



UNIVERSITÀ
DEGLI STUDI
DI PADOVA

Head Office: Università degli Studi di Padova

Department: Centro di Ateneo di Studi e Attività Spaziali "G. Colombo" - CISAS

Ph.D. COURSE IN: Space Sciences, Technologies and Measurements

CURRICULUM: Sciences and Technologies for Aeronautics and Satellite Applications (STASA)

31st SERIES

Neck Protection Development and a Proposal of the Associated Standard for the Motorcyclists

A thesis
on the research project of
Dainese S.p.A.
submitted to the
Università degli Studi di Padova
written with the financial contribution of the People Programme
(Marie Skłodowska Curie Actions)
of the
European Union's Seventh Framework Programme FP7/2007-2013/
under REA grant agreement
n° [FP7-PEOPLE-2013-ITN-608092]

Coordinator: **Prof. Giampiero Naletto**

Supervisor: **Prof. Ugo Galvanetto**

Ph.D. student: **Mohammed Nasim**



UNIVERSITÀ
DEGLI STUDI
DI PADOVA

DAINESE



DAINESE
Settantadue



MOTORcycle
Rider
Integrated
SafeTy

Neck protection development and a proposal of the associated standard for the motorcyclists

Ph.D. Thesis, Università degli Studi di Padova

Dainese S.p.A.

MOTORIST

©Mohammed Nasim, 2018^[1]_{SEP}

All rights reserved.

Published in: Padova, Italy

Essentially all models are wrong, some are useful.

- George E. Box (1976)

Abstract

Motorcyclists (including moped riders) are the most vulnerable road users in terms of injury protection. Though the head and the extremities are the most affected body parts in motorcycle accidents, the occurrence of serious to fatal injuries is often due to the injuries in the cervical spine according to the literature.

Although a variety of neck braces exists in the market to protect the neck from being injured in motorcycle accidents, the effectiveness of those neck braces is not clear due to the lack of scientific evidence of the injury reduction. Moreover, the absence of standard test methods makes the quality assessment process of the braces incomplete. Hence, the development of a common regulation should be the main focus in order to evaluate all the neck braces available in the market and also the future neck protective systems. It is important to define a neck injury assessment process based on the impact conditions of motorcycle accidents. However, a lack of accidental and experimental data on injury mechanisms limits the potential of the standard development research.

The main objective of this study is to contribute to the development of new personal protective equipment (PPE) focusing on neck protection for the motorcyclists. Moreover, the study aims to provide some ideas to develop the standardization procedures for the future EU standards for neck protectors.

New functional prototypes, as neck protective systems, were designed for the motorcyclists. However, more focus has been given on the neck injury mechanisms and new test methods rather than on the development of new neck protectors. For such reason, a new biofidelic finite element (FE) neck model was developed and coupled with Hybrid III head model. In the following steps, a rigid torso was added to the neck model, the neck protective systems were coupled with FE head-neck-torso model and six different test conditions were simulated. The results were analyzed as functions of upper and lower neck forces, head acceleration, head rotation relative to torso, different impact speeds, and available neck injury criteria.

The key suggestions provided in this thesis include modification of the ambient impact test method for motorcyclists' impact protectors, improvement of the design of neck protective systems, advancement of different test methods for neck protectors, investigation for new neck injury assessment process and direction to develop standards for neck protectors.

Summary

The development of new personal protective equipment (PPE) for the motorcyclists focusing to neck protection was the main objective of this thesis. The thesis includes the discussion of the effectiveness of these PPEs and the guidelines of future EU standards for neck protectors, where it has been divided into eleven chapters.

The purpose of this research has been discussed in Chapter 1. A brief description on the research activities and research approach has been summarized.

One of the most important review parts of this thesis on injury biomechanics focusing on neck has been described in Chapter 2. The chapter includes a brief literature review of the anatomical structure of the neck, the statistics of the injuries related to accident found in the literatures, the mechanisms of injury and the mechanical tolerances achieved by volunteer tests, PMHS (Post-mortem human subject) tests and computational models.

A list of PPEs used for motorcyclists' safety along with their functional mechanisms and standards to certify them has been provided in Chapter 3 and Chapter 4. Different standards for different PPEs are used, where some PPEs don't have any standards. The current standards, their effectiveness and drawbacks have been discussed in these chapters.

Chapter 5 summarizes the biomechanical models developed for crash analyses. Different types of physical and numerical models are used as human surrogates for accident reconstruction, evaluation of safety features of the new products and study of the injury mechanisms.

The materials used in the PPEs are mainly energy absorbing materials. Other materials like leathers/textiles in the garments for impact abrasion and cut resistance are also used extensively. Various types of experimental methods applied to test these materials have been explained in Chapter 6.

In Chapter 7, details about the newly developed Dainese finite element neck model have been described including its geometry, construction methods and material properties. In the last part of the chapter, the response of the model in compression, frontal and lateral impacts has been evaluated against experimental results. Some useful studies such as the effects of muscle consideration and body positioning in compressive impacts have also been included in the Appendices.

Chapter 8 discusses the three prototypes, which have been designed based on innovative ideas. The chapter includes the finite element models of those prototypes and the reference PPE (a hybrid neck brace and a helmet).

The models of the virtual test setups for evaluating neck protectors have been demonstrated in Chapter 9. Finally, the evaluation of neck injury reduction by the prototypes developed and existing neck brace using numerical methods has been discussed in the results and discussion sections.

There is no available standard for the neck protectors, though some neck protectors are available in the market and claimed to be certified. The protectors are generally tested based on some internal disciplinarys or other existing standards designed for other purposes than neck protector. These tests are done for commercial purpose and without any proper knowledge on injury biomechanics. In Chapter 10, some suggestions have been provided following the analysis shown in the previous chapters, which could be possibly, included in the future EU standard for neck protector.

Finally, the summary of the work has been concluded with limitations in Chapter 11. The future improvement needed to continue this research has been highlighted at the end of this chapter.

Acknowledgements

All the praises and thanks be to Allah. I am extremely grateful to Him for keeping me in good health during this whole thesis period.

Thanks to Marie Sklodowska Curie Actions for funding the research.

Heartfelt thanks to Marcello Bencini and Nicola Alessi from Dainese S.p.A. for giving me the excellent opportunity to work for Dainese on this interesting topic.

I would like to extend my graceful thanks to Prof. Ugo Galvanetto for accepting me as his Ph.D. student. His tenacious support as a supervisor throughout the entire thesis duration is much appreciable.

I am also thankful to MOTORIST consortium for teaching me the pros and cons of conducting scientific research. I enjoyed being there in every single meeting, discussion, course, workshop and dinner inside this network.

It was a great experience working for Dainese in the R&D Department. I shall always remember the Dainese team, especially the crew of “Ufficio Stile” and “D-air unit” where my desk was located. I should mention a few names that effectively participated in the discussion for this thesis work: Alessandro Cernicchi, David Sheridan, Michele Brasca, Andrea Azzolin and Flavia Papile.

Smile on my well-wishers who helped me in different ways. I would like to mention Sayedus Salehin for his proof reading service of my thesis.

Lastly, my acknowledgement would be incomplete without thanking my family members. My parents and my sister have been my courage from the very beginning. And now, I have more spirit, because of my wife Arani, a new addition to my life. Thanks to her for being patient during this thesis writing period.

Mohammed Nasim

Table of Contents

Chapter 1 Introduction.....	1
1.1 Statement of the Problem.....	1
1.2 Research Objectives.....	2
Chapter 2 Injury Biomechanics of Neck.....	5
2.1 Anatomy.....	5
2.2 Injury Mechanisms.....	9
2.3 Accident Analysis	12
2.4 Mechanical Responses and Tolerances of the Neck.....	15
2.5 Neck Injury Metrics	18
2.5.1 Neck Injury Criterion, NIC	18
2.5.2 Neck Protection Criterion, N_{km}	19
2.5.3 Lower Neck Load Index, LNL.....	19
2.5.4 Beam Criterion (BC).....	20
2.5.5 Neck Injury Index, NII.....	20
2.5.6 Neck Injury Criterion N_{ij}	21
2.5.7 Other Criteria	23
Chapter 3 Personal Protective Equipment (PPE).....	24
3.1 Protective clothing	26
3.2 Gloves	27
3.3 Boots	28
3.4 Impact Protectors	29
3.5 Helmets	30
3.6 Neck Protection Devices.....	31
3.6.1 Neck brace	31
3.6.2 Airbag technology.....	32
Chapter 4 Standards in PPE.....	34
4.1 Standards for protective clothing, gloves and boots	35
4.2 Standards for Impact protectors	37

4.3 Standards for Helmets.....	38
Chapter 5 Biomechanical Models.....	40
5.1 Physical Models	40
5.1.1 Dummies	40
5.1.2 Neck surrogates.....	41
5.2 Computational Models.....	42
5.2.1 Lumped mass (LM) models	43
5.2.2 Multi-body (MB) models.....	44
5.2.3 Finite Element (FE) models.....	46
5.2.3.1 Full-body models	47
5.2.3.2 Neck or Cervical Spine Models	48
5.2.4 Hybrid Models	49
Chapter 6 Experimental Techniques	51
6.1 Drop Weight Impact Tester	51
6.2 Impact Abrasion Apparatus	53
6.3 Impact Cut Resistance Apparatus	56
6.4 Dynamometer.....	56
6.5 Rigid test cones.....	57
Chapter 7 Development of FE Neck Model.....	58
7.1 Model Geometry	59
7.2 Model Construction	61
7.2.1 Vertebrae.....	61
7.2.2 Intervertebral Discs	62
7.2.3 Facet Cartilage and Spinal Cord	62
7.2.4 Segmented D-neck & Hybrid III dummy head.....	63
7.2.5 Ligaments.....	64
7.2.6 Muscles	65
7.2.7 Soft tissues and skin.....	68
7.3 Material Properties.....	68
7.4 The model response in Compression	75

7.4.1 Simulation method for compression	75
7.4.2 Evaluation of D-neck model in compression.....	76
7.5 The model response in frontal impact at 15 g acceleration	79
7.5.1 Simulation method for the impact at 15g acceleration	79
7.5.2 Evaluation of D-neck model in frontal	81
7.6 The model response in lateral impact at 7 g acceleration	83
7.6.1 Simulation method for the impact at 7g acceleration	83
7.6.2 Evaluation of D-neck model in lateral impact	84
Chapter 8 Innovative Protection Systems.....	86
8.1 Reference PPE	86
8.1.1 Helmet model.....	86
8.1.1.1 Finite Element (FE) model Construction.....	87
8.1.1.2 Validation.....	88
8.1.2 Hybrid Neck Brace	89
8.2 New Prototypes.....	91
8.2.1 Soft Neck Brace	91
8.2.2 Neck Collar	94
8.2.3 Airbag Support.....	97
8.2.3.1 Airbag Neck Brace.....	98
8.2.3.2 Airbag Jacket	99
8.3 Physical Comparison	101
Chapter 9 Numerical Analyses	103
9.1 Virtual Test Setups.....	103
9.1.1 Finite Element Model of Anthropomorphic Test Device (ATD)	103
9.1.2 Impact Conditions.....	104
9.2 Results.....	107
9.2.1 Case 1.....	107
9.2.2 Case 2.....	109
9.2.3 Case 3.....	111
9.2.4 Case 4.....	113

9.2.5 Case 5.....	115
9.2.6 Case 6.....	117
9.3 Discussion.....	119
9.3.1 Head Rotation Relative to Torso.....	119
9.3.2 Effect of impact speed	121
9.3.3 Airbag Jacket	122
9.3.4 Neck Injury Criteria	123
Chapter 10 Guidelines for EU Standard	128
10.1 Innocuousness.....	128
10.2 Ergonomics	129
10.3 New Anthropomorphic Test Device (ATD)	129
10.4 Test Methods.....	130
10.5 Neck Injury Risk Assessment	131
10.6 Labelling	133
Chapter 11 Conclusions.....	134
11.1 Summary of the Research	134
11.2 Limitations	135
11.3 Future Work	135
References.....	137
Appendix A.....	154
Appendix B.....	158
Appendix C.....	159
Appendix D.....	160
Appendix E.....	162
The Author	165

List of Figures

Figure 1.1 The summary of the research plan.....	2
Figure 2.1 Different parts of neck anatomy	5
Figure 2.2 Anatomical details of different vertebrae	6
Figure 2.3 The head-neck coupling by occipito-cervical joint. The figure also shows atlanto-axial joint between C1 and C2.....	6
Figure 2.4 The structure of intervertebral disc with nucleus pulposus concentric layers of annulus fibrosus	7
Figure 2.5 The details of the ligaments in human neck	8
Figure 2.6. Lateral view of a human neck detailing muscles.....	8
Figure 2.7 Spinal cord and associated soft tissue	9
Figure 2.8 Possible neck loading modes (top) and examples of four different injury mechanisms (bottom).....	10
Figure 2.9 Summary of the distribution of PTW rider (on the right) and passenger (on the left) injuries greater than AIS1	12
Figure 2.10 Head impact angles leading to neck injuries: (a) in the sagittal plane (ZX) and (b) in the transverse plane (XY).....	14
Figure 2.11. Head-neck response corridors for extension (left) and flexion (right) as reported by Goldsmith and Ommaya (1984)	16
Figure 2.12 Nij kite corridor (blue boundary) and in-position hexagon corridor (black boundary) adopted as the FMVSS 208 final rule.....	22
Figure 2.13 Time dependent neck tensile and shear force tolerances for frontal impact protection according to ECE R94	23
Figure 3.1 PPEs used to reduce different injury risks.....	25
Figure 3.2 Designing of a two-piece leather suits with protective features.....	26
Figure 3.3 Designing of motorcycle gloves with knuckle protection.....	27
Figure 3.4 Design features of motorcycle boot.....	28
Figure 3.5 Impact protection feature of impact protectors – shoulder protector (left) and chest protector (right).....	29
Figure 3.6 General design of protective motorcycle helmet.....	30

Figure 3.7 Different types of neck protecting devices	31
Figure 3.8 The principle of Hybrid Neck Brace.	32
Figure 3.9 Mechanically triggered airbag system with physical connection to the motorcycle.....	33
Figure 4.1 The injury risk zones on a suit.....	35
Figure 4.2 3D explanation of the zoning principle of motorcycle clothing.....	36
Figure 5.1 Different types of crash dummies: (from left to right) Hybrid III 50 th Male Pedestrian, Hybrid III 5 th Female Pedestrian, BioRID II 50 th Male Rear Impact, THOR 50 th Male Frontal Impact, SID IIs 5 th Female Side Impact.....	41
Figure 5.2 The neck ATDs: (a) Hybrid III neck, (b) and (c) modified necks to improve the biofidelity in head-first impacts	42
Figure 5.3 (a) The lumped-mass model of thorax and (b) the lumped-mass model to relate variations in ground reaction forces to mechanical characteristics of specific elements in the model	43
Figure 5.4 Examples of multi-body human models: (a) 5 th percentile MADYMO female model and (b) 50 th percentile MADYMO male model.....	44
Figure 5.5 Multi-body cervical spine models [Reproduced from (a) Camacho et al, 1997 and (b) Van der Horst, 2002	45
Figure 5.6 50 th percentile male dummy and human body occupant models: (a) Hybrid III model developed by LSTC, (b) detailed GHBMC model developed by Global Human Body Model Consortium and (c) detailed THUMS model developed by TOYOTA Motor Corporation and TOYOTA Central R&D	47
Figure 5.7 Finite element full cervical spine models: (a) KTH model with hill muscles [adapted from Brodin et al., 2005], (b) Strasbourg University model with solid elements for passive muscles, (c) Waterloo University model with hill muscles and (d) Chalmers female model with hill muscles and neck soft tissues	49
Figure 5.8 VIRTHUMAN 50 th percentile male hybrid model (right), where the basic skeleton is modelled as multi-body.....	49
Figure 6.1 A list of anvils used in the drop weight impact test for different protectors. They are used for (a) footwear, (b) back and chest protectors, (c) chest protectors (impact distribution test), (d) helmets, (e) limb protectors, and (f) gloves.	51
Figure 6.2 A list of bar impactors used in the impact test for different protectors. They are used for - (a) back and chest protectors, (b) helmets, (c) limb protectors, (d) gloves, and (e) visor (penetration test)	52

Figure 6.3 The experimental set-up of a drop weight impact tester for the impact test ...	52
Figure 6.4 The experimental set-up of headform drop assembly	53
Figure 6.5 A headform used in the tests of helmets.....	53
Figure 6.6 The “Cambridge” type abrasion test machine	54
Figure 6.7 The test specimen of the leather garment mounted on the hinged arm of the Cambridge machine for the impact abrasion test.....	55
Figure 6.8 Base model of the “Darmstadt” type abrasion test machine	55
Figure 6.9 The configuration of the impact cut resistance apparatus	56
Figure 6.10 The dynamometer used for tensile strength test of the samples.....	57
Figure 6.11 (a) A rigid test cone for the restraint test and (b) the performance of the restraint test using the test cone	57
Figure 7.1 FE models of the upper (a) and lower (b) cervical vertebrae	62
Figure 7.2 The construction of vertebral disc with nucleus pulposus and annulus fibrosus	62
Figure 7.3 The position of facet cartilage and spinal cord in the neck model	63
Figure 7.4 Full cervical spine model by replacing the hybrid III neck with the simplified D-neck model.....	64
Figure 7.5 The orientation of ligaments in the neck model	65
Figure 7.6 The position of muscles in the neck model: anterolateral view (left) and right side view (right)	66
Figure 7.7 Dispersion of mass elements to account for the weight of the muscles	66
Figure 7.8 The construction of neck skin and neck soft tissues to develop the complete neck model	68
Figure 7.9 Force-deflection curve for the ligaments defining the three distinct regions..	72
Figure 7.10 Schematic diagram of Hill muscle model with active-passive elements	72
Figure 7.11 (a) The experimental setup with PMHS head and cervical spine and (b) FE model for the simulation replicating the experimental setup.....	76
Figure 7.12 Time lapse of the neck kinematics for the compressive impact with rigid impact surface. The orientations of the surface are (a) -15° and (b) $+15^{\circ}$. The dotted red line represents the neck position in the experiments.	77

Figure 7.13 The comparison between the experimental and simulated results for the impact angles of (a) -15° , (b) 0° and (c) $+15^{\circ}$. The black dotted lines represent the experimental corridors and red solid lines show the response of D-neck model.....	78
Figure 7.14 (a) The test setup with human volunteer and (b) the numerical head-neck model used to perform the sled tests.....	79
Figure 7.15 Prescribed (a) T1 acceleration in impact direction and (b) T1 rotation in the plane of impact based on the NBDL experiments for frontal impact at 15g acceleration	80
Figure 7.16 The activation state of the muscles used in the simulation of sled tests.....	81
Figure 7.17 Time lapse of the neck kinematics with active muscles for the 15g frontal impact. The orientation of the neck skin (top) and the muscles with internal structure (bottom) are shown separately in the figure.	82
Figure 7.18 Simulated response of the active neck model to 15g frontal impact. The response is compared with experimental corridor as a function of acceleration of head centre of gravity (CG).	82
Figure 7.19 Prescribed (a) T1 acceleration in impact direction and (b) T1 rotation in the plane of impact based on the NBDL experiments for frontal impact at 15g acceleration	83
Figure 7.20 Time lapse of the neck kinematics with active muscles for the 15g frontal impact. The orientation of the neck skin (top) and the muscles with internal structure (bottom) are shown separately in the figure.	84
Figure 7.21 Simulated response of the active neck model to 7g lateral impact. The response is compared with experimental corridor as a function of the acceleration of the head centre of gravity (CG).	85
Figure 8.1 Pista GP AGV E2205 Multi Gran Premio reference helmet model to evaluate the neck protectors	86
Figure 8.2 The FE helmet model showing the composite shell (outer semi-transparent layer) and the different regions of the foam liner [chin (green), cheek (red), main (yellow) and top (blue)]	87
Figure 8.3 Compressive stress-strain curves used for modelling the foam parts, which are defined for: (a) pressure yield and (b) yield stress.....	87
Figure 8.4The configuration of the helmet and headform in the simulation environment. The inverted drop tests were simulated at points P and B. The other points according to the Standard ECE R22.05 are R, X and S.....	88

Figure 8.5 The comparison between the experimental and simulated results of the drop tests with helmeted headform at points (a) P and (b) B.....	89
Figure 8.6 Dainese Carbon Hybrid Neck Brace as reference model for comparison.....	90
Figure 8.7 FE Hybrid neck brace model.....	90
Figure 8.8 Stress-strain relationship of PU foam.....	91
Figure 8.9 The concept of soft neck brace was inspired by Dainese Carbon Hybrid Neck brace (left) and energy absorbing foams (right)	91
Figure 8.10 The complete structure of the soft brace (right), which has been designed as layers of different types of foams: two layers of Poron XRD foam, one layer of polyurethane comfort foam and one layer of nitrile butadiene rubber (NBR) placed in between the two Poron layers (left).	92
Figure 8.11 The final prototype of the soft neck brace.....	92
Figure 8.12 FE model of the soft brace.....	93
Figure 8.13 Stress-strain relationship of NBR and PORON energy absorbing polymers	93
Figure 8.14 Dainese developed pressure suit for the astronauts in collaboration with the European Space Agency (ESA), an inspiration for developing the neck collar	94
Figure 8.15 The mechanism of the two elastic bands of different young modulus used as the key feature of the neck collar, where the bands are attached with each other in such a way that the stiffer band allows the flexible band to be elongated smoothly until it reaches to the length of the stiffer band	94
Figure 8.16 The mechanism of the bands, shown in Figure 8.7, where bands were attached with helmet and jacket.....	95
Figure 8.17 The prototype of neck collar: fixing with helmet (left), front view (middle) and side view (right)	95
Figure 8.18 FE model of the neck collar.....	96
Figure 8.19 Force-deflection curves of the bands used to model the neck collar.....	96
Figure 8.20 Airbag technology used as impact protector, which is normally placed inside the jacket	97
Figure 8.21 Two layers of inflated airbag (8mm total thickness) used to compare physically with other neck protectors	97
Figure 8.22 The contact between the helmet and airbag system as neck protector (left) and the position of the airbag layers around neck while inflated (right)	98

Figure 8.23 FE model of airbag neck brace	99
Figure 8.24 Mass of flow rate of Helium used in the simulation	99
Figure 8.25 Dainese D-air street airbag jacket (left), FE model of the airbag jacket (middle) and extra layer of airbag with jacket to provide more restriction on the neck movement (right)	100
Figure 8.26 The drop test performed on airbag jacket according to the standard for back protectors (EN 1621-2:2013)	100
Figure 8.27 Force transmission history from the drop test shown in Figure 8.26.	101
Figure 8.28 Internal pressure of the airbag in the simulation shown in Figure 8.26.	101
Figure 9.1 The extension of the neck model with a torso model.....	103
Figure 9.2 Imaginary sliding test setup (left) and the FE model (right) for frontal impact	104
Figure 9.3 Imaginary sliding test setup (left) and the FE model (right) for rear impact	105
Figure 9.4 Imaginary sliding test setup (left) and the FE model (right) for lateral impact	105
Figure 9.5 Imaginary inverted drop test setup (left) and the FE model (right) for -15° impact angle	106
Figure 9.6 Imaginary inverted drop test setup (left) and the FE model (right) for 0° impact angle.....	106
Figure 9.7 Imaginary inverted drop test setup (left) and the FE model (right) for $+15^{\circ}$ impact angle	107
Figure 9.8 Time-lapse of the response of the ATD model with different neck protective systems for case 1	108
Figure 9.9 The upper and lower neck forces and the resultant head acceleration for case 1	109
Figure 9.10 Time-lapse of the response of the ATD model with different neck protective systems for case 2	110
Figure 9.11 The upper and lower neck forces and the resultant head acceleration for case 2.....	111
Figure 9.12 Time-lapse of the response of the ATD model with different neck protective systems for case 3	112

Figure 9.13 The upper and lower neck forces and the resultant head acceleration for case 3.....	113
Figure 9.14 Time-lapse of the response of the ATD model with different neck protective systems for case 4	114
Figure 9.15 The upper and lower neck forces and the resultant head acceleration for case 4.....	115
Figure 9.16 Time-lapse of the response of the ATD model with different neck protective systems for case 5	116
Figure 9.17 The upper and lower neck forces and the resultant head acceleration for case 5.....	117
Figure 9.18 Time-lapse of the response of the ATD model with different neck protective systems for case 6	118
Figure 9.19 The upper and lower neck forces and the resultant head acceleration for case 6.....	119
Figure 9.20 The calculation of change in head angle representing the head rotation relative to torso (T1)	120
Figure 9.21 The head rotation relative to torso by using different types of neck protective systems for different loading cases	120
Figure 9.22 The upper and lower neck forces and the head rotation relative to torso, with and without hybrid neck brace, at different impact speeds.....	121
Figure 9.23 Time-lapse of the response of the ATD model with airbag neck protective systems for case 1 (top), case 4 (middle) and case 6 (bottom)	122
Figure 9.24 The comparison of upper neck force and the head rotation relative to torso with and without airbag system for cases 1, 4 and 6	123
Figure 10.1 New neck ATD with 3D the printed vertebrae from D-neck model	130
Figure 10.2 The relationship between the neck moment and the head rotation relative to torso of the different neck protective systems for case1: frontal slide (top) and case 4: -15 ⁰ inverted (bottom). The grey corridor represents the flexion-extension corridor, where positive and negative moments indicate extension and flexion respectively	132

List of Tables

Table 2.1. Examples of spinal injuries according to AIS scale	10
Table 2.2 Different types of cervical spine injuries followed by applied load conditions	11
Table 2.3 Neck injury frequencies at different head impact speed.....	13
Table 2.2.4 Neck injury location in the sagittal plane (ZX) in relation with head angle..	14
Table 2.5 Neck injury location in the transverse plane (XY) in relation with head angle	15
Table 2.6. Tolerance limits of the cervical spine	17
Table 2.7 Minimum values for NII injury assessment and coefficients for the Eq. 2.8 ...	21
Table 2.8 Critical values of N_{ij} for FMVSS 208 and peak axial forces for various In- Position (IP) or Out-of-Position (OOP) ATDs	22
Table 4.1 European Standards for motorcycle protective clothing including gloves and boots	37
Table 4.2 European Standards for motorcycle impact protectors.....	38
Table 4.3 European Standard for motorcycle helmet	39
Table 4.4 World Motorcycle Helmet Safety Standards	39
Table 5.1 The history of full cervical spine MB models	45
Table 5.2 The comparison among different types of computational models.....	46
Table 5.3 The history of full cervical spine FE models	48
Table 7.1 Geometries of vertebrae for the design of D-neck model.....	59
Table 7.2 Diameters for spinal cord and spinal canal	60
Table 7.3 Intervertebral disc (IVD) height in the D-neck model.....	61
Table 7.4 The details of muscles' parameters.....	67
Table 7.5 Force-deflection points for modeling the ligaments of lower (C5-C7+) cervical spine.	70
Table 7.6 Force-deflection points for modeling the ligaments of mid (C2-C5) cervical spine	71
Table 7.7 Force-deflection points for modeling the ligaments of upper (C0-C2) cervical spine.	71
Table 7.8 Force-deflection points for modeling the nuchal ligament of whole cervical spine	71

Table 7.9 Material properties used to model the D-neck.....	74
Table 8.1 Material properties of the helmet model.....	88
Table 8.2 The comparison between different types of neck protectors, where “↑” sign means bettering, “↓” sign means worsening and “=” sign means negligible effect due to the differences in design comparing to the reference Dainese Carbon Hybrid Neck Brace.....	102
Table 9.1 The dynamic variable values of upper neck with different neck protective systems.....	124
Table 9.2 The critical values used to calculate NII and Nij.....	124
Table 9.3 The values of NII and Nij using Eq. 2.7 and Eq. 2.9.....	125
Table 9.4 The probability of AIS ≥ 1 injury according to NII criterion	126
Table 9.5 Recalculation of NII functions using the proposed modifications and the prediction of probable AIS3+ injuries	127

Chapter 1

Introduction

1.1 Statement of the Problem

Cervical spine is the major injured region for serious to fatal spine injuries and one of the root causes for such injuries is motor vehicle accident (MVA) [Yoganandan et al, 1989]. The powered two-wheeler (PTW) such as motorbike and moped accidents have been estimated as 18% of the road fatalities in the European Union while the riders accounted for two thirds (63%) of road accident casualties attending a hospital [European Commission, 2017].

The injuries most common to the cervical spine are compression-flexion injuries and burst fractures [Yoganandan et al, 1989, DeWit, 2010], and are mainly due to compression in the sagittal plane [Myers and Winkelstein, 1995]. Various types of injuries to the cervical musculoskeletal system such as vertebral fracture and dislocation, rupture of intervertebral disc, ligament and joints, laceration of spinal cord and vertebral artery are also observed during MVA accidents [Winkelstein and Myers, 1997]. Such injuries are most common in automotive accidents (50.7% of all spine injuries) [Robertson et al., 2002] due to the lag in acceleration between the human head and the vehicle [White and Panjabi, 1990]. It has also severe impact on the motorcycle accidents, as these injuries are common for fatality to the motorcyclists [White et al., 2013; Bambach et al., 2012; Whyte et al., 2016]. The mechanisms of these injuries are mainly based on four basic movement of the head-neck system: flexion, extension, lateral bending and rotation [Chen et al., 2011].

Although a variety of commercial neck braces have been produced to protect the neck from injury in motorcycle accidents, there are lack of scientific evidence and standard test method to assess the effectiveness of those braces in neck injury reduction. Hence, the main priority goes to develop a common regulation to evaluate all the present neck braces and the future neck protective systems. It is important to develop appropriate neck injury criteria that should be included in the evaluation process. However, a lack of experimental data on injury mechanics limits the potential of the standard development research. The finite element human body models are commonly used in the recent era for the analysis of the interaction between helmet and neck brace, which is considered to be a promising tool in this field of research.

1.2 Research Objectives

The concern related to motorcycle accidents has led many organizations to invest on research in the field of motorcyclists' safety. The European Union is one of the biggest contributors in this field, who has financed a lot of past/present projects for motorcyclists' safety. These projects, such as MYMOSA, HUMOS, HEADS, MOTORIST and others are directly and indirectly involved in the safety research for the motorcyclists. The present thesis is a part of the MOTORIST (www.motorist-ptw.eu/) project, which includes three work packages: riders' behaviour, riders' training and active/passive safety. The research presented in this thesis has been done under the work package of active/passive safety. This is an industry based research; all the work described here has been carried out in Dainese S.p.A., a leading Italian gear manufacturer company dealing with the active and passive safety in motorcycle, bicycle, horse riding, winter sports and even some special activities.

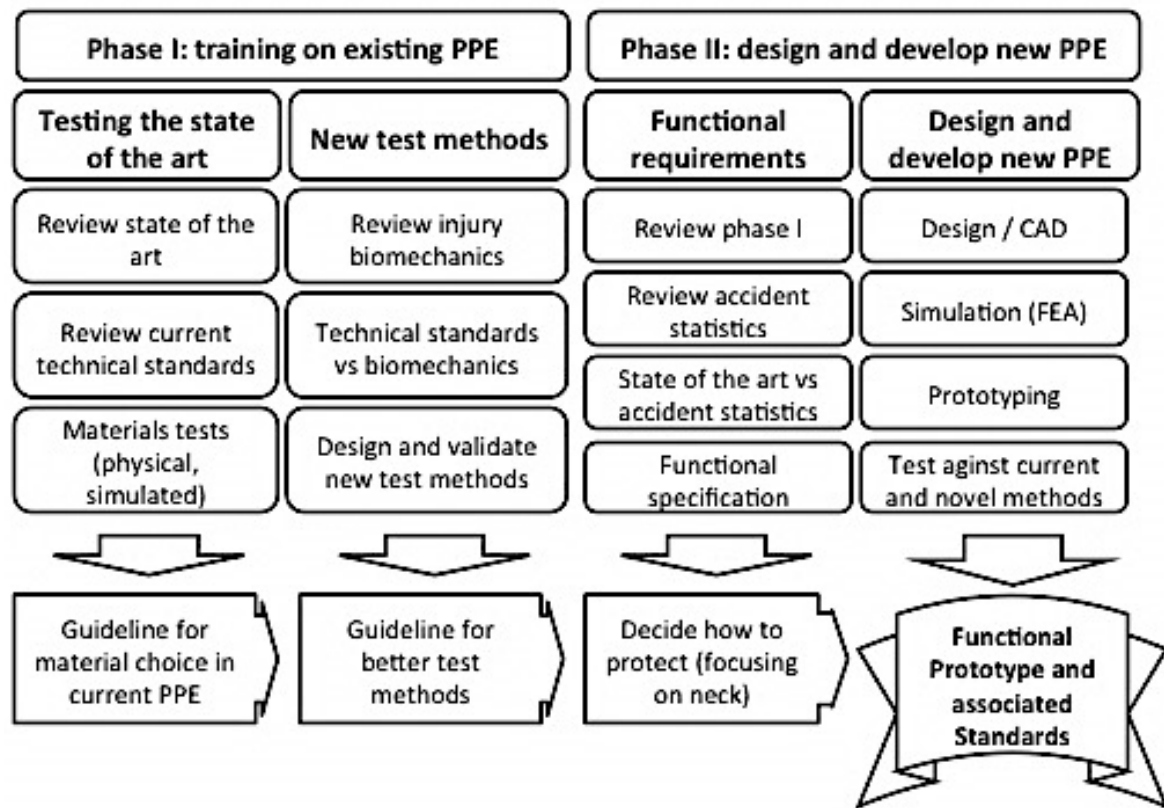


Figure 1.1 The summary of the research plan

The objectives of this research were divided into two phases: training on existing PPE and designing and development of new PPE. The summary of the working plan is shown in Figure 1.1. As it can be seen from the chart, developing PPE with focus to neck was the primary objective, but there were also secondary objectives to perform research on the current PPEs considering their test methods and material selection.

The main objective of this study was to discuss the effectiveness of the existing and future neck protectors. Moreover, the study aimed to establish foundations for the future EU Standards providing some new standardization procedures.

1.3 Research Approach

In the first phase, the existing PPEs and their inherent materials have been reviewed briefly along with their testing procedures according to the Standards. The outcome of this review came out as a deliverable on a survey of Standards in PPE [Nasim et al., 2015]. There is also a published paper based on this review and training, which provides an investigation of the impact properties of the polymeric materials used in the impact protectors [Nasim et al., 2017]. Besides, training on new test methods followed advanced courses on injury biomechanics, ongoing research for the new test methods and their relevancy with biomechanics, attending meeting in CEN/TC162/WG9 (has been described in Chapter 4) and having collaboration with test-houses.

In the second phase, more focus had been given on the neck injury mechanisms and new test methods rather than on the development of new neck protectors. The effectiveness of any new product will remain unclear without any certified evaluation process.

There were some innovative ideas implemented during the whole research period and there were also some new findings. The novelty of this research includes –

Improvement of the test method for impact protector: the test procedure for the ambient impact test according to the associated standard for impact protectors should be improved for practical cases. Nasim et al. (2017) demonstrated that a small change in the temperature around ambient conditions might give different level of protection or even fail the standard criterion, depending on the material and thickness of the soft part used in the protector.

Development of the FE neck model: A novel simple 3D neck model has been developed for analyzing different neck injury mechanism coupling with different types of neck protectors. The model has been validated for several impact conditions to evaluate its biofidelic response similar to that in the real human.

New design for neck protective systems: Three new design concepts have been implemented to prototypes and their performances have been evaluated using physical inspection and numerical methods. The analyses will unveil a better understanding on the neck protective systems to be designed.

Different test methods for neck protectors: New test methods have been suggested with six different test setups using numerical simulation. The boundary conditions of the methods were proposed based on the accident analysis provided in the published literatures.

Investigation for new neck injury assessment process: Currently, there is no neck injury criterion dedicated to motorcycle head-first impacts to predict the overall injury risk for different loading conditions. There is a criterion for motorcycle anthropomorphic test device named as neck injury index (NII), which has been developed for ISO 13232 standard for assessing the risk of injury to the upper cervical spine. In this thesis, neck injury risk was predicted using three different criteria: NII, neck injury criterion (Nij) and beam criterion (BC). Finally, it has been proposed to include to the head rotation relative to torso in the assessment process.

Development of the standard for neck protectors: This thesis creates a platform to motivate the development of standard for the neck protectors. The suggestions for the standard include developing an anthropomorphic test device, new test methods, new neck injury assessment process, labelling, innocuousness and ergonomics.

Chapter 2

Injury Biomechanics of Neck

The biomechanics is the branch of science, which deals with the anatomical study, accidental analysis, experimental measurements and numerical modelling of the living beings like humans, animals and plants, under various boundary conditions. The injury biomechanics, also known as trauma biomechanics is the sub-discipline of biomechanics that is concerned with injury from macroscopic level to tissue level.

This chapter describes briefly the anatomy, accident analysis, injury mechanisms, biomechanical response and tolerances, and injury metrics focusing on the human neck in the context of motorcycle accidents have been described briefly.

2.1 Anatomy

Anatomy is one of the fundamental branches of medical science, which deals with the study of the structure of the human body. The anatomy of the neck comprises of cervical vertebrae, intervertebral discs, ligaments, facet cartilages, nerves, foramina and a complex muscular system (Figure 2.1).

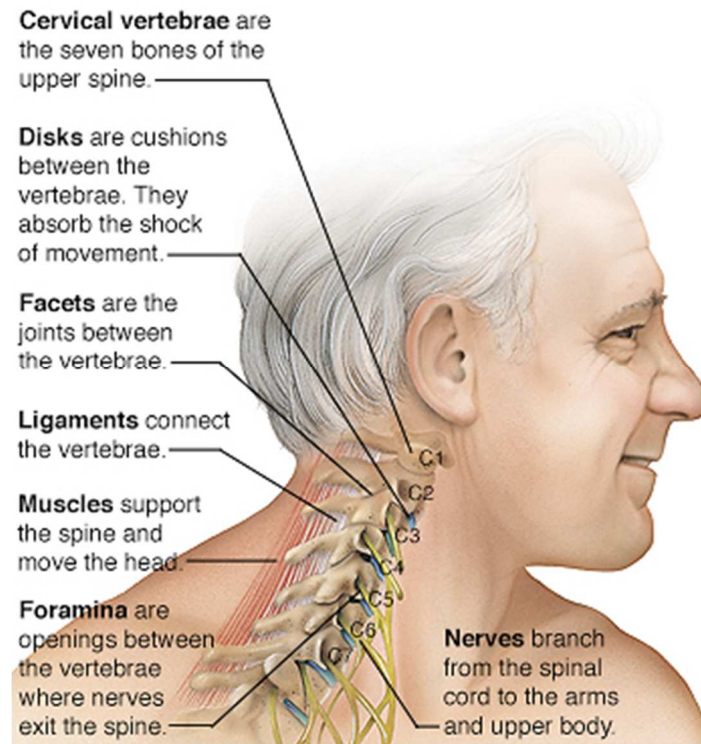


Figure 2.1 Different parts of neck anatomy [Reproduced from www.fairview.org]

The cervical spine of the neck consists of seven vertebrae, which is mainly subdivided into three groups: the upper cervical spine (C1 and C2), the middle cervical spine (C3 – C5), and the lower cervical spine (C6 and C7). The bony structure of each vertebra is constructed with a cancellous (or trabecular) bone core, thin cortical (or compact) bone shell and bony endplates. Figure 2.2 shows the anatomical details of C1 (atlas), C2 (axis), C3 and C4 vertebrae.

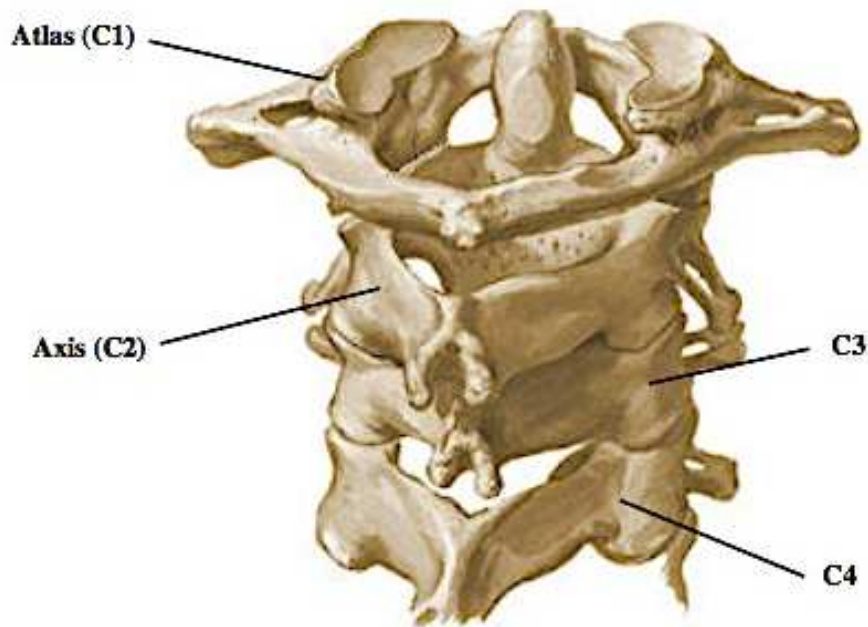


Figure 2.2 Anatomical details of different vertebrae [adapted from Agur and Dalley, 2005]

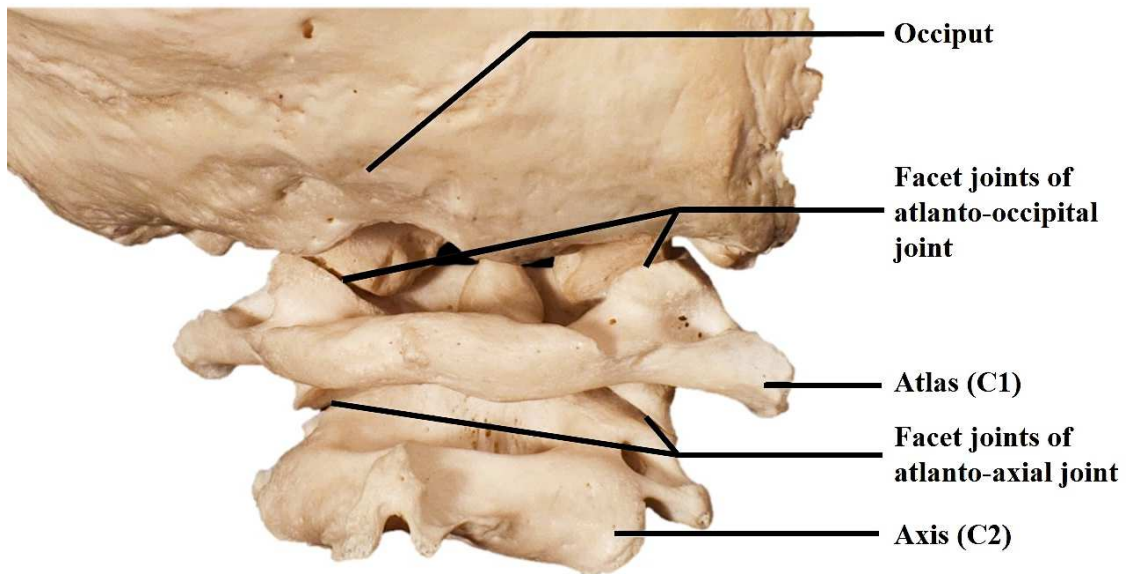


Figure 2.3 The head-neck coupling by occipito-cervical joint. The figure also shows atlanto-axial joint between C1 and C2 [adapted from Muscolino 2013]

The head is supported on the neck by the flexible occipito-cervical joint as shown in Figure 2.3. The figure also shows the atlanto-axial joint between C1 and C2.

The intervertebral disc with a fibro-cartilaginous structure sums up approximately 20 – 33% of the entire height of the spinal column stacking between two adjacent vertebral bodies (Gilad and Nissan, 1986; White and Panjabi, 1990). The intervertebral disc consists of three distinct components: the annulus fibrosus, the nucleus pulposus, and the cartilaginous endplates. The annulus fibrosus, having a composite structure of parallel collagen fibres embedded in a homogenous matrix, encloses the nucleus pulposus forming the outer boundary of the disc as shown in Figure 2.4 [Panzer, 2006]. A cartilaginous endplate acts as a boundary between the superior and inferior surface of the disc and the adjacent vertebrae. The disc helps to absorb the shock of the spinal column and to drive the cervical spine into associated mechanisms when different loading types are applied on it.

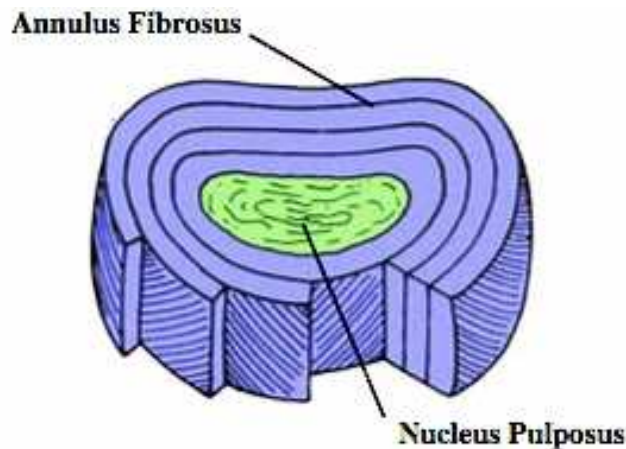


Figure 2.4 The structure of intervertebral disc with nucleus pulposus concentric layers of annulus fibrosus [adapted from White and Panjabi, 1990]

The main function of a ligament is to connect the vertebrae, so that it can resist or restrict the motion of a joint to provide stability to the biological structure (White and Panjabi, 1990). The cervical ligaments from occiput to first thoracic vertebra (T1) are anterior longitudinal ligament, posterior longitudinal ligament, anterior atlanto-occipital membrane, posterior atlanto-occipital membrane, anterior atlanto-axial membrane, posterior atlanto-axial membrane, ligamenta flava, Inter-spinous ligament, capsular ligament, transverse ligament, apical ligament, alar ligament, crus ligament, tectorial membrane and nuchal ligament (figure 2.5). These ligaments are categorized based on their restriction of motion during flexion, extension, translation and rotation.

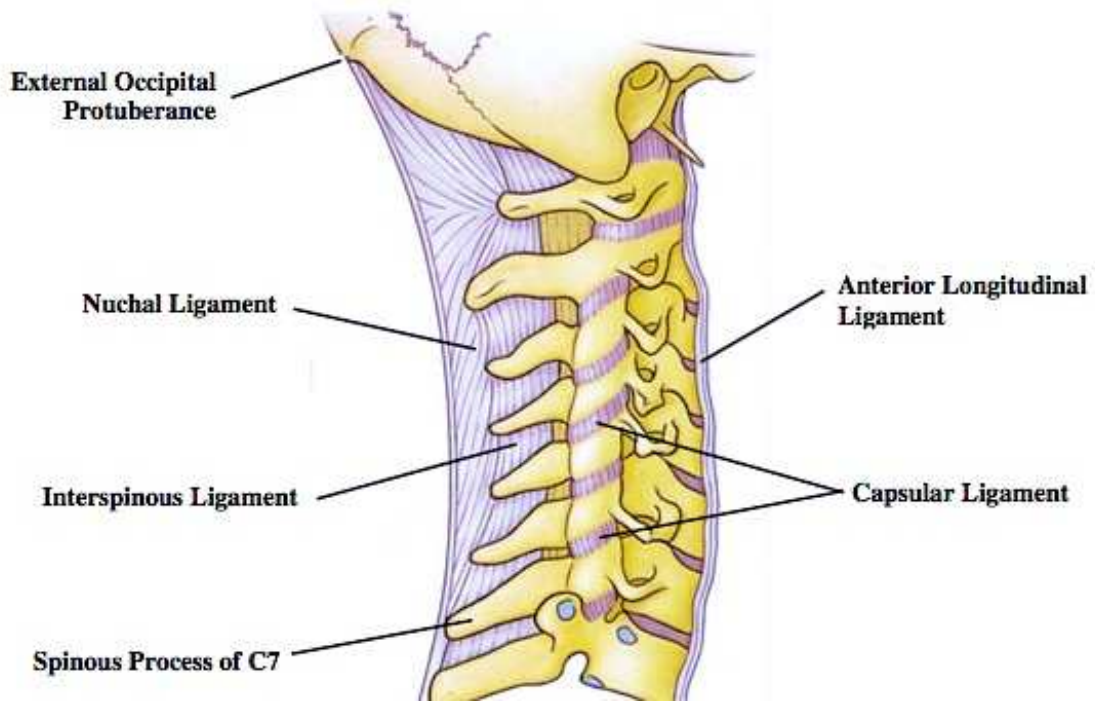


Figure 2.5 The details of the ligaments in human neck [adapted from Moore and Dalley, 2006]

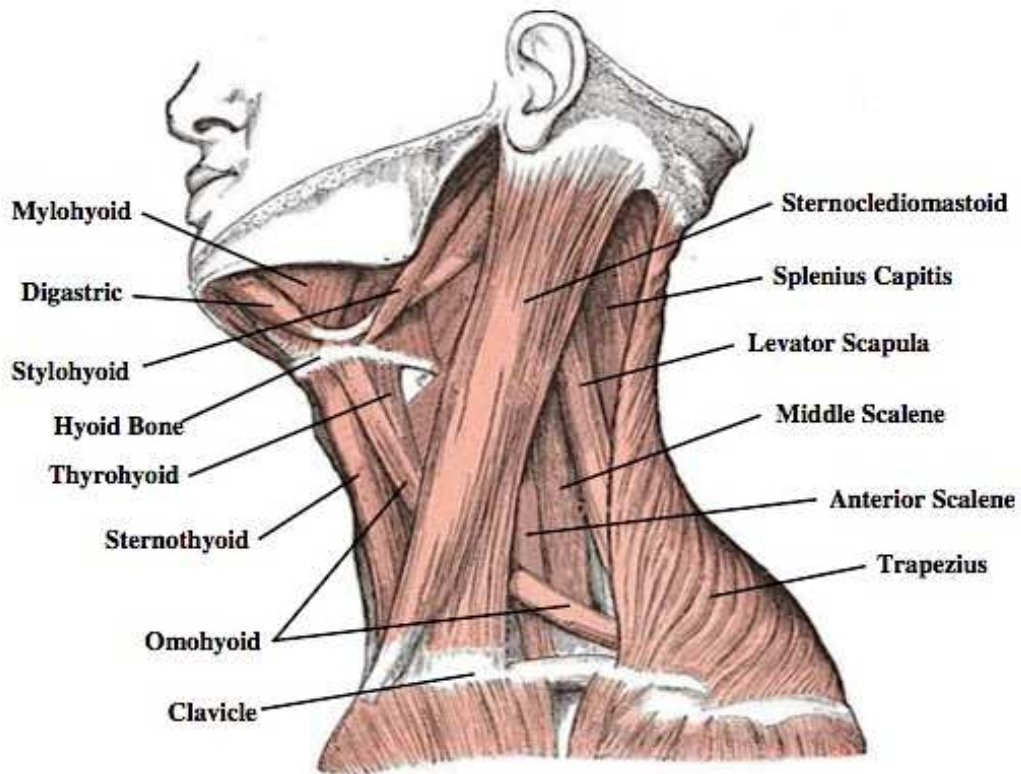


Figure 2.6. Lateral view of a human neck detailing muscles [adapted from Gray, 1918]

The skeletal muscle is a soft tissue with a complex microstructure made up of fascicles, epimysium, perimysium, muscle fibres and tendons. 31 symmetric muscles pairs in the human neck about the medial plane have been identified (Knaub and Myers, 1998). They are oblique capitus inferior, oblique capitus superior, rectus capitus major, rectus capitus minor, longus capitis, longus colli, rectus capitus anterior, rectus capitus lateral, anterior scalene, middle scalene, posterior scalene, sternocleido mastoid iliocostalis cervicis, longissimus capitis longissimus cervicis, multifidus, semisplenius capitus semisplenius cervicis, splenius capitis splenius cervicis, levator scapula minor rhomboid, trapezius, digastric, geniohyoid, mylohyoid, stylohyoid omohyoid, sternohyoid, sternothyroid, and thyrohyoid (some of these muscles are shown in Figure 2.6). These muscles are divided into six groups: hyoid muscles, anterior muscles, lateral muscles, suboccipital muscles, back muscles, and vertebral column muscles (Gray, 1918).

The spinal cord and the associated soft tissues, extending from the medulla oblongata in the brainstem to the lumbar region of the vertebral column, start from the occipital bone and passes through the spinal canal (Fig. 2.7). The canal is formed by the vertebral foramina of all vertebrae.

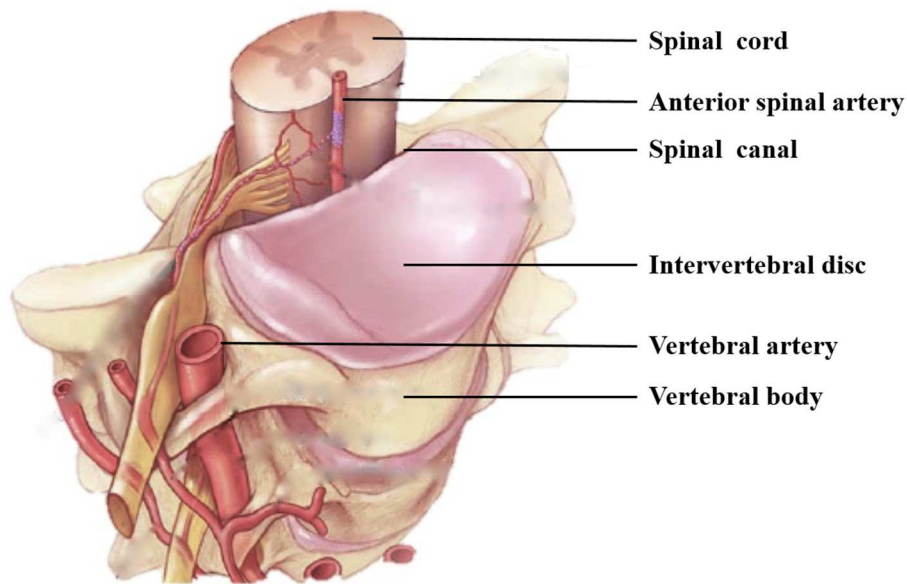


Figure 2.7 Spinal cord and associated soft tissue [adapted from Mayo, 2004]

2.2 Injury Mechanisms

Neck injuries can occur due to two main possible injury mechanisms: a direct impact contacting with a surface or an object and transmission of an impact on other parts of the body (head, thorax, etc). The mechanisms are mainly based on four basic movement of the head-neck system: flexion, extension, lateral bending and rotation [Chen at al., 2011]. These injury mechanisms can produce different types of injuries to the cervical

musculoskeletal system such as vertebral fracture and dislocation, rupture of intervertebral disc, ligament and joints, laceration of spinal cord and vertebral artery [Winkelstein and Myers, 1997]. Viano (2001) reported that the upper cervical spine injuries are usually more serious and life threatening compared to those at the lower levels. AIS (Abbreviated Injury Scale) is widely used to assess the severity of several cervical spine injuries (Table 2.1).

Table 2.1. Examples of spinal injuries according to AIS scale (adapted from AAAM, 2005)

AIS code	Description
1	Abrasion, contusion (hematoma), minor laceration of skin, muscle
2	Minor laceration of vertebral artery Dislocation without fracture of cervical spine
3	Major laceration of vertebral artery Multiple nerve root laceration of cervical spine
4	Spinal cord contusion
5	Spinal cord laceration without cervical spine fracture
6	Decapitation Spinal cord laceration at C3 or higher with fracture

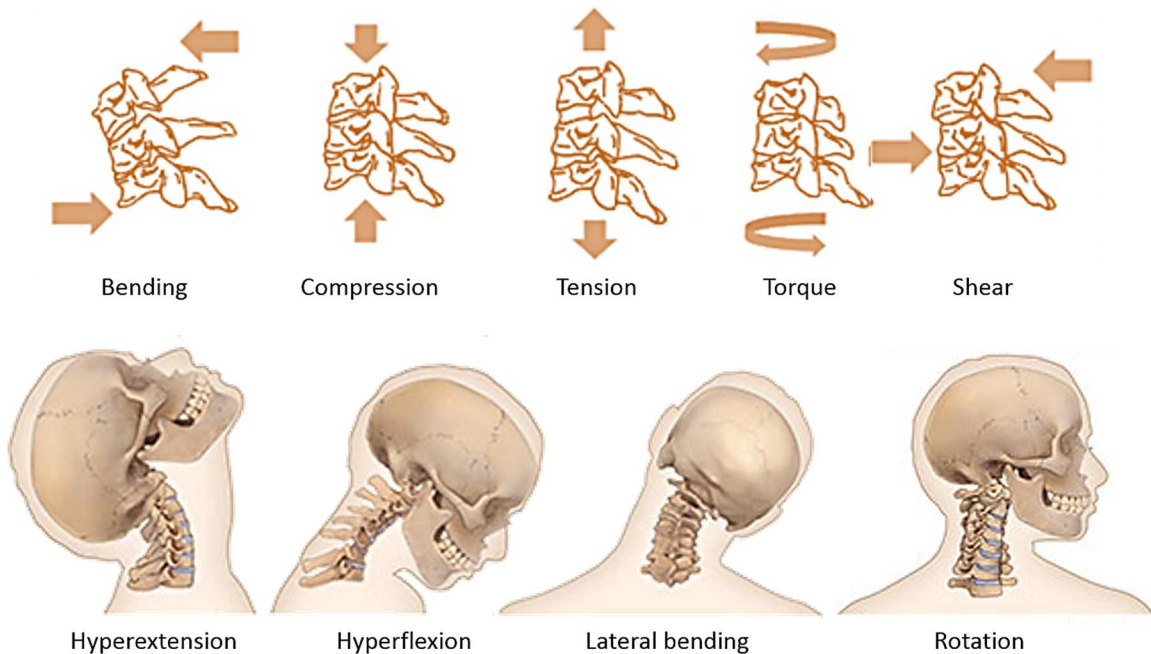


Figure 2.8 Possible neck loading modes (top) [adapted from McElhaney et al. 2002] and examples of four different injury mechanisms (bottom) [adapted from Muscolino 2013]

Table 2.2 Different types of cervical spine injuries followed by applied load conditions (from Winkelstein and Myers, 1997)

Loading modes	Injury Types
Compression	Jefferson's fracture Comminuted fracture of atlas Compression fracture Teardrop fracture
Compression and flexion	Anterior wedge fracture Cervical sprain Unilateral facet dislocation Bilateral facet dislocation Burst fracture Teardrop fracture
Compression and extension	Fracture of Posterior element Clay-shoveler's fracture Hangman's fracture Anterior disc rupture Horizontal vertebral body fracture Teardrop fracture
Tension	Atlanto-occipital dislocation
Tension and flexion	Bilateral facet dislocation Unilateral facet dislocation
Tension and extension	Whiplash Tear of facet joint Tear of intervertebral disc Chip fracture Hangman's fracture Teardrop fracture
Torsion	Atlanto-axial dislocation
Shear	Atlanto-axial subluxation Odontoid fracture Fracture of articular process
Bending	Narrowing of intervertebral foramen Compression of articular process

Several classifications of the neck injury mechanisms have been reported by the researchers [White and Panjabi, 1990; Argenson et al., 2005; Carter et al., 2002; Harris et al., 1986; Allen et al., 1982 and Babcock, 1976]. These mechanisms were divided mainly into three classes: compression, flexion-extension and rotation [Argenson et al., 2005]. Among all the cervical spine injuries, 33% were found to be compression injuries, 28% were flexion-extension injuries and 39% were rotation injuries, where the severity of the injuries was higher for the compression in spite of having lower frequency than for the rotation [DeWit, 2010 Argenson et al., 2005]. The mechanisms of cervical injury at the local level are normally caused by the kinetics of the head-neck-torso assembly. Figure 2.8 shows different injury mechanisms due to different loading conditions on the cervical spine. A list of cervical spine injuries occurred due to these mechanisms is given in Table 2.2.

2.3 Accident Analysis

Motorcyclists (including moped riders) are considered as the most vulnerable road users in terms of injury protection. ACEM, the European Association of Motorcycle Manufacturers reported the injury statistics of 921 PTW (Powered Two Wheeler) riders and 79 PTW passengers involved in the accidents in five European countries: France, Germany, Netherlands, Spain and Italy [ACEM, 2009]. The statistics indicated the total number of 3417 injuries to the PTW riders and 227 injuries to the PTW passengers occurred to the different body parts of those riders and passengers involved in the accident. Based on the AIS (abbreviated injury scale) grading system, the percentages of the frequency of these injuries (greater than AIS1 or minor injuries) to the different body parts are shown in Figure 2.9.

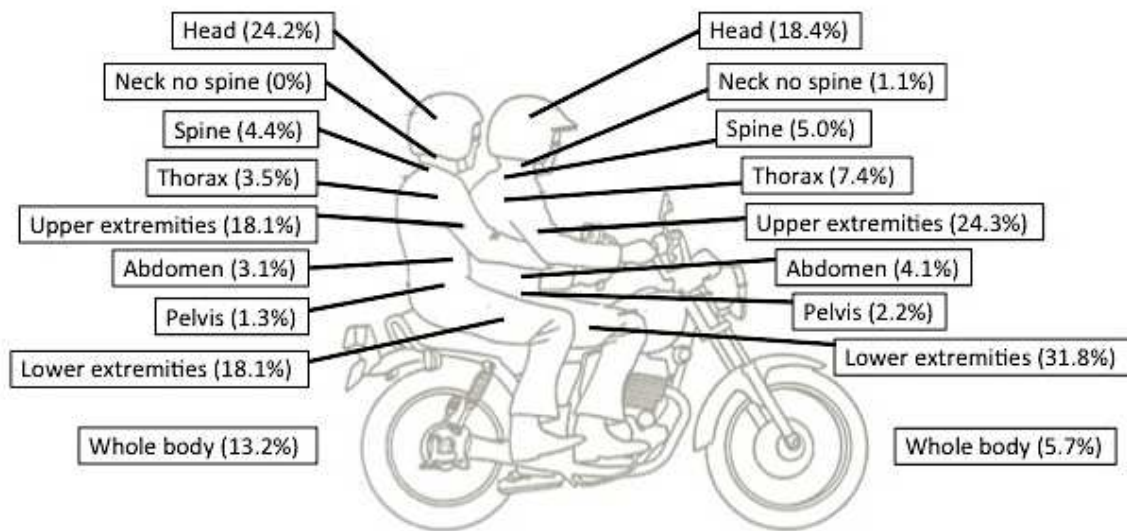


Figure 2.9 Summary of the distribution of PTW rider (on the right) and passenger (on the left) injuries greater than AIS1

The database studies reported that the frequency of cervical spine injury in motorcycle accident is too less comparing to the frequency of injuries to the other body parts [ACEM, 2009; COST 327, 2001]. However, the impact leads to heavy consequences when the injury occurs to the cervical spine. In the AIS scale, COST 327 (2001) showed that 39.3% of the neck injuries were minor (AIS1) and 41% were severe and life threatening (AIS4+) among 61 motorcyclists with neck injuries. These data are in conjunction with the analysis of 76 cases of motorcyclists' real world crash where cervical spine injury was involved [Ooi et al., 2011], which reported that 55.3% of the cases resulted in AIS 3+ injury.

It is difficult to identify the parameters, such as head speed, head angle, and body angle, involved in the accident and resulting in neck injuries. Some of the statistics of these parameters are highlighted in this section according to COST 327 (2001) database, which are mostly relevant to this research work.

Table 2.3 Neck injury frequencies at different head impact speed

Speed of head impact [km/h]	Total		Injuries of the neck							
			Cervical spine strain		Cervical spine fracture		Soft tissue injury		Other	
	n	%	n	%	n	%	n	%	n	%
< 10	2	1.8	1	8.3	-	-	-	-	1	6.7
11 – 20	-	-	-	-	-	-	-	-	-	-
21 – 30	14	12.3	4	33.3	7	13.0	1	3.0	2	13.3
31 – 40	3	2.6	2	16.7	1	1.9	-	-	-	-
41 – 50	14	12.3	1	8.3	10	18.5	3	9.1	-	-
51 – 60	10	8.8	-	-	4	7.4	4	12.1	2	13.3
61 – 70	6	5.3	-	-	4	7.4	1	3.0	1	6.7
71 – 80	13	11.4	-	-	12	22.2	-	-	1	6.7
81 – 90	5	4.4	-	-	2	3.7	1	3.0	2	13.3
91 -100	3	2.6	-	-	3	5.6	-	-	-	-
> 100	4	3.5	-	-	-	-	2	6.1	2	13.3
Unknown	40	35.1	4	33.3	11	20.4	21	63.6	4	26.7
Total	114	100	12	100	54	100	33	100	15	100

Table 2.3 shows the frequency of different types of neck injuries at different levels of head impact speed. The injury is spread at speed of 20-100 km/h and almost all the injury types are present at 30-60 km/h of speed.

Low side impact (body impact angle $<15^{\circ}$) and high side impact (body impact angle $>60^{\circ}$) are the most frequent loading conditions for the occurrence of the neck injuries frequently occur [COST 327, 2001]. Head impact angles leading to neck injuries in the sagittal plane (Figure 2.10a) and transverse plane (Figure 2.10b) are given in Table 2.4 and Table 2.5.

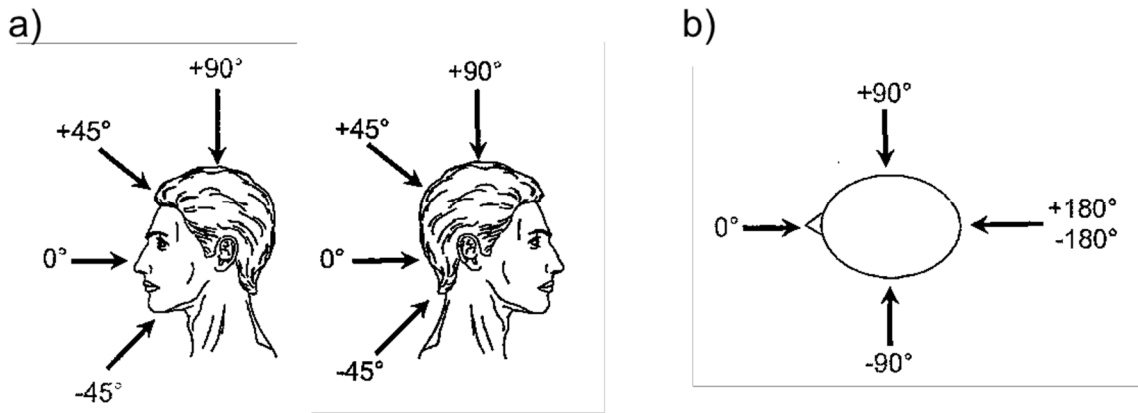


Figure 2.10 Head impact angles leading to neck injuries: (a) in the sagittal plane (ZX) and (b) in the transverse plane (XY)

Table 2.2.4 Neck injury location in the sagittal plane (ZX) in relation with head angle

Head impact angle ZX [°]	Total		Injuries of the neck							
			Cervical spine strain		Cervical spine fracture		Soft tissue injury		Other	
	n	%	n	%	n	%	n	%	n	%
0	52	45.6	2	16.7	34	63.0	6	18.2	10	66.7
1 – 45	14	12.3	4	33.3	2	3.7	6	18.2	2	13.3
46 – 90	3	2.6	-	-	3	5.6	-	-	-	-
91 – 135	1	0.9	-	-	1	1.9	-	-	-	-
136 – 180	5	4.4	-	-	3	5.6	2	6.1	-	-
Unknown	39	34.2	6	50.0	11	20.4	19	57.6	3	20.0
Total	114	100	12	100	54	100	33	100	15	100

Table 2.5 Neck injury location in the transverse plane (XY) in relation with head angle

Head impact angle XY [°]	Total		Injuries of the neck							
			Cervical spine strain		Cervical spine fracture		Soft tissue injury		Other	
	n	%	n	%	n	%	n	%	n	%
0	17	14.9	2	16.7	6	11.1	5	15.2	4	26.7
1 – 45	16	14.0	-	-	8	14.8	7	21.2	1	6.7
46 – 90	7	6.1	1	8.3	5	9.3	-	-	1	6.7
91 – 135	-	-	-	-	-	-	-	-	-	-
136 – 180	12	10.5	1	8.3	6	11.1	1	3.0	4	26.7
(-179) – (-135)	3	2.6	-	-	3	5.6	-	-	-	-
(-134) – (-90)	1	0.9	1	8.3	-	-	-	-	-	-
(-89) – (-45)	4	3.5	1	8.3	3	5.6	-	-	-	-
(-44) – (-1)	15	13.2	-	-	12	22.2	1	3.0	2	13.3
Unknown	39	34.2	6	50.0	11	20.4	19	57.6	3	20.0
Total	114	100	12	100	54	100	33	100	15	100

2.4 Mechanical Responses and Tolerances of the Neck

Numerous human surrogates such as volunteer, cadaver, animal and dummy were used to test the mechanical performance of the human spine. The biomechanical response of the cervical spine has been studied by a number of static and dynamic experiments (both with and without head) with a variation in the load directions [Mertz and Patrick, 1976, 1971; Patrick and Chou, 1976; Schneider et al., 1975; Ewing et al., 1978b; and Nightingale et al., 1997].

Tolerance levels based on volunteer and cadaver tests, performed many years ago [Mertz and Patrick (1967, 1971)], are still reliable and referred to threshold values for different injury risk analyses. The flexion-extension loading corridors of Mertz et al (1973), combining the rotation of the head relative to the torso as a function of bending moment at the occipital condyles, were based on the loading and unloading corridors for sagittal flexion and extension moments established by Mertz & Patrick (1967, 1971).

Goldsmith and Ommaya (1984) conducted sled tests with volunteer and cadaver to account the dynamic neck loading. Figure 2.11 shows the flexion-extension corridors with the pain threshold found in the volunteer tests and the limits for serious injuries achieved in cadaver tests.

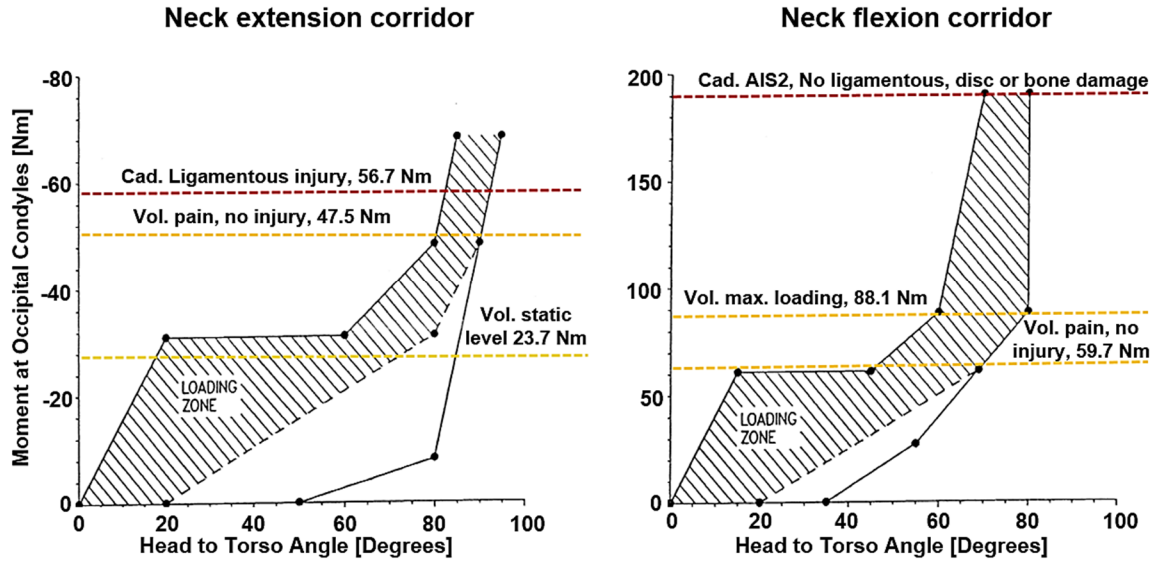


Figure 2.11. Head-neck response corridors for extension (left) and flexion (right) as reported by Goldsmith and Ommaya (1984)

In the advancement of the technologies, the recent studies assessed the motion pattern of each vertebra by X-ray based techniques like cineradiography using volunteer sled tests (e.g. Ono and Kaneoka 1997, 2001; Ono et al. 2006). Nightingale et al. (1997) and Camacho et al. (1997) studied the response of the cervical spine in compressive impacts for rigid and padded impact surfaces. They described the buckling mode of the cervical spine with short interval using high-speed camera.

The tolerance values for the various loading modes on the neck are not widely accepted (King, 2000). The geometry of the cervical spine is too complex and its inherent material properties are nonlinear, where large strains are produced at physiologic loading. Cervical injury mechanisms are sensitive to the initial position of the neck, the loading conditions and boundary conditions imposed by the contact surface [McElhaney and Myers, 1993]. Moreover, the dynamic response (e.g. head acceleration) of female and male volunteers were found to be different in rear-end sled tests due to geometric measures (Linder et al. 2008; Carlsson et al. 2011, 2012, Dehner et al. 2007). The lack of muscle activation during the tests affects the kinematics and injury outcome (e.g. Siegmund 2011). Also, the biomechanical response and tolerance values are age dependent (Yoganandan and Pintar 2000a; Yoganandan et al. 2002).

Table 2.6. Tolerance limits of the cervical spine [taken from Schmitt et al., 2014]

Mechanical response	Test objects	Threshold criterion	Threshold value	Reference
Extension	Volunteers	No-injury (static)	23.7 Nm	Goldsmith and Ommaya (1984)
		Pain	47.3 Nm	Mertz and Patrick (1971)
		No-injury	47.5 Nm	Goldsmith and Ommaya (1984)
	Cadavers	AIS2, ligamentous injury	56.7 Nm	Goldsmith and Ommaya (1984)
Flexion	Volunteers	Pain	59.4 Nm	Mertz and Patrick (1971)
			59.7 Nm	Goldsmith and Ommaya (1984)
		Maximum voluntary loading	87.8 Nm	Mertz and Patrick (1971)
			88.1 Nm	Goldsmith and Ommaya (1984)
	Cadavers	AIS2 (no fractures)	189 Nm	Mertz and Patrick (1971)
			190 Nm	Goldsmith and Ommaya (1984)
Compression	Cadavers	Bilateral facet dislocation	1.72 kN	Myers et al. (1991)
		Compression injuries	4.8-5.9 kN	Maiman et al. (1983)
Tension	Volunteers	No-injury (static)	1.1 kN	Mertz and Patrick (1971)
	Cadavers	Failure	3.1 kN	Shea et al. (1991)
Shear (antero-posterior)	Volunteers	No-injury	845 N	Mertz and Patrick (1971)
	Cadavers	Irreversible damage	2 kN	Goldsmith and Ommaya (1984)
	Functional unit	(Odontoid) fractures	1.5 kN	Doherty et al. (1993)
	Functional unit	Ligament rupture	824 N	Fielding et al. (1974)

The results reported by Mertz & Patrick (1967, 1971) using volunteer tests are the most widely used tolerance values in extension, where the only volunteer withstood a flexion moment of 59.4 Nm with neck pain and had a maximum loading at 87.8 Nm. In the same tests, the static limit for the volunteer was 23.7 Nm and dynamic tolerable value at the base of the skull was 16.7 Nm, which define the tolerance values in flexion. The proposed non-injurious limit is 47.4 Nm and the ligamentous injury limit is 57 Nm. Scaling method was applied to set these limits, which are based on ligamentous damage to a small cadaver at 33.4 Nm. Tolerance data of the neck in lateral bending has not been established acceptably. The volunteer test results reported by Ewing et al (1977) and Wismans and Spenny (1983) show that there was no obvious injury in sled tests performed at 5 to 10 g, which resulted in a lateral bending moment of 20 to 60 Nm and lateral rotation of 52 deg.

A summary of tolerance values of the cervical spine found in the literatures is given in Table 2.6. However, the variations in the values are obvious due to the differences in experimental techniques, loading conditions, variability of the anatomical structures (e.g. geometry or properties such as bone density) and presence of degeneration [Schmitt et al., 2014].

2.5 Neck Injury Metrics

Several neck injury metrics as human neck injury criteria have been proposed by the researchers usually for automotive crash tests using anthropomorphic test devices (ATDs). These metrics provide information on the neck injury risk considering the measurable parameters such as force, moment, acceleration and displacements. The neck injury criteria not only describe injury risk, but sometimes also help to understand the associated issues like seat design or the injury mechanism (Schmitt et al., 2014). However, these criteria have limitations in describing the injury risk for motorcycle crashes due to the restrictions of the defined conditions. Cervical injuries among motorcyclists are usually due to direct impacts on the head, while the criteria proposed for the automotive crashes are due to the inertial loading. Thus, it is important to properly design a neck injury criterion for the assessment of motorcycle accidents. This section provides some available neck injury criteria proposed for the assessment of cervical spine injury risks.

2.5.1 Neck Injury Criterion, NIC

The NIC, introduced by Bostrom et al. (1996), was proposed for loading conditions observed in low speed rear impact and takes the form:

$$NIC = 0.2 a_{rel}(t) + v_{rel}(t)^2 \quad (\text{Eq. 2.1})$$

Where, $a_{rel}(t)$ and $v_{rel}(t)$ are relative acceleration and velocity respect to first thoracic vertebra (T1) respectively. Eriksson and Kullgren (2006) have correlated a NIC of 15 m^2/s^2 with an 18% probability of minor (AIS1) neck injury. However, the head needs to be parallel to T1 to avoid considerable error in injury prediction by this criterion.

NIC_{protraction}, a modification of the NIC for low-speed frontal impact, was introduced by Boström et al. (2000), where NIC of 25 m^2/s^2 with 50% probability of long-term AIS1 neck injuries was proposed. The equations for determining NIC_{protraction} are as follows:

$$NIC_{generic}(t) = 0.2 a_{rel}(t) + |v_{rel}(t)| \quad (Eq. 2.2)$$

$$NIC_{protraction}(t) = |Min(NIC_{generic}(t))| \quad (Eq. 2.3)$$

2.5.2 Neck Protection Criterion, N_{km}

Schmitt et al. (2002) introduced N_{km} criterion with respect to possible injury mechanisms in rear-end collisions. It combines linearly the anterior-posterior shear force (F_x) and sagittal plane bending moment (M_y) as following:

$$N_{km} = \frac{F_x(t)}{F_{int}} + \frac{M_y(t)}{M_{int}} \quad (Eq. 2.4)$$

Where, critical intercept values F_{int} equals to 845 N for both positive and negative shear and M_{int} equals to 47.5 Nm and 88.1 Nm for flexion and extension respectively. The intercepts were chosen to correlate with the human tolerance levels, where a critical N_{km} value 1.0 was proposed, so that, either a moment or a shear force exceeding the intercept value produces a risk of AIS1 neck injuries.

2.5.3 Lower Neck Load Index, LNL

Heitplatz et al. (2003) proposed the LNL index for low speed rear-end collisions, which predicts the lower neck soft tissue injury. LNL combines lower neck tensile and shear forces ($F_i(t)$) and antero-posterior and lateral bending moments ($M_i(t)$) as in the following equation:

$$LNL = \frac{\sqrt{M_x^2 + M_y^2}}{C_{moment}} + \frac{\sqrt{F_x^2 + F_y^2}}{C_{shear}} + \frac{F_z}{C_{tension}} \quad (Eq. 2.5)$$

where, the moment, shear and tension intercept values are proposed to be 15 Nm, 250 N, and 900 N respectively for the Rear Impact Dummy (RID). This criterion has shortcomings in suggesting an injury threshold level and no correlation to real world injury outcome (Bortenschlager et al., 2003).

2.5.4 Beam Criterion (BC)

Bass et al. (2006) proposed this criterion for the lower cervical spine in frontal impacts that exclude head-first impact. A linear combination of the axial force (Fz) and antero-posterior moment (My) measured at the center of the C7-T1 intervertebral disc is used to form the following equation for BC:

$$BC = \frac{Fz}{Fzc} + \frac{My}{Myc} \quad (\text{Eq. 2.6})$$

where, the intercept values Fzc equals 5,660 N (in tension) and 5,430 N (in compression), and Myc equals 141 Nm in flexion. A BC of 1.0 corresponds to a 50% risk of AIS1+ neck injury.

2.5.5 Neck Injury Index, NII

The NII was developed for the motorcycle ATD (MATD) upper neck and is based on the generalized stress ratio for the estimation of strength of materials [ISO 13232-5:2005]. The equation defining NII is as follows:

$$NII = \max \left(\left(\left(\frac{FC}{FCC} + \frac{FT}{FTC} + \left(\left(\frac{Mx}{Mxc} \right)^2 + \left(\frac{MExt}{Mxc} + \frac{MFlex}{MFC} \right)^2 \right)^{1/2} \right)^2 + \left(\frac{Mz}{Mzc} \right)^2 \right)^{1/2}, 3.1 \left(\frac{FC}{FCC} + \frac{FT}{FTC} \right) \right) \quad (\text{Eq. 2.7})$$

where, FC and FT are the measured compressive and tensile forces and MFlex, MExt, Mx, and Mz are the measured flexion, extension, lateral bending and torsion moments respectively. The respective force and moment intercept values are -6530 N, 3340 N, 204.2 Nm, -58 Nm, 62.66 Nm and 47.1 Nm, which were derived by computer simulations. The constant 3.1 in the second term of (eq. 2.7) was calculated based on the 3% probability of an AIS2+ injury when subjected to a 4.17 kN tensile force (Wilber, 1998). The constant was reduced from 3.1 to 1.77 for the assessment of PMHS (post-mortem human subject) injury risk assuming a 50% risk of AIS2+ injury to the PMHS when subjected to a tensile load of 3510 N (Bass et al. 2006).

NII injury assessment is conducted with minimum values of NII for each AIS level. The probability function for NII assessment is based on the following equation:

$$P_{AIS} = 1 - \exp \left(- \left(\frac{NII - a}{b} \right)^{3.5} \right) \quad (\text{Eq. 2.8})$$

where, *a* and *b* are the normalized coefficients of probability function. Table 2.8 shows the minimum values for NII injury assessment and the coefficients for the Eq. 2.8. The coefficient *a* is the same for AIS=4 and AIS=5 injuries since there AIS=4 injuries

were not available in the dataset. The coefficient b has been assumed to be same for each severity level based on 95% confidence interval for μ in ISO 13232-5 Table J.8 [ISO 13232-5:2005]. The probability of injury is assumed to be zero or a low risk of AIS = 1 if NII values less than 1.06.

Table 2.7 Minimum values for NII injury assessment and coefficients for the Eq. 2.8

Severity Level	Min NII	a	b
AIS \geq 1	1.06	1.06 (0.39, 3.02)*	4.38
AIS \geq 2	1.86	1.86 (0.52, 3.48)	4.38
AIS \geq 3	2.29	2.29 (0.76, 3.90)	4.38
AIS \geq 4	4.73	4.73 (2.68, -)	4.38
AIS \geq 5	4.73	4.73 (2.68, -)	4.38
AIS \geq 6	6.13	6.13 (3.65, -)	4.3

*95% confidence interval, based on 95% confidence interval for μ in ISO 13232-5 Table J.8 and assuming $b=4.38$

2.5.6 Neck Injury Criterion N_{ij}

The concept of linearly combining normalized axial load and sagittal plane bending moment in frontal impacts was first proposed by Prasad and Daniel (1984) using piglets as child surrogates. The concept was expanded to include direction of the axial load and bending moment as compression/tension and extension/flexion respectively, which has been adopted by US National Highway Traffic Safety Administration (NHTSA) for neck injury assessment in frontal impacts (Klinich et al., 1996; Kleinberger et al., 1998). N_{ij} forms the following equation (Eq. 2.9), where the intercept values F_{int} and M_{int} vary for compression/tension (F_C/F_T) and flexion/extension (M_F/M_E) respectively.

$$N_{ij} = \frac{F_z(t)}{F_{int}} + \frac{M_y(t)}{M_{int}} \quad (\text{Eq. 2.9})$$

where, F_z is neck axial force and M_y is the neck bending moment in sagittal plane.

The critical values of F_{int} and M_{int} of the upper neck N_{ij} intercepts were adopted by NHTSA and inserted into Federal Motor Vehicle Safety Standard 208 (FMVSS 208) (Eppinger et al., 2000), which have been initially established for three-year-old Hybrid III dummy and validated against experimental tests. Scaling method was applied to extract the critical values for other dummy sizes. A peak compressive force of 4000 N was also adjusted to the FMVSS 208 standard considering the earlier work done by Mertz et al. (1978). Mertz et al. (2003) proposed an in-position N_{ij} of 1.0 in tension and extension for

5% AIS2+ injury risk. Table 2.7 indicates the critical values of axial force and bending moment for all ATDs currently included in FMVSS 208 (Toomey, 2013). The original NHTSA Nij kite and in-position hexagon corridor proposed by American Automobile Manufacturers Association (AAMA) for FMVSS 208 standard are shown in Fig. 2.12 (Eppinger et al. 2000).

Table 2.8 Critical values of Nij for FMVSS 208 and peak axial forces for various In-Position (IP) or Out-of-Position (OOP) ATDs (adapted from Toomey, 2013)

Dummy	Nij Critical Value				Peak Axial Force	
	F _T (N)	F _C (N)	M _F (Nm)	M _E (Nm)	F _T (N)	F _C (N)
HIII 50 th Male - IP	6806	6160	310	135	4170	4000
HIII 5 th Female - IP	4287	3880	155	67	2620	2520
HIII 5 th Female - OOP	3880	3880	155	61	2070	2520
HIII 6yo Child - OOP	2800	2800	93	37	1490	1820
HIII 3yo Child - OOP	2120	2120	68	27	1130	1380
Crabi 12mo Child - OOP	1460	1460	43	17	780	960

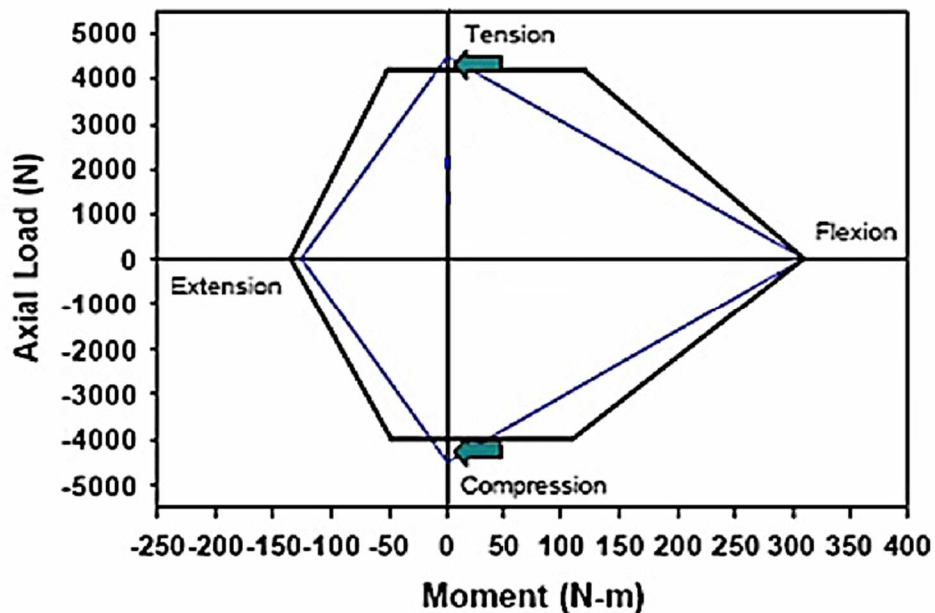


Figure 2.12 Nij kite corridor (blue boundary) and in-position hexagon corridor (black boundary) adopted as the FMVSS 208 final rule [reproduced from Eppinger et al. 2000]

The Economic Commission for Europe (ECE) Regulation No.94 (ECE R94) specifies maximum spinal loads for frontal impact concerning the approval of vehicles with regard

to the protection of occupants. The maximum limit for extension bending moment is 57 Nm. The tolerances of the shear forces and the axial tension force are time dependent (according to Figure 2.13). The European New Car Assessment Program (Euro NCAP) uses the same ECE R94 neck criteria for the frontal impact crash assessment along with NIC and Nkm as part of the whiplash injury criteria, which is conducted to rate the safety of the cars (Toomey, 2013).

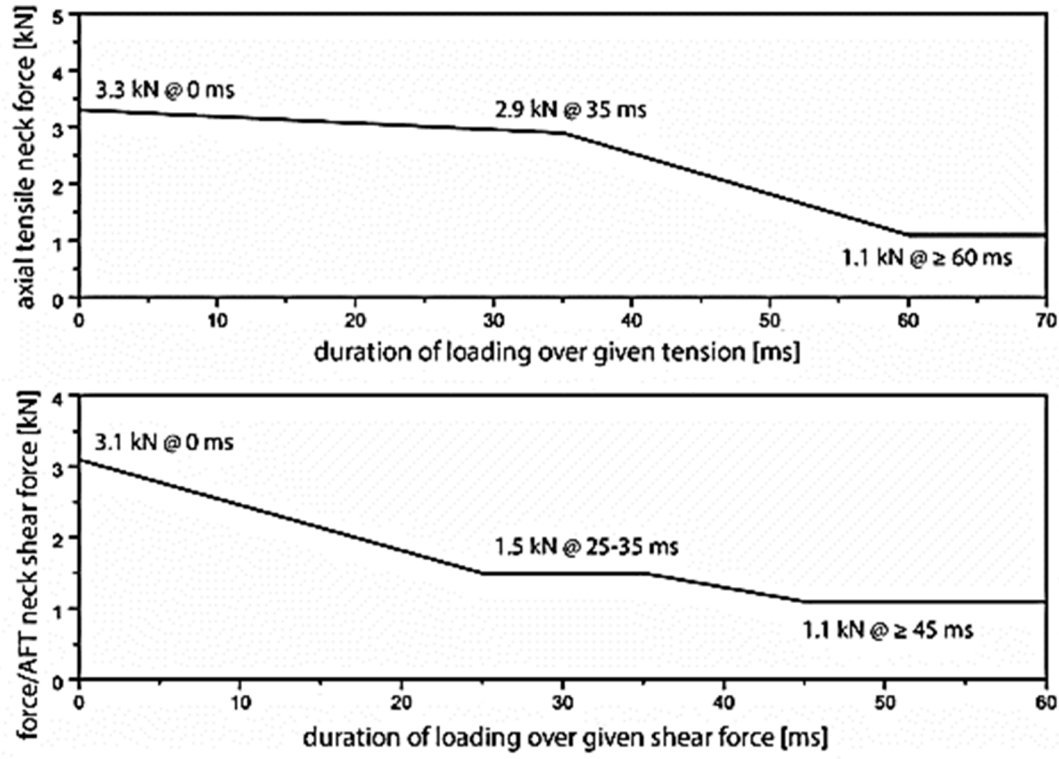


Figure 2.13 Time dependent neck tensile and shear force tolerances for frontal impact protection according to ECE R94 [taken from Schmitt et al., 2014]

2.5.7 Other Criteria

Some additional criteria have been also proposed such as:

- Panjabi et al. (1999) proposed the intervertebral neck injury criterion (IV-NIC), which assumes that the inter-vertebral rotation causes neck pain in a rear-end collision when the physiological intervertebral motion exceeds its limit.
- Viano and Davidsson (2002) proposed the neck displacement criterion (NDC) to assess the risk of soft tissue neck injury.
- Kuppa et al. (2005) proposed a criterion for soft tissue neck injury considering the head-to-torso rotation.
- Munoz et al. (2005) proposed a whiplash injury criterion (WIC) combining the upper and lower neck extension/flexion moment in the sagittal plane.

Chapter 3

Personal Protective Equipment (PPE)

Motorcycle PPE: protection from injury or just for fashion? The question became the subject of scientific discussion to reduce the injury risk during a crash at least since 1976 [de Rome et al., 2011]. A number of researchers have concluded that effective injury prevention is most likely to come from protection systems worn by the rider rather than attached to the motorcycle [Craig, 1983; Nordentoft, 1984; Ouellet, 1987; Spornier 1990].

Researchers have demonstrated the importance of PPE in reducing the frequency and extent of fatality, fracture of the bones, abrasions and lacerations of the skin and soft tissue in motorcycle crashes [Craig, 1983; Nordentoft, 1984; and 34] following the report of Feldkamp and Junghanns (1976) on protective clothing. Figure 3.1 demonstrates the use of PPEs for different parts of the body in contrast with injury risk reduction.

The limitations for injury prevention and reduction are summed up in the report on motorcycle safety by the European Experimental Vehicles Committee in 1993 [EEVC, 1993]. According to the report, the PPEs cannot significantly mitigate [de Rome et al., 2003]:

1. Severe bending, crushing and torsion forces to the lower limbs;
2. Massive penetrating injuries to any part of the body;
3. High energy impacts on the chest or abdomen causing injuries through shock waves, and severe bending forces such as when the torso strikes an upright post.

The design and development of the active and passive motorcycle PPEs are taken into consideration following the general features [Nasim et al., 2015]:

- Shock absorption
- Impact distribution
- Impact abrasion resistance
- Impact cut resistance
- Comfort
- Conspicuity
- Quality and style
- Commitment to safety
- Improved technology
- Affordable protection against climate condition (temperature, wind and rain)



Figure 3.1 PPEs used to reduce different injury risks [adapted www.arrivealive.com]

In this chapter, the key features of different types of PPE have been summarized. The contents provided in this chapter have been briefly adapted from Nasim et al. (2015).

3.1 Protective clothing

Protective clothing includes four categories: one-piece suit, two-piece suit, pants and jackets. The research path for protective clothing has two directions: selection of the optimal materials to protect the riders' body during a crash; and the options for absorbing and/or distributing the impact energy [Haworth, 2006]. Figure 3.2 shows a two-piece leather suits with protective features designed by Dainese [www.dainese.com].



Figure 3.2 Designing of a two-piece leather suits with protective features [www.dainese.com]

The key elements to be considered in defining the injury protection functions of motorcycle clothing are:

- Strength of materials in terms of abrasion, cut, tear or burst resistance. The preference has been given to the leather mainly because of its high abrasion resistance. Textile garments may be constructed in multiple layers of fabrics in order to meet the requirements of the standards.

- Shear forces on body tissue during an impact or while sliding over the ground should be reduced. The material and construction of the inner lining should meet the requirement.
- Burst strength and integrity of seams and fastenings should be ensured so that they do not split during an impact.
- The design in terms of fits and ergonomics in order to prevent safety hazards.

The key elements to be considered for weather factor by motorcycle clothing are:

- Provision for insulation from cold temperatures and ventilation in heat.
- The openings (neck, wrists and waist), coverage of zippers, seams and other fastening points should be designed to prevent wind entry and heat loss.
- Waterproof breathable fabrics seams, pockets, cuffs and neck openings to protect the rider from rain without sweating.

3.2 Gloves

ACEM reported that about 57% of motorcyclists sustain an impact to their hands or wrists during crashes [ACEM, 2004]. Designing of gloves depends on the injury protection functions as well as comfort and style. Figure 3.3 shows a motorcycle glove with protective features including knuckle protection designed by Dainese [www.dainese.com].



Figure 3.3 Designing of motorcycle gloves with knuckle protection [www.dainese.com]

The key elements to be considered in defining the injury protection functions of motorcycle gloves include:

- Robust to provide protection from injuries.
- Strength of materials in terms of abrasion, cut, tear or burst resistance specially the palm and wrists.
- Ease of movement to control the motorcycle without any hazards.
- Coverage of the full hand and wrist
- Fastenings that keep the gloves restrained.
- Impact protection over the knuckle.
- No hard seams or other sharp edges such as studs, staples or buckles penetrating the protective layer of the glove.
- Webbing between the little finger and the next finger to prevent twisting injuries during an impact with a hard surface.
- Comfortable design in terms of fits and ergonomics in order to prevent safety hazards.
- Consideration of the weather factors such as insulation to hold or lose heat, breathable to prevent sweating.

3.3 Boots

According to the report of ACEM (2004), about 56% of motorcyclists sustain an impact to their feet during crashes. The protective design of a motorcycle boot has been exemplified in Figure 3.4 [www.dainese.com].



Figure 3.4 Design features of motorcycle boot [www.dainese.com]

The key elements to be considered in defining the injury protection functions of motorcycle boots include:

- Covering of ankles and shins.
- Impact attenuation for the shins and ankles.
- Fastenings to keep the boots restrained.
- The abrasion and cut resistance of the upper material.
- The impact resistance of the sole.
- The strength of the bond attaching the sole to the adjacent upper part.
- The size and thickness of the sole and inner gap.
- Rigid soles to provide some protection from being crushed in a sliding impact.
- Waterproofing materials for the boots.
- Comfortable design in terms of fits and ergonomics in order to prevent safety hazards.
- Consideration of the weather factors such as insulation to hold or lose heat, breathable to prevent sweating.

3.4 Impact Protectors

The impact protectors are the passive safety equipment used as shields over the key joints of back, chest, elbow, shoulder, hip and knee [Haworth et al., 2006]. Airbag also works as an impact protector for the covered areas when it is inflated. Figure 3.5 demonstrates the impact protective feature of shoulder and chest protectors [www.dainese.com].

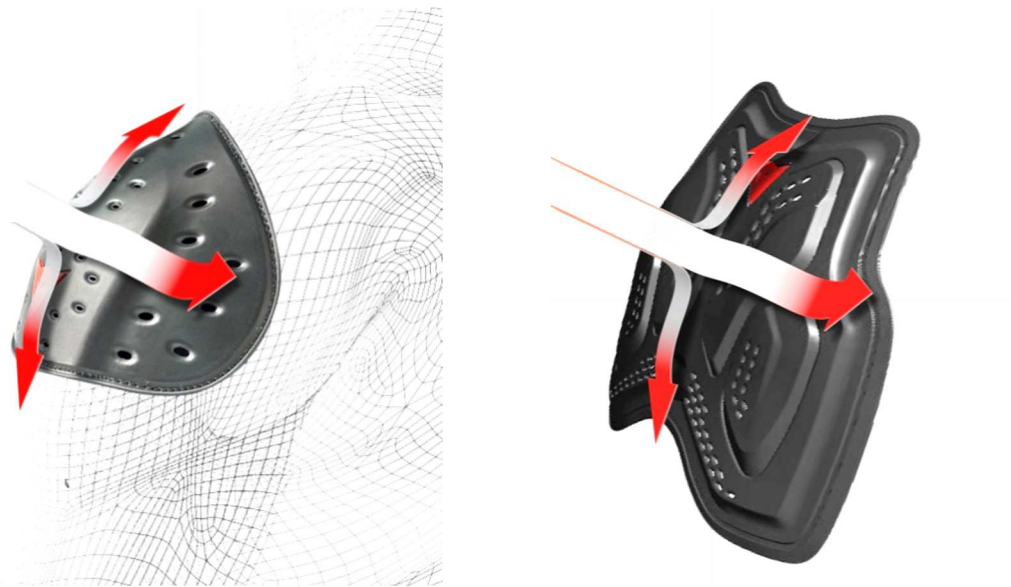


Figure 3.5 Impact protection feature of impact protectors – shoulder protector (left) and chest protector (right) [www.dainese.com]

The key features are:

- Impact attenuation of the impact energy during crashes.
- Fitted and held in place so that they will not move during a crash
- Energy absorption and distribution of an impact to divert pressure and bending stress on the skeleton.
- Materials selection considering the weight and comfortable design in terms of fits and ergonomics in order to prevent safety hazards.

3.5 Helmets

Helmets act as the shields to protect the rider's head from the impact of a collision. The protective feature is not only important while designing a helmet, but also the comfort and ease of movement of the rider is significant. Figure 3.6 shows a schematic diagram of general design of a protective helmet.

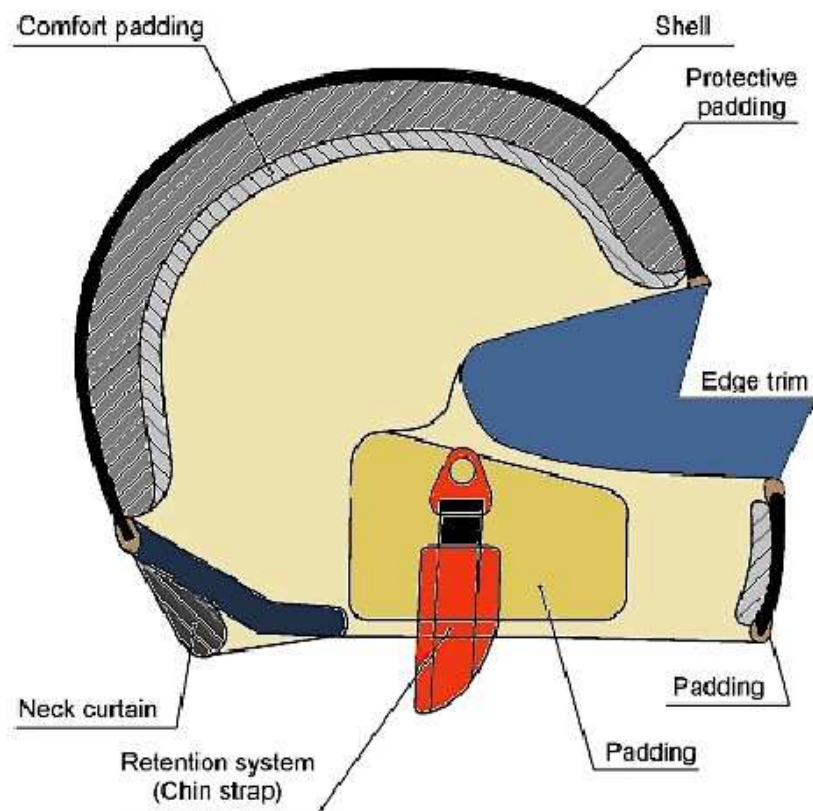


Figure 3.6 General design of protective motorcycle helmet

The key features defined are:

- Impact attenuation of the impact energy during crashes.
- The general shape of the shell as the hard part in order to be fitted.

- Protective padding to absorb impact energy.
- Comfort padding to provide rider's comfort.
- Retention system to restrict the movement during a crash.

Protective lower face-cover as detachable, movable or integral part of the helmet intending to protect the chin of the rider against impacts.

3.6 Neck Protection Devices

The development of motorcycle PPE and standards are in continuous process. Although many PPE are available in the market to protect different body parts during an accident, there is a limited number of PPE developed to protect the neck. The reasons behind that might be the lower frequency of neck injury and unavailability of the standards. Moreover, the effectiveness of this small quantity of neck protecting devices is questionable due to the lack of knowledge in the mechanism of neck injury. The advancement of neck protection devices can be divided into two categories: new products and enhancements of existing products. Figure 3.7 shows different types of neck protecting devices developed by gear manufacturers. Neck brace and the airbag systems can be considered as the most recent and widely known products among all the devices.



Figure 3.7 Different types of neck protecting devices

3.6.1 Neck brace

The neck brace was designed based on the principle that it will restrict the acceleration of head in a controlled manner and hence reduce the bending forces on the cervical spine limiting the head movement such as compression, hyper-flexion and hyper-extension. Such product made of titanium carbon fibre was first developed by BMW. Geisinger et al (2006) conducted simulations using crash dummies, which indicated the reduction of

neck axial forces and bending forces on the cervical spine. Figure 3.8 shows the concept of the neck brace developed by Dainese [www.dainese.com].

Nawrocki et al (2004) designed a similar product named ‘bolster collar’ to support the rider’s neck and head during a crash with focus to injury reduction of the brachial plexus.



Figure 3.8 The principle of Hybrid Neck Brace [www.dainese.com].

3.6.2 Airbag technology

Air bag is the most recent technology but can be the most effective in terms of impact protection. The development of airbag technology is very competitive among a number of companies. Dainese, the first company to introduce air bag in the market since 2011, declares to reduce 80% of the transmitted forces to the body comparing to a back protector (passive device) of level 2 with the current street version. Considering this data and the comfort provided from this kind of device (it only deploys just when needed), it can be considered that the “air” is the future of the neck protection.

There are two kinds of air bag triggering systems - mechanical triggering with physical connection with the motorbike and electronic triggering system. In the mechanical system, the rider must wear the jacket where a cable and small gas cylinder are attached. When the rider is thrown from the motorcycle, the cable is jerked from the motorcycle initiating the inflation process. Thus an “airbag” is provided to protect the areas covered by the device.

The technology started with the mechanical triggering system and currently the electronic triggering system is in a continuous development process to ensure the most effective activation time in real accident scenario. In general, the electronic triggering system consists of sensor to detect the first impact of the rider, algorithm for triggering and pneumatic component. Two kinds of airbag jackets with electronic triggering system exist: stand alone and connected with the motorcycle. The sensor, necessary to detect the accident, is within the jacket in the stand-alone type. In the version connected with motorcycle type, that sensor is installed on the motorcycle where the rider and the motorcycle could be connected by electric cables or a wireless connection. Figure 3.9 shows an example of the stand-alone type airbag jacket with electronic triggering system (racing version) developed by Dainese [www.dainese.com].



Figure 3.9 Mechanically triggered airbag system with physical connection to the motorcycle [www.dainese.com]

Multiple researchers are investigating the development of the airbag technology, which mainly focuses on the improvement of the activation time, the impact resistance performance of the airbag sack, pressurizing and depressurizing. The effect of activation time of the airbag deployment is crucial to ensure the function at the appropriate moment just before the first impact of the rider. The impact resistance performance of the airbag sack is also critical to ensure that the airbag chambers are able to support high pressure, to absorb the energy and are not punctured during a crash. Research on the sack material is also critical as it is important to reduce the weight and increase the breathability for the rider comfort. Moreover, the bouncing effect of the bag due to the volume and the inflation pressure must be avoided so that it does not create another impact hazard.

Chapter 4

Standards in PPE

Standards are set of guidelines to evaluate the finished products in terms of quality, effectiveness and innocuousness. No standards in PPE can claim to be completely protective, but they are designed to provide maximum protection to the users. The first standard for motorcycle PPE, the standard for the limb protector EN1621-1:1997, appeared in Europe in 1997 [www.pva-ppe.org.uk]. The contents provided in this chapter have been briefly adapted from Nasim et al. (2015).

The EU Standards are developed by certain standardization organizations. The organizations are formed by national expertise responsible for researching, proposing and forming the standards. The Organizations may form sub-committees for dealing with different PPEs.

The Standards for motorcyclists' protective clothing, gloves, boot and impact protectors have been developed by the European Committee for Standardization known as CEN [www.cen.eu], which consists of the National Standardization Bodies of 33 European countries. The CEN Technical Board (BT) conducts the standardization activities of CEN and is fully responsible for the execution of CEN's work programme. Standards are prepared by Technical Committees (TCs). Each TC has its own field of operation within which a work programme of identified standards is developed and executed (e.g. TC162 works for protective clothing including hand and arm protection and lifejackets). A Subcommittee, named as Working Group (WG) can be established within a TC in case of large programs of work (e.g. WG9 in TC162 works for protective clothing but only for motorcyclists'). Some small Project Groups (PGs) may be created within a WG by its members in order to define a particular interest for that WG.

Although CEN/TC158 committee deals with head protection, there is no CEN standard in case of motorcycle helmets. Different countries have adopted different standards like DOT for USA, ECE 22.05 for Europe, NBR 7471 for Brazil, AS 1698-2006 for Australia etc. The ECE 22.05, also known as EN 22/05, is actually the most commonly used motorcycle helmet safety standard around the world. The standard, which is theoretically known as "Regulation no 22", has been developed by the Economic Community of Europe (ECE). Some of the motorcycle helmet standards have been developed by private or independent organizations like Snell in the USA, ACU Gold in the UK and BSI (British Standards institution) in the UK.

4.1 Standards for protective clothing, gloves and boots

The clothing standard developed in 2002 as EN13595:2002 was based on the study of Dr. Roderick I. Woods [Woods et al., 1996]. The zone positions according to his proposal are shown on a suit laid out flat in Figure 4.1.

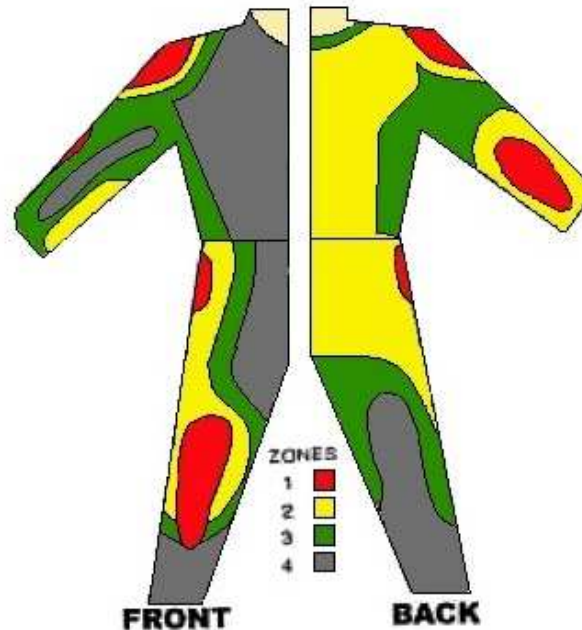


Figure 4.1 The injury risk zones on a suit [Woods et al., 1996]

The risk category zones are defined according to the likelihood that the area of the suit included in the zone will be subjected to mechanical stress, in the event of an accident. There are four zones, as follows:

- Zone 1 – the areas of motorcyclist’s protective garments that have a high risk of damage e.g. impact, abrasion, and tearing.
- Zone 2 – the areas of motorcyclist’s protective garments have a moderate risk of damage e.g. abrasion and tearing.
- Zone 3 – the areas of motorcyclist’s protective garments have a low risk of damage e.g. tearing.
- Zone 4 – the areas of motorcyclist’s protective garments have the lower risk of damage comparing to the other areas.

The example presented in Figure 4.1 is only for protective clothing. Different PPEs have particular test zones according to the Standards. These test zones are defined based on the protection requirements to the relative body parts, the injury type and risks associated with it.

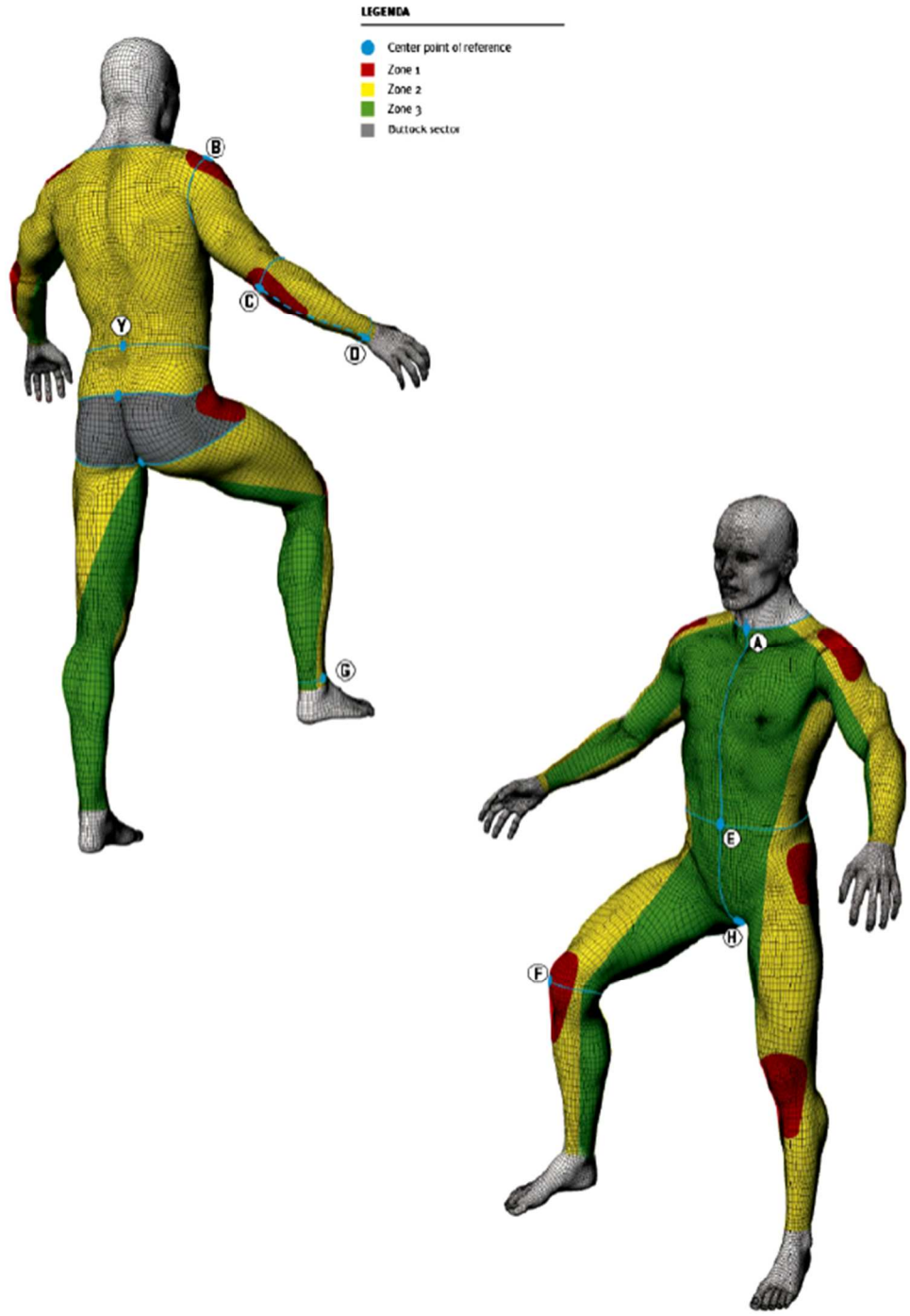


Figure 4.2 3D explanation of the zoning principle of motorcycle clothing

Figure 4.2 shows the modification of Dr. Woods' [Woods et al., 1996] research, which was drawn by Dainese and then proposed by CEN/TC162/WG9 committee in 2012. The figure specifies a method on a 3D human model indicating the boundaries between different injury risk category zones on a motorcycle garment. This method is based on the zoning of the categories of risks, as follows:

- Zones 1 are at high risk of impact and abrasion.
- Zones 2 are at moderate risk of abrasion.
- Zone 3 areas are at low risk of abrasion damage.

This proposal was accepted as the Technical Disciplinary for European Standard (2012) [Dolomiticert, 2012] by the gear manufacturers and test houses for zoning the protective clothing with the approval from CEN. Recently, this zoning principle has been revised and modified slightly in the new Standard prEN 17092.

The Standards EN 13594:2015 for motorcycle gloves [UNI, 2015] and EN 13634:2010 for motorcycle footwear [UNI, 2010] are widely used in many countries of the world. The Standards for gloves emphasize more on impact abrasion and cut resistance tests. Additionally, it has a set of procedures to test the gloves designed for knuckle protection. Likewise, the standards for motorcycle boots also emphasize on impact abrasion and cut resistance tests. Moreover, it includes impact absorption tests for ankle and shin. The summary of the standards for protective clothing, gloves and boots are given in Table 4.1.

Table 4.1 European Standards for motorcycle protective clothing including gloves and boots

Standard number	Standard name	PPE type	Body region	Type of injury
EN 13594	Protective gloves for motorcycle riders - Requirements and test methods	Gloves	Hands and wrists	Abrasions, cuts, impacts
EN 13595 PrEN 17092 (new)	Protective clothing for professional motorcycle riders – Jackets, trousers and one-piece or divided suits – General Requirements	Clothing	Torso, arms and legs	Abrasions, cuts and contusions, bruising
EN 13634	Protective footwear for motorcycle riders - Requirements and test methods	Boots	Feet, ankles, lower legs	Abrasion, cuts, impacts

4.2 Standards for Impact protectors

EN 1621-1:2012 for limb protectors [UNI, 2012], EN 1621-2:2013 for back protectors [UNI, 2013], prEN 1621-3:2010 for chest protectors [CEN, 2010], FprEN 1621-4:2012 for inflatable protectors with mechanical triggering [CEN, 2012] are the state of the art Standards for motorcyclists’ impact protectors. All these Standards mainly aim to protect the associated body regions from an impact. The Standards set different test protocols

with different test zones and protection levels for each individual Standard. Standards for inflatable protectors (e.g. airbag) have some additional tests such as inflation time, activation time etc. The Standards for motorcycle impact protectors are summarized in Table 4.2.

Table 4.2 European Standards for motorcycle impact protectors

Standard number	Standard name	PPE type	Body region	Type of injury
EN 1621-1	Motorcyclists' protective clothing against mechanical impact - Part 1: Motorcyclists' limb joint impact protectors - Requirements and test methods	Limb protectors	Shoulders, elbows, hips and knees	Bruising, contusions and some minor fractures
EN 1621-2	Motorcyclists' protective clothing against mechanical impact - Part 2: Motorcyclists' back protectors - Requirements and test methods	Back protectors	Back	Bruises and strains. Neurological spinal injuries excluded
prEN 1621-3	Motorcyclists' protective clothing against mechanical impact - Part 3: Motorcyclists' chest protectors - Requirements and test methods	Chest protectors	Chest	Fracture of the ribs and compression / damage of lungs
prEN 1621-4	Motorcyclists' protective clothing against mechanical impact - Part 4: Motorcyclists' inflatable protectors - Requirements and test methods	Inflatable body protectors	According to area covered	Injury due to impact and compression

4.3 Standards for Helmets

The ECE 22.05 standard [ECE, 2002] is used in over 50 European countries. Helmets certified to the ECE 22.05 standard are approved for competition events by AMA (American Motorcyclist Association), CCS (Championship Cup Series), FIM (Fédération Internationale de Motocyclisme), Formula-USA and WERA (WERA Motorcycle Roadracing) and are chosen by nearly every professional motorcycle racers competing in

world championship road racing, motocross and off road events, including the ultimate sport of Moto GP. The summary of the ECE 22.05 Standard is presented in Table 4.3.

Table 4.3 European Standard for motorcycle helmet

Standard number	Standard name	PPE type	Body region	Type of injury
ECE 22.05	Uniform provisions concerning the approval of protective helmets and their visors for drivers and passengers of motor cycles and mopeds	Helmets	Head	Skull fracture, intracranial hemorrhage, brain damage, laceration.

Table 4.4 World Motorcycle Helmet Safety Standards

Country	Standards
USA	FMVSS 218 or SNELL M2015
Europe	ECE 22.05
Brazil	NBR 7471
Taiwan	CNS
Australia	AS 1698-2006
Japan	SG or JIS
New Zealand	NZ 5430
Korea	KS G 7001
Malaysia	SIRIM
Thailand	TIS
India	IS 4151
Singapore	PSB
Canada	CSA CAN3-D230-M85

Chapter 5

Biomechanical Models

Human surrogates in biomechanics studies include Dummy (ATD: Anthropomorphic Test Device), Human Volunteers, Human Cadavers (PMHS: Post-Mortem Human Subjects), Animal Models and Computational Models [Crandell et al., 2011]. Biomechanical models are the surrogates of the human body without the actual biological tissues, which represent the kinetics and kinematics of a real human. These models allow us to predict the human behaviour in domains, where the data are unavailable and limited to extract. The models are developed in such a way that those are optimally fitted to experimental data and can be used to analyse the human mechanics for unmeasured conditions. Moreover, such models offer some promising benefits including the prediction of injury mechanisms and injury risks [Wismans et al., 2005].

The biomechanical models can be categorized into two types: physical and computational models. Physical models are used to understand the global response and computational models are used both for global and tissue level responses. The accuracy of the responses for both types of models depends on the biofidelity, which is the accuracy of a model to reproduce the mechanical behaviour of the associated human body parts.

In this chapter, the development of the biomechanical models has been discussed briefly. Owing to the fact that this research aims to develop neck protection, special focus has been given to the state of the art of neck models.

5.1 Physical Models

Crash analyses mainly based on injury criteria are performed using physical models or in other words Anthropomorphic Test Devices (ATDs). The main characteristics needed to develop ATDs are anthropometry and biofidelity like a human being, durability, repeatability and reproducibility of the test results. These ATDs can represent the whole human body or some specific parts of the body.

5.1.1 Dummies

Dummies are the more commonly referred form of ATDs. Currently, the crash test facilities use the automotive crash dummies. Although designing a dummy greatly depends on the crash environments and restraint applications such as automotive, motorcycle or aerospace applications, there is no specific standard dummy developed for motorcycle or airplane crash tests. The dummies differ significantly from the real human body due to the variation in size and gender reflecting on the wide range of occupant population, different material properties of the body parts and difference in joint systems,

behavior due to the absence of active muscles and different loading conditions (Figure 5.1).



Figure 5.1 Different types of crash dummies: (from left to right) Hybrid III 50th Male Pedestrian, Hybrid III 5th Female Pedestrian, BioRID II 50th Male Rear Impact, THOR 50th Male Frontal Impact, SID IIs 5th Female Side Impact (adapted from www.humanetics.com)

In biomechanics studies, the recent dummies are not simply anthropometric manikins like those are used in the fashion houses, but, rather, complex engineering tools made of metal, foams and polymer composites [Crandall et al., 2011]. Hence, the kinematics of the dummies can be improved and the essential levels of biofidelity can be achieved. Moreover, the sensors are instrumented to the appropriate parts of the dummies to record the parameters such as accelerations, forces, and displacements during an impact, but, before that, the validation of the results for certain impact conditions is important.

Modern dummies are specific to loading conditions. They are designed for particular modes of impact: frontal, rear and side impacts. An omnidirectional dummy does not exist due to the complexity of reproducing the humanlike behavior under multiple loading conditions. Perception of dummy responses are dubious for combined crash modes e.g. oblique loading or different mode than the actual designed scenario e.g. rollover [Crandall et al., 2011].

5.1.2 Neck surrogates

The automotive crash-dummies have been developed and validated against the human body (both cadavers and volunteers) due to inertial loadings mainly in particular direction. But the accident scenarios are different for motorcycle crashes due to the difference in restraint systems, where the injuries normally occur due to direct impact

between the body part(s) and object(s). However, neck is one of the body parts that is mostly injured by indirect impacts [ACEM, 2004; MOSAFIM, 2013].

The most common neck ATD used for various impact purposes is of the Hybrid III 50th percentile male dummy. Though this model was designed and is acceptable for automotive frontal and rear-end crashes [Foster et al., 1977], it has immense limitations for other impact conditions, especially for the head-first impacts. The neck of the dummy model is stiffer in axial compression than that of real human [Nelson and Cripton., 2010]. Considering the requirement of biofidelity for the analysis of the head-first or direct impacts, a few modified neck designs have been developed as in Figure 5.2 [Nelson and Cripton, 2010; Withnall et al., 2003]. The modifications were made mainly considering the factors of flexion-extension range of motion and bending stiffness.

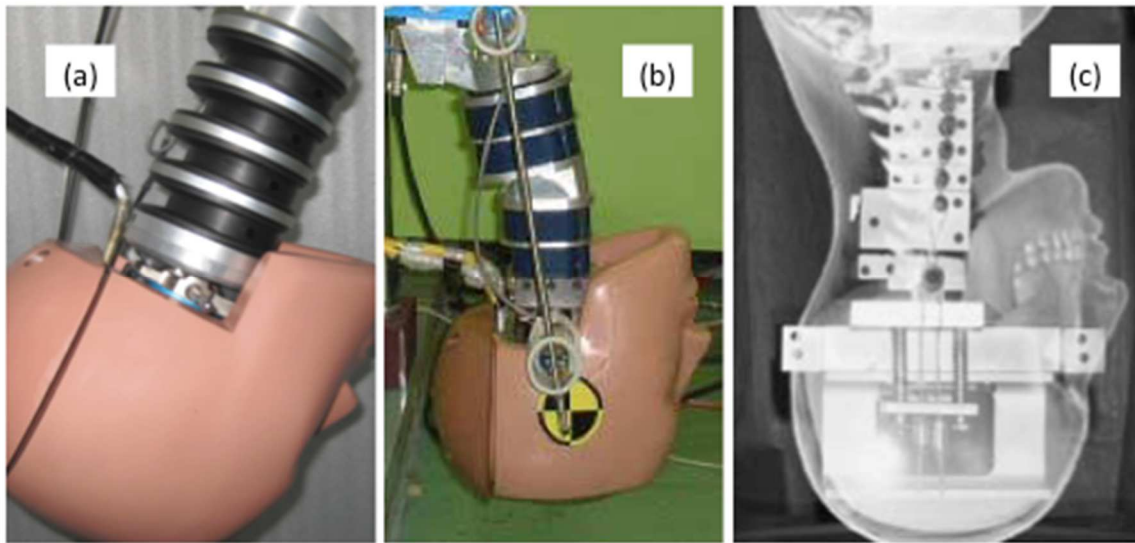


Figure 5.2 The neck ATDs: (a) Hybrid III neck, (b) and (c) modified necks to improve the biofidelity in head-first impacts (reproduced from (a) www.jasti.com, (b) Bhosale, 2008 and (c) Nelson and Cripton, 2010)

5.2 Computational Models

Although the exact humanlike physiological response by any human surrogates is not possible, the use of numerical tools is of great interest to the biomechanics community due to the limitations in the use of physical models and underlying advantages of the computational models. Human volunteer studies can provide only sub-injurious level [Panzer, 2006] and conventional experimental approaches by PMHSs or ATDs are often too complex and expensive to deal with. Moreover, the numerical models have advantages of predicting internal forces and deformations in the biological tissues [Panjabi et al., 1998].

Computational or mathematical models are the analytical representation of a physical phenomenon or event taking into account the inertial effects for all movable parts, where a numerical method is applied to solve equations of motions [Wismans et al., 2005]. Based on the complexity of the mathematical formulations used for these models, computation models can be subdivided into three main groups [Yang et al., 2006]: lumped mass models, multi-body models and finite element models. All models are based on a set of assumptions and have intrinsic limitations on model validation.

5.2.1 Lumped mass (LM) models

Lumped mass models, are usually one or two dimensional, consisting of concentrated masses connected by mass-less elements like springs and dampers. The main advantage of the LM model is its simplicity to develop, but, their use is limited to specific impact conditions that do not involve a large number of contacts or loading direction due to the simplicity [Crandall, 2011]. Two examples of LM human body modelling are shown in Figure 5.3.

Figure 5.3(a) illustrates Lobdell's one-dimensional LM model of the human thorax [Lobdell et al., 1973]. The model consists of rigid bodies with masses m_1 , m_2 and m_3 representing the impactor mass, the sternal effective mass and the vertebral effective mass respectively. These masses are connected by springs and dampers, where, spring k_{12} represents the skin and flesh between impactor and sternum, and the internal spring and dampers represent the connection between sternum and thoracic spine.

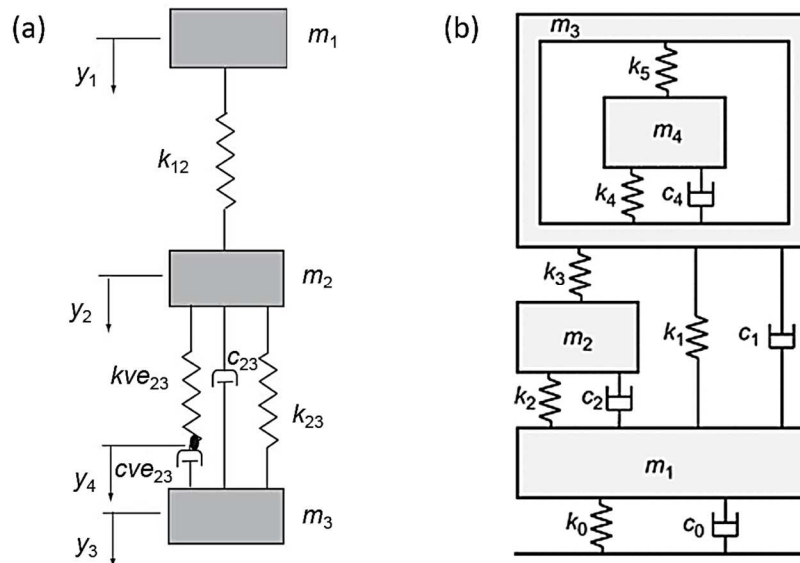


Figure 5.3 (a) The lumped-mass model of thorax (adapted from Lobdell et al., 1973) and (b) the lumped-mass model to relate variations in ground reaction forces to mechanical characteristics of specific elements in the model (adapted from Nigg, 2010)

Figure 5.3 (b) shows a simplified LM model used to determine the relationship between gait mechanics and the impact force during running [Nigg, 2010]. Elements of the system shown in the figure are: lower body rigid mass (m_1) and wobbling mass (m_2), upper body rigid mass (m_3) and wobbling mass (m_4), compressive spring (k_1) and damper (c_1) that connect the upper and lower rigid bodies, spring (k_3) and spring–damper unit (k_2, c_2) connecting the lower wobbling mass to the upper and lower rigid bodies, spring (k_5) and spring–damper unit (k_4, c_4) connecting the upper wobbling mass to the upper rigid mass.

5.2.2 Multi-body (MB) models

In multi-body models, two or three dimensional, the overall human structure, masses, mass distributions, articulations, and joints are modelled with elements in a MB formulation connected by mechanical joints. The number of degrees of freedom between the elements can be constrained in MB models due to the types of joint used in the model.

MB models provide a good balance between the accuracy and the computational cost as the models use ellipsoids and facet surfaces to represent inertial properties and geometry of the body, global response characteristics through prescribed joint properties and nonlinear contact algorithms [Crandall et al. 2011], However, the MB models lack of describing the tissue level failures and modelling the body deformation accurately. Figure 5.4 shows examples of MB models.

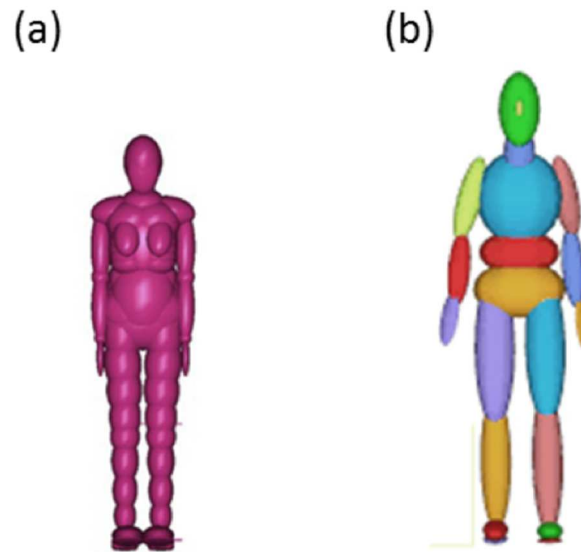


Figure 5.4 Examples of multi-body human models: (a) 5th percentile MADYMO female model [adapted from Xu et al. 2016] and (b) 50th percentile MADYMO male model [adapted from Anderson et al., 2007]

There are a number of full cervical spine MB models developed since one of the first models developed for impact loadings by Williams and Belytschko (1983). Table 5.1 summarizes the advancement of full cervical spine MB models. The history of finite

element cervical spine models is summarized in section 5.2.3.2. Figure 5.5 shows two MB models of cervical spine.

Table 5.1 The history of full cervical spine MB models [Taken from Panzer, 2006]

Model References	Geometry	Muscle Modeling	Validated Impact Cases
Williams & Belytschko, 1983	Simple 3D	Active (Stretch-Reflex)	Frontal, Lateral
Merrill et al., 1984	Traced 2D	Passive	Lateral, Rear
Deng & Goldsmith, 1987	Traced 2D	Passive	Lateral, Rear
De Jager et al, 1994 De Jager et al, 1996	Simple 3D	Passive	Frontal, Lateral
Camacho et al., 1997 Camacho et al., 1999	CT Scan 3D		Axial
Yamazaki et al, 2000	Simple 3D	Active (Hill)	Frontal, Lateral, Rear
Van der Horst, 2002	Simple 3D	Active (Hill)	Frontal, Lateral, Rear
Lee et al, 2004	Actual 3D	Active (Hill)	Frontal

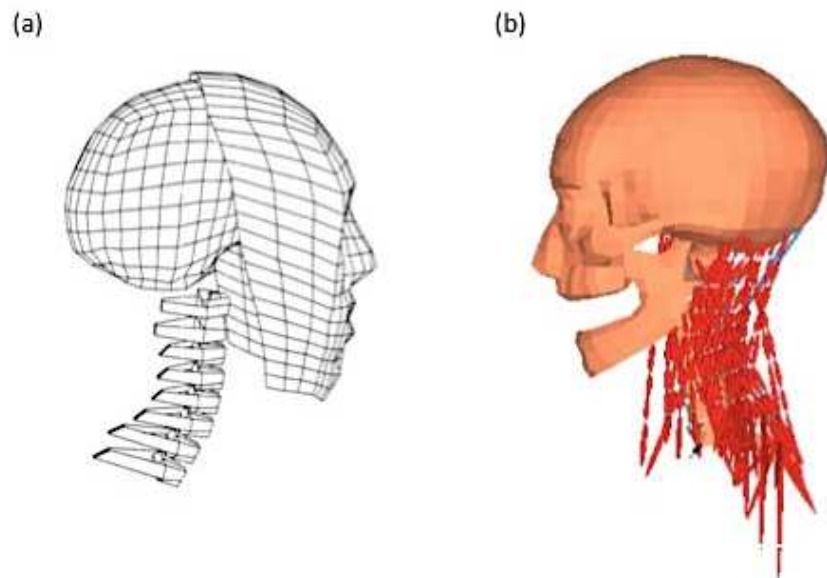


Figure 5.5 Multi-body cervical spine models [Reproduced from (a) Camacho et al, 1997 and (b) Van der Horst, 2002]

5.2.3 Finite Element (FE) models

Finite element methods are the most advanced numerical technique in 3D human modelling, where the model is divided into finite number of volumes, surfaces or lines through elements. The elements are interconnected at a discrete number of nodes associated with the degrees of freedom [Wisman, 2005]. The modelling is normally done using commercial FE solvers.

Constitutive material models are provided to each element based on the mechanical properties of the relevant tissue to be modelled. Moreover, the complex geometry of the tissues can be modelled accurately by means of different advanced imaging techniques like MRI, CT scan etc. Thus, modelling with such anatomical and material details allow understanding the stress distributions in the various tissue structures and the complex mechanisms of injury. The FE models are the most accurate models, in representing the global responses of a real human in various crash conditions, and also the tissue level responses and failure, based on local stress and strain. Hence, FE models have considerable advantages over simpler multibody models, dummies, and in some circumstances even cadavers [Crandell et al., 2011].

There are still some limitations in using the FE models as the quality of the models depends on the accuracy of the geometry and the material properties [Yoganandan et al., 1996]. The experimental data available by PHMS tests or volunteer tests are limited because of the variation in the boundary conditions. Moreover, FE models come with a much higher computational cost and the large parameter studies are more complex and time consuming. The comparisons between different types of computational models are given in Table 5.2.

Table 5.2 The comparison among different types of computational models

Model Type	Advantages	Disadvantages
Lumped mass models	Easy to develop, scale and identify parameters	Highly simplified, no loading distribution
Multi-body models	Realistic kinematics, scaling, low computational time	No tissue level response (deformation)
Finite Element models	Realistic stress and strain distribution, tissue level response	Difficult to validate, high computational time

[Courtesy: Lecture notes of Jeff Crandall, Course on Injury Biomechanics, Munich, 2015]

5.2.3.1 Full-body models

It is extremely challenging to develop full-body models, which will offer responses like a human in crash reconstruction. FE models of the physical crash dummies are widely used for automotive crash analysis. But, mathematical modelling of the real human body is more difficult to develop than a dummy model, which provides improved biofidelity compared to dummy models.

A number of whole body FE human body models (HBMs) are used for automotive crash simulations. The models vary as male or female, adult or child, 5th or 50th or 90th percentile, occupant or pedestrian, frontal or rear or side impact. The most modern and favorite models used by the researchers and companies are e.g. the HUMOS [Robin, 2001], the THUMS [Iwamoto et al., 2002] and the GHBM [Gayzik et al., 2011] models. There are different versions of these models with more biofidelic updates in the later versions and it is a continuous process to make them more accurate for omnidirectional impacts. Most recently, a new VIVA OpenHBM finite element 50th percentile female occupant model has been developed and validated for different impact conditions [Öst et al., 2017b]. THUMS and PIPER child models [www.newsroom.toyota.co.jp; www.piper.com] and Obese HBM [Hwang et al., 2016] are recent progresses in human body modeling. Figure 5.6 shows examples of 50th percentile male dummy and human body occupant models.

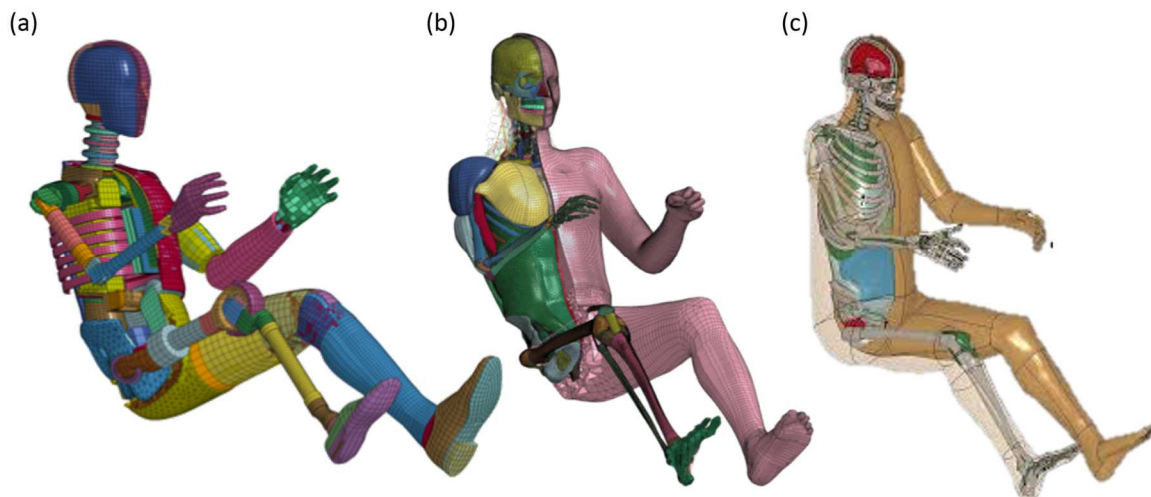


Figure 5.6 50th percentile male dummy and human body occupant models: (a) Hybrid III model developed by LSTC [adapted from Eliasson and Wass, 2015], (b) detailed GHBM model developed by Global Human Body Model Consortium [adapted from www.ghbmc.com] and (c) detailed THUMS model developed by TOYOTA Motor Corporation and TOYOTA Central R&D [adapted from www.dynamore.se] (some parts are hidden)

5.2.3.2 Neck or Cervical Spine Models

Cervical spine modeling is the main attribute of a neck model. Cervical spine FE models are historically divided into two groups: cervical spine segment model and full cervical spine model. Cervical spine segment model is the numerical model that represents a segment or a combination of segments of the cervical spine, usually modeled as vertebra-disc-vertebra with or without ligaments. These models are validated against the experimental data of simple quasi-static loading that focuses on the stress-strain behavior of the local tissues [Panzer, 2006].

In full cervical spine model, the numerical models consist of the whole cervical spine model, where the model exists from T1 vertebra to the skull. Kleinberg (1993) developed the first FE model of full cervical spine. In the advancement of FE cervical spine modeling, the first detailed upper cervical spine model was developed by Halldin et al. (2000). Models developed by Meyer et al. (2004), Panzer (2006) Östh et al. (2016) are some of the other advanced and recent FE cervical spine models (Figure 5.7). Table 5.3 summarizes the history of full cervical spine FE models.

Table 5.3 The history of full cervical spine FE models [Updated from Panzer, 2006]

Model References	Geometry	Muscle Modeling	Validated Impact Cases
Kleinberger, 1993	Simple 3D		Frontal, Axial
Dauvilliers et al, 1994	Simple 3D		Frontal, Lateral
Yang et al., 1998	MRI Scan 3D		Axial, Lateral
Deng et al., 1999 Deng and Fu, 2002	Actual 3D	Active (Hill)	Frontal
Halldin et al., 2000 Brolin & Halldin, 2004 Brolin et al., 2005 Hedenstierna et al, 2009	CT Scan 3D	Active (Hill) Passive (Hyperelastic) with Active (Hill)	Frontal, Lateral, Axial
Meyer et al., 2004 Meyer et al., 2018	CT Scan 3D	Passive	Frontal, Lateral, Rear, Axial
Zhang et al., 2006	Traced 3D		
Panzer, 2006 Panzer et al., 2011	Actual 3D	Active (Hill)	Frontal, Lateral
Östh et al., 2016 Östh et al., 2017a	CT Scan 3D	Active (Hill)	Rear

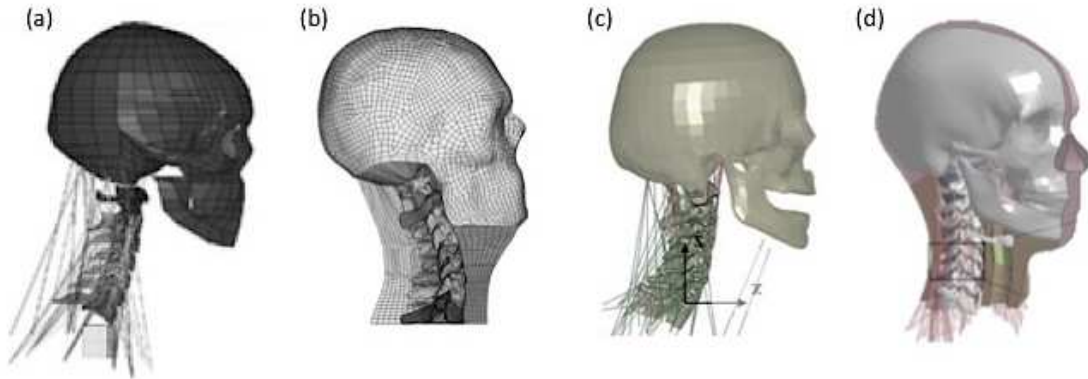


Figure 5.7 Finite element full cervical spine models: (a) KTH model with hill muscles [adapted from Brodin et al., 2005], (b) Strasbourg University model with solid elements for passive muscles [adapted from Meyer et al., 2004], (c) Waterloo University model with hill muscles [adapted from Panzer, 2006] and (d) Chalmers female model with hill muscles and neck soft tissues [adapted from Östh et al., 2017a]

5.2.4 Hybrid Models

Besides subdividing the computational models into three main groups, there is an auxiliary type of model exists called “hybrid model”. The numerical techniques, combining rigid bodies and deformable segments, are applied to hybrid models. An example of hybrid modelling is the external interfaces between MADYMO and the FE based crash codes allowing integrated multi-body finite element simulations [Wismans et al., 2005].

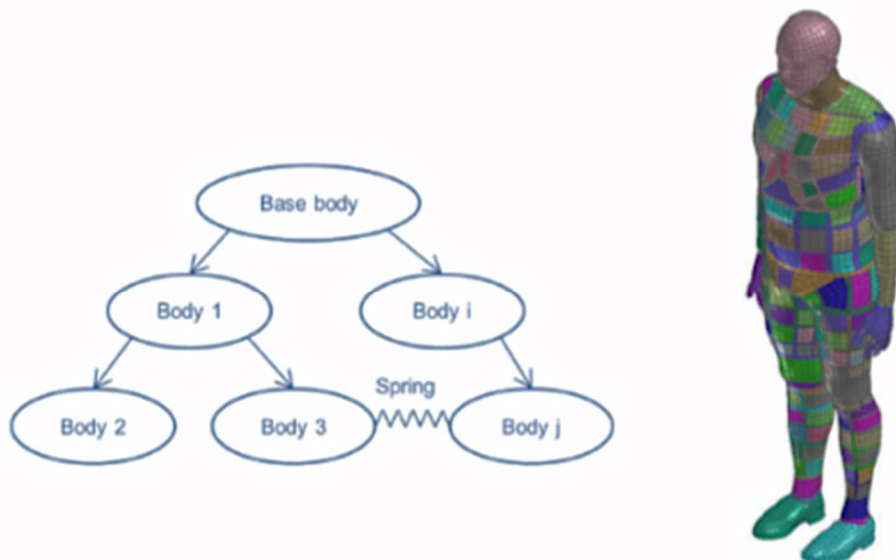


Figure 5.8 VIRTUMAN 50th percentile male hybrid model (right), where the basic skeleton is modelled as multi-body (adapted from Lindstedt et al., 2016)

Figure 5.8 shows another example of hybrid model of a virtual human body model, developed as VIRTHUMAN. A multi-body system represents the basic skeleton forming an open structure, where rigid bodies are connected via joints through non-linear springs and dampers [Lindstedt et al., 2016].

Chapter 6

Experimental Techniques

Different experimental procedures are applied to test the characteristics of the PPEs according to the Standards described in Chapter 4. These experiments are important to evaluate the quality of the finished products. The techniques, presented in this chapter, are commonly used for testing the PPEs and their inherent materials, but not necessarily all of them have been used in the development of the neck protectors. However, these techniques are imperative in material testing and in the development of the neck protector standards. The contents provided in this chapter have been briefly adapted from Nasim et al. (2015).

6.1 Drop Weight Impact Tester

A dropping apparatus with a mass ('falling weight'), known as bar impactor, is dropped freely to perform the impact tests for the impact protectors. The mass is released in order to drop along a guided vertical path onto the sample placed on a test anvil. The centre of the mass of the falling weight lies over the centre of the anvil. The force transmitted through the sample is the resultant force recorded by a load cell placed inside the anvil. The performance levels of an impact protector, followed by the values defined in the Standards, are defined based on this resultant force. Figure 6.1 and Figure 6.2 show several anvils and bar impactors respectively, which are used in the drop assembly (Figure 6.3) for the impact absorption tests according to the relevant standards. This apparatus with flat impactor and flat anvil was used in this research work for dynamic loading test to determine the stress-strain behaviour of the foam materials. Nasim and Brasca (2016) and Nasim et al. (2017) reported the impact properties of polymers using this drop weight technique. The analyses are briefly summarized in Appendix A.

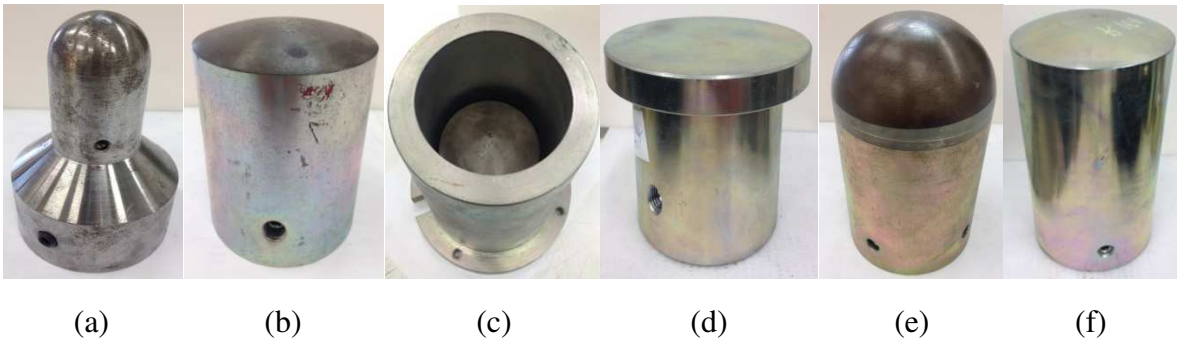


Figure 6.1 A list of anvils used in the drop weight impact test for different protectors. They are used for (a) footwear, (b) back and chest protectors, (c) chest protectors (impact distribution test), (d) helmets, (e) limb protectors, and (f) gloves.

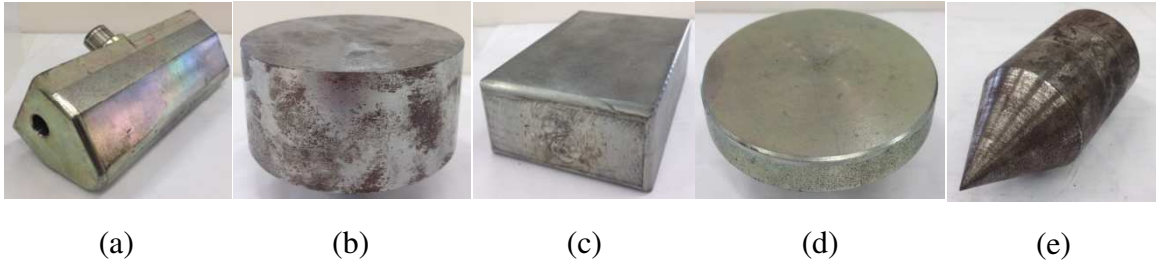


Figure 6.2 A list of bar impactors used in the impact test for different protectors. They are used for - (a) back and chest protectors, (b) helmets, (c) limb protectors, (d) gloves, and (e) visor (penetration test)



Figure 6.3 The experimental set-up of a drop weight impact tester for the impact test

There is a modification for the impact test of the motorcycle helmets. In the impact test for other protectors, the falling weight is the sum of the guided mass and the bar impactor. But, according to the helmet Standard ECE 22.05 [ECE, 2002], the free fall guidance system includes the helmeted headform as shown in Figure 6.4. The metallic headform (as in Figure 6.5) is fitted with a three-axis accelerometer. The measuring

assembly adopts a system to bring the point of impact into correspondence with the centre of the anvil.



Figure 6.4 The experimental set-up of headform drop assembly [Reproduced from www.mavet.it]

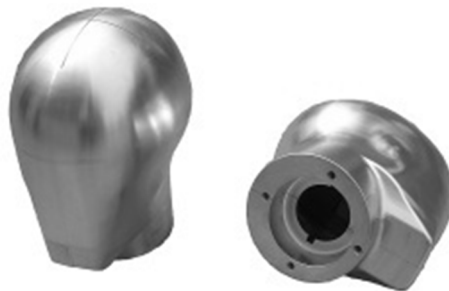


Figure 6.5 A headform used in the tests of helmets [Reproduced from www.mavet.it]

6.2 Impact Abrasion Apparatus

During the development of the standard EN 13695:2002 for motorcycle protective clothing, a number of existing test methods were proposed and discussed. And the final choice came between the “Cambridge” machine as shown in Figure 6.6 built by Dr Roderick Woods of the Protective Clothing Research Facility (PCRF) at Cambridge University [www.pva-ppe.org.uk], and the “Darmstadt” machine as shown in Figure 6.8,

which is currently in use by several textile weavers and motorcycle clothing manufacturers.

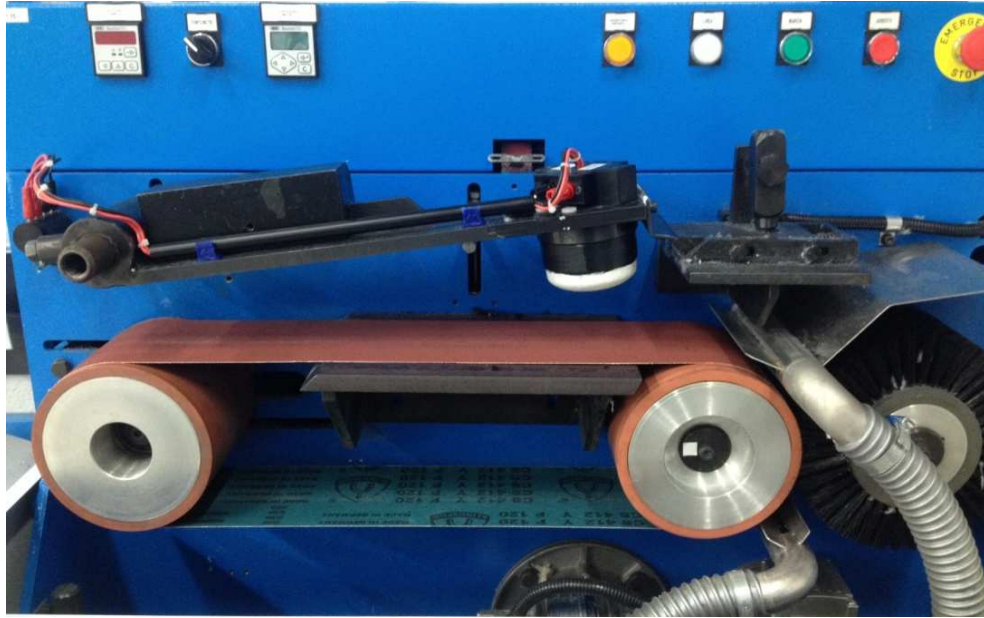


Figure 6.6 The “Cambridge” type abrasion test machine

The Cambridge machine (Figure 6.6) consists of a heavy-duty abrasive belt of known grit value spinning at a constant speed of eight meters per second or just under 18 miles per hour. The hinged arm carrying the test specimen of garment material is released and falls onto the moving belt as shown in Figure 6.7. Two fine copper wires are attached across the both side of the specimen. An electronic timer starts recording the time taken from contact to perforation where the time starts when the first wire facing towards the belt is cut and stops when the second copper in the other side is cut. The time interval between the countdown starts and stops indicates the pass/fail criteria in the test method and also the abrasive protection levels of the garment. The device has also been adopted for use in other standards, where there is a requirement for products to be tested for their abrasion resistance against road surfaces, such as roller skating protectors.

The Darmstadt machine (Figure 6.8), which consists of a concrete surface, is based on the principle of having rotary system of one or more suspended sample holders from the centre. An electric motor spins the sample holders to a specific number of revolutions per minute. Then the sample holders are unlocked from the central shaft, continue to spin falling onto the concrete and gradually come to rest. The test sample is judged on the basis of the creation of any holes in the test samples. The Darmstadt machine has been introduced in the new Standard for motorcycle clothing PrEN 17092:2017 [CEN, 2017] due to fact that the current version of the machine has demonstrated the progress in repeatability of the result after many round robin tests, which was not the same with the

Cambridge machine. Moreover, the supporters of this machine claim that it mimics the action of clothing in a real accident more accurately, a reduction in speed from initial velocity to a halt.



Figure 6.7 The test specimen of the leather garment mounted on the hinged arm of the Cambridge machine for the impact abrasion test

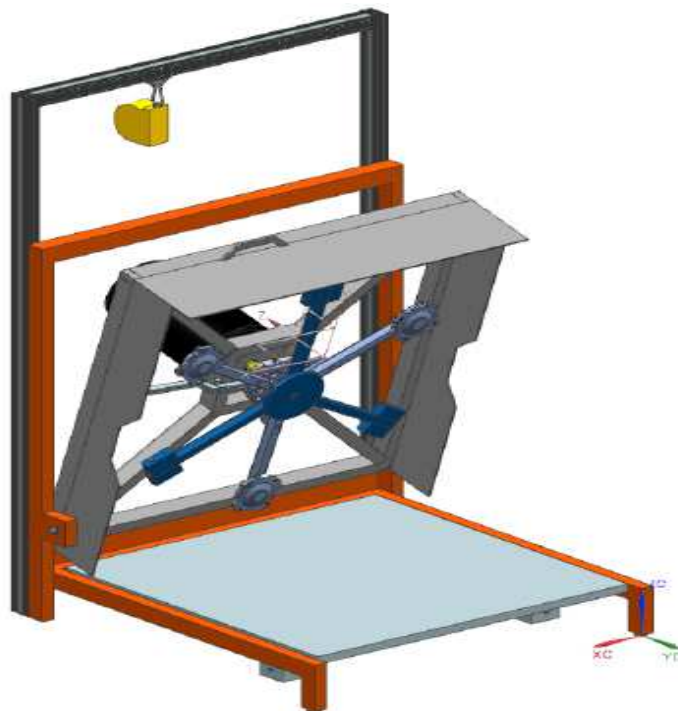


Figure 6.8 Base model of the "Darmstadt" type abrasion test machine

6.3 Impact Cut Resistance Apparatus

The impact cut resistance apparatus (Figure 6.9) is used to measure the cut resistance of the full thickness of the clothing in the various zones based on the impact. A test specimen taken from the clothing is mounted over a block containing a rectangular hole. A striker of fixed mass with a sharp blade fitted to its lower surface is dropped with a defined energy level so that the blade impacts the sample directly above the rectangular hole. The maximum penetration of the blade through the material is measured. The measurement of penetration defines the cut resistance characteristic of the clothing material.

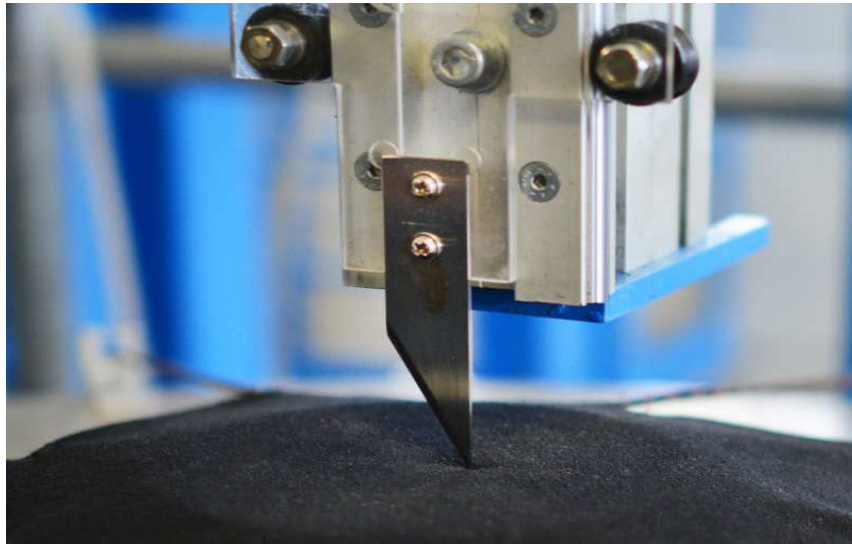


Figure 6.9 The configuration of the impact cut resistance apparatus

6.4 Dynamometer

Dynamometers are used for the tensile strength test of the seam and zipper, textiles, leathers and rubber joints. The type of dynamometer shown in Figure 6.10 (a) is normally used for the tensile strength test of the seam, zippers and fasteners. The samples are clamped over a test rig containing a high pressure rubber diaphragm, which is then inflated under the seam or zipper until either the sample is torn or the stitching is given away. The rig measures the pressure required to burst the seam or zipper.

Another type of dynamometer is shown in Figure 6.10 (b), which is useful for measuring the tensile strength of textile and leather garments and elastic bands used for the retention system. A sample of approximately 20 cm is clamped with the two arms of the test rig. The upper arm continues to create stress on the sample at fixed strain or stress rate until the sample is torn. This test rig has been used to measure the stress-strain behaviour of some samples, which was needed to set the material properties in the simulation for this research work.

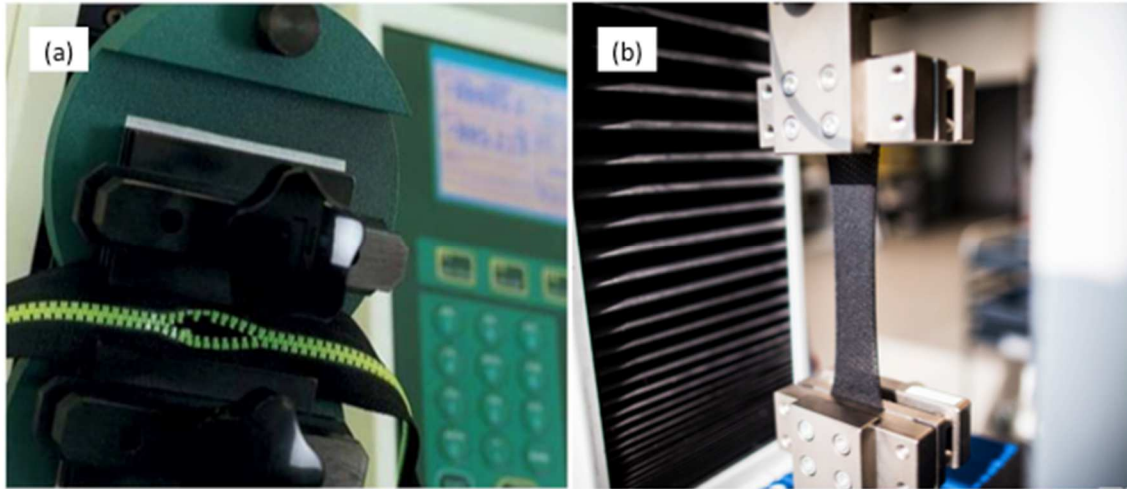


Figure 6.10 The dynamometer used for tensile strength test of the samples

6.5 Rigid test cones

Five rigid test cones for the sleeves and five rigid cones for the legs of the test garments, and also six cones for the gloves, are used for the restraint test. Figure 6.11(a) shows a test cone used in the restraint test. The cones are fitted with hooks to enable a longitudinal force to be applied to its smaller end. Then the cones are gradually pulled, as exemplified in Figure 6.11(b), to apply a force to the test over 20 – 60 seconds until the required maximum force is reached according to the standards. The cones need to sustain the maximum force remaining inside the sample.



Figure 6.11 (a) A rigid test cone for the restraint test and (b) the performance of the restraint test using the test cone

Chapter 7

Development of FE Neck Model

The inspiration of developing the Dainese neck (D-neck) model was to understand the real dynamics of neck during a motorcycle crash. Since the biofidelic full-body or neck models described in Section 5.2.3 have been developed focusing on car crash simulations, the application of those models on the study of injury mechanisms in motorcycle accidents remain limited due to the different impact scenarios. For the construction of full cervical spine model, the head model was chosen from hybrid III model developed by Livemore Software Technology Corporation (LSTC). Despite the availability of both dummy and FE models of the hybrid III neck, the application of that neck is incredibly limited for direct impact conditions; the neck is too stiff in compression and less sensitive than flexible human neck [Yoganandan, 1989; Myers et al., 1991; Foster et al., 1977; Nelson and Cripton, 2010]. The response of hybrid III neck in compressive impact has been indicated in Appendix B.

Although the accurate shaped models derived from CT/MRI scan provide an approximation to a certain population of spines, these models cannot perfectly represent the exact global size of that population. Here, for constructing the D-neck model, the statistical shape of 50th percentile male cervical spine by choosing the mean geometries found from the literatures [Bazaldúa et al., 2011; Ulbrich et al., 2014; Sengül et al., 2006; Gilad and Nissan, 1987; Panjabi et al., 2001; Przybylski et al., 1998] and the adjustment of the shapes of the cervical spine by looking at the available published figures [Moore and Dalley, 2006; Filler, 2004] have been considered. As it is a simple 3D model, some parts could not be kept geometrically accurate like those of a human. In spite of this disadvantage, this model has been proven to be a good tool to analyze the dynamics of the neck for compressive as well as direct impacts and to utilize in applications for analyzing the injury risk. Such applications have been reported in this thesis by using the FE model of a commercial motorcycle helmet and neck protective systems.

The D-neck model has potential to develop an anthropomorphic test device (ATD) for neck protector standards - another reason to be inspired in developing the model. Although a biofidelic neck ATDs for head-first impacts are available [Nelson and Cripton, 2010; Withnall et al., 2003], their affirmation in the Standard market has not been adopted promisingly. The simplicity of the geometry and modelling of the D-neck can provide valuable inputs in developing new test methods for neck protector standards, which is extremely demanding topic in recent time. The material models need to be

adjusted with that of the new ATD to construct a durable structure and re-evaluated with the achieved results to make balance with biofidelity.

7.1 Model Geometry

Firstly, the curvature of the neck between the vertebral bodies (superior face of C2 and inferior face of C7) was considered as 30° in the sagittal plane by drawing two straight lines and later each vertebra was translated and rotated to fit inside this angle.

Table 7.1 Geometries of vertebrae for the design of D-neck model [Bazaldúa et al., 2011; Sengül et al., 2006; 7; Panjabi et al., 2001]

Vertebral dimensions in mm	C1	C2	C3	C4	C5	C6	C7
<i>Vertebral body</i>							
A-P diameter	21.6*	14	14.7	17	17	17.4	17.4
Transverse diameter	14.6*	18.3	19.1	20.8	20.8	23	23
Vertebral height	10.3*	22.1	13	12.5	11.5	12	13
Lamina height	-	11.5	12.3	11.4	11.3	12.2	14.3
Spinous process length	-	21.3	15.5	15.4	16.6	21.8	29.1
Articular process diameter (Both superior and inferior)	8.5	11.3	11.3	11.3	11.3	12	12
Articular process height	6	12.1	10.6	11	10.2	10.2	11
Outer A-P diameter	46.2	-	-	-	-	-	-
Outer transverse diameter	50	-	-	-	-	-	-
Inner A-P diameter	31	-	-	-	-	-	-
Inner transverse diameter	28.7	-	-	-	-	-	-
<i>Dens</i>							
Height	-	14.5	-	-	-	-	-
A-P diameter	-	7.5	-	-	-	-	-
Transverse diameter	-	11	-	-	-	-	-
Cortical bone thickness	0.5	0.58	0.58	0.58	0.58	0.68	0.68

*For the simplicity of atlas geometry, the anterior arch and tubercle had been drawn as vertebral body.

In order to design each vertebra, initially the vertebral body was shaped as an ellipse by using the antero-posterior (A-P) and transverse diameters (the dimensions considered to design the vertebrae are given in Table 7.1). The positions of the adjacent vertebrae were defined considering the required disc height between two consecutive vertebrae. Approximate height of 5mm was taken initially for all the cervical discs [Gilad and Nissan, 1987; Przybylski et al., 1998].

Cervical spinal canal dimensions [Ulbrich et al., 2014] were estimated to shape the posterior part of the vertebral bodies. Conical cylinders were drawn for the spinal canal and spinal cord using the diameters related to three different vertebrae (see Table 7.2). The posterior parts of the vertebrae such as pedicle, spinal process, articular process, and lamina were drawn around the canal dimensions to complete each vertebra. In this process, the lamina width, transverse process and transverse foramen were not included in any of the vertebrae including C1 and C2.

The dens (odontoid process) was adjusted with vertebral body of axis. The outer shape of atlas was initially drawn as an ellipse followed by the distance between both lateral most edge of the transverse foramen and the maximum A-P dimension of the vertebral canal. The anterior arch of the atlas was kept at a distance of 1.2 mm from the dens and the facet cartilages of 0.55 mm were added to atlas and dens to cover the gap.

Table 7.2 Diameters for spinal cord and spinal canal [Ulbrich et al., 2014]

Diameters in mm	C1	C3	C7
Spinal cord	8.3	7.8	6.8
Spinal canal	15.2	12.4	12.2

In the next step, the intervertebral discs (IVDs) were developed as the volume between the inferior and superior boundaries of two consecutive vertebrae. The superior surface of nucleus was drawn as an ellipse on the superior surface of the disc considering approximately the half of the A-P and transverse diameters of the disc surface. Then closed ellipsoidal cylinder was drawn from the superior surface of the nucleus, where the inferior surface was projected to the inferior surface of the disc. The remaining volume of the disc was taken as AF. After mesh generation, the C7+ disc was drawn in such a way that the stacked vertebrae and the discs could dimensionally match with the replaced hybrid III neck parts as shown in Figure 7.4.

Lastly, first thoracic (T1) vertebra was added with the D-neck to make it a full neck model. The geometry of T1 is not new, but dimensionally scaling up of C7 vertebra in XYZ direction. The posterior boundary from the superior surface of the vertebral body of T1 and the superior surface of hybrid III neck bracket were kept aligned in the same

plane. C7+ vertebral disc was reconstructed as C7T1 to cover the gap between the two adjacent vertebrae completely. The dimensions of the IVDs originated in the D-neck model are given in the Table 7.3.

Table 7.3 Intervertebral disc (IVD) height in the D-neck model [Gilad and Nissan, 1987; Przybylski et al., 1998]

Height in mm	C23	C34	C45	C56	C67	C7T1
IVD anterior	7.3	7.2	5.5	6.1	8.2	6.0
IVD posterior	9.5	6.0	5.0	4.0	5.6	5.5

7.2 Model Construction

The geometry of the D-neck was based on the values found in the literatures as described in Section 7.1. The total height of the neck (C1-C7) was the summation of the total vertebral height and the total disc height. The lordotic angle between the vertebral faces of C2 and C7 in the sagittal plane was measured as 10°.

The CAD (computer aided design) and mesh generation of all the parts of D-neck was constructed in LS-PrePost V.4.3 and then coupled with Hybrid III head and upper neck bracket as described in the following Section 7.2.4. Then the neck bracket was replaced with T1 vertebra and muscles, neck skin and neck soft tissues were added one by one. Overall 169060 elements were used to model the complete neck (excluding the head components of the hybrid III). The global coordinate system was considered with X-axis (forward), Y-axis (left) and Z-axis (Upward). The gravity loading was ignored in all the simulations.

7.2.1 Vertebrae

The geometry of the lower and middle cervical spine (C3-C7) as in Figure 7.1b was the main basis of the D-neck, which was taken from a morphometric study of 150 cervical vertebrae [Bazaldúa et al., 2011] The upper cervical spine (C1-atlas and C2-axis), as shown in Figure 7.1a, was developed mainly following the geometry of 40 human C1 and C2 vertebrae [Sengül et al., 2006]. The bones of the cervical spine were modelled as two parts: cortical bone and cancellous bone. The cortical bone was modelled as triangular shell and the cancellous bone was modelled as tetrahedron. The thickness of the cortical bone (C1=0.5mm, C2-C5=0.58mm and C6-T1=0.68mm) was taken slightly higher than that is found in the literature [Panjabi et al., 2001] as bony endplate was not considered for this model.

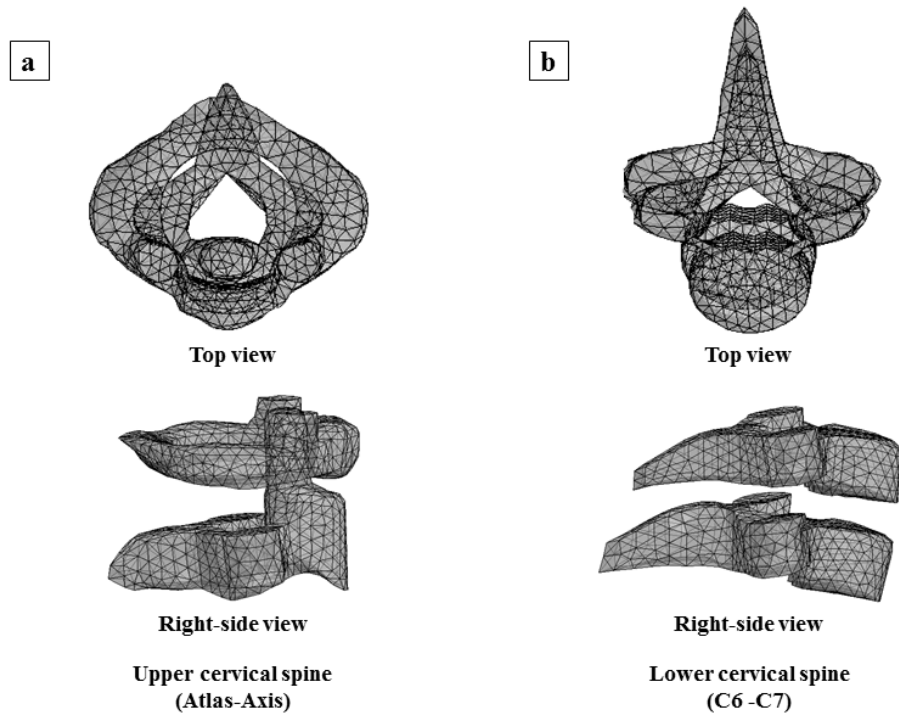


Figure 7.1 FE models of the upper (a) and lower (b) cervical vertebrae

7.2.2 Intervertebral Discs

The intervertebral disc (IVD) consisted of two parts (Figure 7.2): nucleus and annulus fibrosus (AF). Fiber laminae and ground substance were considered as singular part to model the AF. Tetrahedral solid elements were used to model both nucleus and AF.

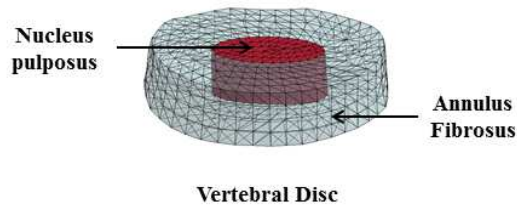


Figure 7.2 The construction of vertebral disc with nucleus pulposus and annulus fibrosus

7.2.3 Facet Cartilage and Spinal Cord

Hypothetic spinal cord was also introduced replacing the guided cable from the Hybrid III model and solid compressible hyper-elastic elements were assumed for modeling it [Clarke, 2011]. The adjustment of facet cartilage and spinal cord with segmented D-neck model (C1-C7) is shown in Figure 7.3.

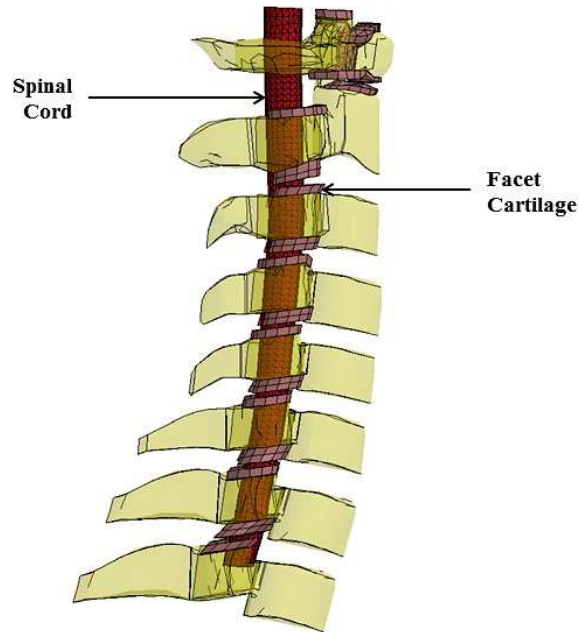


Figure 7.3 The position of facet cartilage and spinal cord in the neck model

The facet cartilage was modelled with solid elastic elements from the facet surfaces [Östh, 2016; Yamada, 1970]. Single element thickness with the superior facet and double element thickness with the inferior facet were used. The existence of synovial fluid between the facet cartilages was neglected.

7.2.4 Segmented D-neck & Hybrid III dummy head

In this thesis, the detailed hybrid III model developed by LSTC was used for the head model. The head model consists of different parts: head skin, head cap skin, skull, skull cap, head base, head accelerometer (placed at the center of gravity (CG)), head blast left, head blast right and head mount-storm. The weight of these parts was calculated as 4.67 kg. The hybrid III neck upper disc (HNUD) was modified with rigid shell elements and was provided the same material properties as in the cortical bone of first thoracic vertebra (T1), which was considered as the replacement of the occipital condyles. The hybrid III upper neck bracket (HUNB) was considered as T1. The segmented D-neck (C1-C7) model was coupled with the head model between HNUD and HUNB as shown in Figure 7.4 and then the ligaments were constructed. Automatic surface to surface contact between the C1 and HNUD was assigned. Lastly, the rigid T1 vertebra (the principle moments of inertia: $I_{xx} = 0.0014 \text{ kgm}^2$, $I_{yy} = 0.0018 \text{ kgm}^2$ and $I_{zz} = 0.0028 \text{ kgm}^2$) was constructed by geometrically enlarging the C7 vertebra and then the C7+ vertebral disc was redesigned to cover the gap between C7 and T1. The nodes of the superior and inferior surfaces of the spinal cord were rigidly constrained with HNUD and T1.

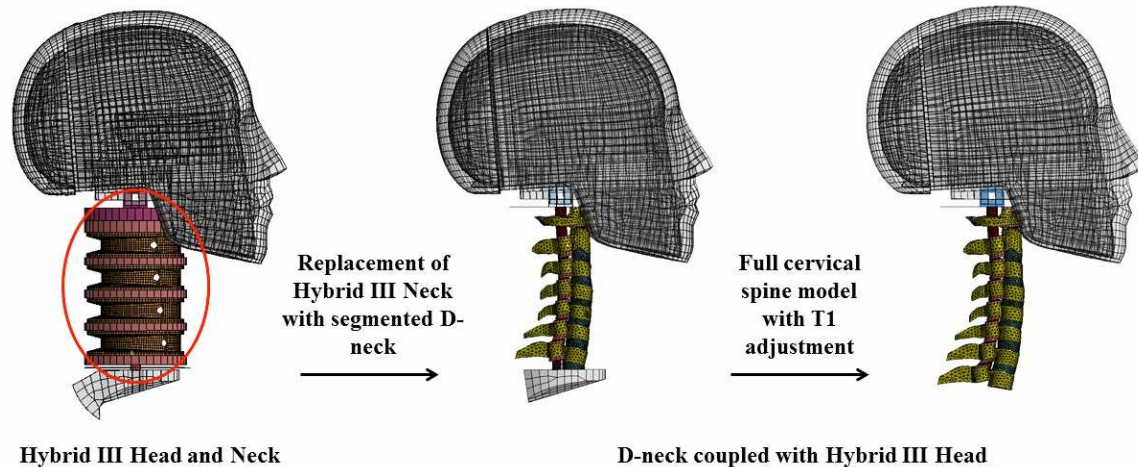


Figure 7.4 Full cervical spine model by replacing the hybrid III neck with the simplified D-neck model

7.2.5 Ligaments

The ligaments were adjusted with the D-neck after the neck had been coupled with the hybrid III. Anterior longitudinal ligament (ALL), posterior longitudinal ligament (PLL), anterior atlanto-occipital membrane (AAOM), posterior atlanto-occipital membrane (PAOM), anterior atlanto-axial membrane (AAAM), posterior atlanto-axial membrane (PAAM), ligamenta flava (LF), Inter-spinous ligament (ISL), capsular ligament (CL), transverse ligament (TL), apical ligament, alar ligament, crus ligament, tectorial membrane and nuchal ligament were adjusted in the model based on their biological positions as shown in Figure 7.5 [Moore and Dalley, 2006; Agur and Dalley, 2005; Gray, 1918; Yoganandan et al., 2000b].

All the ligaments except TL were modelled with total of 359 discrete elements and non-linear elastic spring material [Panzer, 2006]. For the simplicity, rate-independent force-deflection curves for the force generation in the discrete elements were provided based on three different regions (more details in Section 7.3) [Chazel et al., 1985; Hayashi, 2003]. TL was modelled as an elastic shell providing stability and allowing rotational movement between the atlas and the axis, which is also important to restrain the translational motion between these vertebrae [Panjabi et al., 1998].

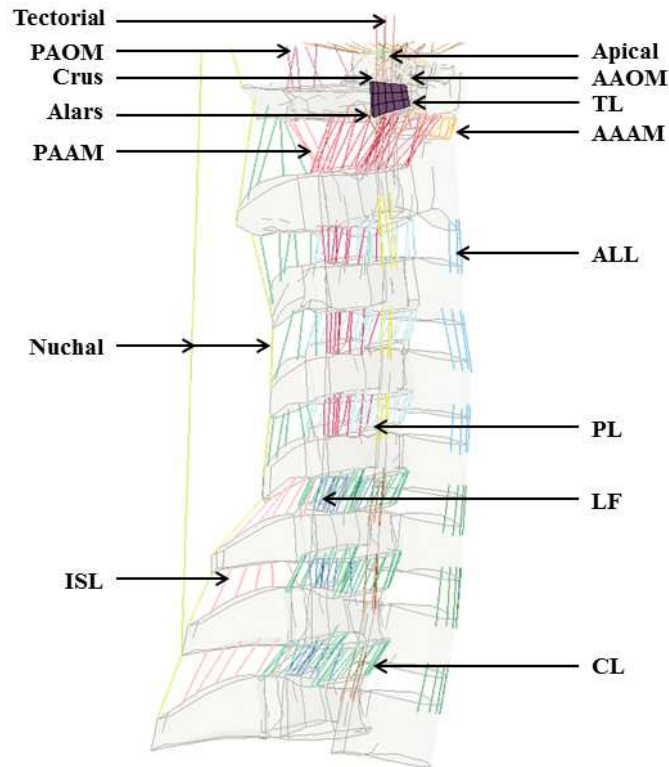


Figure 7.5 The orientation of ligaments in the neck model

7.2.6 Muscles

In the next phase of the neck model development, the muscles were integrated based on the descriptions provided in clinical anatomy literatures (Figure 7.6). The vertebrae and skull were taken as reference for all the muscles, though the origin or insertion points could not be modelled perfectly as they would be in a full body model. The muscles, that have insertion or origin points at the level of T1 or below, were constrained to the base of neck soft tissues and skin described in the next Section 7.2.7.

The muscles were modelled using a number of 1D spring elements with multiple separate segments to account for the force generation between the origin and insertion points. Total 1968 spring elements were used to model 94 separate muscle pairs (188 segments in total), which represent 25 different muscles of the neck. A symbolic simple hyoid bone was added at C3 level, with the material model and properties identical to cortical bones, to define the insertion point of infrahyoid and suprahyoid muscles. The length of each muscle was calculated as the straight distance from origin to insertion point. The data of physiological cross-sectional area (PCSA) and muscle volume were taken from the information provided by Knaub and Myers (1998). The maximum isometric force (F_{max}) was calculated from the PCSA and a maximum muscle stress of 50 N/cm^2 [Winters and Stark, 1988]. The geometric details of the cervical spine muscle segments are given in Table 7.4.

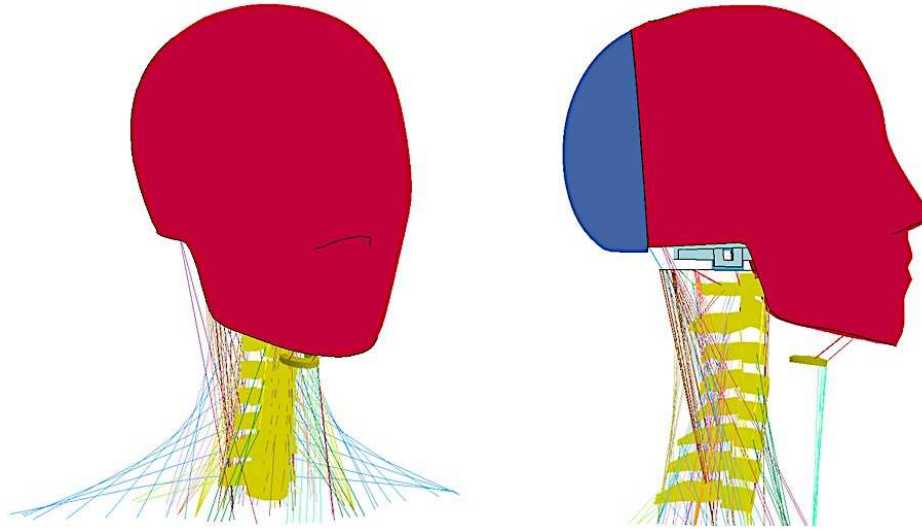


Figure 7.6 The position of muscles in the neck model: anterolateral view (left) and right side view (right)

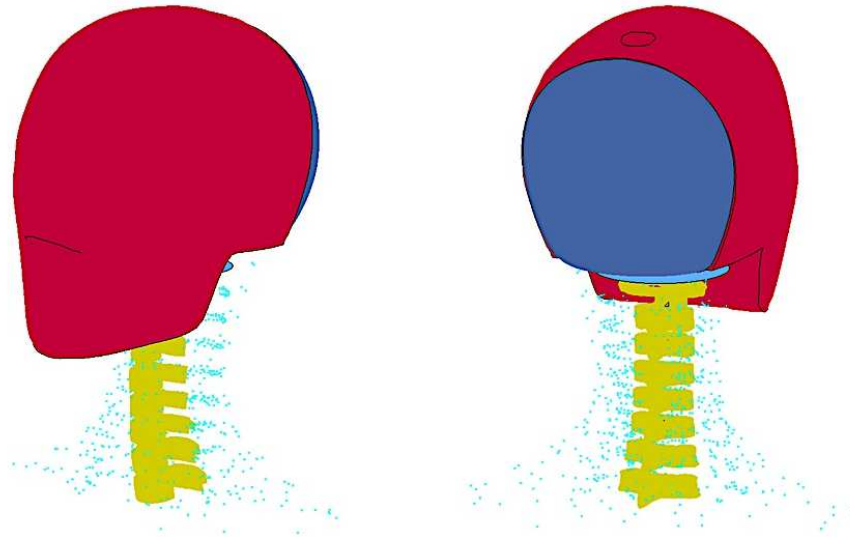


Figure 7.7 Dispersion of mass elements to account for the weight of the muscles

The neck curvature of the superficial neck muscles, during neck flexion or extension or lateral bending for the changing load direction, were accounted by dividing the muscle segment into equal length elements in series that elongate over the complete cervical spine. The intermediate nodes connecting two serial spring elements were constrained to the closest vertebra, so that the muscle elements could be forced to follow the neck curvature [Brolin et al, 2005; Panzer, 2006]. For this reason, one element from the posterior part of each vertebral body was changed to rigid element. To account for the weight of the muscles, mass elements were added, as discrete elements were used to model the muscle. The mass of each element, located on a muscle segment node, was calculated based on the volume of the muscle segment. The distribution of muscle mass in the D-neck is shown in Figure 7.7.

Table 7.4 The details of muscles' parameters

Muscle	Multiple segments	Total no. of springs	Average Length (mm)	PCSA (cm²)	F_{max} (N)	Volume (cm³)
Oblique Captias Inferior	1	3	36.16	1.95	97.5	8.13
Oblique Capitas Superior	1	3	19.56	0.88	44	3.03
Rectus Capitus Major	1	3	41.8	1.68	84	5.37
Rectus Capitas Minor	1	3	12.57	0.92	46	1.82
Longus Capitas	4	31	81.92	1.37	17.1	11.09
Longus Colli	8	44	99.5	2.75	19.6	13.79
Rectus Capitis Anterior	1	4	19.45	1.30	65	1.36
Rectus Capitis Lateral	1	2	10.5	1.30	65	1.74
Anterior Scalene	4	20	90.29	1.88	23.5	9.56
Middle Scalene	6	30	92.95	1.36	11.35	10.38
Posterior Scalene	3	9	70.94	1.05	17.5	6.38
Sternocleido Mastoid	2	23	195	4.92	123.1	56.09
Illiocostalis Cervicis	4	18	87.22	1.04	13	7.21
Longissimus Capitis	5	30	101.85	0.98	98	12.33
Longissimu Cervicis	5	23	94.65	1.49	14.9	9.71
Multifidus	6	12	30.36	2.35	19.58	24.64
Semisplenius Capitus	9	66	149.82	5.52	30.65	44.67
Semisplenius Cervicis	4	20	90.6	3.06	38.25	24.19
Splenius Capitis	4	33	155.27	3.09	38.65	30.67
Splenius Cervicis	3	21	139.74	1.43	23.85	14.38
Levator Scapula	4	28	122.94	3.12	39	37.83
Minor Rhomboid	2	6	63.68	1.02	25.5	7.47
Trapezius	9	54	158.07	13.73	76.28	132.09
Infrahyoid	3	3	101.074	1.33	11.08	12.19*
Suprahyoid	1.5	3	34.5	1.02	17	5*

*Assumed.

7.2.7 Soft tissues and skin

The neck soft tissues and skin were added to the model, as these are important parts for coupling the neck protectors with the D-neck, so that the more accurate response can be achieved by defining appropriate contact between the neck protectors and the human skin. The shape of the neck-skin was adopted from the 50th percentile male avatar of the commercial software CLO[®]. The avatar was merged acceptably with the hybrid III head by using transforming and scaling methods. Then the required skin part, as shown in Figure 7.8, was cut from the whole avatar model. The upper section of the skin was cut from the bottom of the head and head cap of hybrid III head, and the lower section of that was cut from the clavicle keeping the cut plane at second thoracic vertebra (T2) level. The skin was modeled with brick elements. The thickness of the skin in the model has been assumed as 0.9mm [Griffin et al., 2017].

In the final construction of the neck model (Figure 7.8b), soft tissues were modeled using tetrahedron element inside the empty space of the skin (Figure 7.8a). The main reason of adding the soft tissues is to achieve real dynamics of the skin during the accident simulations. The trachea cavity passing through the hyoid bone was also added in the soft tissues. Contact between the soft tissues and the spine model was neglected, as it was assumed that the muscles were separately modelled to generate force among the vertebrae according to their origin and insertion points.

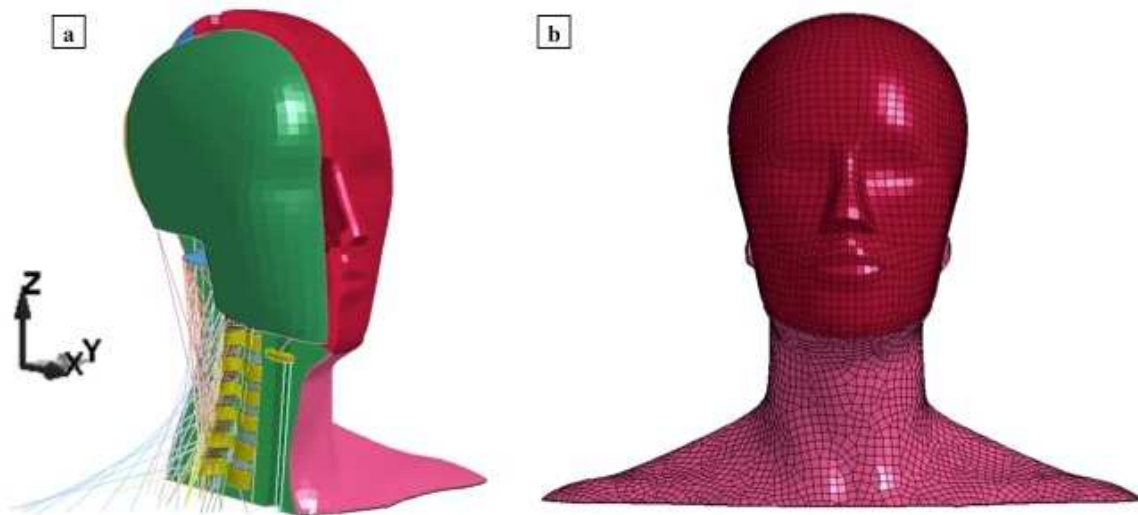


Figure 7.8 The construction of neck skin and neck soft tissues to develop the complete neck model

7.3 Material Properties

The correct material properties are important to develop a biofidelic model [Yoganandan et al, 1996]. However, the experimental data for many cervical spine tissues are often limited, not in a compatible format for numerical modeling or even not yet available in the literatures (Panjabi, 1998). All the material models used in the D-neck model have

been selected from the LS- DYNA material library [Hallquist, 2006] based on the suitable match with the material properties of the cervical spine tissues found in the literature.

Isotropic power law plasticity material model was used for the bones, so that the onset of bone damage can be identified when a load is applied [Panzer, 2006; Currey, 2004; Kopperdahl, and Keaveny, 1998]. The elastoplastic behaviour of this model with the yield point obeys a linear stress-strain relationship for elastic part (Eq. 7.1) and a non-linear function defining the yield stress for the plastic part (Eq. 7.2).

$$\sigma = E \cdot \varepsilon \quad \text{Eq. 7.1}$$

$$\sigma = k \cdot \varepsilon^n = k \cdot (\varepsilon_{yp} + \varepsilon_p)^n \quad \text{Eq. 7.2}$$

where, E is the Young's modulus, ε_{yp} is the yield strain, ε_p is the effective plastic strain, and k and n are parameters of the yield function.

The nucleus pulposus of the intervertebral disc exhibits viscoelastic characteristic that behaves like a solid in dynamic conditions, but like a fluid in quasi-static conditions [Iatridis et al., 1996]. The material constitutive law of pure viscoelasticity was used to model the nucleus pulposus [Yang, and Kish, 1988; Zhang et al., 2006; Östh, 2016]. The explicit stress relaxation functions can be described with the help of linear rheological models as in Eq. 7.3 below [Hermann and Peterson, 1968]:

$$G(t) = G_\infty + (G_0 - G_\infty)e^{-\beta t} \quad \text{Eq. 7.3}$$

where, $G(t)$ is the shear relaxation modulus G_∞ is long-term shear modulus, G_0 is short-term shear modulus and β is the decay constant at time t . The convolution of strain rate history leading to the integral form of linear viscoelasticity is given in Eq 7.3, which is also known as the Boltzmann superposition principle:

$$\sigma(t) = \int_0^t G(t - \tau)\dot{\varepsilon}(\tau)d\tau \quad \text{Eq. 7.4}$$

In the equation, t refers to time and τ is a time variable of integration.

Isotropic elastic material model was used to model annulus fibrosus of discs, facet cartilage, and transverse ligament [Yang and Kish, 1988; Halldin et al., 2000; Zhang et al., 2006; Östh et al., 2016; Chazel et al., 1985; Yamada, 1970]. A linear stress-strain relationship, as given in Eq. 7.1, was assumed in these cervical spine tissues.

Hyper-elastic ogden material model for spinal cord [Clarke, 2011] and neck soft tissues [Östh, 2017a; Engelbrektsson, 2011] was considered. The advantage of this material model is the better adjustment possibilities to experimental curves. In addition to the real numbers for the integer exponent in the ordinary polynomial, the principal stretches

instead of strain invariants are used in the strain energy function (Ogden, 1984). The strain energy of the Ogden hyper-elastic formulation can be defined with Eq. 7.5.

$$W = \sum_{n=1}^N \frac{\mu_n}{\alpha_n} (\lambda_1^{\alpha_n} + \lambda_2^{\alpha_n} + \lambda_3^{\alpha_n} - 3)$$

Eq. 7.5

where, n is the number of terms considered for the Ogden model, μ_n and α_n are a set of material constants and λ_i is the principal stretch.

Each discrete element of the ligaments was provided with nonlinear elastic spring model [Panzer, 2006], where force generation in the element is calculated based on the following Eq. 7.6.

$$F = f(\delta L) + g(\delta L) \cdot h\left(\frac{dL}{dt}\right)$$

Eq. 7.6

where, $f(\delta L)$ represents the quasi-static force-deflection curve and $h\left(\frac{dL}{dt}\right)$ provides the dynamic scaling factor and $g(\delta L)$ means the deflection based curve that scales $h\left(\frac{dL}{dt}\right)$. Only rate independent force-deflection curve was considered to the ligaments using the studies found in the literatures [Chazel et al., 1985; Hayashi, 2003].

The three definite points (A, B, and C) of the force-deflection curves of the ligaments are shown in Figure 7.9. The force-deflection points based on the study provided by Chazal et al. (1985) for lower, mid and upper cervical spine ligaments are given in Table 7.5, Table 7.6 and Table 7.7 respectively. The points for nuchal ligament (Table 7.8) were calculated with the data provided by Hayashi (2003) and the ligament length measured from the D-neck model.

Table 7.5 Force-deflection points for modeling the ligaments of lower (C5-C7+) cervical spine [Panzer, 2006; Chazel et al., 1985].

Ligament	Point 1		Point 2		Point 3	
	d (mm)	F(N)	d (mm)	F(N)	d (mm)	F(N)
ALL	1.37	15.66	5.02	124.56	6.5	145
PLL	1.53	18.42	4.72	146.45	6.1	188
LF	2.69	26.96	7.16	115.20	9.4	1.29
ISL	2.06	7.84	4.98	35.45	6.7	39
CL	2.06	27.87	5.95	155.66	7.8	181

Table 7.6 Force-deflection points for modeling the ligaments of mid (C2-C5) cervical spine [Panzer, 2006; Chazel et al., 1985]

Ligament	Point A		Point B		Point C	
	d (mm)	F(N)	d (mm)	F(N)	d (mm)	F(N)
ALL	1.22	10.04	4.48	79.89	5.8	93
PLL	0.88	6.96	2.71	55.31	3.5	71
LF	1.86	25.29	4.95	108.05	6.5	121
ISL	1.94	7.84	4.69	35.45	6.3	39
CL	2.69	18.48	7.78	103.20	10.2	120

Table 7.7 Force-deflection points for modeling the ligaments of upper (C0-C2) cervical spine [Panzer, 2006; Chazel et al., 1985].

Ligament	Point A		Point B		Point C	
	d (mm)	F(N)	d (mm)	F(N)	d (mm)	F(N)
ISL (C12)	1.94	7.84	4.69	35.45	6.3	39
CL (C01)	1.50	49.28	4.35	275.20	5.7	320
CL (C12)	3.06	48.36	8.85	270.04	11.6	314
AAOM (C01)	4.99	35.73	14.42	199.52	18.9	232
PAOM (C01)	4.78	12.78	13.81	71.38	18.1	83
AAAM (C12)	2.19	40.50	6.33	226.18	8.3	263
PAAM (C12)	2.53	17.09	7.32	95.46	9.6	111
Apical	2.11	32.96	6.10	184.04	8.0	214
Alars	3.72	54.98	10.76	307.02	14.1	357
Crus	3.30	67.14	9.54	374.96	12.5	436
Tectorial	3.14	11.70	9.08	65.36	11.9	76

Table 7.8 Force-deflection points for modeling the nuchal ligament of whole cervical spine [Hayashi, 2003]

Ligament	Point A		Point B		Point C	
	d (mm)	F(N)	d (mm)	F(N)	d (mm)	F(N)
Nuchal	2.42	22.27	12.43	47.72	19.8	62.36

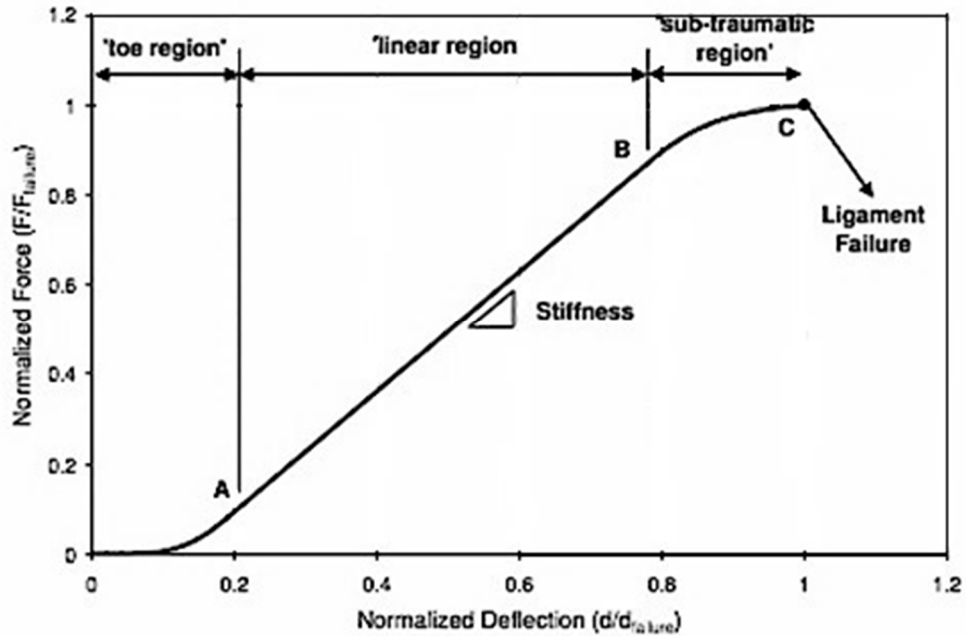


Figure 7.9 Force-deflection curve for the ligaments defining the three distinct regions [adapted from Panzer, 2006]

The classical Hill-type muscle material model was assigned to each 1D discrete element used for modeling the muscles. Such material model can explain active (contracted) and passive (relaxed) muscle behaviours. Figure 7.10 shows a schematic diagram of Hill muscle model with contractile element (CE) to account for the active muscle forces, and a parallel elastic element (PE) and a dampening element (DE) to account for passive muscle forces.

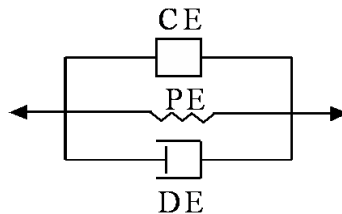


Figure 7.10 Schematic diagram of Hill muscle model with active-passive elements

Neglecting the DE, the total force in the muscle (F^M) is the sum of the contractile force and parallel elastic force (Eq. 7.7). When the muscle is inactive, the entire resistance to elongation is provided by the PE element.

$$F_M = F_{PE} + F_{CE} \quad \text{Eq. 7.7}$$

Active muscle force is calculated following Eq. 7.8, which is a function of muscle length, velocity, and active state dynamics [Winters and Woo, 1990].

$$F_{CE} = a(t) \cdot F_{max} \cdot F_{TL}(L) \cdot F_{TV}(v) \quad \text{Eq. 7.8}$$

where, tension-length (F_{TL}) and tension-velocity (F_{TV}) provide nonlinear relationships based on the current state of length and velocity of the muscle, while active state dynamics $a(t)$ is a time-dependent function. The function is often scaled by the peak isometric force F_{max} (refer to Table 7.4).

The Gaussian-shaped tension-length relationship (Eq. 7.9) was given by Winters and Woo (1990).

$$F_{TL} = e^{-S_k \cdot (|L| - L_{opt})^2} \quad \text{Eq. 7.9}$$

where, L_{opt} is the optimum stretch and S_k is a model parameter.

Equation (Eq. 7.10) provided by Fung (1993) can be used to describe tension-velocity relationship, which accounts the shortening effect of muscle force.

$$F_{Tv} = \frac{1 + \frac{v}{v_{max}}}{1 - \frac{v}{v_{max} \cdot CE_{sh}}} \quad \text{for, } v < 0 \quad \text{Eq. 7.10}$$

where, the muscle velocity v is for shortening, v_{max} and CE_{sh} are model parameters.

Equation (Eq. 7.11) provided by Winters and Woo (1990) can be used to describe tension-velocity relationship for the lengthening effect of muscle force.

$$F_{Tv} = \frac{1 + \frac{v}{v_{max}} \cdot \frac{CE_{ml}}{CE_{shl}}}{1 - \frac{v}{v_{max} \cdot CE_{sh}}} \quad \text{for, } v > 0 \quad \text{Eq. 7.10}$$

where, the muscle velocity v is for lengthening, v_{max} , CE_{shl} and CE_{ml} are model parameters.

The mathematical model to represent the force in the parallel elastic element F_{PE} using an exponential relationship was proposed by Winters and Stark (1985):

$$F_{PE} = \frac{F_{max}}{e^{K_{sh}} - 1} \cdot \left[e^{\frac{K_{sh}}{L_{max}} \cdot (L - L_0)} - 1 \right] \quad \text{for, } L > L_0 \quad \text{Eq. 7.11}$$

where, F_{max} is the maximum force and L_0 is the initial length of the muscle, and K_{sh} and L_{max} are model parameters.

Table 7.9 Material properties used to model the D-neck

Tissue	Constitutive law	Material properties	Reference
Cortical bone	Power law plasticity [018] Rigid (T1) [020]	$E=16.7$ GPa, $\nu=0.3$	Panzer, 2006; Currey, 2004
Cancellous bone	Power law plasticity [018] Rigid (T1) [020]	$E=0.291$ GPa, $\nu=0.3$	Kopperdahl & Keaveny, 1998; Panzer, 2006;
Nucleus pulposus	Viscoelastic [006]	$K=1.72$ GPa, $G_0=17.8$ kPa, $G_f= 7.1$ kPa, $\beta=1/s$	Yang and Kish, 1988; Östh, 2016
Annulus fibrosus	Isotropic elastic [001]	$E=0.025$ GPa, $\nu=0.4$	Zhang et al., 2006 *
Spinal cord	Incompressible hyperelastic [077_O]	$G=188.2$ kPa, $\nu=0.45$, $\mu_1= 99.4$ kPa, $\alpha_1=4.7$	Clarke, 2011 *
Facet cartilage	Isotropic elastic [001]	$E=0.63$ GPa, $\nu=0.1$	Östh, 2016; Yamada, 1970 *
Transverse ligament	Isotropic elastic [001]	$E=0.04$ GPa, $\nu=0.3$	Halldin et al., 2000; Chazel et al., 1985; *
Other ligaments	Nonlinear elastic [S04]	Table 7.5 – 7.8	Panzer, 2006; Chazel et al., 1985; Hayashi, 2003
Neck skin	Isotropic elastic [001]	$E=0.006$ GPa, $\nu=0.4$	Östh, 2017a; Manschot and Brakkee, 1988; *
Neck soft tissues	Incompressible hyperelastic [077_O]	$G=3$ kPa, $\nu=0.499$, $\mu_1= 0.03$ kPa, $\alpha_1=20$	Östh, 2017a; Engelbrektsson, 2011
Muscles	Hill-type muscle [S15]	$\sigma_{max} = 0.5$ MPa $S_k = 6.25$ $L_{opt} = 1.05$ $V_{max} = 4 (L_{opt}) /s$ $CE_{sh} = 0.55$ $CE_{shl} = 0.1065$ $CE_{ml} = 1.3$ $L_{max} = 0.6$ $K_{sh} = 3$	Winters and Stark, 1988 Winters, 1995 Winters, 1995 Zajac, 1989 Winters and Woo, 1990 Winters and Woo, 1990 Winters and Woo, 1990 Winters, 1995 Winters, 1995

*Modified with assumption

Neural excitation (Eq. 7.12) and active state dynamics (Eq. 7.13) states the muscle activation for the Hill muscle [Winters and Stark, 1985].

$$\frac{d}{dt} E(t) = \frac{u(t) - E(t)}{\tau_{ne}} \quad \text{Eq. 7.12}$$

$$\frac{d}{dt} a(t) = \frac{u(t) - a(t)}{\tau_a} \quad \text{Eq. 7.12}$$

where $u(t)$ is the idealized neural input ($0 < u(t) < 1$), τ_{ne} is the neural excitation time constant and τ_a is the active state time constant. The muscle is in the activation state only when $E(t) > a(t)$.

The overall material properties and constitutive laws used to model the different parts of the D-neck are given in Table 7.9.

7.4 The model response in Compression

7.4.1 Simulation method for compression

The D-neck model was evaluated against the experimental results for compressive loadings [Nightingale et al., 1996a; Nightingale et al., 1996b; Nightingale et al., 1997; Camacho et al., 1997]. In the experiments (Figure 7.11a), the entire head and the spine through the second thoracic vertebra of a PMHS (T2) was used to conduct an axial impact. The impact anvil was made of steel cylinder with 152.5 mm of diameter and 40 mm of thickness for rigid surface tests. Further thick Teflon surface was added in order to conduct frictionless impacts. The impact angles between -15° and 30° were set for performing the tests with 10 specimens. The initial speed of the impacts was on the order of 3.2 m/s. A three-axis load cell under the impact surface for measuring the impact forces on the head and a six-axis load cell at the first thoracic vertebra (T1) for measuring the forces and moments on the neck were implemented in the experimental setup. Also, two accelerometers were added to the head and T1.

Figure 7.11b shows the computational model of the experimental setup. The initial velocity was set to 3.2 m/s [Camacho et al., 1997; Halldin et al., 2000]. The rigid ($E=207$ GPa, $\rho=8$ g/cm³) anvil (diameter of 152.5 mm and height of 40 mm) was modelled with brick elements, where one layer of 10 mm on the top was added as Teflon and modelled with isotropic elastic-plastic material ($G=0.5$ GPa, $\rho=2.2$ g/cm³). The co-efficient of friction was taken as 0.04 for the contact between the head and the impact surface. The impact surface was oriented to three different angles: 0° , $+15^\circ$ and -15° as shown in the Figure 7.11b. A fixed mass of 16 kg from the torso was assigned to T1 in the model to maintain the similarity with the experiments.

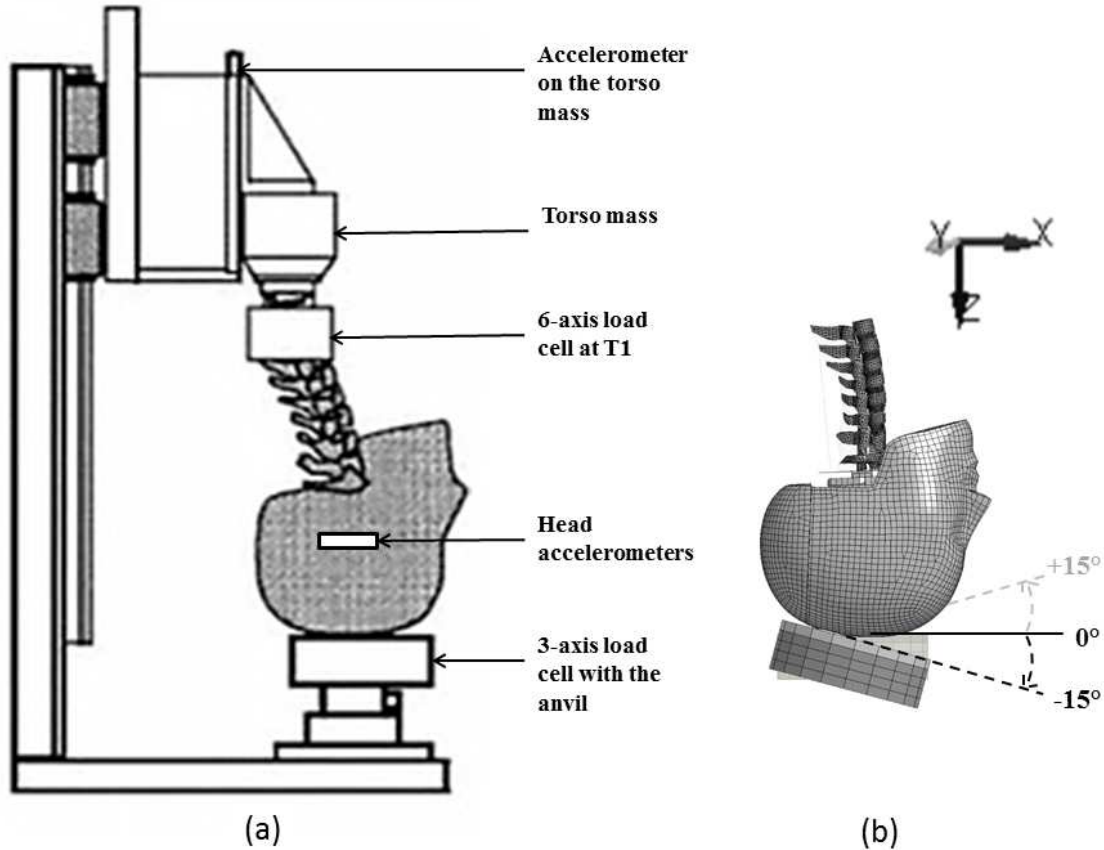


Figure 7.11 (a) The experimental setup with PMHS head and cervical spine [adapted from Nightingale et al., 2016] and (b) FE model for the simulation replicating the experimental setup

The explicit FE solver LS-DYNA[®] R6.1.1, using Intel[®] Xeon[®] CPU @ 3.60 GHz, was utilized to run the simulations. The cervical spine model used in this simulation consisted of 94997 elements. The time needed to run one simulation of 60 milliseconds on quad core processor was approximately 1 hour and 8 minutes.

7.4.2 Evaluation of D-neck model in compression

The global response of D-neck model was compared in two ways. The first way was involved in comparing the neck motion. The kinematics of the D-neck model was in good agreement with that in the experiments. Figure 7.12 shows the time lapse of the comparable neck kinematics till 18ms from the time of impact. The red lines in the figure represent the approximate outer boundaries of the PMHS neck from the experiments. The lines were drawn from the published figures [Camacho et al., 1997], where the figures from both experiment and simulation were overlapped with each other for comparing the identical sizes. The motion of the D-neck agrees comparatively more with the PMHS neck for -15° impact.

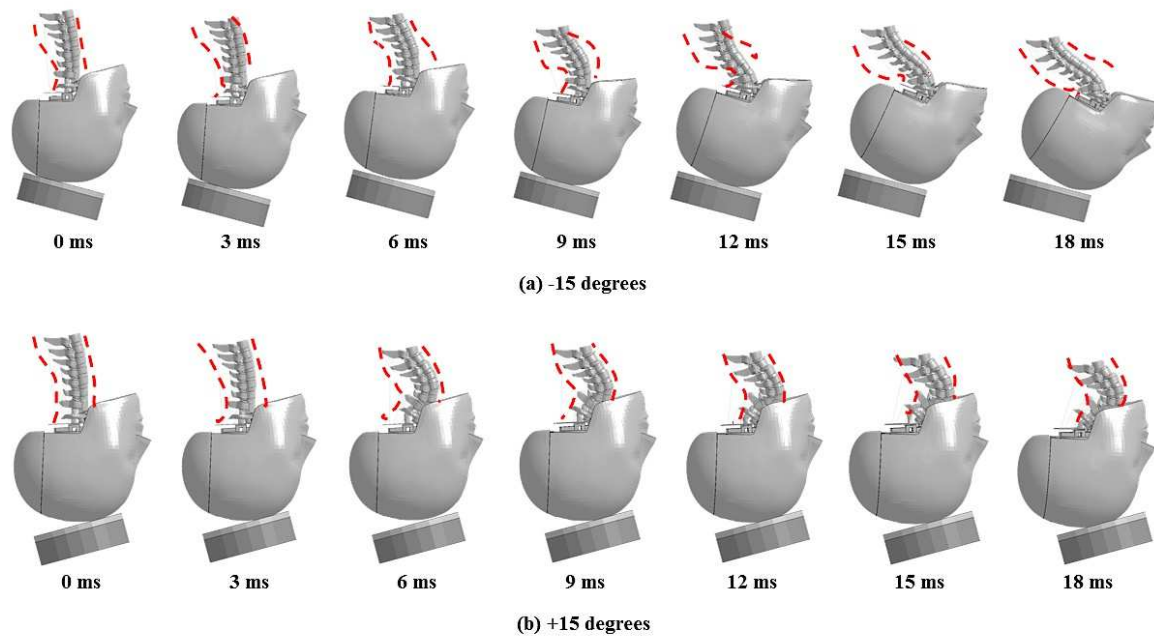


Figure 7.12 Time lapse of the neck kinematics for the compressive impact with rigid impact surface. The orientations of the surface are (a) -15° and (b) $+15^{\circ}$. The dotted red line represents the neck position in the experiments by Nightingale et al.

The second way of comparison followed the approach of other researchers based on the boundary conditions [Camacho et al., 1997; Halldin et al., 2000]. The simulated D-neck response was compared with the published experimental corridors [Camacho et al., 1997] as shown in Figure 7.13. The experimental corridors were developed for the impact tests on rigid surface followed by the experiments performed on the PMHS specimens [Nightingale et al., 1996a; Nightingale et al., 1996b; Nightingale et al., 1997]. The data were filtered at 1000 Hz following the SAE J211 specifications. Apparently, there are some differences in the head acceleration, though the neck force of D-neck is in excellent agreement with experimental corridors. Moreover, the second peak of the head acceleration is observed in the simulations as the head re-bounces after the impact. The reason is assumed to be that the hybrid III head model consists of one rubbery skin layer modeled with viscoelastic constitutive laws, where the PMHS skin was absent in the experiments. Hence, the hybrid III head gives more elastic response than the PMHS head. Further comparison of the upper neck shear and axial forces and the neck moment at occipital condyles are given in Appendix C.

Extensions of this study with full-body and muscles integration to the D-neck model are provided in Appendices D and E.

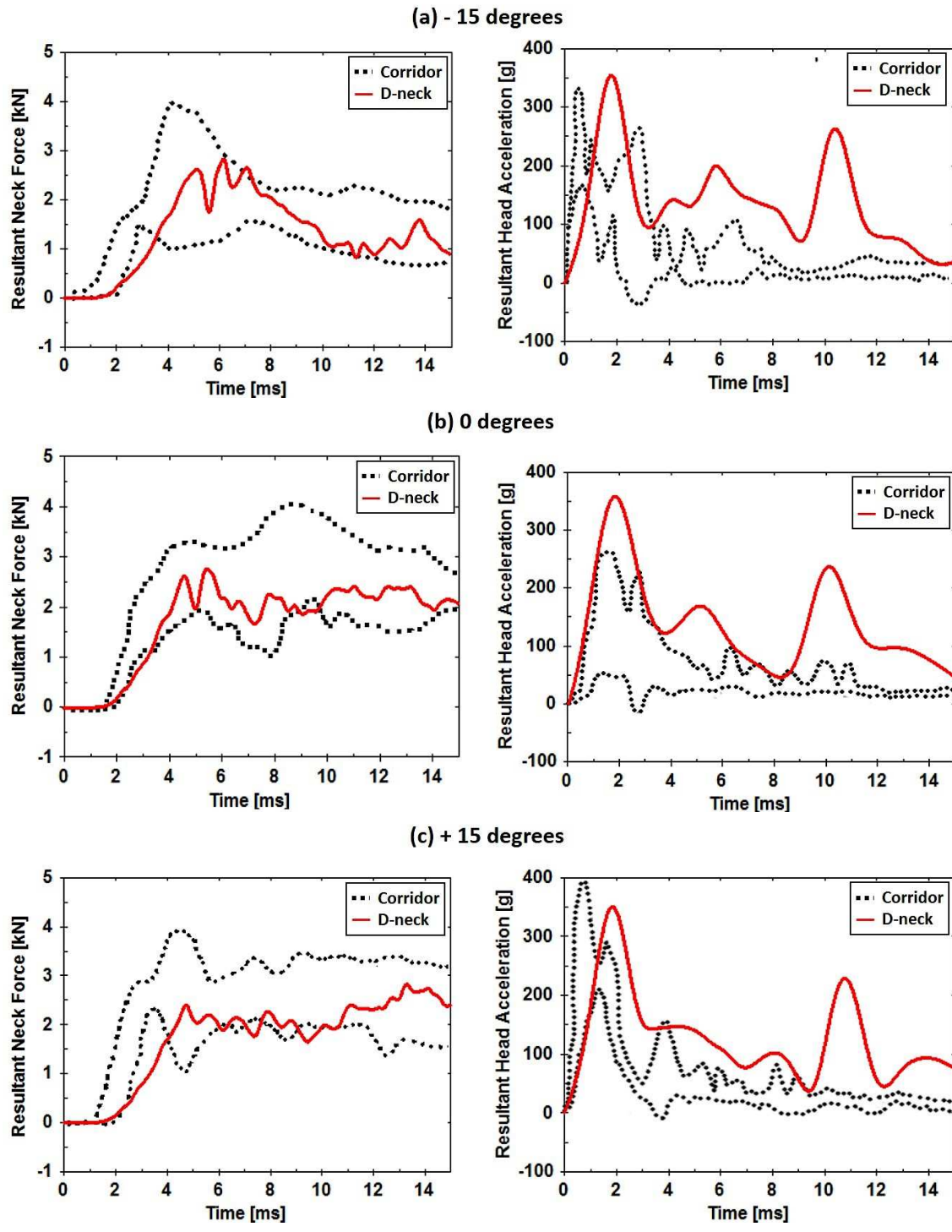


Figure 7.13 The comparison between the experimental and simulated results for the impact angles of (a) -15°, (b) 0° and (c) +15°. The black dotted lines represent the experimental corridors [Camacho et al., 1997] and red solid lines show the response of D-neck model.

7.5 The model response in frontal impact at 15 g acceleration

7.5.1 Simulation method for the impact at 15g acceleration

The kinematic response of the D-neck model for inertial loading in frontal impact was evaluated against the sled tests performed at the Naval Biodynamics Laboratory (NBDL) [Ewing et al., 1978a; Thunissen et al., 1995]. The test data were taken from studies on human volunteers subjected to 15g sled acceleration ($1g = 9.81 \text{ m/s}^2$).

The young and well-trained volunteers were allowed to sit on a rigid seat mounted on a HYGE accelerator in an upright position, and accounted to short duration accelerations for frontal impact. The volunteers were sufficiently constrained to vertical or lateral displacement of the T1 vertebra by means of occupant restraint systems like shoulder straps with inverted V-pelvic strap and a lap belt. The resulting three-dimensional motions of the head and T1 were monitored using an assembly of accelerometers and cameras mounted to the test subject as shown in Figure 7.14a.

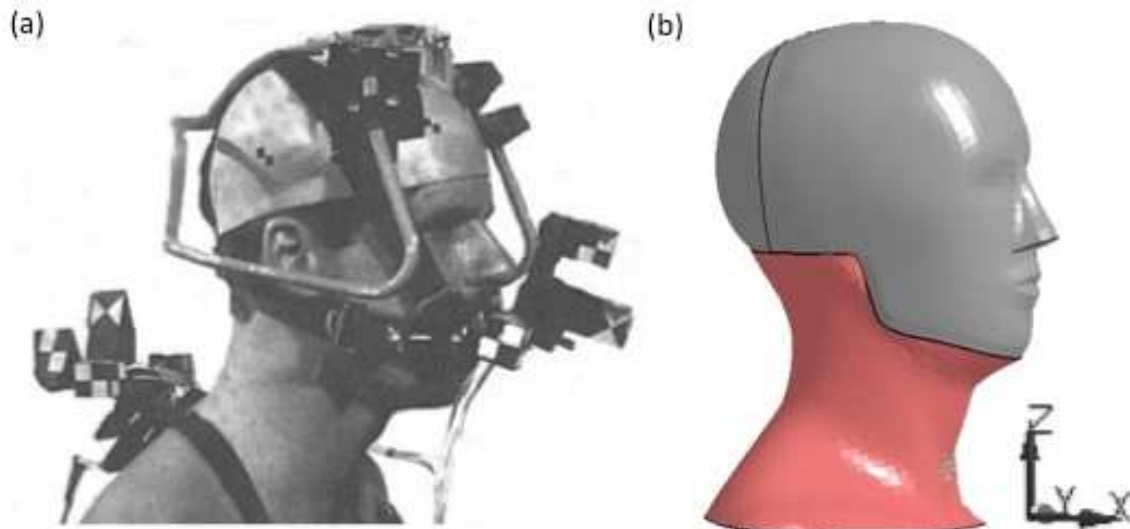


Figure 7.14 (a) The test setup with human volunteer and (b) the numerical head-neck model used to perform the sled tests

The full neck model (shown in Figure 7.14b) was used to simulate the frontal impact at 15g sled acceleration, which consists of the head, eight vertebrae, intervertebral discs, ligaments, neck musculature, neck skin and neck soft tissues as described in Section 7.2. The global coordinate system, as shown in Figure 7.14b, was considered.

The initial head angle in the experiment was 0 degrees and the lordotic angle of the cervical spine was not reported. The head angle was defined as the angle between the Frankfort plane and the horizontal plane, where the Frankfort plane is defined as the imaginary plane passing through the upper margin of the ear canals and the inferior margin of the orbit. The lordotic angle is the normal inward curvature of the spine in the

cervical and lumbar region. The average neck length and average head mass of 8 volunteers participated in the tests were 16.1 cm and 4.76 kg respectively. In the simulation, the model parameters were: the head angle of 0 degree, the lordotic angle of 10 degrees, the head mass of 4.67 kg and neck length of 15.14 cm. The neck length was measured as the initial distance between the head anatomical origin (AO) and the T1 vertebra. On the hybrid III head, the AO was taken from the head-neck joint beam, passing through the hole of the neck bracket occiput and representing the occipital condyle of the model.

Although T1 vertebra was sufficiently constrained with the sled, the T1 acceleration was different from the sled acceleration due to the time lag for transferring acceleration from the sled to the T1. It was assumed that the T1 acceleration (Ewing et al., 1968) with a significant amount of T1 rotation (Wismans et al., 1986) in the frontal X-direction is the medium for transferring the sled acceleration to the head during the sled tests. The average T1 X-acceleration and T1 Y-rotation from the recorded experimental data (Thunnissen et al., 1995) were provided as boundary conditions in the simulation (Figure 17.15) while all other motions for the T1 were constrained.

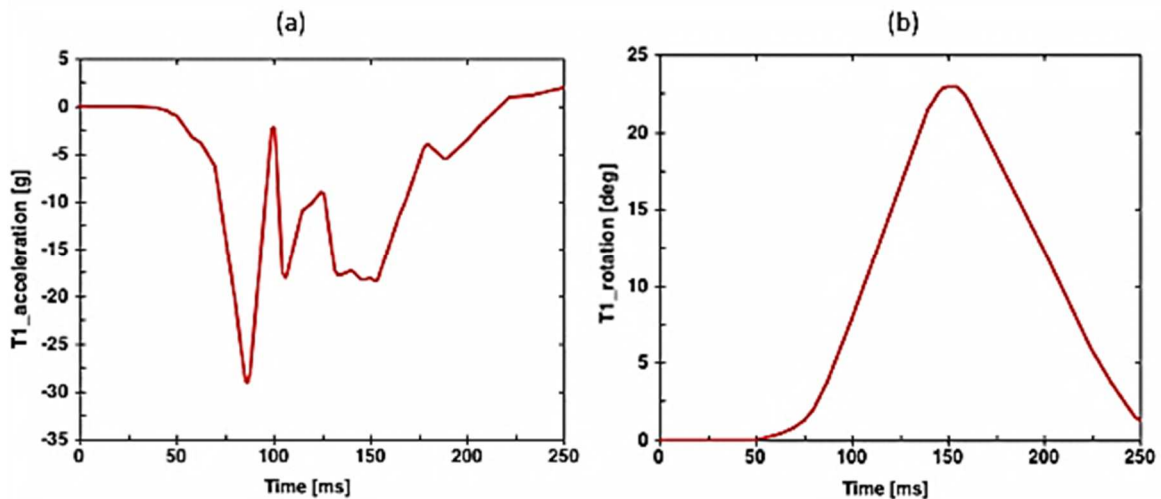


Figure 7.15 Prescribed (a) T1 acceleration in impact direction and (b) T1 rotation in the plane of impact based on the NBDL experiments for frontal impact at 15g acceleration

The activation of the muscles was provided according to the resulting active state values defined in Figure 7.16. It was reported that the neck muscles activate around 74 ms after the onset of sled acceleration in rear impact (Siegmund et al., 2003). Therefore, the active state values were chosen considering that the idealized neural input $u(t)$ initiated at 74 ms and held for 100 ms. The same active state values were used to evaluate the response of the neck model for 7g lateral impacts.

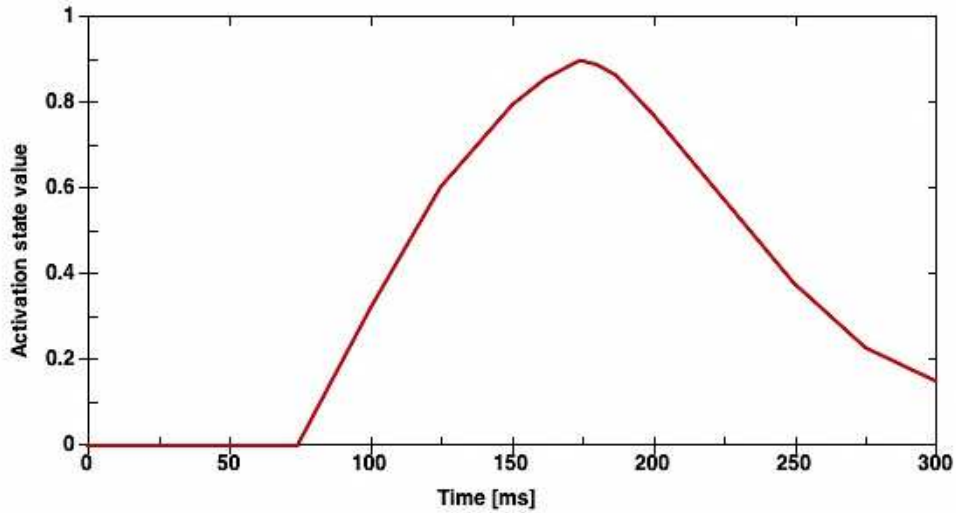


Figure 7.16 The activation state of the muscles used in the simulation of sled tests

The simulation was run with the explicit FE solver LS-DYNA[®] R6.1.1 using Intel[®] Xeon[®] CPU @ 3.60 GHz. The simulation, successfully running till 210 ms, took 6 hours and 39 minutes using quad core processor.

7.5.2 Evaluation of D-neck model in frontal

The graphical response of the active neck model for frontal impact is shown in Figure 7.17. The figure clarifies both the orientation of the neck skin and the muscles with internal structure during the simulation. Although the simulation lasted for 210 ms, the results have been analyzed upto 190 ms due to the instabilities found in the results after that period. The results upto 190 ms are sufficient to evaluate the model response, as the analyses using this model that will be shown in Chapter 9 last for up to 30 ms. However, the head only translates during the first 90 ms without any rotation, because of its inertia resulting in the head lag [Wismans et al., 1987]. Shortly after this the head started to rotate forward allowing the cervical spine to bend in flexion. The head reached its maximum flexion at about 160 ms. The muscle activation started after 74 ms reducing the tensile forces in the cervical spine and continued till the deactivation time.

Figure 7.18 compares the trends in acceleration-time history between the head-neck model in the simulation and the experimental results from the NBDL tests. The comparison shows that there are similarities in the pattern of the acceleration-time profiles. It can be seen from the figure that there is small oscillations in the head accelerations till 70 ms. Moreover, there are some differences in the response of the simulated model than that of the human volunteers.

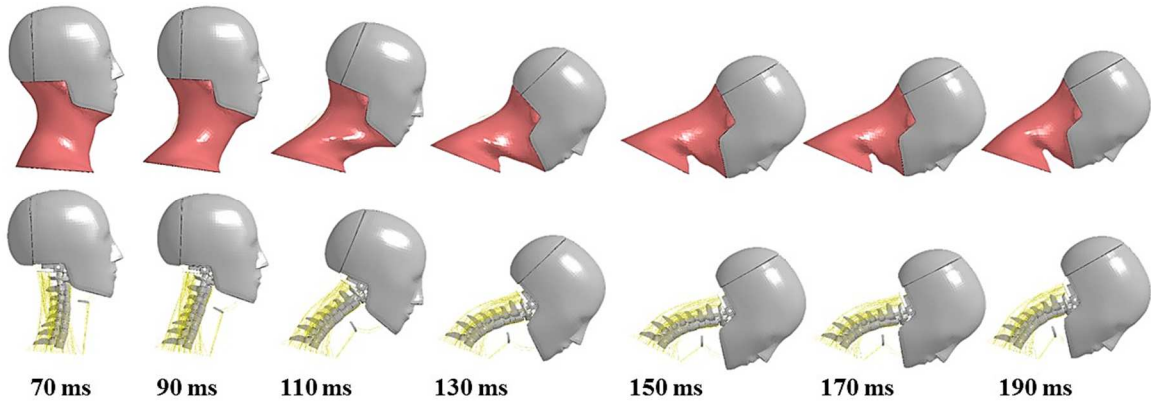


Figure 7.17 Time lapse of the neck kinematics with active muscles for the 15g frontal impact. The orientation of the neck skin (top) and the muscles with internal structure (bottom) are shown separately in the figure.

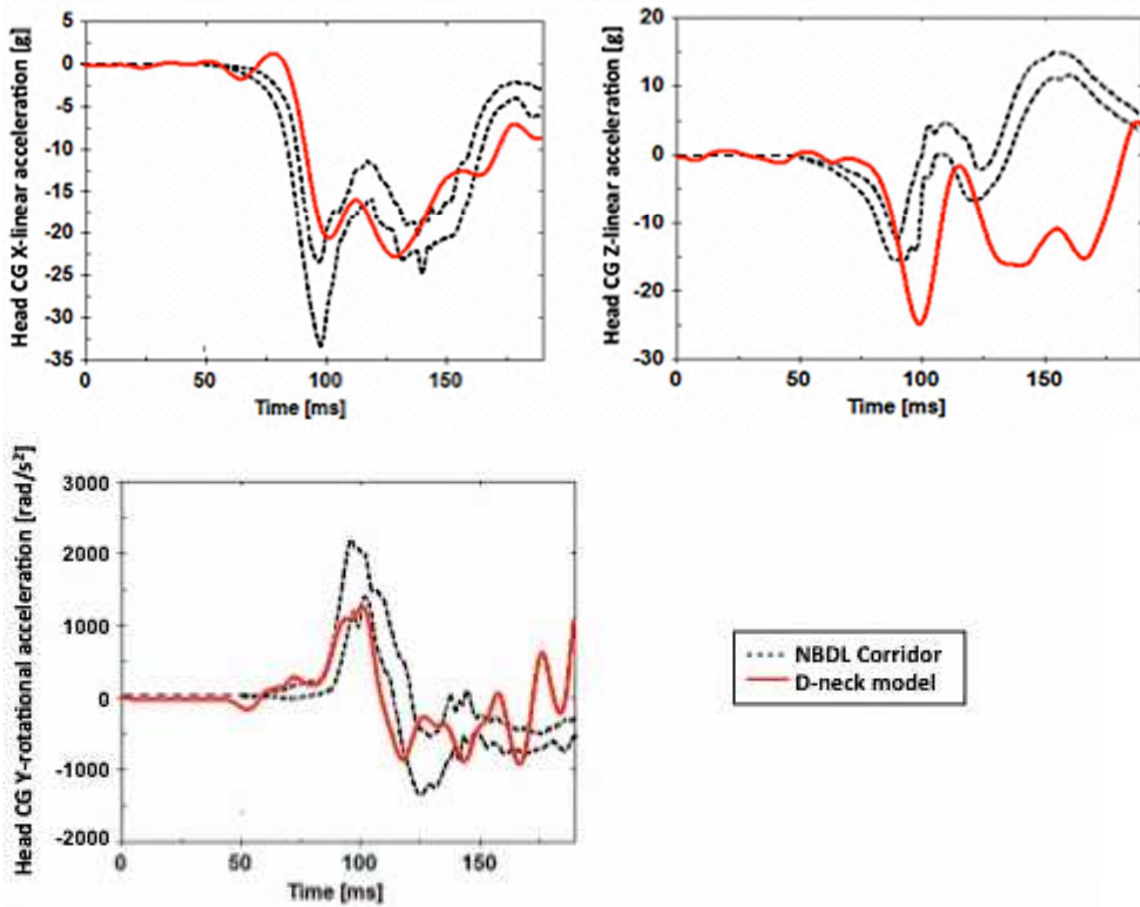


Figure 7.18 Simulated response of the active neck model to 15g frontal impact. The response is compared with experimental corridor as a function of acceleration of head centre of gravity (CG).

Noticeably, the prediction of the peak X-linear acceleration by the head-neck model lagged behind that of the experimental corridors with small delay. After 160 ms, the prediction of the model does not agree well with the NBDL corridor.

There is also an apparent gap between the simulation and the experimental responses for the peak Z-linear acceleration, where the model over-predicts the peak at 100 ms. However, the prediction of the vertical (Z) acceleration of the head CG by the model shows different path than that of the experimental corridors. Lastly, the model response for rotational acceleration around Y-axis agrees well with the experimental results till 170 ms.

7.6 The model response in lateral impact at 7 g acceleration

7.6.1 Simulation method for the impact at 7g acceleration

Similar experimental and simulation methods applied to 15g frontal impact tests were considered, but with small changes, to estimate the global response of the D-neck model in lateral impact at 7g sled acceleration. In addition to the constrained system considered to T1 vertebra by the restraint belts, a chest strap was used to reduce the force on the right shoulder. Moreover, to limit the upper torso motion, the right shoulder of the test subject was encountered with a lightly padded wooden board. Based on the experimental results (Thunnissen et al., 1995), the average Y-acceleration and X-rotation, provided as the prescribed boundary conditions to T1, are shown in Figure 17.19.

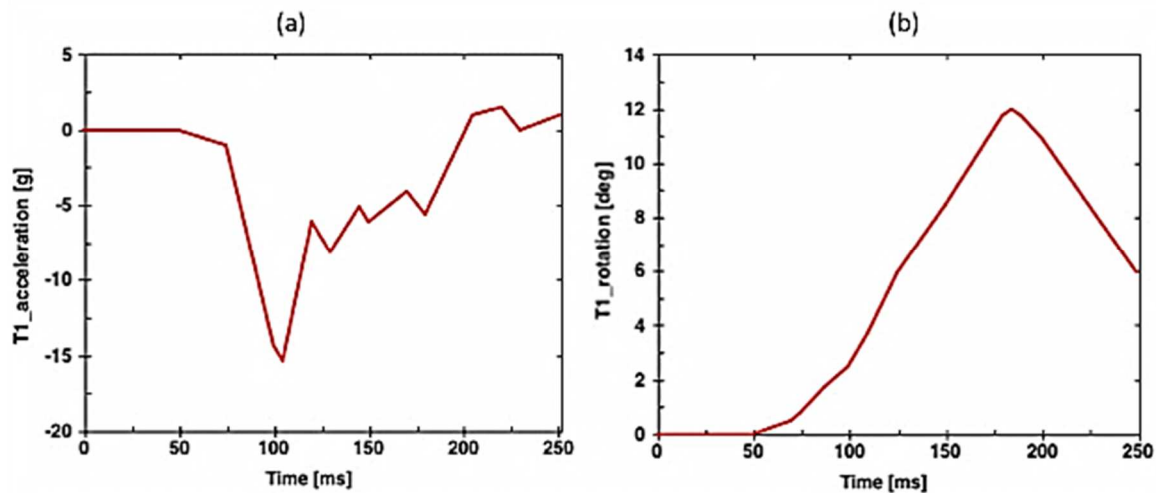


Figure 7.19 Prescribed (a) T1 acceleration in impact direction and (b) T1 rotation in the plane of impact based on the NBDL experiments for frontal impact at 15g acceleration

The identical simulation environment was set as described in Section 7.5.1. The simulation took 5 hours and 58 minutes to run till 190 ms using quad core processor.

7.6.2 Evaluation of D-neck model in lateral impact

Figure 7.20 illustrates the kinematics of the neck skin and the active muscles with internal structure of the neck model at 7g lateral impact. The head started to rotate laterally allowing the cervical spine to bend in lateral flexion and slightly in torsion after 90 ms. The results have been analyzed upto 160-170 ms due to the instabilities observed in the results afterwards, although the simulation lasted for 190 ms. The time is sufficient to evaluate the model response in lateral impact, as the further analyses using this model in Chapter 9 will be shown for direct impact to head upto 30ms.

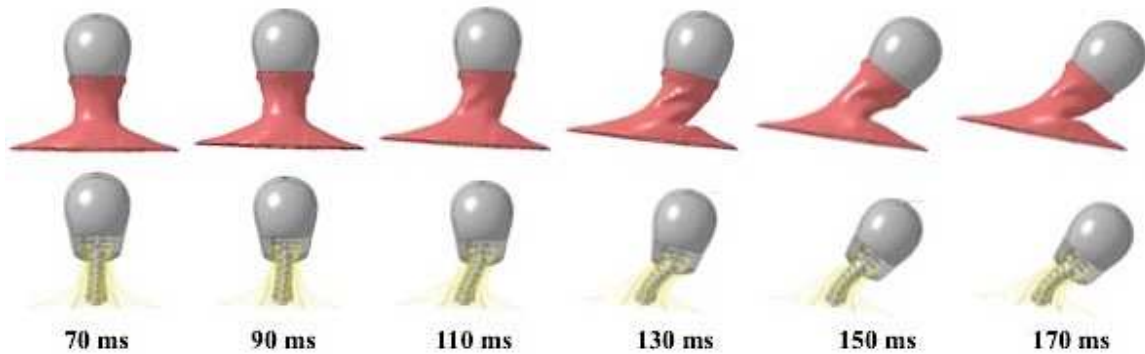


Figure 7.20 Time lapse of the neck kinematics with active muscles for the 15g frontal impact. The orientation of the neck skin (top) and the muscles with internal structure (bottom) are shown separately in the figure.

The global acceleration response in terms of time of the simulated head-neck model was compared to the NBDL experimental data for 7g lateral impact as shown in Figure 7.21. The figure shows that the trends in acceleration-time history of the model agree well with experimental corridors. However, there are areas where the response of the model differs from the responses of the volunteers.

There are lags of the model response due to oscillations in the acceleration-time curve in the forward X-direction and the response goes significantly different after 155ms. The response agrees well in the lateral Y-direction except a slight lag in the peak linear acceleration. The linear acceleration in the upward Z-direction agrees well before 140 ms.

The prediction of the lateral bending of the neck model by head CG rotational acceleration around X-axis agrees too well with NBDL corridor, but there are small differences in the prediction of the neck torsion by head CG rotational acceleration around Z-axis.

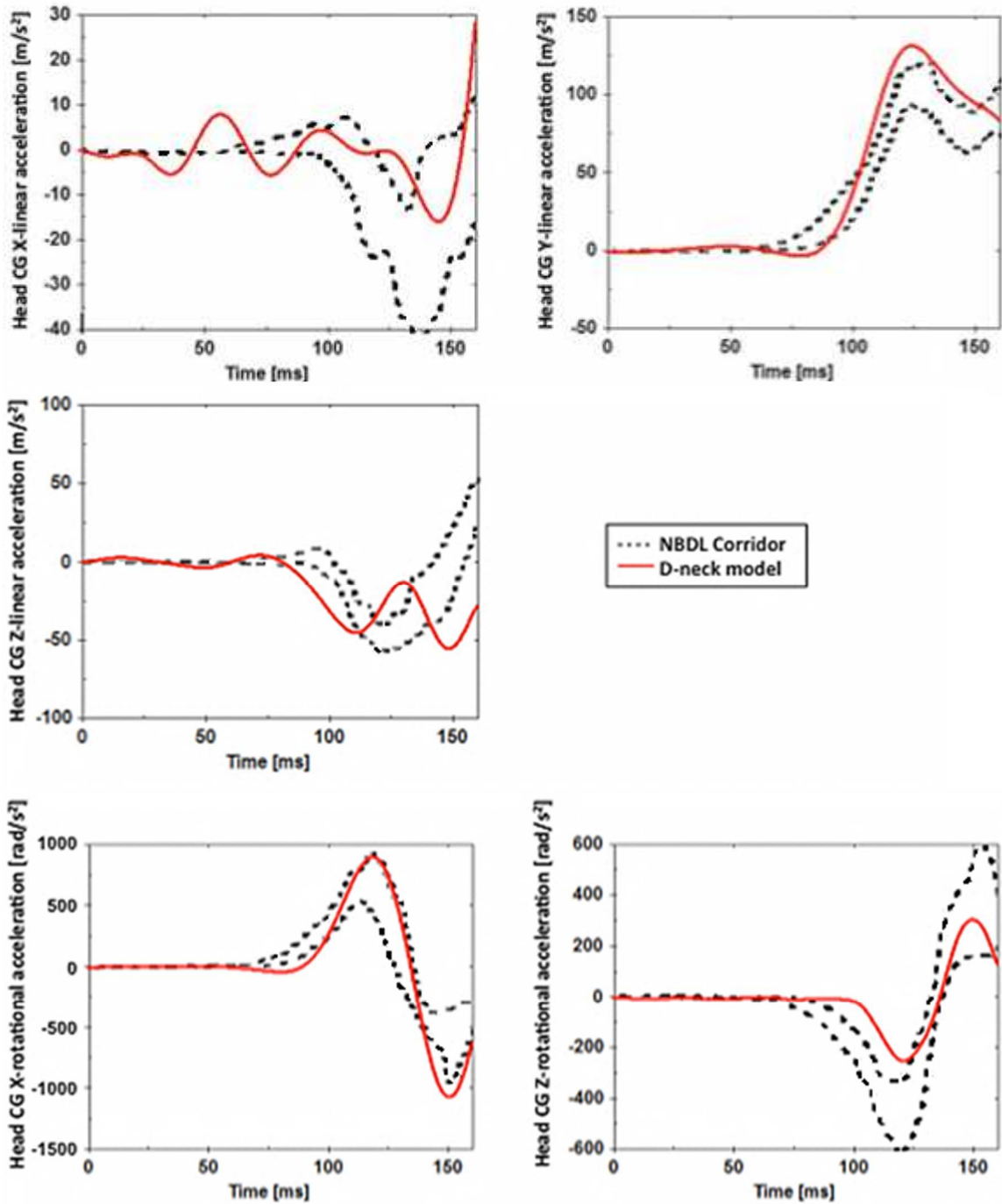


Figure 7.21 Simulated response of the active neck model to 7g lateral impact. The response is compared with experimental corridor as a function of the acceleration of the head centre of gravity (CG).

Chapter 8

Innovative Protection Systems

A variety of neck braces exist in the market as explained in Section 3.6 (Figure 3.7 and 3.8 referable). Although the effectiveness of those neck braces is not clear due to the lack of scientific evidences of the injury reduction, the trade of those devices in the market suggests the demand of production. Currently, there is no official standard regulation for neck protectors. Therefore, the achievement of minimum safety criterion cannot be assessed.

This chapter explains the development of a few prototypes based on innovative ideas. The focus has been given on understanding the mechanism of these devices and also their injury reduction capability using numerical simulation described in Chapter 9. The results will definitely guide the researchers and designers to select from the comparable parameters while designing neck protectors and also while developing a standard.

8.1 Reference PPE

8.1.1 Helmet model

The most of severe injuries produced at the cervical spine region are produced due to an indirect loading [ACEM, 2004; MOSAFIM, 2013]. Hence, it is necessary to include head and torso for studying the neck injury mechanism and protection. Moreover, the helmet is compulsory to wear according to the law in the European countries and also in the most of the countries around the world. Considering these facts, Pista GP AGV E2205 Multi Gran Premio helmet model (Figure 8.1), a product of Dainese S.p.A., was used for evaluating the design and effectiveness of different neck protection systems.



Figure 8.1 Pista GP AGV E2205 Multi Gran Premio reference helmet model to evaluate the neck protectors [adapted from www.Dainese.com]

8.1.1.1 Finite Element (FE) model Construction

The helmet FE model, as in Figure 8.2, was generated by the CAD model of the aforementioned commercial racing helmet. The helmet consists of three parts: outer shell, inner foam liner and restraint system [Cernicchi, 2008]. The carbon fiber reinforced shell of the helmet was modelled with orthotropic composite material model with Chang [Chang and Chang, 1987] failure formulation. In reality, the shell has different orientations of fibers in different regions. For the sake of simplicity, one unique fiber orientations [(0), (45), (0)] had been chosen considering the fact that this study does not focus on helmet optimization.

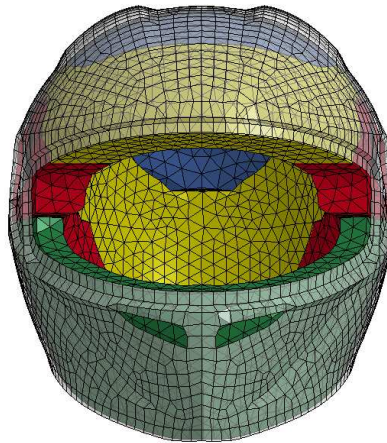


Figure 8.2 The FE helmet model showing the composite shell (outer semi-transparent layer) and the different regions of the foam liner [chin (green), cheek (red), main (yellow) and top (blue)]

The inner EPS (expanded polystyrene) foam liner has four different regions: main (50 kg/m^3), cheek (60 kg/m^3), chin (60 kg/m^3) and top (35 kg/m^3). The liner was modelled with isotropic crushable foam material model and stress-strain curves were provided to the foam material properties as shown in Figure 8.3.

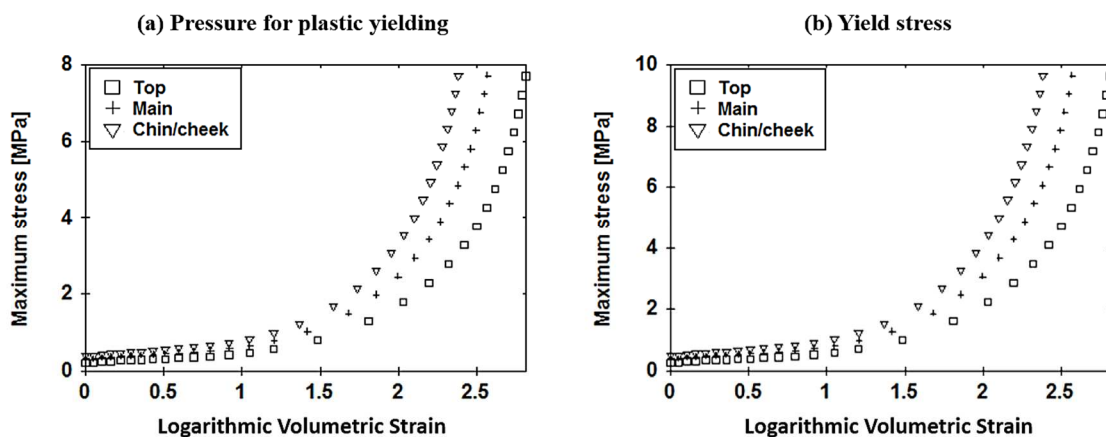


Figure 8.3 Compressive stress-strain curves used for modelling the foam parts, which are defined for: (a) pressure yield and (b) yield stress

The restraint system, which has negligible effect in the study of compressive impacts, was modelled with 2 nonlinear elastic discrete elements. The values of the results might be affected for other impacts, but the assumption is that the dynamics of the neck and the comparison in the results will be negligibly affected. The material properties used for modelling the helmet are given in Table 8.1.

Table 8.1 Material properties of the helmet model

Part	Constitutive law	Elastic Modulus [MPa]	Poisson's ratio
Outer shell	Orthotropic composite [054]	$E_a, E_b = 50000$	$\nu_{ba} = 0.085$
Top EPS	Isotropic crushable foam [075]	12.93	0.01
Main EPS	Isotropic crushable foam [075]	19.06	0.01
Chin/Cheek EPS	Isotropic crushable foam [075]	25.02	0.01
Restraint system	Nonlinear elastic spring [S04]	1	-

8.1.1.2 Validation

The helmet has been validated based on the European helmet standard ECE R22.05 [ECE, 2002]. The standard includes drop tests at two extreme conditions: -20°C and 50°C . Both flat and kerbstone shaped anvils are used for performing the tests, which are performed on five points as indicated in Figure 8.4: P, B, R, X and S. Impact velocities of 7.5 ms^{-1} (for points P, B, R and X) and 5.5 ms^{-1} (for point S) are needed. Then the final evaluation for pass/fail criteria is done using the value of the peak resultant linear acceleration measured at the center of gravity (CG) of the headform.

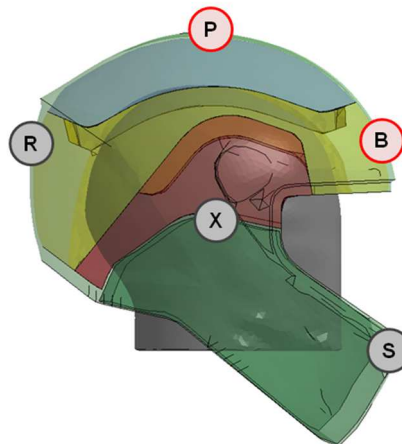


Figure 8.4The configuration of the helmet and headform in the simulation environment. The inverted drop tests were simulated at points P and B. The other points according to the Standard ECE R22.05 are R, X and S [ECE, 2002].

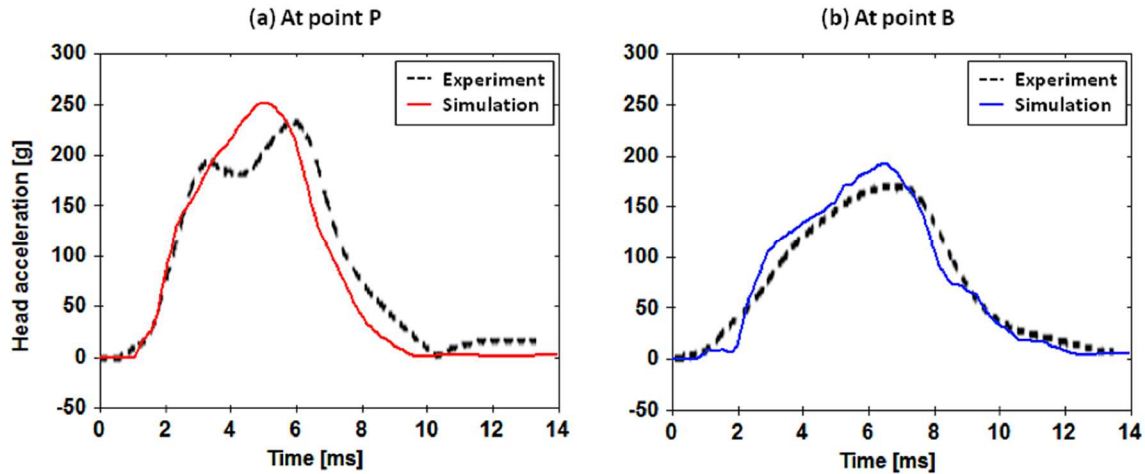


Figure 8.5 The comparison between the experimental and simulated results of the drop tests with helmeted headform at points (a) P and (b) B.

For the validation purpose, the experiments were carried out at points P and B with 7.5 ms^{-1} of initial velocity. Evaluation of the simulated results based on these two points are sufficient, as these points include the impact on EPS main and top liners. All the impacts simulated for this study were performed on the helmets around these liners. Only flat anvil and room temperature were chosen for the drop tests. The headform size was “J” according to the Standard. The simulations were performed with same boundary conditions as in the experiments. The linear accelerations of the simulations and the experiments, as a function of time, were compared in Figure 8.5. The results are in good agreement except for a slight over estimation of the peak acceleration in the simulations. The reason for the small difference may be the commercial helmet includes also the comfort padding, which has some impact on the results. Moreover, the helmet FE model used here acceptably serves the objectives of this study as the helmet optimization or comparison among different helmets is not the main objectives.

8.1.2 Hybrid Neck Brace

It is important to consider at least one reference neck protection device that exists in the market for comparing the newly designed prototypes and their effectiveness. The reason is the unavailability of certified standard for neck protectors for the assessment. Moreover, the comparison with the reference model will help to understand the mechanism needed to produce any neck protectors with more effectiveness. Commercial Dainese carbon hybrid neck brace (as shown in Figure 8.6) has been chosen for the evaluation purpose.



Figure 8.6 Dainese Carbon Hybrid Neck Brace as reference model for comparison [adapted from www.Dainese.com]

The FE hybrid neck brace model, shown in Figure 8.7, was generated in LS-PrePost V.3.3 using the CAD file of the aforementioned neck brace. The foam liner is made of Polyurethane (PU) foam (0.4g/cm^3). Low-density foam constitutive material law [MAT_057] for the tetrahedral elements was used to model the PU foam. Stress-strain relationship (Figure 8.8) from dynamic compression test was provided to the material properties.

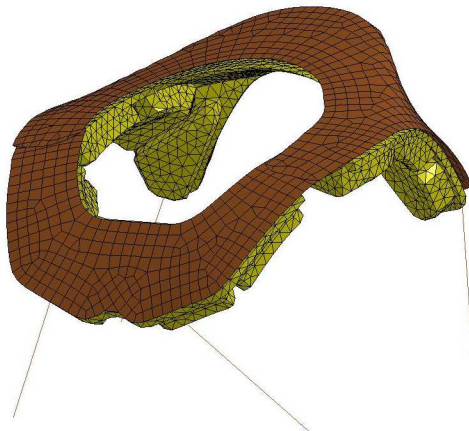


Figure 8.7 FE Hybrid neck brace model

The shell liner is made of carbon fibre composite. For modeling the liner, material properties and element generation similar to that used for modeling the shell of the helmet (described in Section 8.1.1.1) were considered. The thickness of the liner was taken as 2 mm. The restraining system consists of shoulder belts, which was modeled with four discrete elements similarly to the modeling of retention system of the helmet.

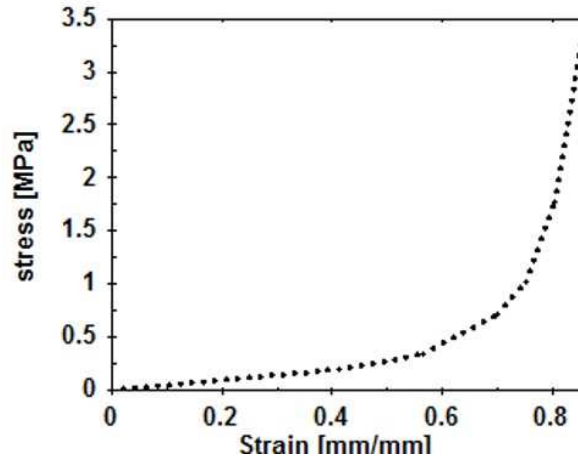


Figure 8.8 Stress-strain relationship of PU foam

8.2 New Prototypes

8.2.1 Soft Neck Brace

The concept of the soft neck brace was inspired by the Dainese hybrid neck brace and energy absorbing foams as shown in Figure 8.9. The idea was to replace the hard layer of the hybrid neck brace made of carbon fibre with soft energy absorbing foam, which also works as energy damping pad.



Figure 8.9 The concept of soft neck brace was inspired by Dainese Carbon Hybrid Neck brace (left) [adapted from www.Dainese.com] and energy absorbing foams (right)

The soft brace has been designed as layers of different types of foams: two layers of Poron® XRD foam, one layer of polyurethane comfort foam and one layer of nitrile butadiene rubber (NBR) placed in between the two Poron layers (Figure 8.10 (left)). The complete structure of the soft brace has been made with 5 pieces of such layered structure and these pieces were joined by elastic bands as shown in Figure 8.10 (right). The shape

and placement of the pieces followed the geometry of hybrid neck brace. The total thickness of the layered foam structure has been kept identical to the height of the hybrid neck brace.



Figure 8.10 The complete structure of the soft brace (right), which has been designed as layers of different types of foams: two layers of Poron XRD foam, one layer of polyurethane comfort foam and one layer of nitrile butadiene rubber (NBR) placed in between the two Poron layers (left).

The final prototype of the soft neck brace (Figure 8.11) has been constructed by placing the layered structure foams inside soft elastic fabrics, where retention system has been integrated to keep the brace firmly attached with the shoulder. The simplicity in design of this brace overcomes the complexity while wearing the bulky structure of hybrid neck brace and also makes it comfortable while riding.



Figure 8.11 The final prototype of the soft neck brace

Figure 8.12 shows the FE model of the prototype of soft neck brace. The geometry of the soft brace was designed and the mesh was generated in LS-PrePost V.3.3. The model consists of four parts: Nitrile Butadiene Rubber (NBR), PORON[®] XRD foam, soft elastic fabric and restraining system.

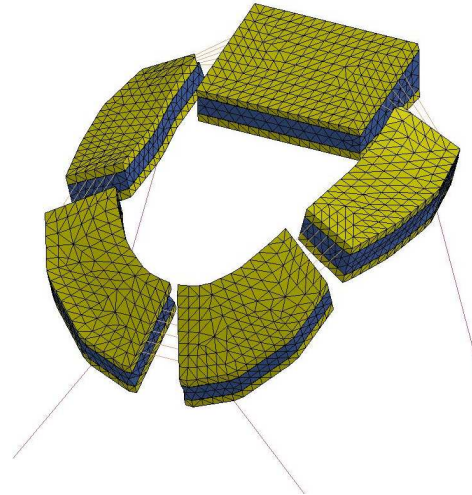


Figure 8.12 FE model of the soft brace

The foam parts were modeled with tetrahedral elements and were tied with each other as shown in Figure 8.12. The material properties and constitutive law for NBR (0.18 g/cm^3) was assigned according to Nasim et al. (2017). The same constitutive law of low-density foam [MAT_057] was used for modeling the PORON foam (0.245 g/cm^3). The stress-strain curves for NBR and PORON used in the model are shown in Figure 8.13, which were achieved from dynamic compression tests.

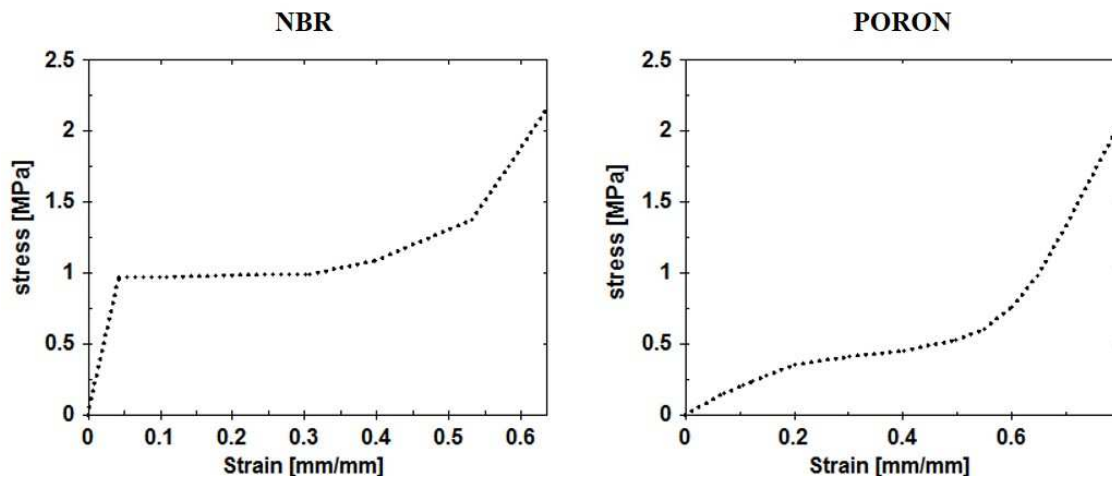


Figure 8.13 Stress-strain relationship of NBR and PORON energy absorbing polymers

The soft fabric and the restraining system were modeled with discrete elements. The force-deflection curve, achieved by tensile tests, was provided to model the soft fabric as shown in Figure 8.13. The modeling of the restraining system was kept similar to that for the helmet and hybrid neck brace.

8.2.2 Neck Collar

The neck collar was designed using two elastic bands of different young modulus and one soft elastic fabric. The design has been inspired by Dainese developed pressure suit (Figure 8.14) for the astronauts in collaboration with the European Space Agency (ESA). The suit aims to counteract the stretching of the spine in space, which might be the cause of the lower back pain to the astronauts.



Figure 8.14 Dainese developed pressure suit for the astronauts in collaboration with the European Space Agency (ESA), an inspiration for developing the neck collar [adapted from www.Dainese.com]

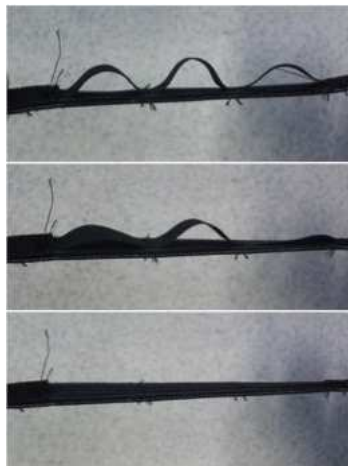


Figure 8.15 The mechanism of the two elastic bands of different young modulus used as the key feature of the neck collar, where the bands are attached with each other in such a way that the stiffer band allows the flexible band to be elongated smoothly until it reaches to the length of the stiffer band



Figure 8.16 The mechanism of the bands, shown in Figure 8.7, where bands were attached with helmet and jacket

The mechanism of the collar has been demonstrated in Figure 8.15, where the two bands are attached with each other in such a way that the stiffer band allows the flexible band to be elongated smoothly until it reaches to the length of the stiffer band. The two band mechanisms have been considered in this design, so that the neck moment at occipital condyle could be reduced. The combined mechanism of these bands attached with helmet and jacket are shown in Figure 8.16.



Figure 8.17 The prototype of neck collar: fixing with helmet (left), front view (middle) and side view (right)

Finally, the bands were sewed on a soft and elastic woven fabric from four positions of the neck: front, back, right and left (Figure 8.17). The woven fabric was given the similar shape of a neck, which was in accordance with the shape of Dainese Balaclava, a product used as wind-stopper for the motorcyclists. For opening purpose, three zippers were

joined with the bands from front and two sides. The design lacks of proper fixing method with helmet and jacket, as the loose fixing will result in malfunctioning of the design.

The prototype of neck collar has three different parts to create force between helmet and jacket: soft fabric, combined band and stiffer band, so that the sudden movement of the head can be restricted. These parts were modeled with assemblies of discrete elements (as illustrated in Figure 8.18) according to the positions used in the design. It was sufficient to model collar with discrete elements as the mechanism of the design depends on force generated by helmet and jacket. The force-deflection curves (Figure 8.19), resulted from the tensile tests using the instrument shown in Figure 6.10b, were used in the non-linear elastic constitutive material law [MAT_S04] to model the soft fabric and combined bands. The stiffer band was also modeled with discrete element using the same material properties as in the helmet retention system.

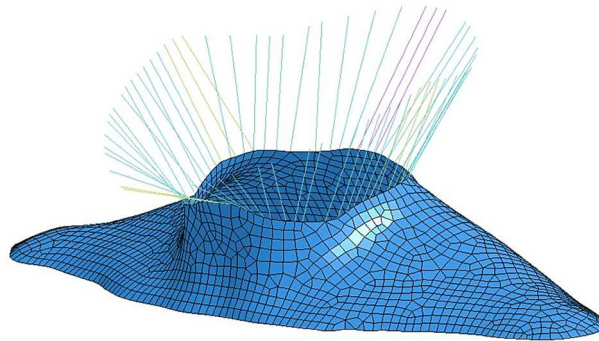


Figure 8.18 FE model of the neck collar

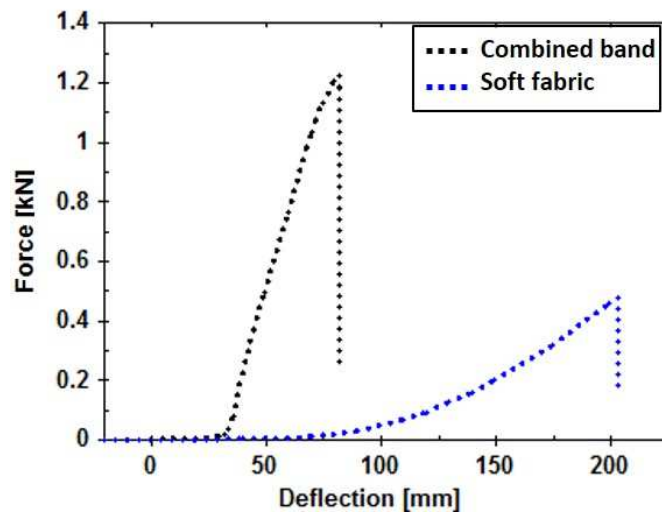


Figure 8.19 Force-deflection curves of the bands used to model the neck collar

The Jacket was also modeled to properly investigate the function of the collar. The jacket was assumed to be made of elastic Nappa leather, which is widely used in motorcycle

jacket. Quadrilateral elastic ($E=36.6$ MPa $\nu=0.4$) [MAT_001] shell elements were used to model the jacket.

8.2.3 Airbag Support

The airbag technology has been proven to be very efficient in terms of impact protection. The use of this technology in the jacket (Figure 8.20) has somehow influence in restricting the neck movement. The neck protector with airbag technology has advantage over the bulky neck braces on the rider's dynamics, as the system will only work when inflated during crashes. The mechanism of the airbag technology has been described in Section 3.7.



Figure 8.20 Airbag technology used as impact protector, which is normally placed inside the jacket [adapted from www.Dainese.com]

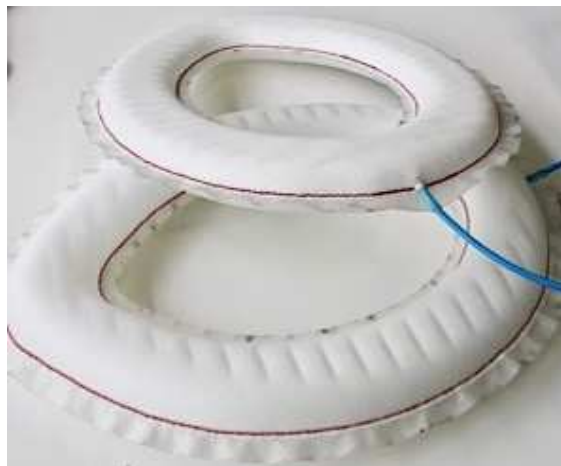


Figure 8.21 Two layers of inflated airbag (8mm total thickness) used to compare physically with other neck protectors



Figure 8.22 The contact between the helmet and airbag system as neck protector (left) and the position of the airbag layers around neck while inflated (right)

Figure 8.21 and Figure 8.22 show the two inflated layers of airbag system, developed for the physical understanding of its mechanism and comparison with other neck protectors. The thickness of the two layers while inflated was kept as 8 cm. Though these layers were mechanically inflated, electrical triggering system could be utilized in future prototypes using advanced algorithms.

The prototype of airbag system with only such two simple layers loses the practicality concerning the final design. Because the system needs to be supported by the jacket when it is designed as an integrated part of a jacket or by any means when it is constructed as a stand-alone product, even some helmet manufacturers tried to integrate airbag system inside the helmet for head and neck support. Hence, considering the practical reasoning, airbag neck brace and airbag jacket with different levels of layers, as elaborated in the following Sections 8.2.3.1 and 8.2.3.2, have been simulated and compared with other neck protectors to evaluate their injury reduction capability. However, the prototype with simple two layers was useful for mechanical analysis.

8.2.3.1 Airbag Neck Brace

The airbag neck brace (Figure 8.23) is a stand-alone neck protective design, where the airbag layer replaces the carbon composite shell from the hybrid neck brace (as described in Section 8.1.2). The geometry, mesh generation and material properties of the PU foam in the airbag brace is identical with that in the hybrid neck brace.

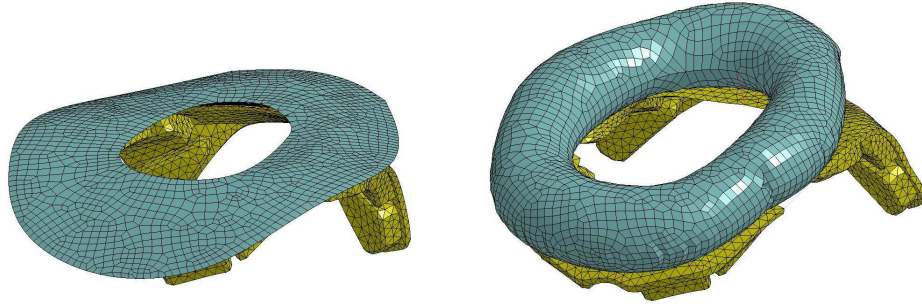


Figure 8.23 FE model of airbag neck brace

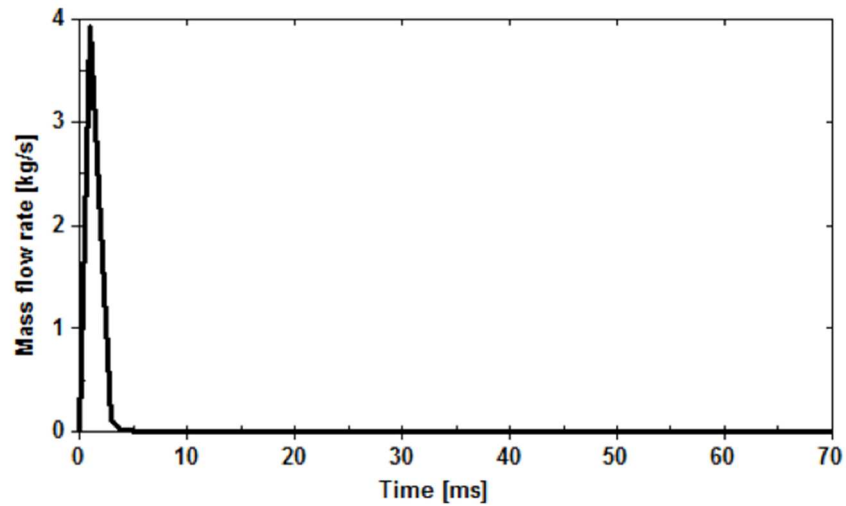


Figure 8.24 Mass of flow rate of Helium used in the simulation

Fabric material model [MAT_Fabric_034] was used to model the airbag membranes ($E_a=E_b=2.5$ GPa, $\nu=0.33$). Moreover, simple airbag model was used for inflating the airbag with gas properties of Helium ($C_v=3.12$ kJ/kgK, $C_p=5.19$ kJ/kgK, $T=298$ K). The mass flow rate of helium inside the airbag was defined according to Figure 8.24. The time to reach maximum flow rate was kept too short to inflate the airbag properly during the impact, because the initial time for the simulations were in close proximity to the time of impact. The amount of mass flow rate was selected based on trial and error, so that the required pressure inside the bag could be achieved. The validation of the airbag system has been provided in the next section (8.2.3.2) using an airbag jacket.

8.2.3.2 Airbag Jacket

The model of the airbag jacket was developed from the CAD file of commercial airbag jacket (street version) produced by Dainese S.p.A. To provide more restriction on the movement of the neck covering the gap between head and shoulder, extra layer of airbag was added as shown in Figure 8.25 (right). The overall thickness of the two layers was calculated as 11.5 cm. The airbag and its inflation were modeled similarly as described in the previous section (8.2.3.1) for airbag neck brace.

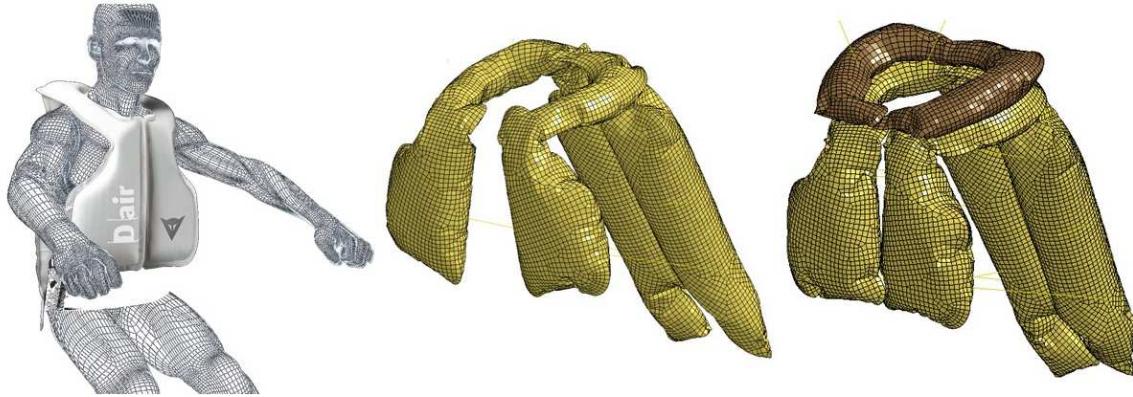


Figure 8.25 Dainese D-air street airbag jacket (left), FE model of the airbag jacket (middle) and extra layer of airbag with jacket to provide more restriction on the neck movement (right)

The modeling of the airbag was compared with the experimental results. The drop test on the airbag back area was simulated (as shown in Figure 8.26) according to the standard for back protectors EN 1621-2:2013 [UNI, 2013]. Figure 8.27 shows the transmitted force history recorded at the anvil and Figure 8.28 indicates the pressure history inside the airbag. Practically, 1.6 bar reaches at 100 ms from the time of impact. From the drop tests performed in-house on the back of the street airbag jacket, the force transmission was found to be 2.5 kN on average. In the simulation, a peak transmission of 3.18 kN was observed. The pressure inside the bag was higher than in the real case. The reason might be that the mass flow rate of the Helium was not modelled according to the real condition, as complete inflation with a short time was desired in the simulation. However, the model is acceptable based on the evaluation of force transmission.

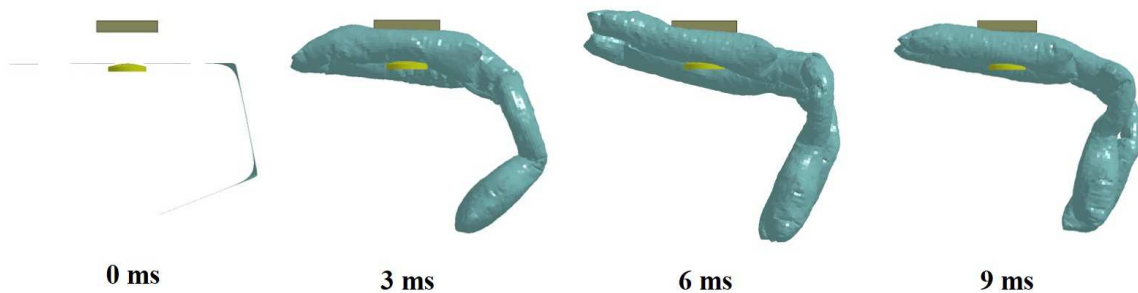


Figure 8.26 The drop test performed on airbag jacket according to the standard for back protectors (EN 1621-2:2013)

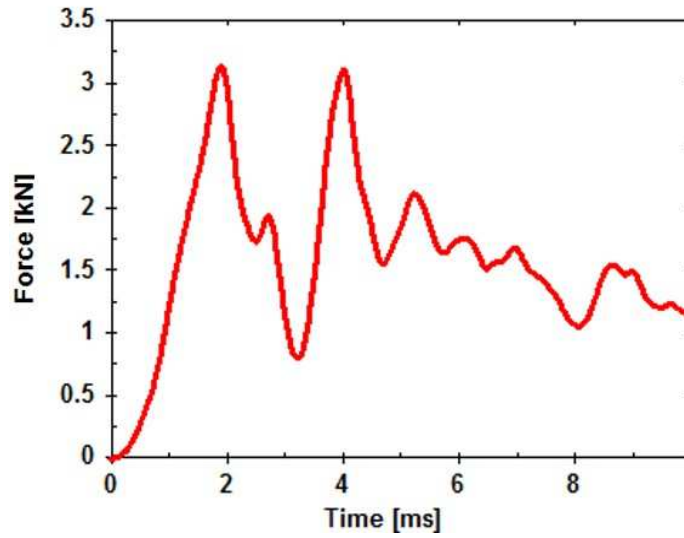


Figure 8.27 Force transmission history from the drop test shown in Figure 8.26.

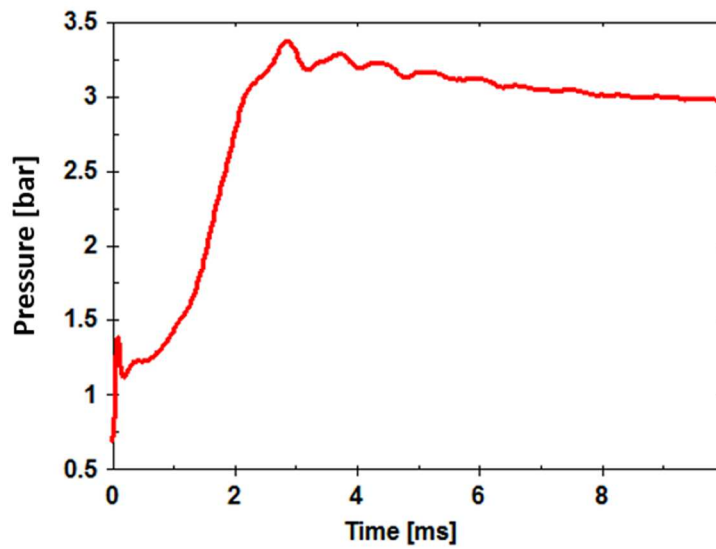






Figure 8.28 Internal pressure of the airbag in the simulation shown in Figure 8.26.

8.3 Physical Comparison

The physical analyses of the newly developed prototypes described in Section 8.2 have been compared with the reference neck brace described in Section 8.1. Table 8.2 summarizes the overall comparison. The assessment of injury reduction has been done using numerical methods, which has been outlined in Chapter 9.

Table 8.2 The comparison between different types of neck protectors, where “↑” sign means bettering, “↓” sign means worsening and “=” sign means negligible effect due to the differences in design comparing to the reference Dainese Carbon Hybrid Neck Brace

Type	Weight (gm)	Comfort to wear	Comfort while riding	Rider’s dynamics	Functional possibility	Challenges
 Hybrid neck brace	610	Ref.	Ref.	Ref.	Extension, flexion, lateral bending, rotation	<ul style="list-style-type: none"> - Placing and keeping the brace affirmed - Flexibility on the rider’s dynamics
 Soft neck brace	235	↑	↑	=	Extension, flexion, lateral bending, rotation	<ul style="list-style-type: none"> - Position of the foams - Shape of the foams - Flexibility on the rider’s dynamics
 Neck collar	90	↓	↑	↑	Extension, flexion, lateral bending, tension, translation	<ul style="list-style-type: none"> - Fixing the system with helmet & jacket - Opening
 Airbag system	220 (deflated)	↑	↑	↑	Extension, flexion, lateral bending, rotation, compression	<ul style="list-style-type: none"> - Adjusting the required thickness while inflated - Shaping the area that needs to be covered

Chapter 9

Numerical Analyses

Owing to the fact that there are no standard test procedures for the neck protectors, this chapter includes numerical test methods with appropriate boundary conditions following the data found in the literature. This chapter provides a brief analysis of the neck injury reduction capabilities of the neck protective systems described in Chapter 8. The analyses reported in this chapter will help understanding the functional mechanisms of different designs of neck protective systems and their protective characteristics to various impact loading. However, the results cannot be fully guaranteed, as simple geometry of the neck model has been used. Another limitation of the results is that the systems might not have been positioned accordingly to extract the maximum injury reduction scheme. Moreover, numerical models of human body always have limitations to mimic the response of a real human.

9.1 Virtual Test Setups

9.1.1 Finite Element Model of Anthropomorphic Test Device (ATD)

The complete neck model was enhanced with a torso model (Figure 9.1), so that the neck protective systems could be positioned according to the designed specifications. The shape of the torso was taken from the 50th percentile male avatar of the designing software CLO® as it was chosen for the neck skin.

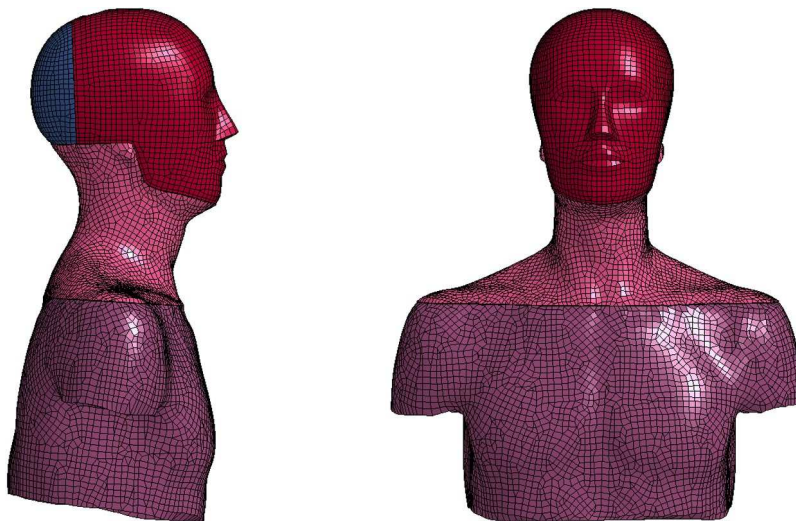


Figure 9.1 The extension of the neck model with a torso model

The torso was modelled as rigid ($E=70$ GPa, $\nu=0.3$) with the material model MAT_020 from the LS-DYNA material library. The torso mass of 16 kg from T1, which was

assigned for the validation (see Section 7.4), was released and reassigned to the torso model. However, the torso was rigidly constrained with T1.

9.1.2 Impact Conditions

Six different loading conditions for the impact tests were assumed based on the accident database (provided in Chapter 2) to evaluate the neck injury reduction characteristic of the neck protectors (as described in Chapter 8). Three of the cases were considered as sliding: frontal (Figure 9.2), rear (Figure 9.3) and lateral (Figure 9.4); and three other cases were inverted: -15° (Figure 9.5), 0° (Figure 9.6) and $+15^{\circ}$ (Figure 9.7). The sliding and inverted impacts were imagined as the low-side and high-side impacts respectively during motorcycle crashes.

Case 1: Frontal Slide

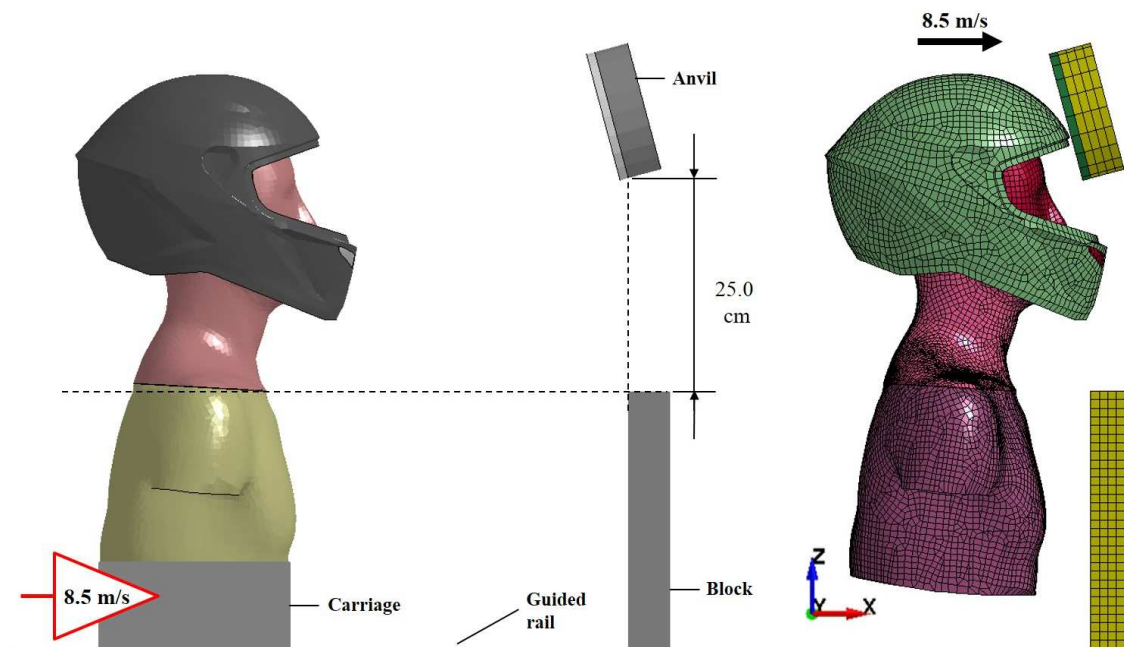


Figure 9.2 Imaginary sliding test setup (left) and the FE model (right) for frontal impact

In the sliding cases, it was assumed that the ATD would be placed on a carriage and the velocity of 8.5m/s would be given to this carriage. The carriage can move only in translational direction. For all the sliding cases, the rigid anvil was placed at $+15^{\circ}$ angle and a Teflon layer was added for frictionless contact. A rigid block was placed in front of the impact direction to restrict the ATD's forward motion after the impact. This block is important from the design aspect of a test setup and also to create proper neck curvature. The distance of the blocks was chosen in such a way that sufficient flexion, extension and lateral bending of the neck could be achieved. For this reason, initially several simulations were run to choose the required distance.

Case 2: Rearward Slide

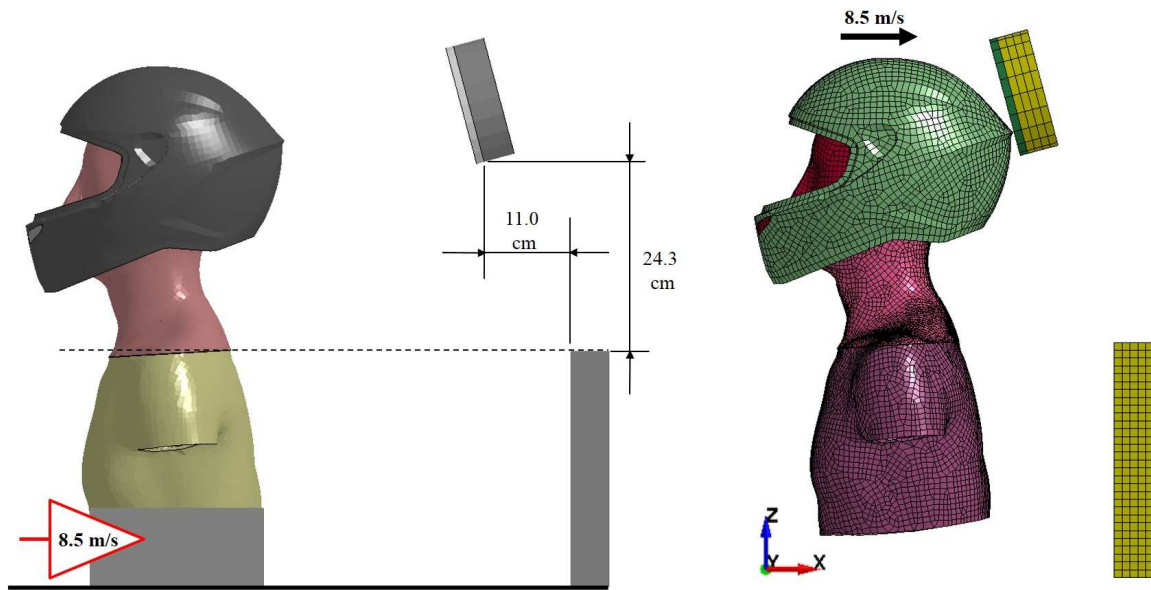


Figure 9.3 Imaginary sliding test setup (left) and the FE model (right) for rear impact

Case 3: Lateral Slide

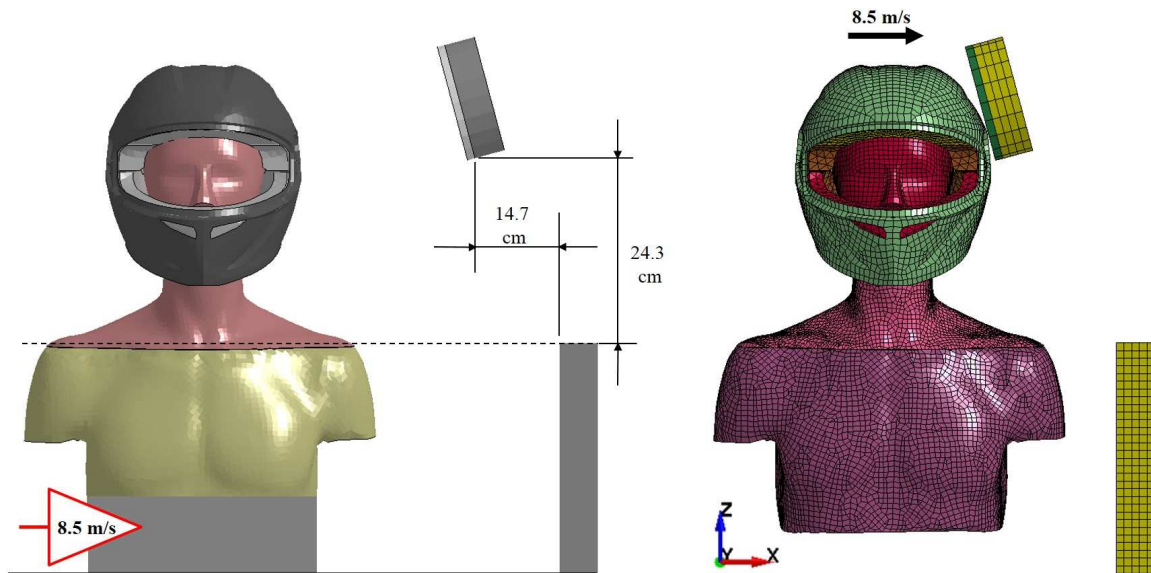


Figure 9.4 Imaginary sliding test setup (left) and the FE model (right) for lateral impact

For the inverted drop cases, the boundary conditions were based on the experiments explained in Section 7.4.1. The impact velocity of 3.2 m/s was sufficient to create injuries to the cervical spine [Nightingale et al., 1996; Nightingale et al., 1997]. The carriage was allowed to move in the axial direction while other directions were made constrained. There was no need of block in these cases.

Case 4: Inverted -15°

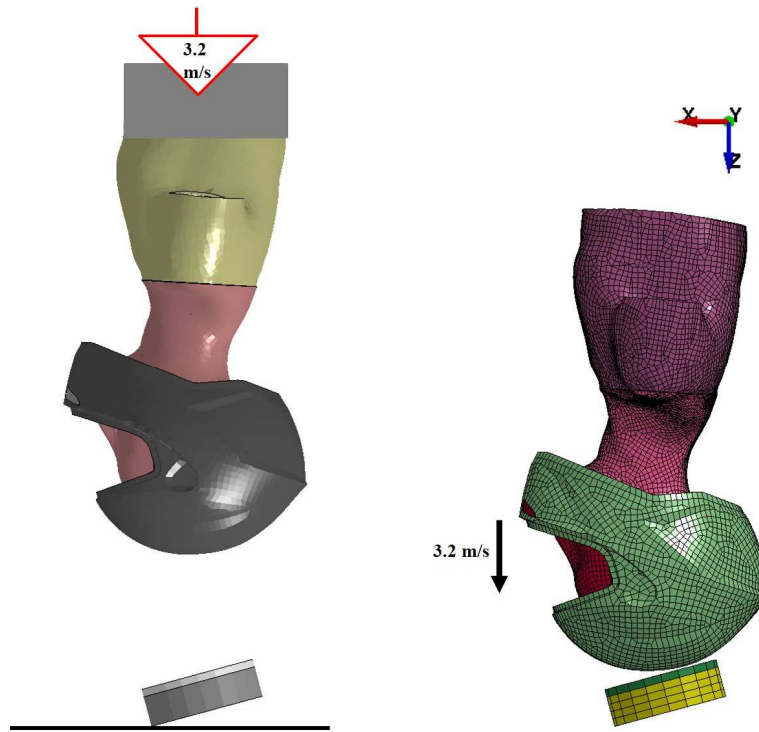


Figure 9.5 Imaginary inverted drop test setup (left) and the FE model (right) for -15° impact angle

Case 5: Inverted 0°

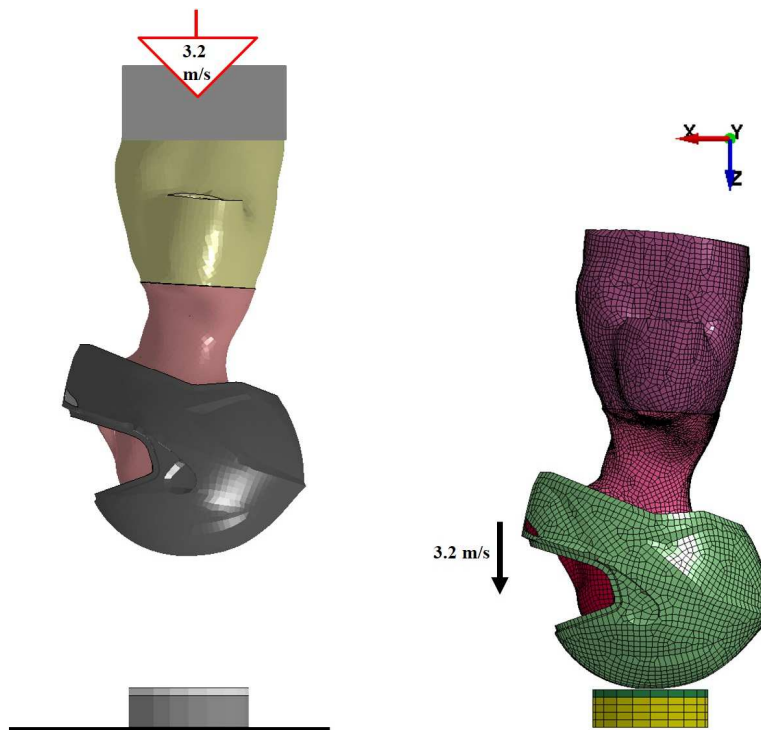


Figure 9.6 Imaginary inverted drop test setup (left) and the FE model (right) for 0° impact angle

Case 6: Inverted +15°

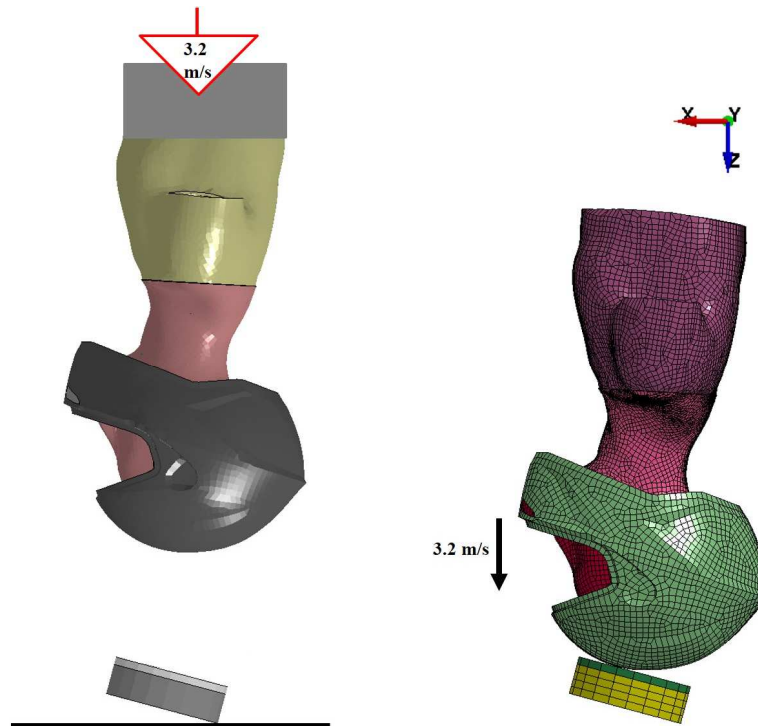


Figure 9.7 Imaginary inverted drop test setup (left) and the FE model (right) for +15° impact angle

9.2 Results

The simulation results for evaluating the neck protective devices were analyzed till 30ms from the impact. The experimental results in compression indicated that injury occurred in less than 10 ms and peak axial force in less than 15 ms [Nightingale et al., 1996; Nightingale et al., 1997]. Similar data was assumed for frontal, rear and lateral impacts. Although the response of D-neck was not evaluated in rear impact, the results achieved in such impact condition are assumed to be acceptable. Since the response of the model showed good agreement in other impacts, especially to the compressive impacts. All the simulations run for the evaluation were head-first impacts, which led the neck in compression loading mode either alone or combining with other loading modes.

9.2.1 Case 1

The kinematics of the ATD model with different neck protective systems for case 1 is shown in Figure 9.8. It was observed that the front part of all the braces (hybrid, soft and airbag) hit the block before the helmet had an impact with the anvil, which might affect the results. However, it represents the real crash condition considering that there is ground contact of the body parts before the head hits the impact object. Moreover, it can be considered as an advantage or disadvantage of the design feature depending on the assessment results.



Figure 9.8 Time-lapse of the response of the ATD model with different neck protective systems for case 1

Figure 9.9 compares the upper and lower neck forces and the resultant head acceleration for various neck protective systems. It is apparent that the neck shear force becomes higher by restricting the head rotation with hard braces such as hybrid and airbag braces. The hybrid brace resulted in the highest peak compressive force, which indicates the higher possibilities of neck injury comparing to other protective systems. The neck collar performed best in terms of controlling the neck shear force, but results in slightly higher compressive force comparing to no coupled neck systems. The peak resultant head acceleration was slightly increased by using airbag brace as the inflation of the airbag has influence on the helmet. The first and second peak T1 resultant forces were similar for all the systems.

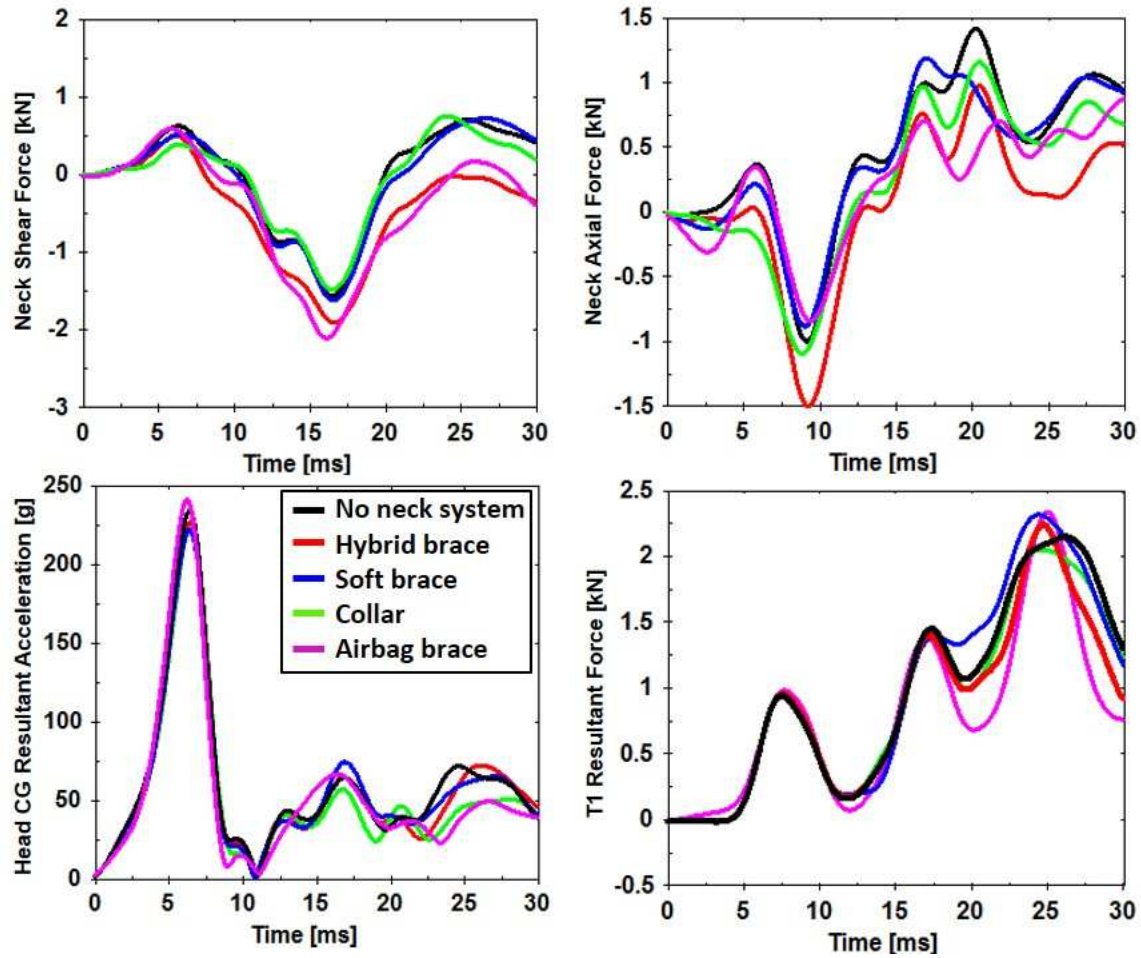


Figure 9.9 The upper and lower neck forces and the resultant head acceleration for case 1

9.2.2 Case 2

The response of the ATD model with different neck protective systems for case 2 is illustrated in Figure 9.10. It shows that the helmet did not have any contact with the brace models before 20 ms. The collar was the only system that had effect all the time. However, it seems that the distance of the rigid block (see Figure 9.3) should be reduced for improving the evaluation process of the neck protective systems in flexion loading mode.

The neck protective systems were compared based on the upper and lower neck forces and resultant head acceleration as shown in Figure 9.11. It is difficult to predict and compare the effectiveness of the systems as the helmet contacted the braces after 20ms. Based on the simulation results, the neck collar showed better control of the neck parameters, but a slight increase in the head acceleration. Interestingly, restricting the neck movement increased the neck axial force by using any neck protective system.



Figure 9.10 Time-lapse of the response of the ATD model with different neck protective systems for case 2

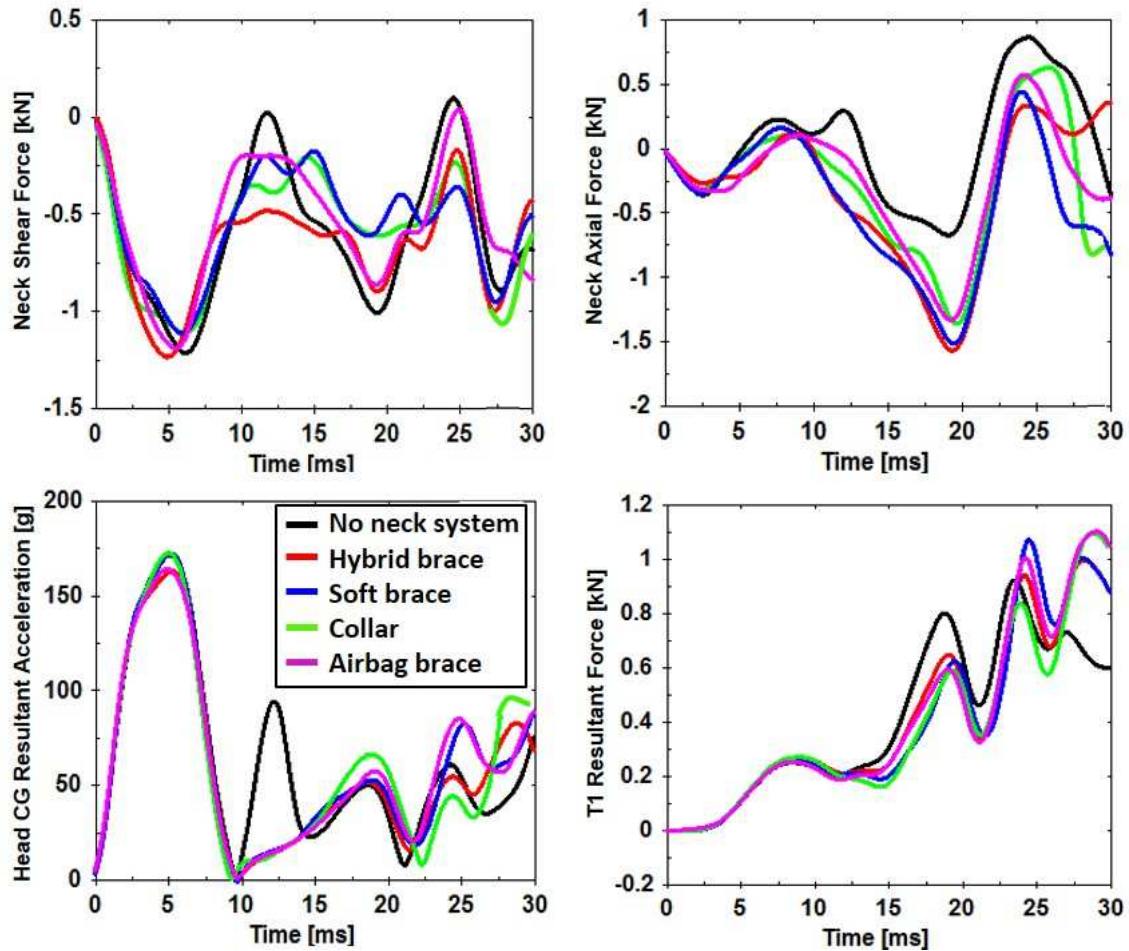


Figure 9.11 The upper and lower neck forces and the resultant head acceleration for case 2

9.2.3 Case 3

The lateral bending of the ATD model with different neck protective systems in case 3 is shown in Figure 9.12. The bending of the neck occurred after having an impact with the anvil and in the opposite direction of the impact velocity. The helmet came in contact with the neck braces after 8 ms, where collar had different mechanisms by creating force between the helmet and the jacket immediately after the head started to rotate.

The comparison of the systems based on the upper and lower neck forces and resultant head acceleration is shown in Figure 9.13. It is evident that the use of hybrid brace increased the neck shear force due to its stiff material in the hard shell. For other systems, the shear force was reduced. However, neck tensile force was increased for those systems. The head acceleration was slightly increased and the T1 force was reduced by using the airbag brace. For other protective systems, the first peak head acceleration and T1 force were almost identical.



Figure 9.12 Time-lapse of the response of the ATD model with different neck protective systems for case 3

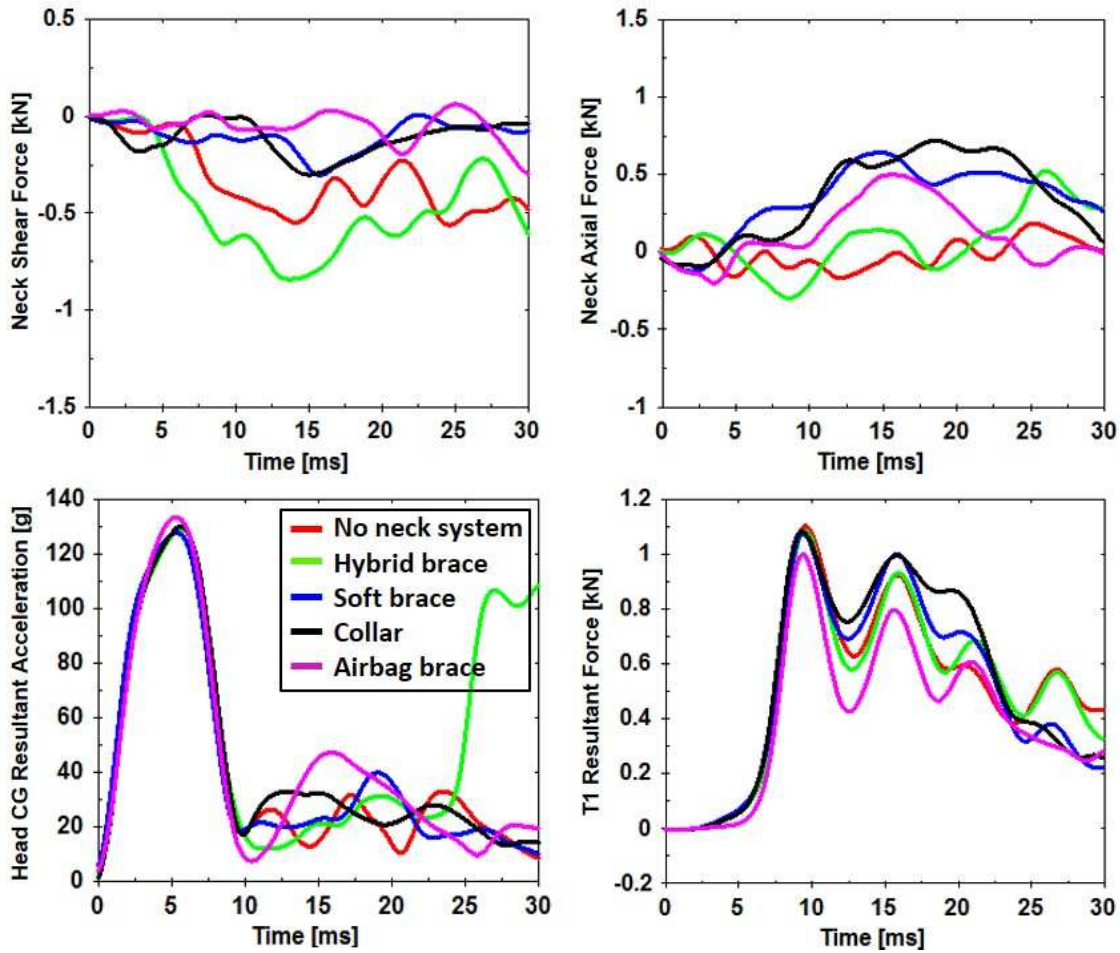


Figure 9.13 The upper and lower neck forces and the resultant head acceleration for case 3

9.2.4 Case 4

Figure 9.14 shows the response of the ATD model in compression-extension mode with different neck protective systems according to case 4. The kinematics of the neck depends on the position of the braces.

The comparison of the systems based on the upper and lower neck forces and resultant head acceleration is shown in Figure 9.15. For some instances, all the systems resulted in reducing the shear force while the force was increased in some points. However, the shear force was reduced by using the airbag brace after the peak was reached. The peak compressive force (positive sign represents compressive force) was increased significantly by using the hybrid brace. The peak head acceleration was similar or lower when there were neck protective systems. T1 force was also similar for all the systems except for the airbag brace, by which the force was slightly reduced.

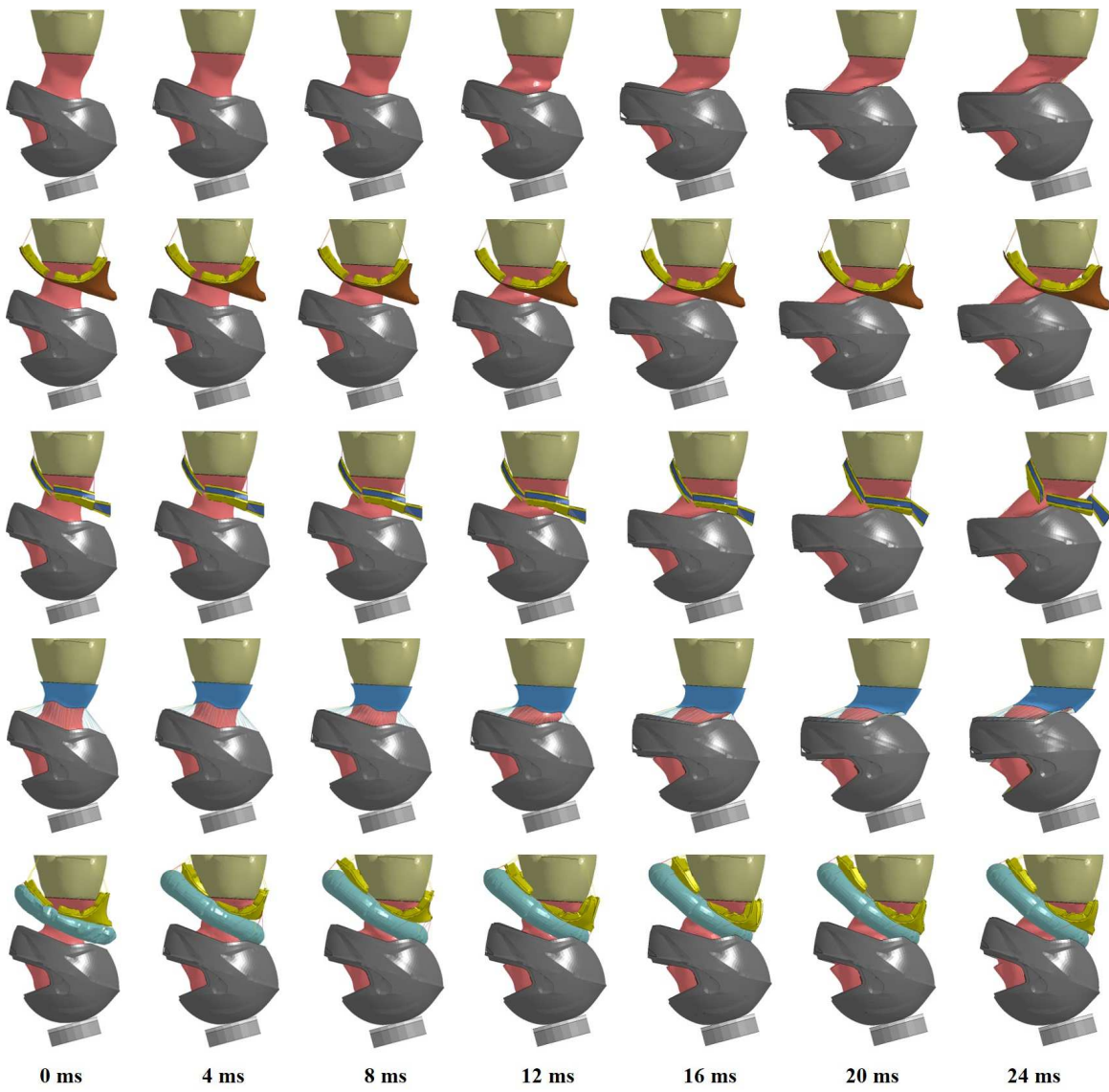


Figure 9.14 Time-lapse of the response of the ATD model with different neck protective systems for case 4

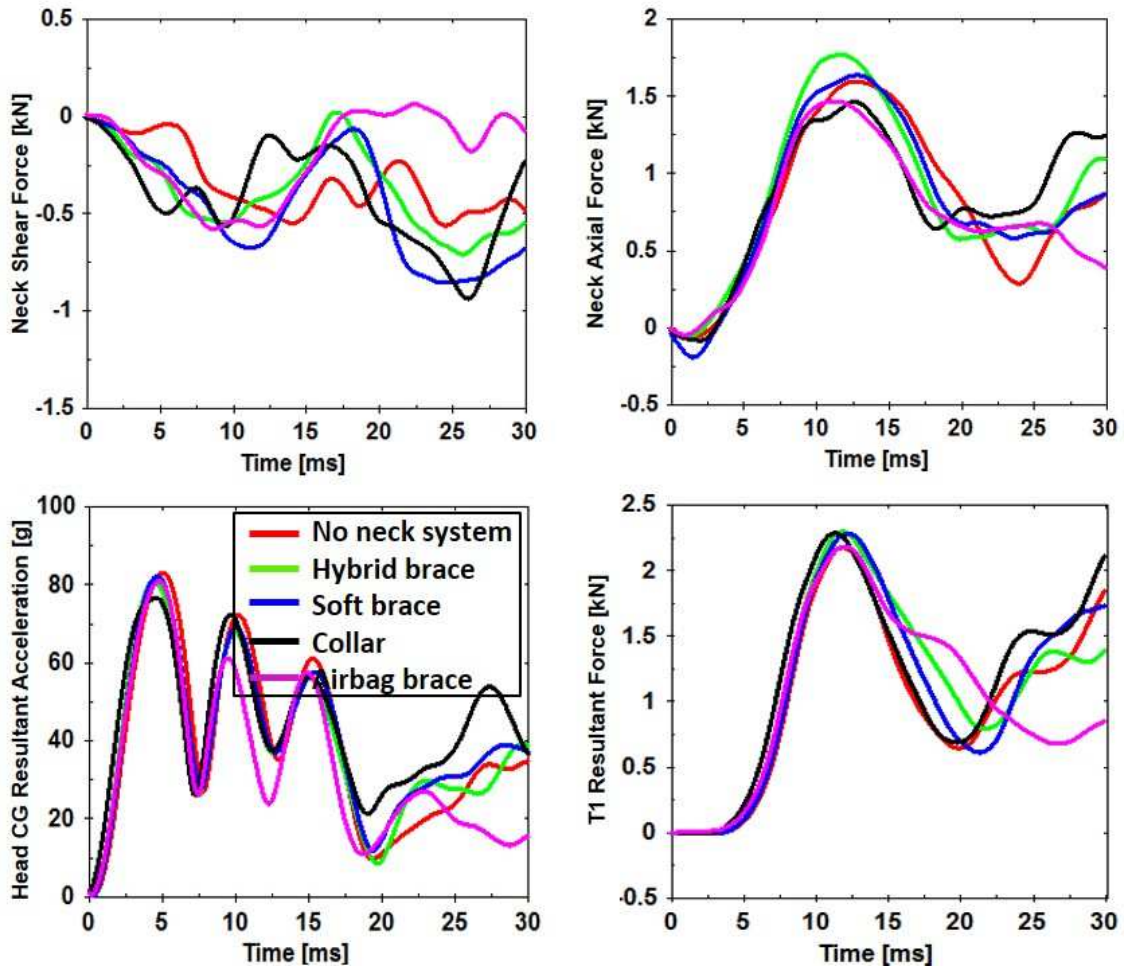


Figure 9.15 The upper and lower neck forces and the resultant head acceleration for case 4

9.2.5 Case 5

Figure 9.16 shows the response of the ATD model in pure compression mode according to case 5. The ATD model was coupled with different neck protective systems.

The comparison of the systems based on the upper and lower neck forces and resultant head acceleration is shown in Figure 9.17. The neck shear force was increased when the braces were used. However, there was a slight reduction in the peak neck compressive force (positive sign represents compressive force) by using the hybrid and airbag braces. The peak head acceleration was identical for all the systems. The first peak T1 force was similar except for the soft brace, by which it was slightly increased.

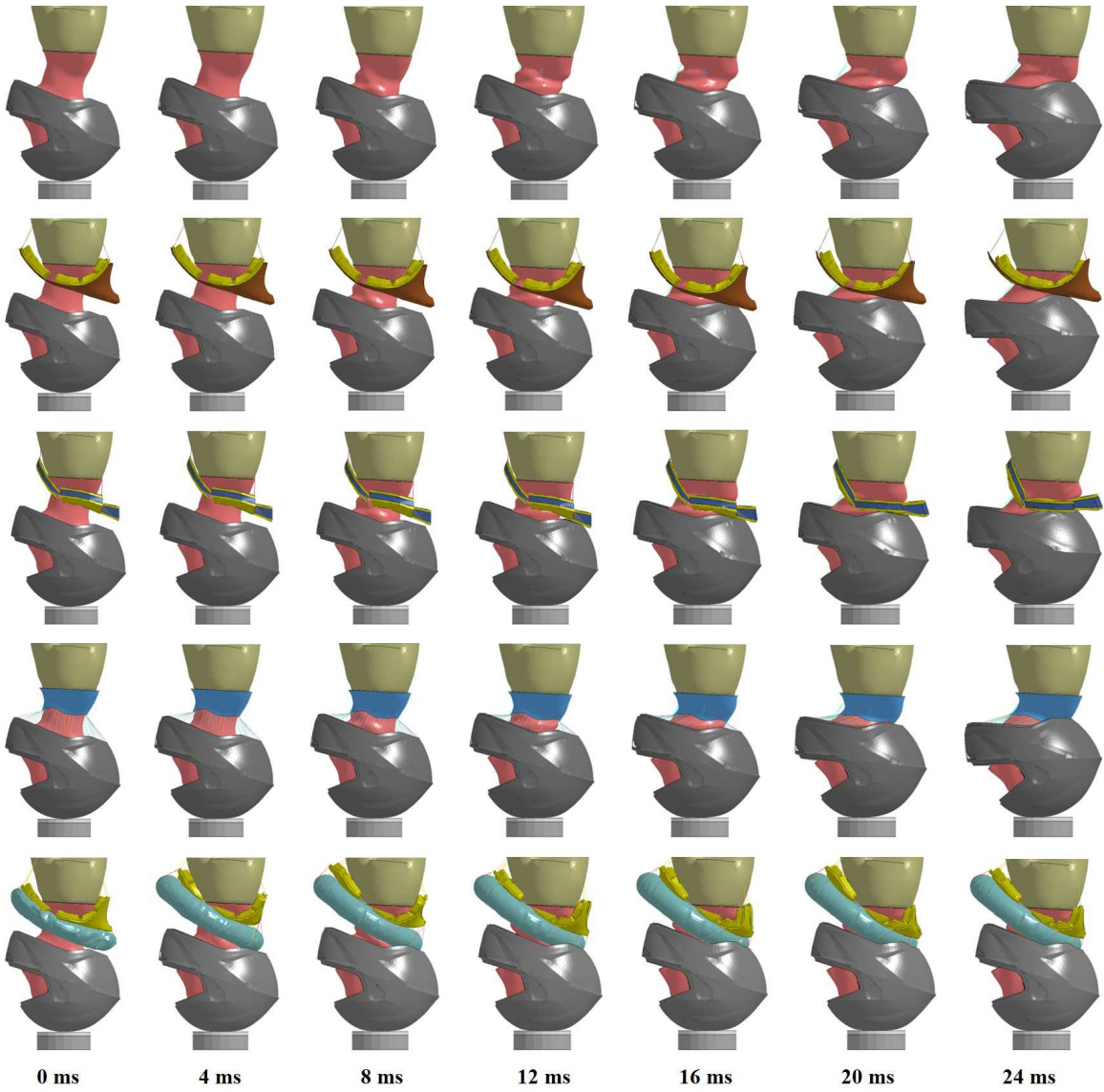


Figure 9.16 Time-lapse of the response of the ATD model with different neck protective systems for case 5

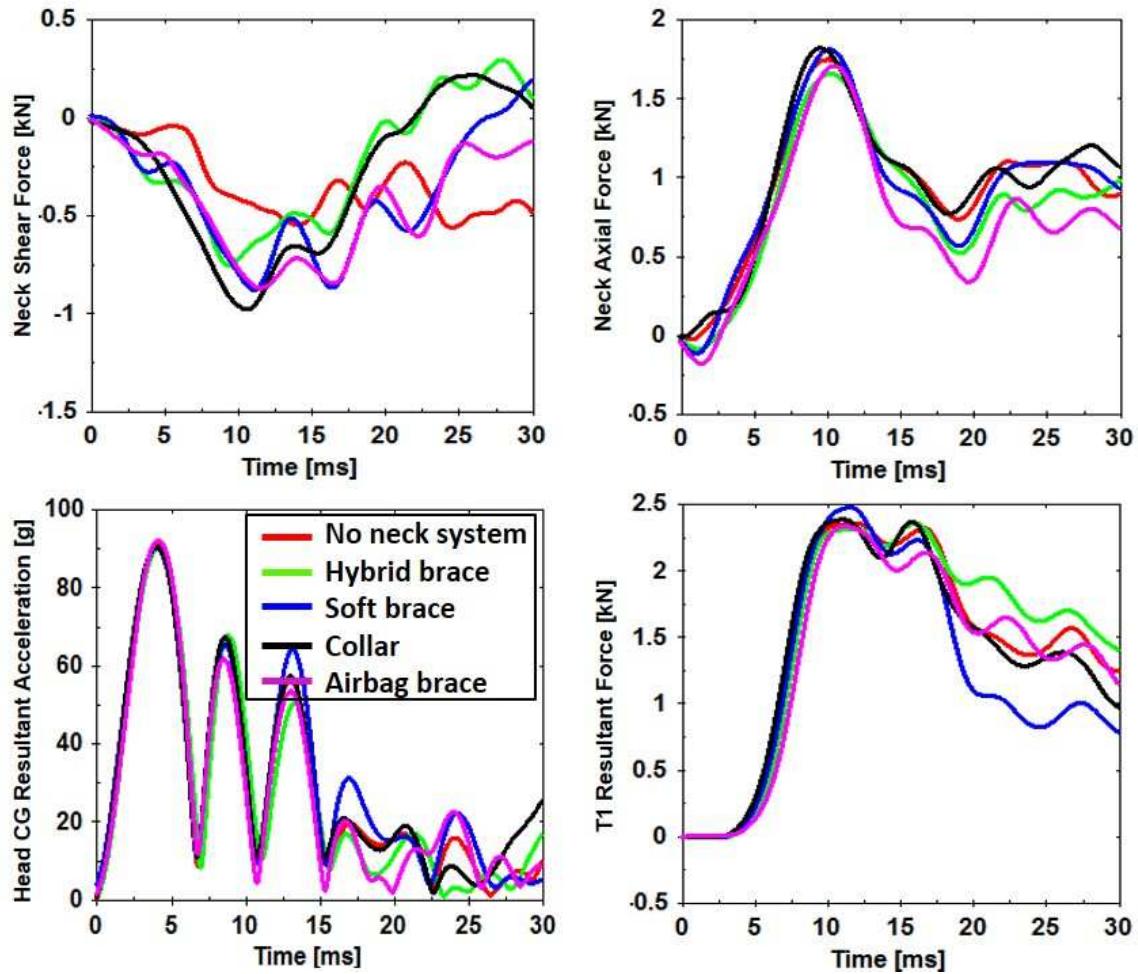


Figure 9.17 The upper and lower neck forces and the resultant head acceleration for case 5

9.2.6 Case 6

Figure 9.18 shows the response of the ATD model according to case 6 in compression-flexion mode. The ATD model was coupled with different neck protective systems. It was assumed that the helmet would have contact with front part of the braces, because of the flexion moment of the neck, but it contacted with the rear and lateral parts of the braces due to the compression of the neck.

The upper and lower neck forces and the resultant head acceleration of the neck protective systems are shown in Figure 9.19. The neck shear force was reduced by all the systems except the neck collar. In this case, the hybrid brace showed the most reduction of the neck shear force. However, the peak neck compressive force was increased (positive sign represents compressive force) by the hybrid and other braces. The hybrid brace also showed an increase in the peak T1 resultant force. The peaks of the head acceleration were similar for all the systems.

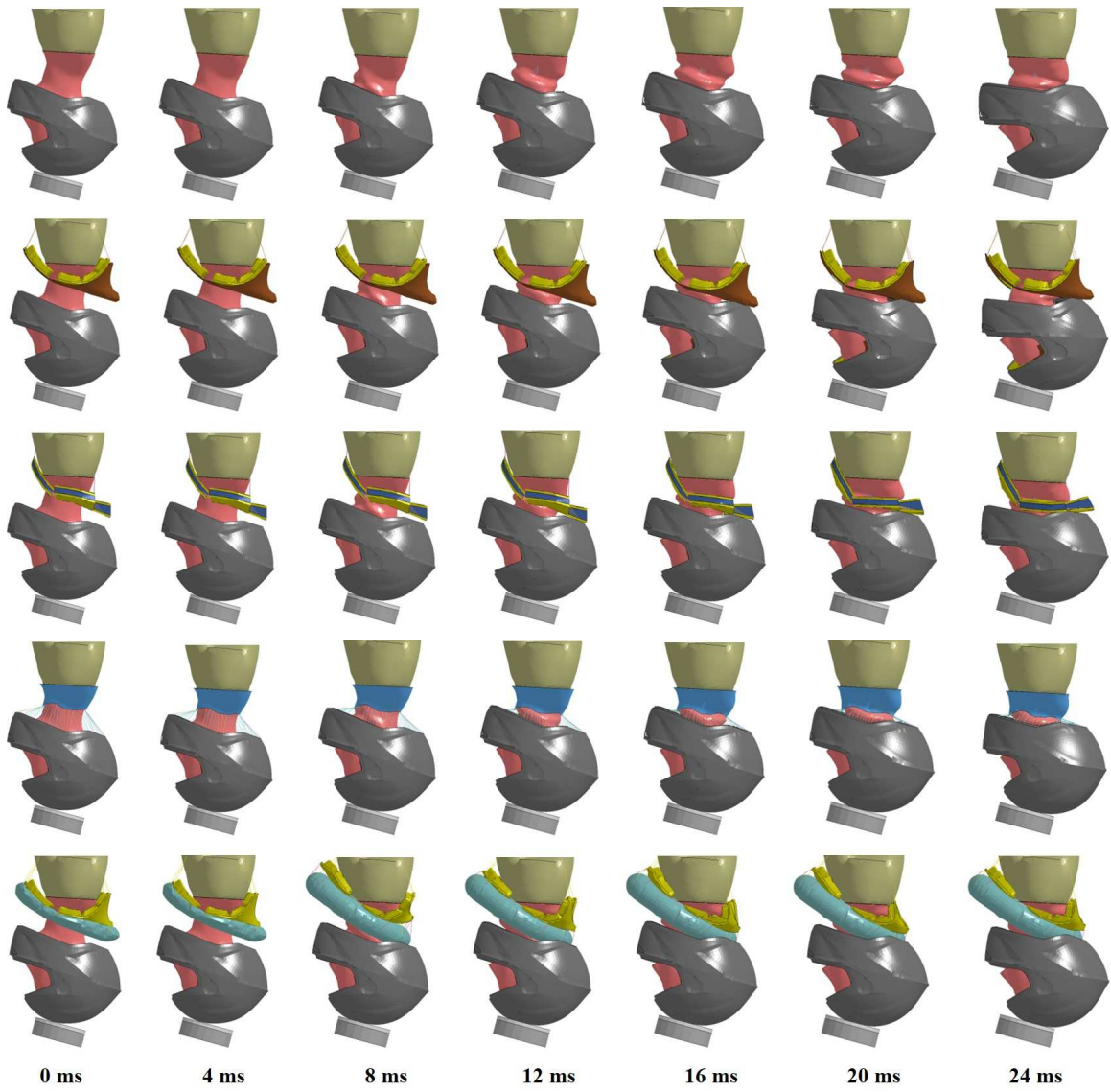


Figure 9.18 Time-lapse of the response of the ATD model with different neck protective systems for case 6

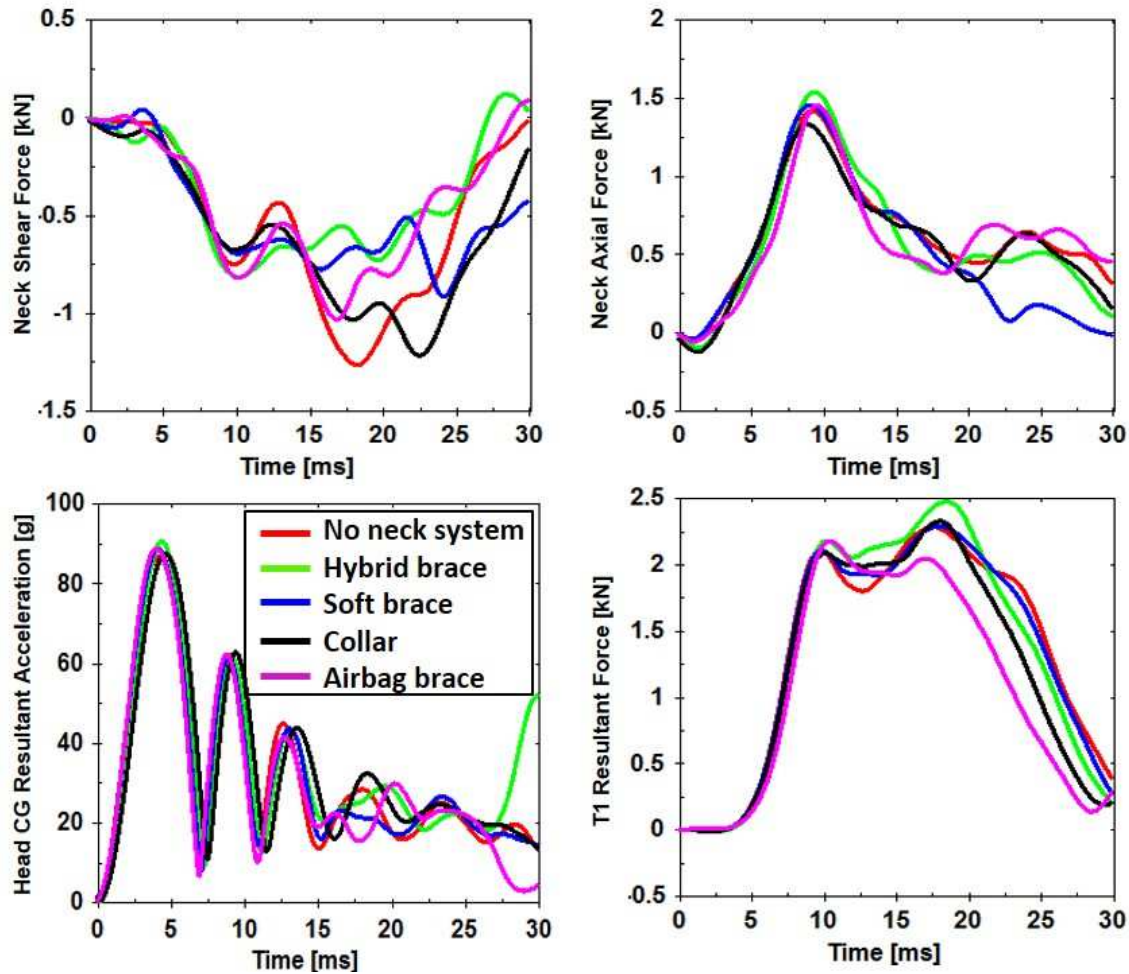


Figure 9.19 The upper and lower neck forces and the resultant head acceleration for case 6

9.3 Discussion

The results shown are based on a specific helmet. They will be different with other helmet models. However, it is almost impossible to pick one protective system as the best, which will protect the neck during all kinds of impact loadings. It is important to define the loading condition for which the system will work. Moreover, the position of the systems around the neck is an important factor to maximize the protective features. For the evaluation method, it is also important to choose the suitable neck injury metrics.

9.3.1 Head Rotation Relative to Torso

All the neck protective systems developed based on the principle of restricting the neck movement by means of the relative rotation of the head with respect to torso. However, the effectiveness of such restriction in reducing the neck forces and moment was not mentioned in the literature. In the present section, the head rotation with respect to torso for the neck protective systems (shown in Chapter 8) has been compared. The rotation was calculated as change in θ (Figure 9.20), where θ is the head link angle at the center

of gravity (CG) of the head. The T1 was assumed as the reference of the torso. The positive and negative angle values indicate the flexion and extension mode respectively.

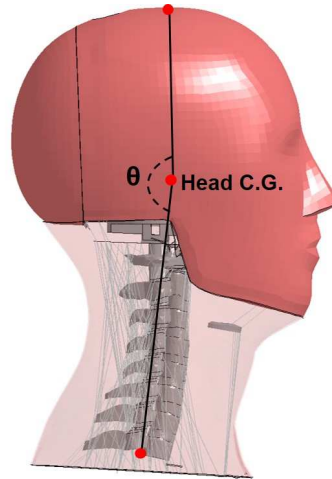


Figure 9.20 The calculation of change in head angle representing the head rotation relative to torso (T1)

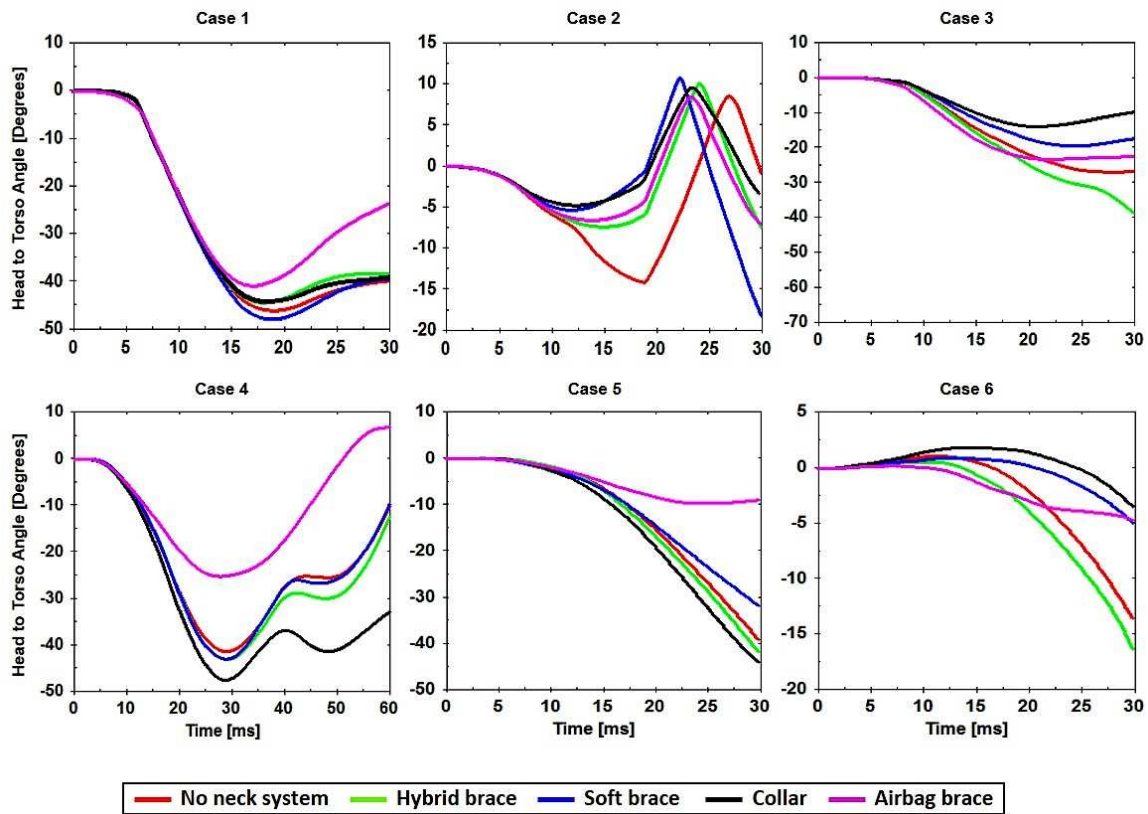


Figure 9.21 The head rotation relative to torso by using different types of neck protective systems for different loading cases

Figure 9.21 shows the differences in head rotation for all the cases due to the coupling of neck protective systems to the ATD. The hybrid brace reduced the head rotation for all the cases, but for case 6 after reducing the rotation in flexion mode, it increased in

extension mode. The foam brace could not restrict the rotation significantly. However, it reduced the head rotation for case 2. The neck collar had a better control on the head rotation in all the sliding cases, but it did not function for restricting the rotation in compressive loading. Finally, the airbag brace performed the best in restricting the head rotation as it could cover the gap between the head and torso to greater extent than other systems.

9.3.2 Effect of impact speed

The results discussed in Section 9.2 were based on a specific impact speed for each case. The consequence of changing the speed on neck protection with the hybrid neck brace has been presented in Figure 9.22. Case 6 had been randomly chosen to investigate the effect. Two more simulations at 2 m/s and 5m/s, additional to 3.2 m/s, were run for the investigation.

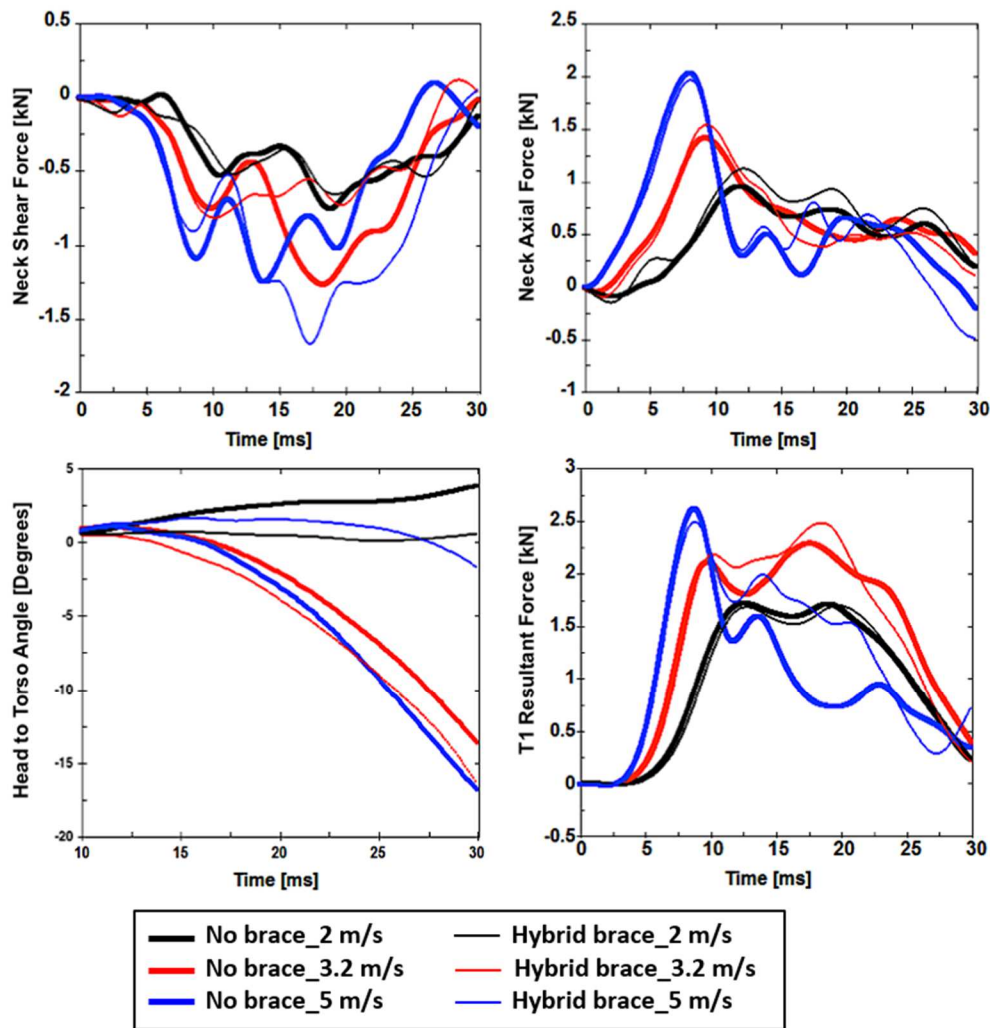


Figure 9.22 The upper and lower neck forces and the head rotation relative to torso, with and without hybrid neck brace, at different impact speeds

Figure 9.22 shows that the peak neck compressive force (positive sign represents compressive force) with brace was higher comparing to that without brace at the lower impact speeds. However, it showed different behavior for the neck shear force. The force appeared to be increased and decreased at different points on the shear force curves. However, the force increased extensively at 5 m/s impact when the brace was used.

The first peak T1 force was similar at all the impact speeds, but the force increased afterwards by using the hybrid brace at higher speeds. The differences of the head rotation curves, with and without braces, were highest at 5 m/s.

9.3.3 Airbag Jacket

The effect of airbag jacket with two layers on neck protection was investigated for cases 1, 4 and 6. The aim of this investigation was to understand the mechanism of neck injury reduction by restricting the neck movement. Figure 9.23 shows the response of the ATD model with airbag jacket.

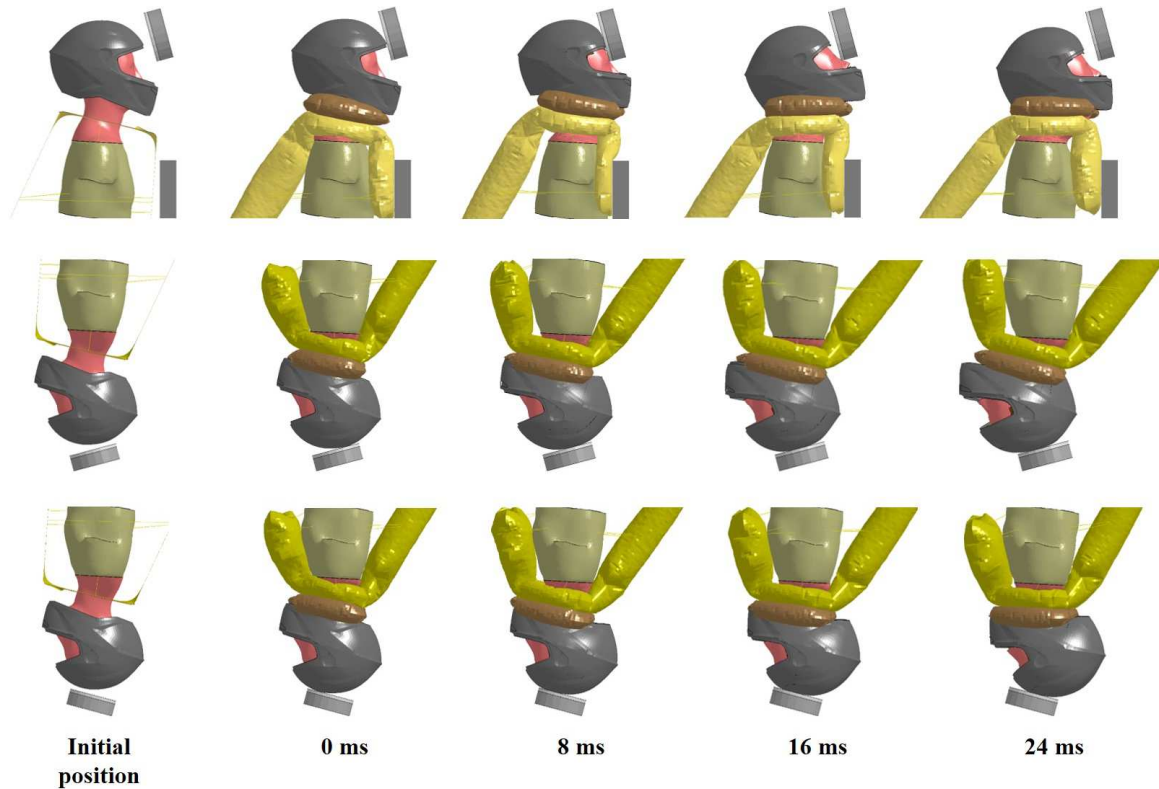


Figure 9.23 Time-lapse of the response of the ATD model with airbag neck protective systems for case 1 (top), case 4 (middle) and case 6 (bottom)

The upper and lower neck forces and the head rotation, with and without airbag neck protective systems, are compared for cases 1, 4 and 6 in Figure 9.24. The airbag jacket showed similar effects to those produced by the airbag brace on head rotation. For case 1, the jacket could not reduce the neck shear force but there was a decrease in the

compressive force. The shear force was not reduced for case 4 by the airbag jacket, but it was reduced for case 6. However, the compressive force (positive sign represents compressive force) was reduced significantly by the airbag jacket.

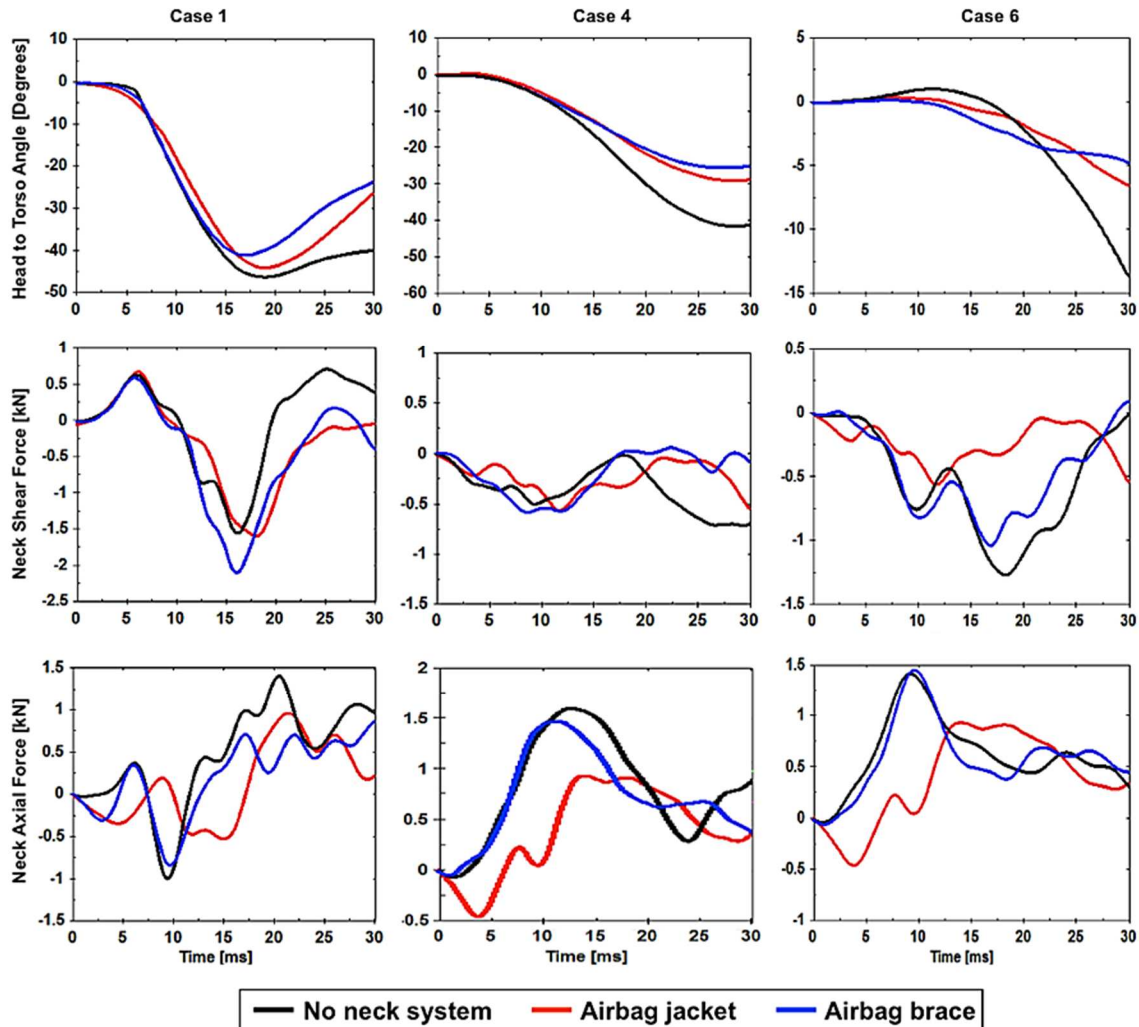


Figure 9.24 The comparison of upper neck force and the head rotation relative to torso with and without airbag system for cases 1, 4 and 6

9.3.4 Neck Injury Criteria

It is important to evaluate the neck protective systems with at least one suitable neck injury metric. In Section 2.7, the available neck injury metrics, found in the literature, were discussed. However, in the present analysis, an appropriate neck injury criterion could not be related, because of the use of different neck model and loading conditions. Based on the acceptance of neck injury criteria in the standards (ISO 13232-5 [ISO, 2005] and FMVSS 208 [Kleinberger, 1998], the results were analyzed using NII (Neck Injury Index) and Nij (Neck Injury Criterion) for predicting the injury risk in the upper neck for cases 1 and 4.

The dynamic variable values from the simulation with different neck protective systems are given in Table 9.1. The values were taken as the maximum values within 30ms from the impact. All the data were filtered at 1000 Hz according to SAE J211 specifications.

Table 9.1 The dynamic variable values of upper neck with different neck protective systems

Case	Neck system	F _C (N)	F _T (N)	M _{flx} (Nm)	M _{ext} (Nm)	M _X (Nm)	M _Z (Nm)
Frontal slide (case 1)	No system	2088	152	55.01	22.63	9.27	21.65
	Hybrid brace	2705	158	57.3	14.82	8.75	21.89
	Soft brace	2440	477	52.69	13.66	4.63	14.64
	Collar	2452	399	62.77	19.69	11.38	27.52
	Airbag brace	2470	173	19.58	19.06	5.28	14.44
	Airbag jacket	1337	1040	30.3	19.7	8.5	25.7
-15° Inverted (case 4)	No system	1425	1816	73.63	23.78	12.37	19.0
	Hybrid brace	2180	1481	76.64	10.51	10.91	40.31
	Soft brace	1352	1635	82.34	16.92	8.57	21.39
	Collar	1262	1451	73.37	26.19	10.82	26.03
	Airbag brace	1345	1292	94.58	17.91	9.2	40.59
	Airbag jacket	1122	1097	81.6	12.88	8.26	24.73

The values of NII and Nij were calculated using Eq 2.7 and Eq 2.9 respectively. In this present discussion, NII was calculated as NII-left and NII-right using the left and right functions of Eq. 2.7 respectively. The critical values used to define the NII and Nij are shown in Table 9.2 (details in Sections 2.5.5 and 2.5.6).

Table 9.2 The critical values used to calculate NII and Nij

Criterion	F _C (N)	F _T (N)	M _{flx} (Nm)	M _{ext} (Nm)	M _X (Nm)	M _Z (Nm)
NII	6530	3340	204.2	58	62.66	47.1
Nij	6160	6806	310	135	NA	NA

Table 9.3 shows the calculated values of NII and Nij. The probability of injury is assumed to be zero or a low risk of AIS = 1 if NII values less than 1.06. The minimum values of NII to calculate the probability of injury are given in Table 2.7. However,

according to the values calculated, both NII-left and NII-right could predict the probability of AIS \geq 1 neck injury by using Eq.8. The values of the probability are shown in Table 9.4. For a small number of impacts for case 4, it was possible to calculate the probability of AIS \geq 2 and even AIS \geq 3 neck injury when the min NII values were reached. The results showed that the probability of AIS \geq 1 injury became higher, using the NII-right function, when any protective system was used. The NII-left values were reduced by using airbag brace and soft brace for case 1 and that was significantly reduced by using airbag jacket for case 4.

Nij greater than 1 corresponds to 22% risk of AIS 3+ neck injury [Bass et al., 2008]. From Table 9.3, Nij values never reached to 1 for any of the impact scenarios. However, the risk of neck injury by using the hybrid neck brace appeared to be the highest according to the values of Nij. The values were lowest for the airbag jacket.

Table 9.3 The values of NII and Nij using Eq. 2.7 and Eq. 2.9

Case	Neck system	Value		
		NII-left	NII-right	Nij
Frontal slide (case 1)	No system	1.138	1.132	0.516
	Hybrid brace	1.117	1.431	0.624
	Soft brace	1.062	1.601	0.566
	Collar	1.305	1.534	0.600
	Airbag brace	0.916	1.333	0.542
	Airbag jacket	1.159	1.600	0.363
-15 ⁰ Inverted (case 4)	No system	1.609	2.362	0.504
	Hybrid brace	1.607	2.409	0.601
	Soft brace	1.476	2.159	0.506
	Collar	1.558	1.946	0.450
	Airbag brace	1.626	1.838	0.523
	Airbag jacket	1.251	1.551	0.445

Table 9.4 The probability of AIS ≥ 1 injury according to NII criterion

Case	Neck system	$P_{AIS \geq 1}$	
		NII-left	NII-right
Frontal slide (case 1)	No system	0.0177	0.0164
	Hybrid brace	0.0129	0.0812
	Soft brace	0.0005	0.1162
	Collar	0.0544	0.1026
	Airbag brace	-	0.0605
	Airbag jacket	0.0224	0.1160
-15° Inverted (case 4)	No system	0.1178	0.2571
	Hybrid brace	0.01174	0.2652
	Soft brace	0.0907	0.2220
	Collar	0.1075	0.1830
	Airbag brace	0.1212	0.1627
	Airbag jacket	0.0427	0.1060

Bass et al. (2008) reported that, there is a poor correlation between the predictions of injury risk using NII and injury data by the cadaveric experiments. The NII underestimate the risk and severity of the injuries observed in the cadaveric tests. The reasons were assumed that the development of NII was based on specific types of injuries and data, and also the possible biofidelic limitation of the ATD used in the system. Bass et al. (2008) proposed a new neck injury risk assessment for NII ($NII_{cadaver}$) based on the cadaveric experimental dataset, which improved the predictive capability of the neck injury risk to both upper and lower cervical spines. The proposal came after performing a survival analysis for AIS3+ injuries using NII, which determined the NII-right coefficient to be 1.77 rather than 3.1. The proposal also determined the coefficients a and b of the Eq. 2.8 to be -0.87 and 3.03 respectively by performing a normal distribution.

The NII was recalculated using the proposed $NII_{cadaver}$ and probability of AIS3+ was predicted using the aforementioned normalized coefficients of the probability function. The results are shown in Table 9.5. Apparently, the calculations with the proposed modifications were more acceptable, as it showed similar consequences discussed the in results section. No significant reduction of the probability of injury risk was observed by using any neck protective system; even the probability was increased for some impact

scenarios. However, the use of NIICadaver is limited to cadaveric specimen similar to those in the experiments according to Bass et al. (2008), because the experimental cadavers had predominantly flexion/compression and flexion/tension dynamics and were more elderly which might have increased the occurrence of injuries in the experiments.

Table 9.5 Recalculation of NII functions using the proposed modifications by Bass et al. (2008) and the prediction of probable AIS3+ injuries

Case	Neck system	Value			
		$NII_{\text{cadaver-left}}$	$NII_{\text{cadaver-right}}$	$PAIS_{3+} (NII_{\text{cad-left}})$	$PAIS_{3+} (NII_{\text{cad-right}})$
Frontal slide (case 1)	No system	1.138	0.647	0.4846	0.3938
	Hybrid brace	1.117	0.817	0.4809	0.4269
	Soft brace	1.062	0.914	0.4714	0.4450
	Collar	1.305	0.876	0.5122	0.4380
	Airbag brace	0.916	0.761	0.4453	0.4163
	Airbag jacket	1.159	0.913	0.4881	0.4450
-15° Inverted (case 4)	No system	1.609	1.349	0.5587	0.5192
	Hybrid brace	1.607	1.376	0.5585	0.5234
	Soft brace	1.476	1.233	0.5390	0.5004
	Collar	1.558	1.111	0.5513	0.4799
	Airbag brace	1.626	1.049	0.5612	0.4692
	Airbag jacket	1.251	0.885	0.5034	0.4397

Chapter 10

Guidelines for EU Standard

Studies found that effective injury prevention is most likely to come from protection systems worn by the rider rather than those attached to the motorcycle [de Rome et al., 2012]. No PPE is currently in existence, which can provide complete protection during an accidental impact, though a significant proportion of motorcycle injuries may be reduced by the use of certified PPE.

There is a very close relation between PPE and injury biomechanics. The importance of PPE has been demonstrated as reducing the frequency and extent of fatality, fracture of the bones, abrasions and lacerations of the skin and soft tissues in motorcycle crashes. Though the urge of developing a PPE is based on the injury biomechanics; the designing of a PPE not only depends on the protection from the injuries but also on the wearer's comfort and style.

It is important that the PPE conform to relevant EU directives regarding health and safety or environmental protection marked with "CE". This present chapter provides some guidelines, which could be strongly considered in the future standard for motorcyclists' neck protectors.

10.1 Innocuousness

Innocuousness of a PPE defines the quality of being harmless of that PPE. The existing neck braces in the market were developed using energy absorbing materials. Moreover, new neck protecting devices could be developed using garment materials used in the motorcycle clothing as shown in Chapter 8. So, the innocuousness defined in the standards for motorcycle clothing and impact protectors could be considered for the innocuousness of neck protectors. According to the innocuousness requirements of EN 13688 [Nasim et al., 2015], used in the standard for motorcycle protective garments, PPE materials and parts can not contain, release or degrade to release any harmful substances generally known to be toxic, carcinogenic, mutagenic, allergenic, teratogenic or otherwise harmful. The innocuousness requirements of EN 340 [Nasim et al., 2015] are used in the standard for motorcycle impact protectors. The color fastness to water of the constituent materials of protective clothing which likely could come into contact with the skin of the user, need to be tested according to EN ISO 105-E01 for textiles and according to EN ISO 11642 for leather [Nasim et al., 2015]. In case of any inflatable system to be adopted, an additional evaluation of heat exposure in accordance with the

ergonomic test should be conducted. Gas generators containing pyrotechnic components can generate hot gases when fired [Nasim et al., 2015].

10.2 Ergonomics

This section is based on the ergonomics tests according to the existing standards for gloves, boots, protective clothing and impact protectors. The neck protector should be examined visually for design features that may interfere with riding or present a hazard to the rider. The ergonomic exercises should be carried out to detect any sharp edges or sharp points such as studs, rivets and staples or other items in both external and internal body that might injure the users. Moreover, string type designs should not be allowed as it might result in strangling of the neck. However, the strings could be attached on the garments, so that they do come in direct contact with the neck.

The protector should be put on by an assessor of suitable size with experience of riding a motorcycle, if applicable, using the restraint systems supplied with the protector. Similarly, to the other existing standards, a set of questions could be set to assess the protector, where the assessor should fill the questionnaire with “Yes” in order to make the assessment process passed. Some sample questions are, but not limited to, as follows [Nasim et al., 2015]:

- “Is it possible to put on the protector and to operate the fasteners and adjusters without impediment?”
- “Is it possible to put on the gloves or helmet while using the protector?”
- “Is the protector free from any rough, sharp or hard components, or other features that might cause irritation or that would make riding hazardous?”
- “Can you get on and off a motorcycle?”
- “Can you comfortably reach the controls of the motorcycle?”
- “Can you turn your head and torso sufficiently when on a motorcycle?”
- “Can you confirm that the adjustment system, if present, does not cause discomfort while performing the movements?”
- “Does the adjustment system, if present, securely hold the protector in place?”

10.3 New Anthropomorphic Test Device (ATD)

It is important to develop one biofidelic test setup to conduct impact tests and to evaluate the neck protecting devices for the motorcyclists. The most common ATD used for automotive purposes is the hybrid III dummy. There are other biofidelic ATDs used in the automotive crash analyses (e.g. BioRID, THOR, SID). But, these ATDs are not validated for the impact loadings observed in the motorcycle accidents. Some modified neck ATDs are available, which could be used for direct impacts as described in Section 5.1.2. However, the geometry of the D-neck model has potential to develop a new neck

ATD, because of its simplified geometry and biofidelic response in direct compressive impacts. Based on the need and potentiality of the D-neck model, it was 3D printed and the vertebrae were arranged sequentially as shown in Figure 10.1 (left). Further, rubber as intervertebral discs were placed inside the adjacent vertebrae. To create force of ligaments and passive muscles, elastic bands were considered. Then, the neck model was coupled with the hybrid III head model as shown in the Figure 10.1 (right). It is just a preliminary prototype that was initiated to develop, but further investigations and developments are needed to finalize the neck ATD.

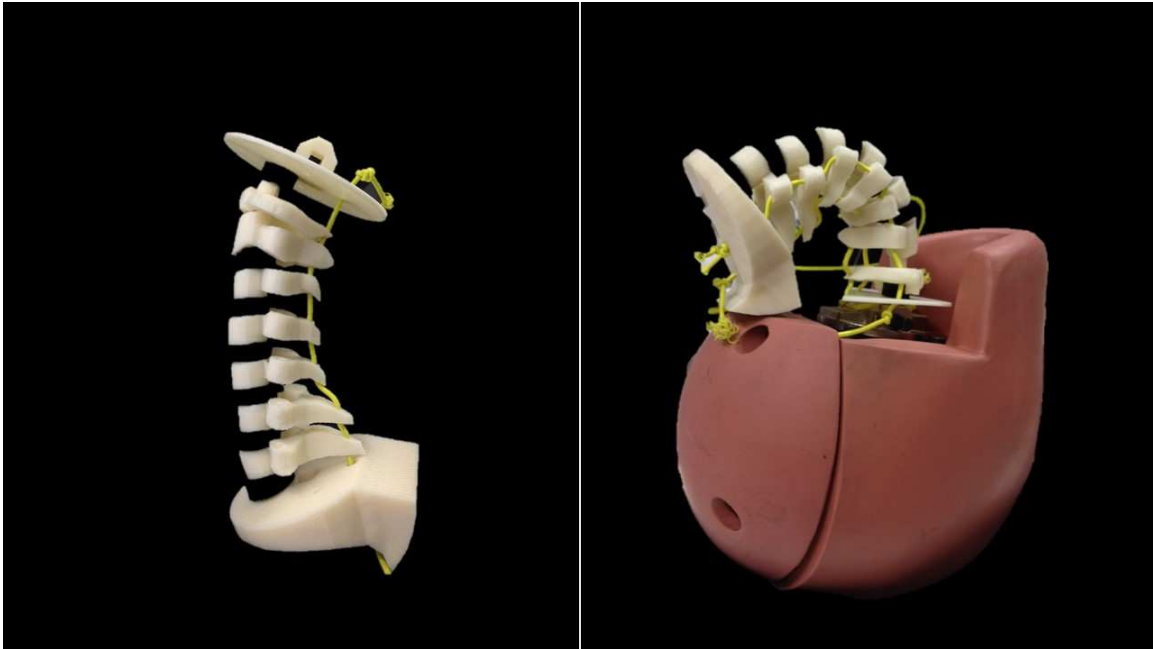


Figure 10.1 New neck ATD with 3D the printed vertebrae from D-neck model

10.4 Test Methods

Testing of a PPE is the most important concern in the standards. The neck injury mechanisms in motorcycle accidents are not clear and hence it is difficult to suggest appropriate test methods for neck protectors of motorcyclists. The injury mechanisms and the biomechanics of the neck by using different types of neck protectors are still under research. However, based on the accident data found in the literatures and also considering the methodologies applied in the existing PPEs, six different setups were designed in this thesis (Section 9.2.2). All the tests were based on the direct impacts to the helmet as this thesis already reported that the main mode of occurring the neck injury is by direct impacts to head and then the transfer of the force from head to neck. Standard helmets must be considered to perform the tests and the neck protectors should be properly restrained with the ATD according to the restraint systems considered in the design.

Repeatability of the results is an important factor in the standards. Hence, each test should be performed at least three times to guarantee the test results. The test samples should be prepared at specific temperature and humidity to ensure the compatibility with the weather condition.

10.5 Neck Injury Risk Assessment

An assessment procedure of the test results must be included in the standard. This might be done as pass/fail criteria or defining two or more protection levels, as found in the existing standards described in Chapter 4. Varieties of neck injury metrics, which are used to assess the neck injury risk, were described in Section 2.5. But, only Neck Injury Index (NII) was developed for motorcycle crash analysis. The NII was validated for predicting the risk of injury to the upper cervical spine of the motorcycle riders, which has been adopted in the standard of ISO 13232-5 [ISO 13232-5:2005]. The upper neck injury risk prediction using NII injury criterion was calculated for this thesis (see Section 9.4.1). However, the capability of NII is limited, as it cannot predict the injury risk in the whole cervical spine region.

All the neck protective systems were developed based on the assumption of restricting the neck movement by restricting the head rotation. But, there is no neck injury criterion, which includes the head rotation. Goldsmith and Ommaya (1984) conducted sled tests with volunteer and cadaver and recommended the flexion-extension corridors accounting the dynamic neck loading (Figure 2.11). The corridors indicated the pain and injury thresholds as a function of head rotation relative to torso. The pain thresholds found in the volunteer tests were at 47.5 Nm (for extension) and 59.7 Nm (for flexion). Also, the limits for serious injuries achieved in cadaver tests were at 56.7 Nm (for extension) and 190 Nm (for flexion).

The aforementioned flexion-extension corridors were used to show the relationship between the neck moment and the head rotation relative to torso, with and without the neck protective systems considered for this thesis. Figure 10.2 (for case 1 and case 4 from Chapter 9) shows that all the curves were inside the corridor for case 4, but, for case 1, the curves went outside of the corridor at maximum rotational angles. The head rotation was lowest for the airbag brace, but resulted in highest neck moment. Hence, restriction of the neck movement, by restricting the head rotation, cannot guarantee the neck injury reduction. However, a proper corridor is needed, which will account for the impact loadings observed in the motorcycle crashes.

Based on the above discussion, it is important to develop appropriate neck injury criteria, which will be able to predict the neck injury in the whole cervical spine region of the motorcycle riders. Investigations are needed to verify the significance of the head rotation

on the neck injuries considering the impact conditions of the motorcycle crashes and then to include the head rotation in the neck injury assessment process.

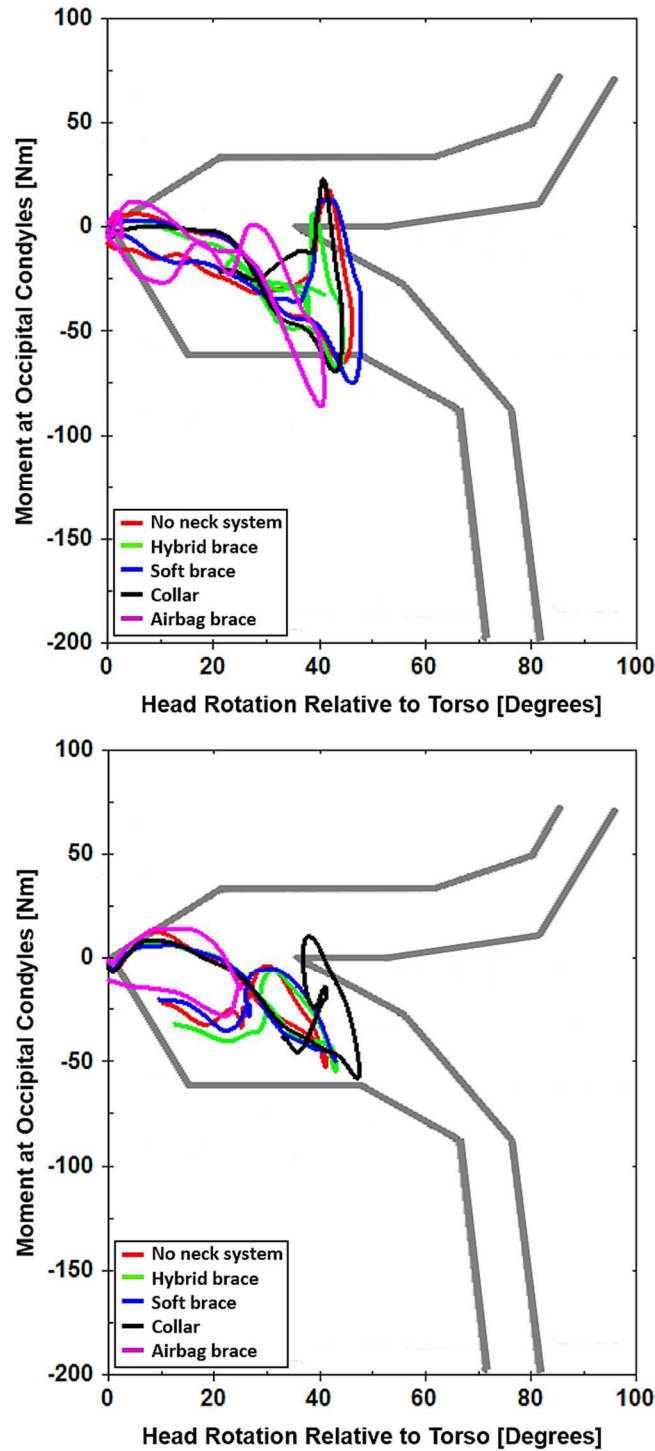


Figure 10.2 The relationship between the neck moment and the head rotation relative to torso of the different neck protective systems for case1: frontal slide (top) and case 4: -15° inverted (bottom). The grey corridor represents the flexion-extension corridor proposed by Goldsmith and Ommaya (1984), where positive and negative moments indicate extension and flexion respectively

10.6 Labelling

The information of each product claiming to be protective according to the standard must be provided with the product. This could be done by the mean of perfectly legible pictogram permanently attached with the product or other instruction guides, though these methods might supply limited information to the users. However, the labelling should contain at least the following information [Nasim et al., 2015]:

- A mean of identification of the manufacturer or its authorized representative, for example a trademark.
- The place of production.
- The commercial name of the product, style code or other means of identification.
- Size of the product.
- A level of protection or other means to indicate the quality of the product. This indication must be based on the tests performed to assess the protectors.
- Specification of the type of helmet needs to be used to meet the provided quality. This should be done according to the type of helmet used in the standard tests.
- Specification of the type(s) of road, where the neck protector would be suitable to be used.
- A warning about the limitations of the product while using, if any.
- Care and cleaning instructions.
- A trademark of the “CE marking” should be provided, which literally means the “European Conformity” declared by the manufacturer that the product complies with the essential requirements of the relevant European health, safety and environmental protection legislation.

Chapter 11

Conclusions

11.1 Summary of the Research

Although a variety of neck braces were designed to protect the neck from injury in motorcycle accidents, the effectiveness of those neck braces in reducing the injury risk is not clear due to the lack of scientific evidences. Moreover, there are no current standard test methods for neck protectors.

Three new functional prototypes of neck protective systems were designed for the motorcyclist riders. Additionally, a new biofidelic finite element (FE) neck model was developed and coupled with Hybrid III head model, which was validated for different impact conditions. In order to develop an anthropomorphic test device, a rigid torso was added with the neck model. The new neck protective systems and the existing hybrid neck brace were coupled with FE head-neck-torso model and six different test conditions were simulated. Focus was given on the neck injury risk assessment while comparing the results with different neck protectors.

It is not possible to highlight one specific protective system as the best, which will protect the neck during all kinds of impact loadings. The response of the neck with different neck protective systems is complicated as it exhibits different behaviour at different loading conditions. As an example, the neck shear force was increased by using the hybrid brace at frontal impact, but that force was reduced by the same brace at $+15^0$ inverted impact. Moreover, the behaviour of neck with a coupled protective system is dependent on the impact speeds.

However, the quality of the neck protective systems was analyzed using NII (Neck Injury Index) and Nij (Neck Injury Criterion) for predicting the injury risk in the upper neck. Though these injury metrics were validated for the impact conditions different from those considered in this thesis, these metrics were used based on their acceptance in the standards (ISO 13232-5 and FMVSS 208). The injury risk predictions for different neck protective systems could not be correlated between these two criteria. The analysis was continued using the NII_{cadaver} proposed by Bass et al. (2008) and more realistic injury risks were predicted. The results indicated the need of a proper neck injury criterion, which will be capable of predicting the injury risk in the whole cervical spine region during different motorcycle impact conditions and can be integrated in the future standard for motorcycle neck protectors. This thesis suggested investigating the significance of the

neck moment and the head rotation relative to torso in the neck injury assessment process.

11.2 Limitations

There are some limitations of this thesis. The key limitations are:

- The results shown are based on a specific helmet. They might be different with other helmet models.
- The neck model was not validated for the frontal, rear and lateral head-first impacts similarly to the loading conditions used in the evaluation process.
- Limitation of this study is primarily due to the lack of dynamic muscle response. The actual muscle active states during the motorcycle crashes are unknown. In this thesis, only one active state was used in the simulations for the evaluation of the neck protective systems, which was taken from the volunteer response in a sled test.
- The position of neck protective systems, with respect to neck, might play an important role in the analyses. However, the thesis did not show any comparison placing the systems in different positions.
- In the simulations, one fixed position of the neck was considered before the impact. It will be interesting to analyze the results by pre-positioning the neck with different orientations.
- For simplicity, the retention systems of the neck protectors were modeled with discrete elements. The results might be slightly different for some cases when the proper modeling of the retentions systems (probably with shell elements) would be used.

11.3 Future Work

In this thesis, the evaluation of the neck protective systems was provided based on the response of the simplified finite element D-neck model. Other biofidelic human head-neck models could be used to compare the results achieved by the simplified neck model.

It is important to assess the neck protective systems with different helmet models, so that the functionality of the systems will be more exposed.

Some challenging problems for the prototypes were indicated in Table 8.1. In the future, these challenges must be overcome to make the prototypes ready for the production.

A guideline of the standard test procedures was indicated in the previous chapter. In the next step, a standardization committee should be formed including the experts from the biomechanics community, test-houses and gear manufacturers. The committee will focus on the standard development for neck protectors.

Finally, at least one suitable design of the experimental setup is needed for testing the neck protectors. Neck anthropomorphic test device should be adopted in the experimental setup, which should be able to calculate the head position relative to torso, the upper neck axial and shear forces and the neck bending moment at occipital condyles.

References

- AAAM, AIS 2005: the injury scale. In: Gennarelli T, Wodzin E (eds) Association of Advancement of Automotive Medicine, Des Plaines, 2005.
- ACEM, MAIDS in-depth investigation of accidents involving powered two wheelers: Final report 1.2. Association of European Motorcycle Manufacturers (ACEM), Brussels, 2004.
- ACEM, Motorcycle Accidents in Depth Study (MAIDS) V2.0, 2009.
- Agur, A.M.R., and Dalley, A.F., 2005. Grant' s Atlas of Anatomy 11th Ed. Lippincott Williams and Wilkins, Philadelphia.
- Allen, B.L., Ferguson, R.L., Lehmann, T.R., O'Brien, R.P., 1982. A mechanistic classification of closed, indirect fractures and dislocations of the lower cervical spine. *Spine*, 7 (1), 1-27.
- Anderson R.W.G., Streeter L.D., Ponte G., McLean, A.J., Pedestrian reconstruction using multibody madymo simulation and the polar II dummy: a comparison of head kinematics. Proceedings of the 20th International Technical Conference on the Enhanced Safety of Vehicles (ESV), 2007.
- Argenson, C., de Peretti, F., Ghabris, A., Eude, P., Lovet, J., and Hovorka, I., 2002. Classification of Lower Cervical Spine Injuries. *European Journal of Orthopaedic Surgery and Traumatology* 7(4), 215 – 229.
- Babcock, J.L., 1976. Cervical spine injuries. *Arch Surg*, 111, 646-51.
- Bambach M.R., Grzebieta R.H., McIntosh A.S., Injury typology of fatal motorcycle collisions with roadside barriers in Australia and New Zealand. *Accid. Anal. Prev.* 49, 253–260, 2012.
- Bass C.R., Donnellan L., Salzar R., Lucas S., Folk B., Davis M., Rafaels K., Planchak C., Meyerhoff, K., Ziemba A., Alem N., A new neck injury criterion in combined vertical/frontal crashes with head supported mass. In *Proceeding of International Research Council on the Biomechanics of Impact*, Madrid (Spain), September 2006, 75-91, 2006.
- Bass C.R., Crandall J.R., Salzar R.S., Rafaels K., Damon A., Lucas S., Assessing the Neck Injury Index (NII) using experimental cadaver tests, In: *Proceedings of IRCOBI conference*, pp 253–265, 2008.
- Bazaldúa C. J. J.; González, L. A.; Gómez, S. A.; Villarreal, S. E. E.; Velázquez, G. S. E.; Sánchez, U. A.; Elizondo-Omaña, R. E. & Guzmán, L. S., Morphometric study of

cervical vertebrae C3-C7 in a population from northeastern Mexico. *Int. J. Morphol.*, 29(2):325-330, 2011.

Bhosale P.V., Modeling of Motorcycle Anthropometric Test Device Neck Using Reverse Engineering Technique. ASME. ASME proceedings, Volume 17: Transportation Systems, 2008.

Bortenschlager K., Kramberger D., Barnsteiner K., Hartlieb M., Ferdinand L., Leyer H., Muser M., Schmitt K.-U., Comparison tests of BioRID II and RID-2 with regard to repeatability, reproducibility and sensitivity for assessment of car seat protection potential in rear-end impacts. *Stapp Car Crash J* 47:473–488, 2003.

Boström O., Bohman K., Håland Y., Kullgren A., Krafft M., New AIS1 long-term neck injury criteria candidates based on real frontal crash analysis. In: Proceedings of IRCOBI conference, pp 249–264, 2000.

Boström O., Svensson M., Aldman B., Hansson H., Håland Y., Lövsund P., Seeman T., Suneson A., Säljö A., Örtengren T., A new neck injury criterion candidate based on injury findings in the cervical spinal ganglia after experimental neck extension trauma. In: Proceedings of IRCOBI conference, pp 123–136, 1996.

Brolin, K., and Halldin, P., Development of a Finite Element Model of the Upper Cervical Spine and a Parameter Study of Ligament Characteristics. *Spine* 29(4), 376 – 385, 2004.

Brolin, K., Halldin, P., and Leijonhufvud, I., 2005. The Effect of Muscle Activation on Neck Response. *Traffic Injury Prevention* 6, 67 – 76. 2005.

Camacho D.L.A., Nightingale R.W., Robinette J.J., Vanguri, S.K., Coates, D.J., and Myers, B.S., Experimental Flexibility Measurements for the Development of a Computational Head-Neck Model Validated for Near-Vertex Head Impact. Proceedings from the 41st Stapp Car Crash Conference, 473 – 486. SAE 973345, 1997.

Camacho D.L.A., Nightingale, R.W. and Myers B.S., Surface Friction in Near-Vertex Head and Neck Impact Increases Risk of Injury. *Journal of Biomechanics* 32, 293 – 301, 1999.

Carlsson A, Linder A, Davidsson J, Hell W, Schick S, Svensson M, Dynamic kinematic responses of female volunteers in rear impacts and comparison to previous male volunteer tests. *Traffic Inj Prev* 12(4):347–357, 2011.

Carlsson A, Siegmund G, Linder A, Svensson M, Motion of the head and neck of female and male volunteers in rear impact car-to-car impacts. *Traffic Inj Prev* 13(4):378–387, 2012.

Carter, J.W., Compressive Cervical Spine Injury: The Effect of Injury Mechanisms on Structural Injury Pattern and Neurologic Injury Potential. PhD Thesis. University of Washington, 2002

CEN, Motorcyclists' protective clothing against mechanical impact - Part 3: Motorcyclists' chest protectors - Requirements and test methods, prEN 1621-3:2010, 2010.

CEN, Motorcyclists' protective clothing against mechanical impact - Part 4: Motorcyclists' inflatable protectors - Requirements and test methods, FprEN 1621-4:2012, 2012.

CEN, PrEN 17092:2017, Protective clothing for professional motorcycle riders – Jackets, trousers and one-piece or divided suits – General Requirements, 2017.

Cernicchi, A., Galvanetto, U., Iannucci, L., Virtual modelling of safety helmets: practical problems. *Int. J. Crashworthiness* 13, 451–467, 2008.

Chang F.-K. and Chang K.-Y., A progressive damage model for laminated composites containing stress concentrations. *Journal of Composite Materials*, 21 (9), 834–855, 1987.

Chazel, J., Tanguy, A., Bourges, M., Gaurel, G., Escande, G., Guillot, M., and Vanneuville, G., 1985. Biomechanical Properties of Spinal Ligaments and a Histological Study of the Supraspinal Ligament in Traction. *Journal of Biomechanics* 18(3), 167 – 176.

Chen H., Zhang L., Wang Z., Yang K.H., King I., Biomechanics of the neck, *Theor. Biomech.*, 386–402, 2011.

Clarke E. C. 2011. Spinal Cord Mechanical Properties. In: Bilston L. E., editor, *Neural Tissue Biomechanics*. Springer.

COST 327. Motorcycle safety helmets. European Co-operation in the field of Scientific and Technical research (COST) project, European Commission, Brussels, Belgium, 2001.

Craig G.R., Sleet R., Wood S.R., Lower limb injuries in motorcycle accidents. *Injury* 15, 1983, 163-166.

Crandall J.R., Bose D., Forman J., Untaroiu C.D., Arregui-Dalmases C., Shaw C.G., Kerrigan J.R., Human Surrogates for Injury Biomechanics Research. *Clinical Anatomy*, 24. 362-71, 2011.

Currey, J.D., 2004. Tensile Yield in Compact Bone is Determined by Strain, Post-Yield Behaviour by Mineral Content. *Journal of Biomechanics* 37, 549 – 556.

- Dauvilliers, F., Bendjellal, F., Weiss, M., Lavaste, F., and Tarriere, C., Development of a Finite Element Model of the Neck. Proceedings from the 38th Stapp Car Crash Conference, 77 – 91. SAE 942210, 1994.
- De Jager, M., Suren, A., Thunnissen, J., and Wismans, J., A Three-Dimensional Head-Neck Model: Validation for Frontal and Lateral Impacts. Proceedings from the 38th Stapp Car Crash Conference, 93 – 109. SAE 942211, 1994.
- De Jager, M., Suren, A., Thunnissen, J., and Wismans, J., A Global and a Detailed Mathematical Model for Head-Neck Dynamics. Proceedings from the 40th Stapp Car Crash Conference, 93 – 109. SAE 962430, 1996.
- de Rome L., Ivers R., Fitzharris M., Du W., Richardson D., Haworth N., Heritier S., Motorcycle protective clothing: Protection from injury or just the weather? Accident Analysis and Prevention 43 (6), 2011.
- de Rome L., Gibson T., Haworth N., Ivers R., Sakashita C., Varnsverry P., Improving consumer information about motorcycle protective clothing products, Reports for the Motor Accidents Authority of NSW (MAA), Australia, 2012.
- de Rome L., Stanford G., Wood, B., Motorcycle Protective Clothing, Road Safety Research, Policing and Education Conference, Sydney, 2013.
- Dehner C, Elbel M, Schick S, Walz F, Hell W, Kramer M, Risk of injury of the cervical spine in sled tests in female volunteers. Clin Biomech (Bristol, Avon) 22(6):615–622, 2007.
- Deng, Y.C., Goldsmith, W., Response of a Human Head/Neck/Upper-Torso Replica to Dynamic Loading-II: Analytical/Numerical Model. Journal, 1987.
- Deng, Y.C., Li, X., and Liu, Y., Modeling of the Human Cervical Spine Using Finite Element Techniques. Proceedings from the 43rd Stapp Car Crash Conference. SAE 1999-01-1310, 1999.
- Deng, Y.C., and Fu, J., Simulation and Identification of the Neck Muscle Activities During Head and Neck Flexion Whiplash. Proceedings from the 46th Stapp Car Crash Conference. SAE 2002-01-0017, 2002.
- DeWit J. A., Cervical spine segment finite element model validation and verification at traumatic loading levels for injury prediction. Proceedings from the IRCOBI conference, 59-77, 2010.
- Doherty B, Esses S, Heggeness M, A biomechanical study of odontoid fractures and fracture fixation. Spine 18(2):178–184, 1993.

Dolomiticert, Protective clothing for professional motorcycle riders – Jackets, trousers and one-piece or divided suits – General Requirements, Technical Disciplinary for European Standard, 2012.

ECE, Economic Community of Europe (ECE), ECE 22.05: Uniform provisions concerning the approval of protective helmets and their visors for drivers and passengers of motor cycles and mopeds, Agreement No. 22, Revision 4, 2002.

ECE, Regulation No.94. Uniform provisions concerning the approval of vehicles with regard to the protection of occupants in the event of a frontal collision. United Nations Economic Commission for Europe –Transport Division, May 8, 2007.

EEVC, Report on motorcycle Safety. An EEVC Paper, Report of the Ad-hoc Group on Motorcycle Safety, 1993. European Experimental Vehicles Committee Brussels, pp. 75, 1993.

Eliasson E., Wass J., Industrialisation of a Finite Element Active Human Body Model for Vehicle Crash Simulations, Master's Thesis, Chalmers University of Technology, 2015.

Engelbrektsson, K., Evaluation of material models in LS-DYNA for impact simulation of white adipose tissue. MSc. Thesis. Chalmers University of Technology, Gothenburg, Sweden, 2011.

Eppinger R., Sun E., Kuppala, S. Saul R., Supplement: development of improved injury criteria for the assessment of advanced automotive restraint systems – II. NHTSA Docket No. 2000-7013-3, March, 2000.

Eriksson L., Kullgren A., Influence of seat geometry and seating posture on NICmax long-term AIS 1 neck injury predictability. Traffic Injury Prevention, 7, 61-9, 2006.

European Commission, Traffic Safety Basic Facts 2017 – Motorcycles & Mopeds, ec.europa.eu/transport/road_safety/sites/roadsafety/files/pdf/statistics/dacota/bfs2017_momotoped.pdf, 2017.

Ewing, C.L., Thomas, D.J., Beeler, G.W., Patrick, L.M., and Gillis, D.B., Dynamic Response of the Head and Neck of the Living Human to –Gx Impact Acceleration. Proceedings from the 12th Stapp Car Crash Conference 424 – 439. SAE 680792, 1968.

Ewing CL, Thomas DJ, Lustik L, Muzzy WH III, Willems GC, Majewski P. Dynamic response of the human head and neck to +Gy impact acceleration. Proc. Stapp Conf., 21st, New Orleans, Paper no. 770928, pp. 547–86. Warrendale, PA: Soc. Automot. Eng., 1977.

Ewing C.L., Thomas D.J., Lustik L., Willems G.C., Muzzy III W.H., Becker E.B., and M.E. Jessop. Dynamic response of human and primate head and neck to +Gy impact

acceleration. Report DOT HS-803-058, Naval Aerospace Medical Research Laboratory, Pensacola, 1978a.

Ewing CL, Thomas DJ, Lustick L, Muzzy WH III, Willems GC, Majewski P., Effect of initial position on the human head and neck response to +Y impact acceleration. Proc. Stapp Conf., 22nd, Ann Arbor, Mich., Paper no. 780888, pp. 101–38. Warrendale, PA: Soc. Automot. Eng., 1978b.

Feldkamp G., Junghanns K., The typical traffic accident in adolescents: The motorcycle accident - some epidemiologic features and the effectiveness of safety helmets and clothing. Proceedings of IRCOBI Amsterdam, 1976.

Fielding J, Cochran G, Lawsing J, Hohl M Tears of the transverse ligament of the atlas. J Bone Joint Surg 56A(8):1683–1691, 1974.

Filler A. G., Do You Really Need Back Surgery: A Surgeon's Guide to Neck and Back Pain and How to Choose Your Treatment, Oxford University Press, 2004.

Foster J.K., Kortge J.O., and Wolanin M.J., Hybrid III-A Biomechanically-Based Crash Test Dummy. Proceedings from the 21st Stapp Car Crash Conference. SAE Technical Paper 770938, 1977.

Fung, Y.C., Biomechanics: Mechanical Properties of Living Tissue 2nd Ed. Springer, New York, NY, 1993.

Gayzik F.S., Moreno D.P., Vavalle N.A., Rhyne A.C., Stitzel J.D., Development of the Global Human Body Models Consortium Mid-Sized Male Full Body Model. Proceedings of the 39th International Workshop. Injury Biomechanics Research, 2011.

Geisinger A., Andreas, Diehl-Thiele T., Kreitmeier H., Bachmann J., Müller P., Leatt C., Innovation in Development of BMW Motorrad Riders Equipement to reduce the Risk of Injury as shown with the Neck-Brace System, Proceedings of the 6th International Motorcycle Conference, Institut Für Zweiradsicherheit (IFZ), Cologne, 2006 p178-218.

Gilad, I., and Nissan, M., 1986. A Study of Vertebra and Disc Geometric Relations of the Human Cervical and Lumbar Spine. Spine 11(2), 154 – 157.

Goldsmith W, Ommaya AK (1984) Head and neck injury criteria and tolerance levels. In: Aldman B, Chapon A (eds) The biomechanics of impact trauma. Elsevier Science Publishers, Amsterdam, pp 149–187

Gray, H., Anatomy of the Human Body. Lea & Febiger, Philadelphia; Bartleby.com – 2000, 1918.

Griffin M. F., Leung B. C., Premakumar Y., Szarko M. and Butler P. E., Comparison of the mechanical properties of different skin sites for auricular and nasal reconstruction. *Journal of Otolaryngology - Head and Neck Surgery*, 46:33, 2017.

Halldin, P.H., Brolin, K., Kleiven, S., von Holst, H., Jakobsson, L., and Palmertz, C., Investigation of Conditions that Affect Neck Compression-Flexion Injuries Using Numerical Techniques. Proceedings from the 44th Stapp Car Crash Conference. SAE 2000-01-SC10, 2000.

Hallquist J.O., LS-DYNA Keyword Users Manual. Livermore Software Technology Co., Livermore, CA., 2006.

Harris, J.H., Edeiken-Monroe, B., Kopaniky, D.R., 1986. A practical classification of acute cervical spine injuries. *Orthopedic Clinics of North America*, 17 (1), 15-30.

Haworth N., De Rome L., Rowden P., Motorcycle protective clothing: Stage 1 review of literature and development of a safety 'star rating' system (RSD-0299), Report to VicRoads, 2006.

Hayashi K., 2003. Mechanical Properties of Soft Tissues and Arterial Walls. In: Holzapfel G.A., Ogden R.W. (eds) *Biomechanics of Soft Tissue in Cardiovascular Systems*. International Centre for Mechanical Sciences (Courses and Lectures), vol 441. Springer, Vienna

Hedenstierna S., Halldin P., Siegmund G.P., Neck muscle load distribution in lateral, frontal, and rear-end impacts: a three-dimensional finite element analysis. *Spine*, 34(24):2626–33, 2009.

Heitplatz F., Sferco R., Fay P., Reim J., Kim A., Prasad P., An evaluation of existing and proposed injury criteria with various dummies to determine their ability to predict the levels of soft tissue neck injury seen in real world accidents. In: Proceedings of 18th ESV conference, 2003.

Herrman L.R. and Peterson F.E., A numerical procedure for viscoelastic stress analysis. In Proceedings of ICRPG Mechanical behavior working group. Orlando, 1968.

Hwang E., Hu J., Chen C., Klein K.F., Miller C.S., Reed M.P., Rupp J.D., Hallman J.J., Development, Evaluation, and Sensitivity Analysis of Parametric Finite Element Whole-Body Human Models in Side Impacts, *Stapp Car Crash J.*, 60:473-508, 2016.

Iatridis, J.C., Weidenbaum, M., Setton, L.A., and Mow, V.C., 1996. Is the Nucleus Pulposus a Solid or a Fluid? Mechanical Behaviors of the Nucleus Pulposus of the Human Intervertebral Disc. *Spine* 21, 1174 – 1184.

ISO 13232-5, Motorcycles – test and analysis procedures for research evaluation of rider crash protective devices fitted to motorcycles – Part 5: Injury indices and risk/benefit analysis, International Standards Organization, Geneva. 2005.

Iwamoto M., Kisanuki Y., Wantanabe I., Furusu K., Miki, K., Hasegawa J. Development of a finite element model of the Total Human Model for Safety (THUMS) and application to injury reconstruction. Proceedings from Conference of IRCOBI, Munich, Germany, 2002.

K.D. Klinich, R.A. Saul, G. Auguste, S. Backaitis, M. Klienberger, Techniques for developing child dummy protection reference values, 1996.

King A.I., Fundamentals of impact biomechanics: Part I—Biomechanics of the Head, Neck, and Thorax, Biomedical Engineering, 2:55-81, 2000.

Kleinberger M., Sun E., Eppinger R., Kuppa S., Saul R., Development of improved injury criteria for the assessment of advanced automotive restraint systems, 1998.

Kleinberger, M., Application of Finite Element Techniques to the Study of Cervical Spine Mechanics. Proceedings from the 37th Stapp Car Crash Conference, 261 – 272. SAE 933131, 1993.

Knaub K. and Myers B.S., Project F.2(c) Cervical Spine Muscle. National Highway Traffic Safety Administration, NHTSA-98-3588-133, 1998.

Kopperdahl, D.L., and Keaveny, T.M., Yield Strain Behavior of Trabecular Bone. Journal of Biomechanics 31, 601 – 608, 1998.

Kuppa S., Saunders J., Stammen J., Mallory A., Kinematically based whiplash injury criterion. In: Proceedings of 19th ESV conference, paper no. 05-0211, 2005.

Linder A, Carlsson A., Svensson M., Siegmund G., Dynamic responses of female and male volunteers in rear impacts. Traffic Inj Prev 9:592–599, 2008.

Lindstedt L., Vychytil J., Dziewonski T., Hyncik L., numerical tests of the virtual human model response under dynamic load conditions defined in federal aviation regulation part 23.562 and 25.562 – preliminary study, Archive of Mechanical Engineering, Vol. LXIII (4), 2016.

Lobdell T., Kroell C., Schneider D., Hering W., Nahum A., Impact response of the human thorax. In: King W, Mertz H, editors. Human Impact Response Measurement and Simulation. New York: Plenum Press. p 201–245, 1973.

Maiman D, Sances A, Myclebust J, Larson S, Houterman C, Chilbert M, El-Ghatit A (1983) Compression injuries of the cervical spine: a biomechanical analysis. Neurosurgery 13(3):254–260

Manschot, J.F.M., Brakkee, A.J.M., 1986. The measurement and modelling of the mechanical properties of human skin in vivo – II. The model. *J. Biomech.* 19 (7), 517–521.

Mayo Foundation for Medical Education and Research, 2004.

McElhaney J, Nightingale R, Winkelstein B, Chancey V, Myers B (2002) Biomechanical aspects of cervical trauma. In: Nahum Melvin (ed) *Accidental injury—biomechanics and prevention*. Springer, New York

McElhaney JH, Myers BS. 1993. Biomechanical aspects of cervical trauma. In *Accidental Injury—Biomechanics and Prevention*, ed. AM Nahum, JW Melvin, pp. 311–61. New York: Springer-Verlag

Merrill, T., Goldsmith, W., and Deng, Y.C., Three-Dimensional Response of a Lumped Parameter Head-Neck Model Due to Impact and Impulsive Loading. *Journal of Biomechanics* 17(2), 81 – 95, 1984.

Mertz H, Patrick L (1967) Investigation of the kinematics and kinetics of whiplash. In: *Proceedings of 11th stapp car crash conference*, pp 2952–2980, SAE 670919

Mertz H, Patrick L (1971) Strength and response of the human neck. In: *Proceedings of 15th stapp car crash conference*, pp 207–255, SAE 710855

Mertz HJ, Neathery RF, Culver CC. 1973. Performance requirements and characteristics of mechanical necks. In *Human Impact Response: Measurement and Simulation*, ed. WF King, HJ Mertz, pp. 263–88. New York: Plenum

Mertz H.J., Hodgson V.R., Thomas L.M., Nyquist G.W., An assessment of compressive neck loads under injury-producing conditions. *Physician and Sports Medicine*, 6(11), 95–106, 1978.

Mertz J.H., Irwin A.L., Prasad P., Biomechanical and scaling bases for frontal and side impact injury assessment reference values. *47th Stapp Car Crash Conference Proceedings*, 155-188, 2003.

Meyer F., Bourdet N., Deck C., Willinger R., and Raul J.S., Human Neck Finite Element Model Development and Validation Against Original Experimental Data. *Proceedings from the 48th Stapp Car Crash Conference*, 177 – 206. SAE 2004-22-0008, 2004

Meyer F., Deck C., Willinger R., Protection from motorcycle neck-braces using FE modeling, *Sports Engineering*, 2018.

Moore K.L., and Dalley A.F., *Clinically Oriented Anatomy* 5th Ed. Lippincott Williams and Wilkins, Philadelphia, 2006.

MOSAFIM, Motorcyclist road SAFety Improvement through better behaviour of the equipment and first aid devices. Final Technical Implementation Report, 2013.

Munoz, D., Mansilla, A., Lopez-Valdes, F., Martin, R., A study of current neck injury criteria used for whiplash analysis, proposal of a new criterion involving upper and lower neck load cells. In Proceedings of the 19th International Technical Conference on the Enhanced Safety of Vehicles (ESV), Washington D.C., June 6-9, 2005.

Muscolino J.E., Advanced Treatment Techniques for the Manual Therapist: Neck, Lippincott, Williams and Wilkins publishers, 2013.

Myers, B.S., McElhaney, J.H., Richardson, W.J., Nightingale, R.W., and Doherty, B.J., The Influence of End Condition on Human Cervical Spine Injury. Proceedings from the 35th Stapp Car Crash Conference, 391 – 399. SAE 912915, 1991.

Myers B.S. and Winkelstein B.A., Epidemiology, Classification, Mechanism and Tolerance of Human Cervical Spine Injury. Critical Reviews in Biomedical Engineering 23(5&6):307-409. 1995.

Nasim M., Brasca M., Cernicchi, A., Silani A., Standards in PPE, A survey, http://www.motorist-ptw.eu/wp-content/uploads/2015/10/MOTORIST-D3.5_Standards-in-PPE-a-survey.pdf, 2015.

Nasim M., Brasca M., Impact properties of polymeric materials used for motorcyclists' personal protective equipment, International Conference on Impact Loading of Structures and Materials, Turin, Italy, 2016.

Nasim M., Brasca M., Khosroshahi S. F., Galvanetto U., Understanding the impact properties of polymeric sandwich structures used for motorcyclists' back protectors, Polymer Testing. Vol. 61, pp. 249–257, 2017.

Nasim M., Cernicchi, A., Galvanetto U., The Effect Of Human Body Positioning On Neck Injuries During Compressive Impacts, Proceeding of International Conference on Impact Loading of Structures and Materials, Xi'an, China, 2018.

Nawrocki A., Demus J., Maklewska E., Mielicka E., Clothing protecting brachial plexus of motorcycle riding during collision. Fibres and Textiles in Eastern Europe, 2004,12(3) pp 53-57.

Nelson T. S., Cripton P. A., A new biofidelic sagittal plane surrogate neck for head-first impacts. Traffic Injury Prevention 11, 309-319, 2010.

Nigg, B. M., Biomechanics of Sport Shoes. Calgary, AB: Topline Printing Inc., 2010.

Nightingale, R.W., McElhaney, J.H., Richardson, W.J., and Myers, B.S., Dynamic Responses of the Head and Cervical Spine to Axial Impact Loading. *Journal of Biomechanics* 29(3), 307 – 318, 1996a.

Nightingale R. W., McElhaney J. H., Richardson W. J., Best T. M. and Myers B. S., Experimental cervical spine injury: relating head motion, injury classification. and injury mechanism. *Journal of Bone Joint Surgery*. 78-A(3) :412-421, 1996b.

Nightingale, R.W., McElhaney, J.H., Camacho, D.L., Kleinberger, M., Winkelstein, B.A., and Myers, B.S., The Dynamic Responses of the Cervical Spine: Buckling, End Conditions, and Tolerance in Compressive Impacts. *Proceedings from the 41st Stapp Car Crash Conference*, 451 – 471. SAE 973344, 1997.

Nightingale R.W., Sganga J., Cutcliffe H., ‘Dale’ Bass C.R., Impact responses of the cervical spine: A computational study of the effects of muscle activity, torso constraint, and pre-flexion, *Journal of Biomechanics* 49, 558–564, 2016.

Nordentoft E.L., Larsen C.F., Behrendorff I., The problem of leg injuries in motorcycle riders. In: Cesari, D., Charpenne, A. eds. *Proceedings of the International Conference of the Research Council on the Biomechanics of Impact*. IRCOBI, Delft, 1984.

Ogden, R.W., *Non-Linear Elastic Deformations*. Ellis Horwood Ltd., Chichester, Great Britain, 1984.

Ono K, Kaneoka K, Motion analysis of human cervical vertebrae during low speed rear impacts by the simulated sled. In: *Proceedings of IRCOBI conference*, pp 223–237, 1997.

Ono K, Kaneoka K, Human cervical vertebra motions and whiplash injury mechanism in low speed rear collision. In: *Proceedings of IIWPG/IRCOBI symposium on dynamic testing for whiplash injury risk, isle of man*, 2001.

Ono K, Ejima S, Suzuki Y, Kaneoka K, Fukushima M, Ujihashi S, Prediction of neck injury risk based on the analysis of localized cervical vertebral motion of human volunteers during low-speed rear impacts. In: *Proceedings of IRCOBI conference*, pp 103–113, 2006.

Ooi S.S., Wong S.S, Yeap J.S., Umar R., Relationship between Cervical Spine Injury and Helmet Use in Motorcycle Road Crashes. *Asia-Pacific Journal Public Health*, Vol. 23(4) pp: 608-619, 2011.

Östh J., Brolin, K., Svensson, M. Y., Linder ,A., A female ligamentous cervical spine finite element model validated for physiological loading. *J. Biomech. Eng.* 138(6), 2016.

Östh J., Mendoza-Vazquez, M., Sato, F., Linder , A., Svensson, M. Y., Brolin, K., A female head–neck model for rear impact simulations. *Journal of Biomechanics* 51 49–56, 2017a.

- Östh J., Mendoza-Vazquez M., Linder A., Svensson M.Y., Brodin K., The VIVA OpenHBM Finite Element 50th Percentile Female Occupant Model: Whole Body Model Development and Kinematic Validation. Proceedings of the IRCOBI Conference, Antwerp, Belgium, 2017b.
- Ouellet J.V., Hurt H.H., Thom D., Collision performance of contemporary crash bar and motorcycle rider leg injuries. Accident reconstructions: Automobiles, tractors, semitrailers motorcycles and pedestrians The Engineering Society for Advancing Mobility Land Sea Air and Space (SAE), Warrendale, PA 15096, pp. 2829 – 2842, 1987.
- Panjabi, M.M., Crisco, J.J., Lydon, C., and Dvorak, J., The Mechanical Properties of Human Alar and Transverse Ligaments at Slow and Fast Extension Rates. *Clinical Biomechanics* 13(2), 112 – 120, 1998.
- Panjabi M., Wang J., Delson N., Neck injury criterion based on intervertebral motions and its evaluation using an instrumented neck dummy. In: Proceedings of IRCOBI conference, pp 179–190, 1999.
- Panjabi, M.M., Chen, N.C., Shin, E.K., and Wang, J-L., The Cortical Shell Architecture of Human Cervical Vertebral Bodies. *Spine* 26(22), 2478 – 2484, 2001.
- Panzer M. B., Numerical modelling of the human cervical spine in frontal impact. PhD Thesis. University of Waterloo, 2006.
- Panzer M.B., Fice J.B., Cronin D.S., Cervical spine response in frontal crash. *Med Eng Phys.* 33:1147–1159, 2011.
- Patrick LM, Chou, CC. Response of X-ray study of the human neck in flexion, extension and lateral flexion. Veh. Res. Inst. Rep. VRI-7-3, Warrendale, PA: Soc. Automot. Eng., 1976.
- Prasad P., Daniel R.P., A biomechanical analysis of head, neck, and torso injuries to child surrogates due to sudden torso acceleration, in: 28th Stapp Car Crash Conf., 1984.
- Przybylski, G.J., Patel, P.R., Carlin, G.J., and Woo, S.L-Y., 1998. Quantitative Anthropometry of the Subatlantal Cervical Longitudinal Ligaments. *Spine* 23(8), 893 – 898.
- Robertson A., Branfoot T., Barlow I.F., and Giannoudies P.V., Spinal Injury Patterns Resulting From Car and Motorcycle Accidents. *Spine* 27(24), 2825 – 2830, 2002.
- Robin S., Human Model for Safety - A Joint Effort Towards the Development of Refined Human-Like Car Occupant Models. Proceedings from 17th International Conference for the Enhanced Safety of Vehicles, 2001.

Schmitt K.-U., Muser M., Walz F., Niederer P., Nkm—a proposal for a neck protection criterion for low speed rear-end impacts. *Traffic Inj Prev* 3(2):117–126, 2002.

Schmitt K.-U., Niederer P.F, Cronin D.S., Muser M.H., Walz F., *Trauma biomechanics: an introduction to injury biomechanics*, Forth Ed., Springer, 2014.

Schneider LW, Foust DR, Bowman BM, Snyder RG, Chaffin DB, Abelnour TA, Baum JK. Biomechanical properties of the human neck in lateral flexion. *Proc. Stapp Conf.*, 19th, San Diego, Paper no. 751156, pp. 455–86. Warrendale, PA: Soc. Automot. Eng. 1975.

Sengül G., Kadioglu H., *Morphometric Anatomy of the Atlas and Axis Vertebrae*, *Turkish Neurosurgery* 16, 69-76, 2006.

Shea M, Edwards W, White A, Hayes W, Variations of stiffness and strength along the human cervical spine. *J Biomech* 24(2):95–107, 1991.

Siegmund G.P., Sanderson D.J., Myers B.S., and Inglis J.T., Awareness affects the response of human subjects exposed to a single whiplash-like perturbation. *Spine* 28(7); 671– 679, 2003.

Siegmund G What occupant kinematics and neuromuscular responses tell us about whiplash injury. *Spine* 36(25S):S175–S179, 2011.

Sporner A., Langwieder K., Polauke J., *Passive safety for motorcyclists. From the leg protector to the airbag*. SAE Technical Paper Series, 1990.

Thunnissen J.G.M., Wismans J.S.H.M., Ewing C.L., and Thomas D.J., Human volunteer head-neck response in frontal flexion: a new analysis. In *Proceedings of the 39th Stapp Car Crash Conference*, pages 439–460. Society of Automotive Engineers, SAE Paper No. 952721, 1995.

Toomey D., *Cervical Spine Tolerance And Response In Compressive Loading Modes Including Combined Compression And Lateral Bending*, PhD thesis, Wayne State University, 2013.

Ulbrich E. J., Schraner C., Boesch C., Hodler J., Busato A., Anderson S. E., Eigenheer S., Zimmermann H., Sturzenegger M., Normative MR cervical spinal canal dimensions. *Radiology* 271, 172-182, 2014.

UNI Ente Italiano di Normazione, *Protective footwear for motorcycle riders - Requirements and test methods*, UNI EN 13634:2010, 2010.

UNI Ente Italiano di Normazione, *Motorcyclists' protective clothing against mechanical impact - Part 1: Motorcyclists' limb joint impact protectors - Requirements and test methods*, UNI EN 1621-1:2012, 2012.

UNI Ente Italiano di Normazione, Motorcyclists' protective clothing against mechanical impact - Part 2: Motorcyclists' back protectors - Requirements and test methods, UNI EN 1621-2:2013, 2013.

UNI Ente Italiano di Normazione, Protective gloves for motorcycle riders - Requirements and test methods, UNI EN 13594:2015, 2015.

Viano D., Crashworthiness and biomechanics, Euromotor Course, June 11–13 2001, Göteborg, 2001.

Viano D., Davidsson J., Neck displacements of volunteers, BioRID P3 and Hybrid III in rear impacts: implications to whiplash assessment by a neck displacement criterion (NDC). *Traffic Inj Prev* 3:105–116, 2002.

White A.A., and Panjabi M.M., *Clinical Biomechanics of the Spine*. 2nd Ed. J.B. Lippincott Co., Philadelphia, 1990.

White D., Lang J., Russell G., Tetsworth K., Harvey K., Bellamy N., A comparison of injuries to moped/scooter and motorcycle riders in Queensland, Australia. *Injury* 44, 855–862, 2013.

Whyte T., Gibson T., Anderson R., Eager D., Milthorpe B., Mechanisms of head and neck injuries sustained by helmeted motorcyclists in fatal real-world crashes: Analysis of 47 in-depth cases. *J. Neurotrauma*, 2016.

Wilber V.H., American Automobile Manufacturers Association Comments to Docket No. NHTSA Docket No. 98-4405; Notice 1 Advanced Technology Airbags: Attachment C. American Automobile Manufacturers Association, December 17, 1998 (NHTSA Docket 98-4405-79), 1998.

Williams, J.L., and Belytschko, T.B., A Three-Dimensional Model of Human Cervical Spine for Impact Simulation. *Journal of Biomechanical Engineering* 105, 321 – 331, 1983.

Winkelstein, B.A., Myers, B.S., The biomechanics of cervical spine injury and implications for injury prevention. *Medicine & Science in Sports & Exercise*, 29 (7), 246-55, 1997.

Winters, J.M., and Stark, L., Analysis of Fundamental Human Movement Patterns Through the Use of In- Depth Antagonistics Muscle Models. *IEEE Transactions in Biomedical Engineering* 12, 826 – 839, 1985.

Winters, J.M., and Stark, L., Estimated Mechanical Properties of Synergistic Muscles Involved in Movements of a Variety of Human Joints. *Journal of Biomechanics* 21(12), 1027 – 1041, 1988.

Winters, J.M., and Woo, S.L.Y., Multiple Muscle Systems: Biomechanics and Movement Organization. Springer-Verlag, New York, 1990.

Winters, J.M., How Detailed Should Muscle Models be to Understand Multi-Joint Movement Coordination?. Human Movement Science 14, 401 – 442, 1995.

Wismans J., Spenne D.H., Performance requirements for mechanical necks in lateral flexion. Proc. Stapp Conf., 27th, San Diego, Paper no. 831613, pp. 137-48. Warrendale, PA: Soc. Automot. Eng., 1983.

Wismans, J., van Oorashot, H., and Woltring, H.J., Omni-Directional Human Head-Neck Response. Proceedings from the 30th Stapp Car Crash Conference 313 – 331. SAE 861893. 1986.

Wismans J., Philippens M., van Oorschot E., Kallieris D., and Mattern R., Comparison of human volunteer and cadaver head-neck response in frontal flexion. In Proceedings of the 31st Stapp Car Crash Conference. Society of Automotive Engineers, SAE Paper No. 872194, 1987.

Wismans J., Happee R., van Dommelen J., Computational Human Body Models. In: Gilchrist M.D. (eds) IUTAM Symposium on Impact Biomechanics: From Fundamental Insights to Applications. Solid Mechanics and Its Applications, vol 124. Springer, Dordrecht, 2005.

Withnall C., Shewchenko N., Wiley K., Rogers N., An Improved Dummy Neck for the ISO 13232 Motorcycle Anthropometric Test Dummy, Paper No. 418, Proceedings of the 18th International Technical Conference on the Enhanced Safety of Vehicles, Nagoya, Japan, 2003.

Woods R.I., Johnson J. S., Mansdorf S.Z., Eds., Specification of motorcyclists' protective clothing designed to reduce road surface impact injuries, Performance of Protective Clothing: Fifth Volume ASTM STP 1237, American Society for Testing and Materials, Philadelphia, pp 3-22, 1996.

www.arrivealive.co.za, accessed date: 13th October, 2015.

www.cen.eu/, accessed date: 6th October, 2015.

www.dainese.com, accessed date: 13th October, 2015; and 25th January, 2017.

www.dynamore.se, accessed date: 26th July, 2018.

www.fairview.org/patient-education/85973, accessed date: 7th August, 2018.

www.ghbmc.com, accessed date: 26th July, 2018.

www.humaneticsatd.com/crash-test-dummies, accessed date: 25th July, 2018.

www.jasti.co.jp/en/support, accessed date: 25th July, 2018.

www.mavet.it, accessed date: 13th October, 2015.

www.newsroom.toyota.co.jp/en/detail/12497148, accessed date: 27th July, 2018.

www.piper-project.org/downloads, accessed date: 27th July, 2018.

www.pva-ppe.org.uk/standards, accessed date: 13th October, 2015.

Xu J., Shang S., Qi H., Yu G., Wang Y., Chen P., Simulative investigation on head injuries of electric self-balancing scooter riders subject to ground impact. *Accident Analysis & Prevention*. 89. 128-141, 2016.

Yamada H., 1970. *Strength of biological materials*. Williams & Wilkins, Baltimore, MD.

Yang, K.H., and Kish, V.L., Compressibility Measurement of Human Intervertebral Nucleus Pulposus. *Journal of Biomechanics* 21, 865, 1988.

Yang K.H., Hu J., White N.A., King A.I., Chou C.C., Prasad P., Development of numerical models for injury biomechanics research: A review of 50 years of publications in the Stapp Car Crash Conference. *Stapp Car Crash J* 50:429–490, 2006.

Yoganandan N., Pintar F., Haffner M., Jentzen J., Mainma D.J., Weinshel S.S., Larson S.J., Nichols H., and Sances A., Epidemiology and Injury Biomechanics of Motor Vehicle Related Trauma to the Human Spine. *Proceedings from the 33rd Stapp Car Crash Conference*, 223-242. SAE 892438, 1989.

Yoganandan N., Kumaresan S., Voo L., and Pintar F.A., Finite Element Applications in Cervical Spine Modeling. *Spine* 21(15), 1824 – 1834, 1996.

Yoganandan N., Pintar F., (eds) *Frontiers in whiplash trauma: clinical and biomechanical*. IOS Press, Amsterdam, 2000a.

Yoganandan, N., Kumaresan, S., and Pintar, F.A., Geometric and Mechanical Properties of Human Cervical Spine Ligaments. *Journal of Biomechanical Engineering* 122, 623 – 629, 2000b.

Yoganandan N., Kumaresan S., Pintar F., Gennarelli T., Pediatric biomechanics. In: Nahum Melvin (ed) *Accidental injury—biomechanics and prevention*. Springer, New York, 2002.

Zajac, F.E., 1989. Muscle and tendon: properties, models, scaling, and application to biomechanics and motor control. *Crit. Rev. Biomed. Eng.* 17 (4), 359–411.

Zhang, Q.H., Teo, E.C., Ng, H.W., and Lee, V.S., Finite Element Analysis of Moment-Rotation Relationships for Human Cervical Spine. *Journal of Biomechanics* 39, 189 – 19, 2006.

Appendix A

Impact Properties of Polymers Used for Impact Protectors

The impact behavior of a number of samples, made of materials commonly used for manufacturing body impact protectors, was studied. Nitrile butadiene rubber as the soft layer and polyethylene thermoplastic as the hard layer as shown in Figure A.1 were considered. The variables for the analyses were the thickness of the layers, the sample temperature and the distribution of the vent holes in the sample.

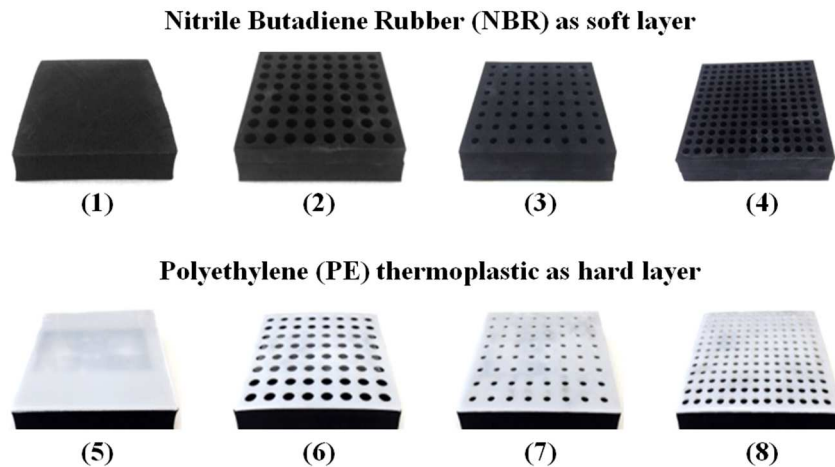


Figure A.1 Samples for the impact test: (1-4) NBR only and (5-8) sandwich of NBR and PE layers; sample configurations: solid (1, 5), vent holes with 8mm diameter (2, 6), vent holes with 5mm diameter (equal number of holes as for the sample with 8mm diameter) (3, 7) and vent holes with 5mm diameter (equal volume of void as for the sample with 8mm diameter) (4, 8).

Figure A.2 shows the force distribution capability of the hard part and the stability of the impact properties fairly dependent on the thickness of the soft part.

Figure A.3 and Figure A.4 are the numerical illustrations comparing the von Mises stress distribution in the samples due to the change in thickness of the hard part.

Figure A.5 shows that a reasonable distance between two consecutive vent holes is required for achieving optimal impact protection.

The impact behavior of NBR is considerably dependent on the temperature. The peak transmitted force abruptly increases in a range of about $\sim 16^{\circ}\text{C}$, where such increase appears with a shift as a function of the thickness of NBR layer. Such behavior raises a question on the feasibility of the testing procedures for the ambient impact test for the impact protectors, because a small change in the temperature around the ambient condition might give different level of protection or even fail the standard criterion. However, it depends on the material and thickness of the soft part used in the protector.

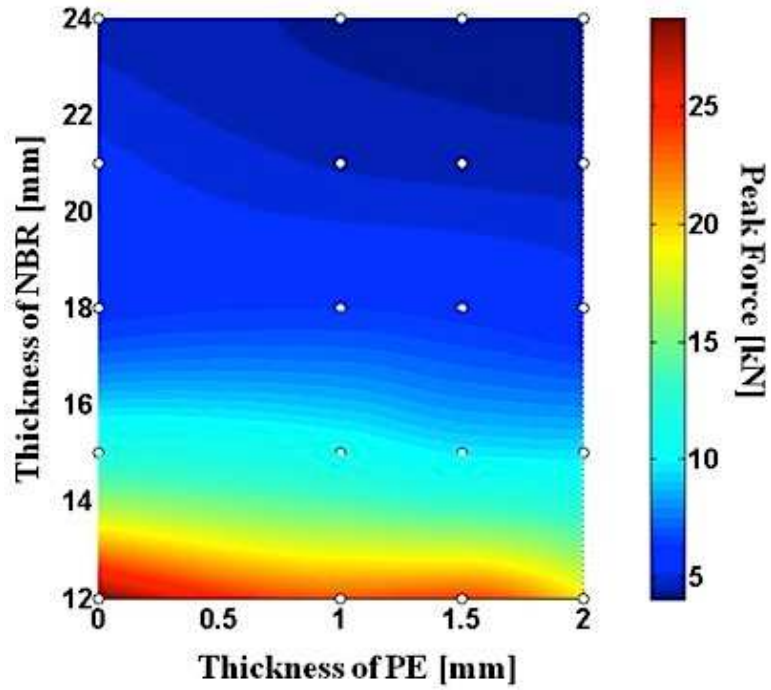


Figure A.2 The surface contour representing the peak transmitted force as a function of thickness of NBR and PE layers. The interpolated values from the experimental impact results (marked by 'o') were used to construct the figure.

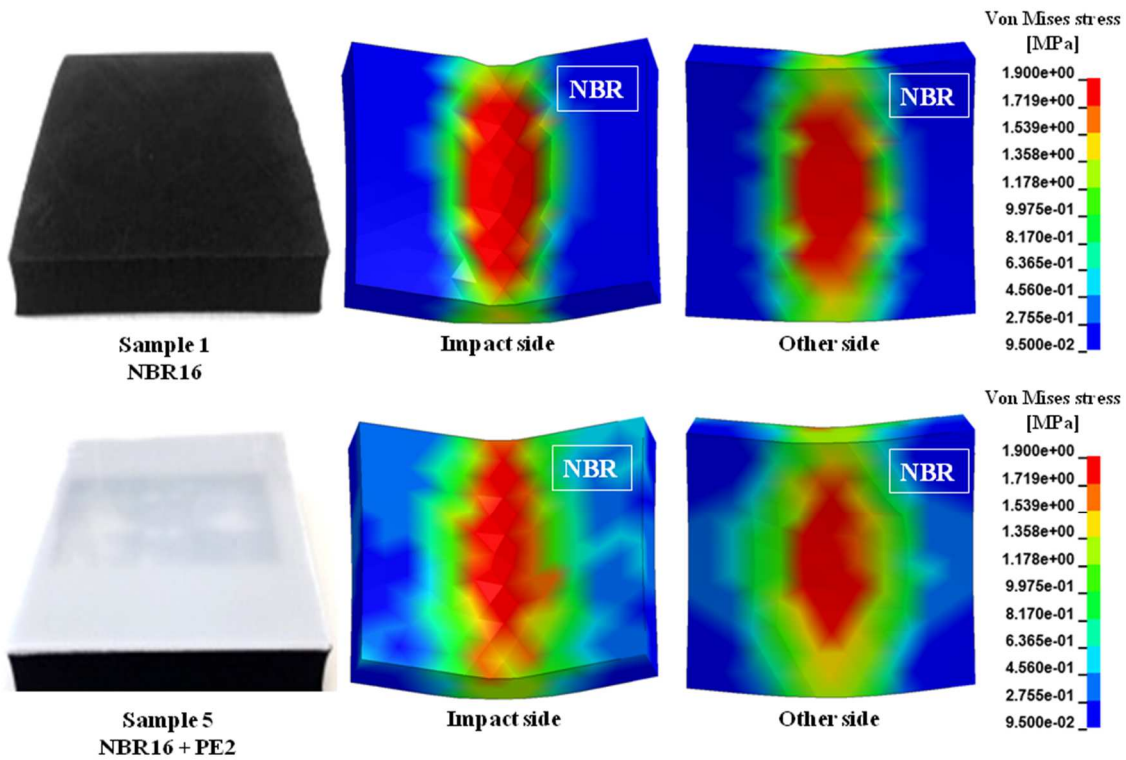
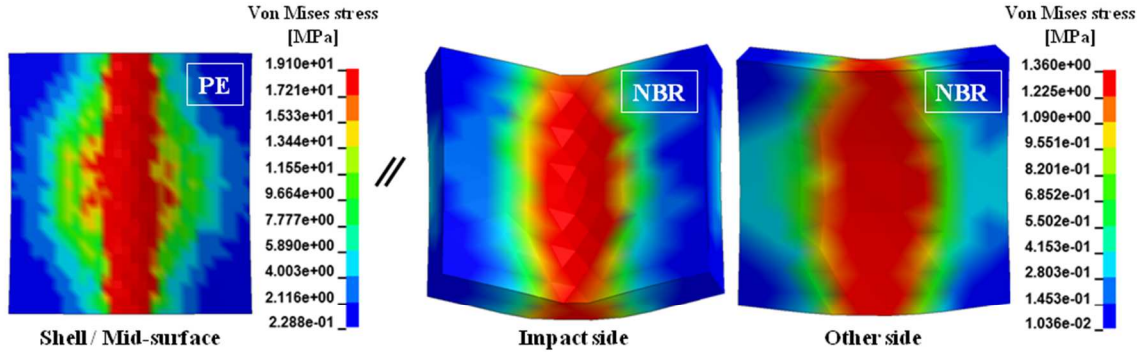
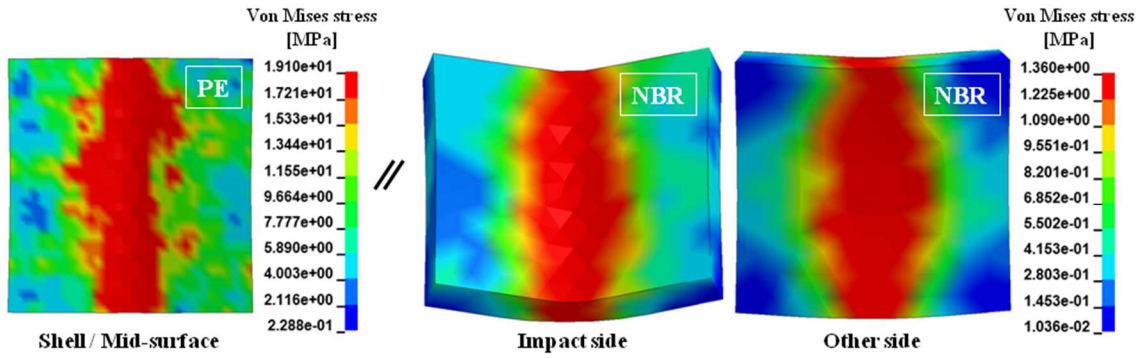


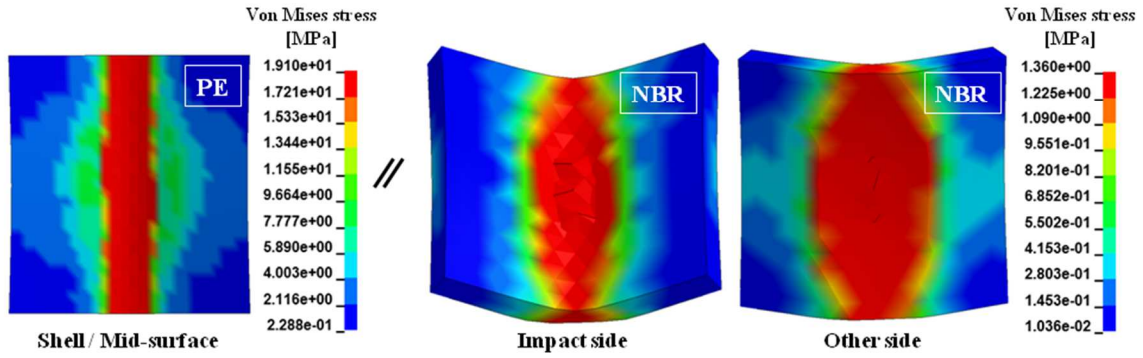
Figure A.3 The comparison of the von Mises stress distribution between the samples type 1 and 5 at the moment the transmitted force reaches the peak value. The thicknesses of NBR and PE layers are 16mm and 2mm respectively.



(a) Sample type 5 – NBR16 + PE1



(b) Sample type 5 – NBR16 + PE2



(c) Sample type 5 – NBR12 + PE2

Figure A.4 Contour maps showing the von Mises stress distribution in the sandwiches (sample type 5) with different thicknesses of NBR and PE layers at the moment the transmitted force reaches the peak value.

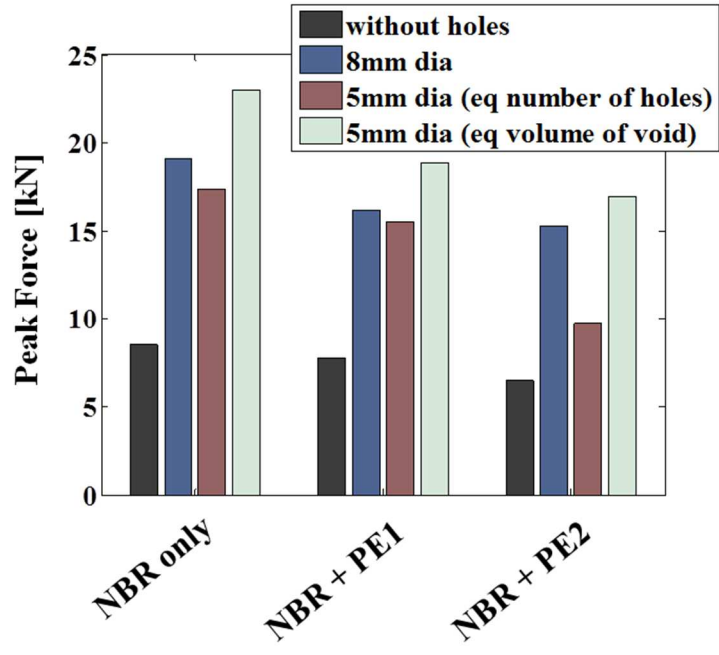


Figure A.5 Impact behavior due to the arrangement of vent holes in the samples of NBR only, NBR with PE of 1 mm and NBR with PE of 2 mm. The thickness of the NBR layer in all the samples is 16mm.

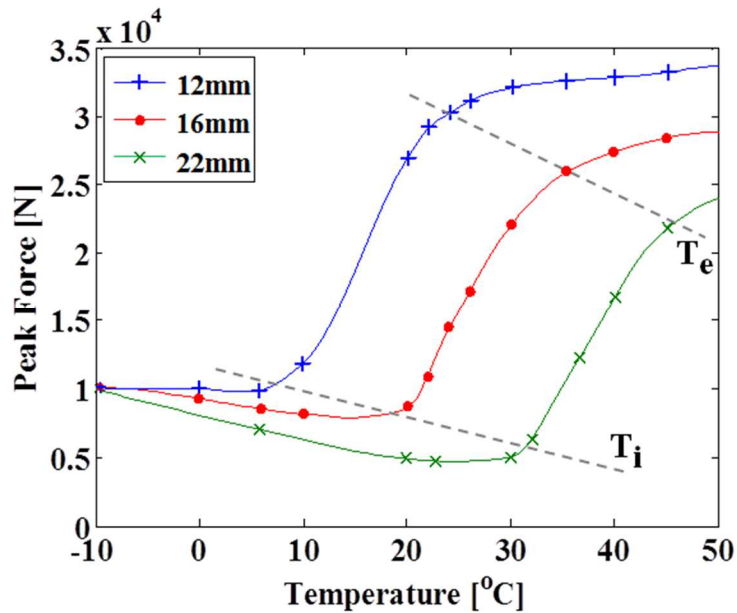


Figure A.6 The peak transmitted force through NBR samples (sample type 1) of 12mm, 16mm and 22mm of thickness as a function of temperature. The markers and the solid lines represent the experimental values and the fitted curves by interpolation respectively.

Appendix B

Stiffness of Hybrid III Neck

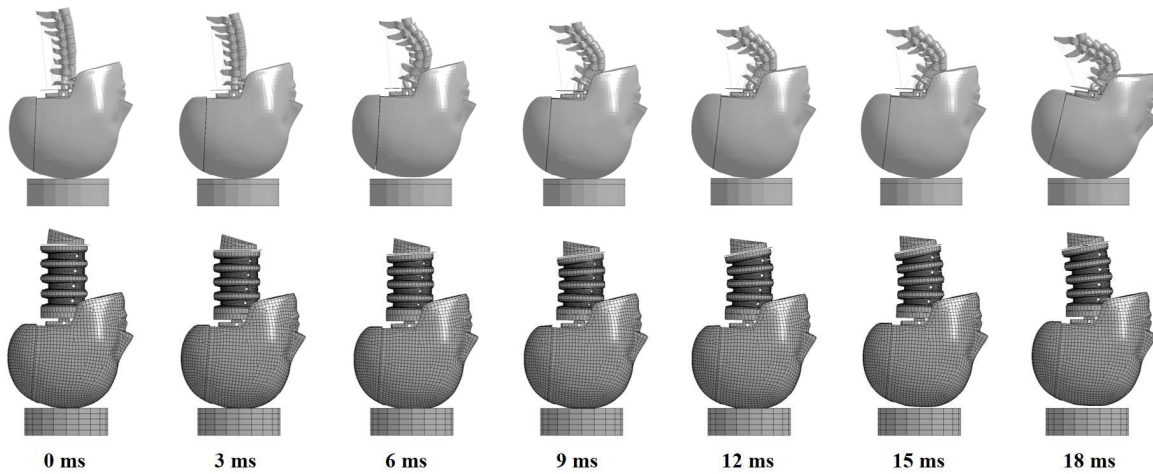


Figure B.1 Time lapse of the neck kinematics of the D-neck and hybrid III neck for the compressive impact. The orientation of the impact surface is 0° according to the experiments by Nightingale et al. (1996a, 1996b and 1997)

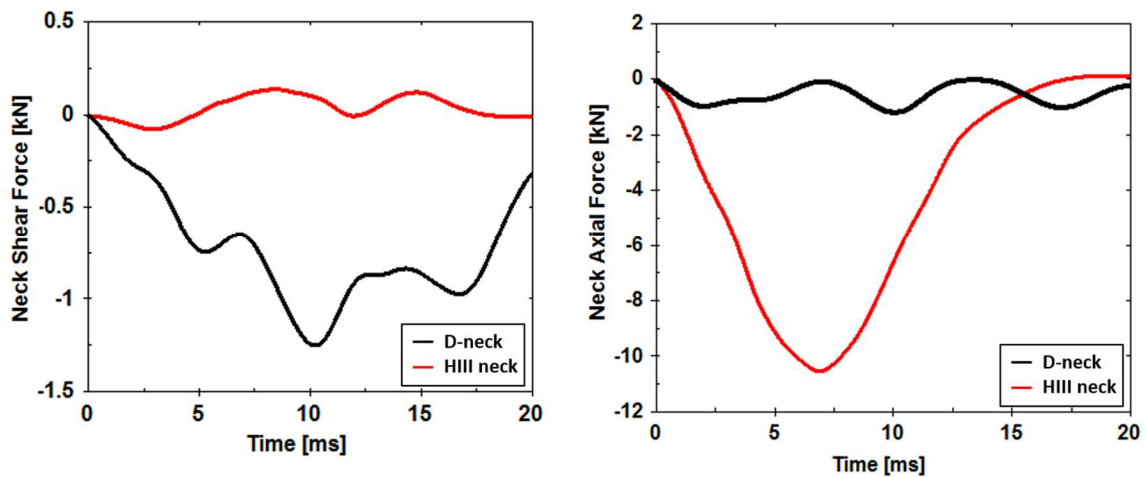


Figure B.2 Comparison of the upper neck forces between the D-neck and hybrid III neck

Appendix C

The Upper Neck Forces During Compressive Impacts

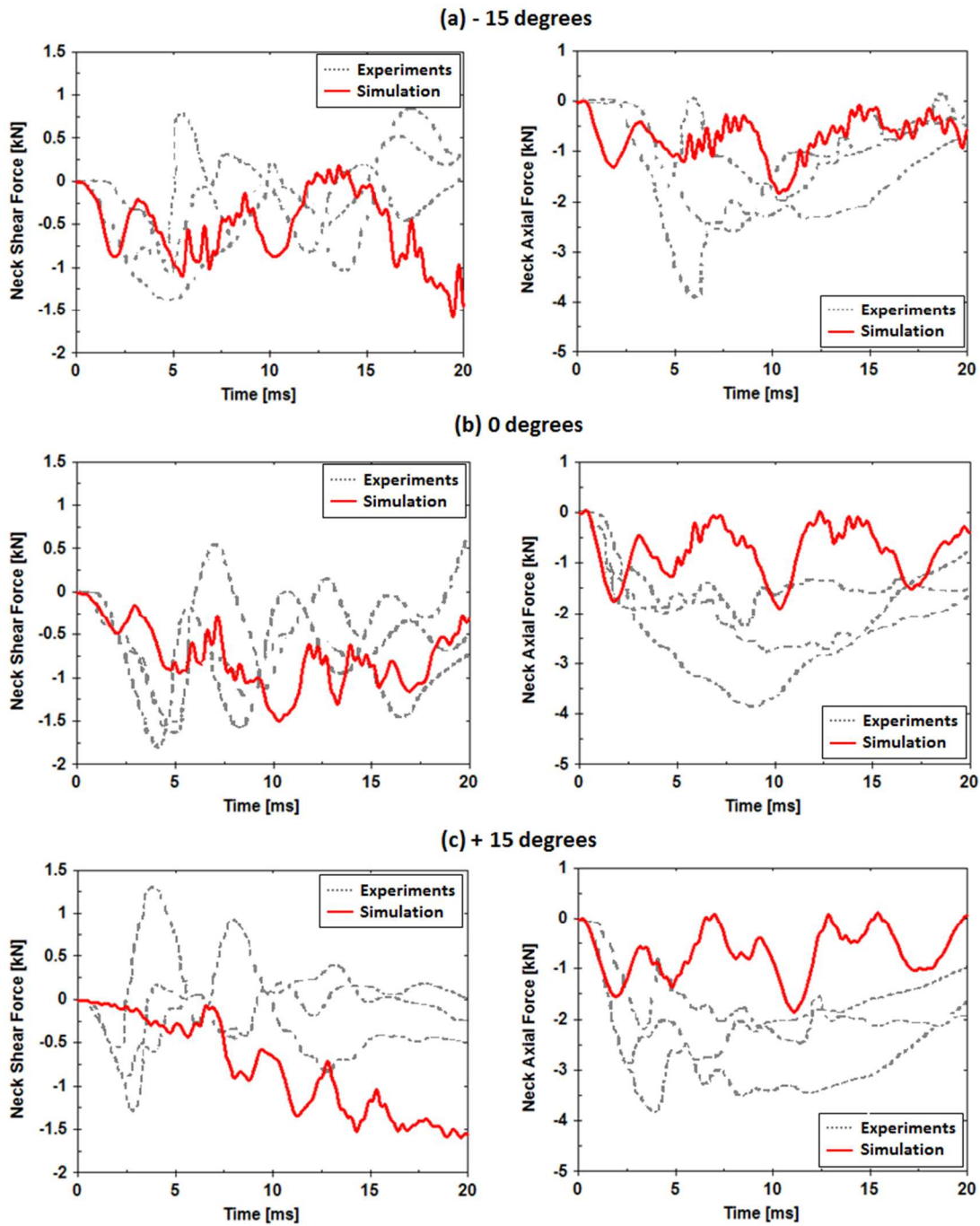


Figure C.1 The comparison of the upper neck forces between the experimental and simulated results for the impact angles of -15° (a), 0° (b) and $+15^{\circ}$ (c). The dotted grey and solid red lines represent the responses of the cadaveric necks [Nightingale et al., 1997] and D-neck model respectively.

Appendix D

Effect of Human Body Position in Compressive Impacts

This work was presented at a conference [Nasim et al., 2018]. The aim of the study was to understand the effect of boundary conditions applied to T1 in compressive impacts (described in Section 7.4), so that it can provide significant input in developing a future standard test method for neck protection devices. In this study, we further investigated the consequence of the full body impacts in three different positions: standing, seated and flexible (Figure D.1). In the full-body drop tests, the fixed torso mass of 16 kg to T1 was released and the spine from the Hybrid III model was rigidly constrained with the T1 from the D-neck model. The force-time histories of the neck are shown in Figure D.2. According to our simulations, the boundary condition applied to T1-constrained test seems to be appropriate for defining a test setup for the neck. It will be important to investigate with lower torso masses in order to develop a simpler setup.

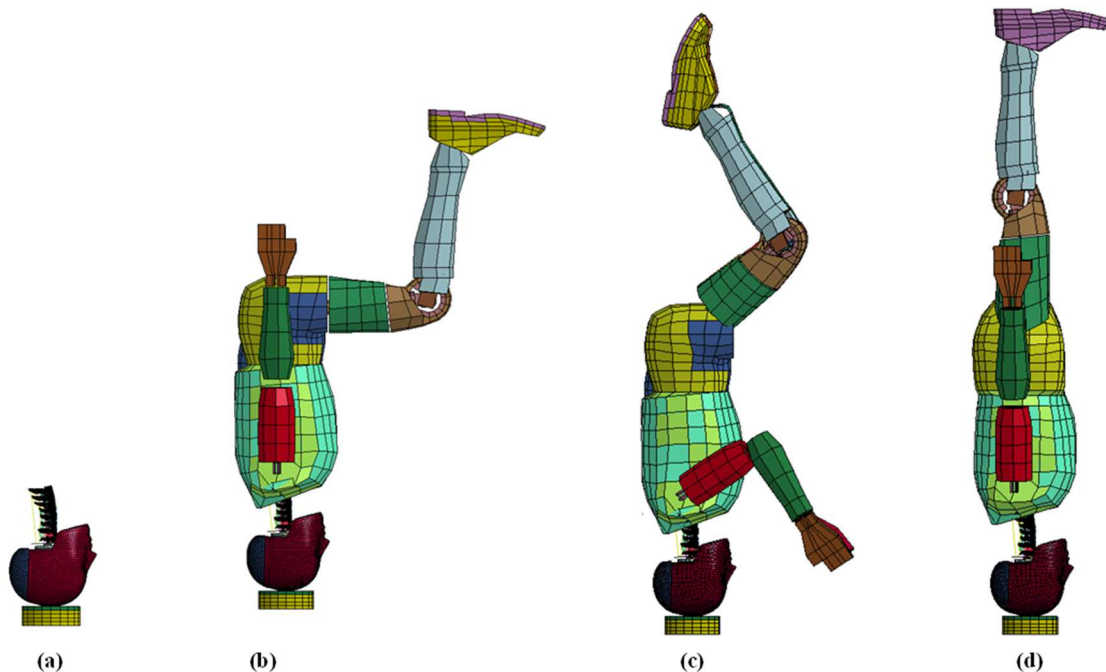


Figure D.1 The simulated drop configurations: (a) T1-constrained, (b) full-body sitting, (c) full-body flexible and (d) full-body standing.

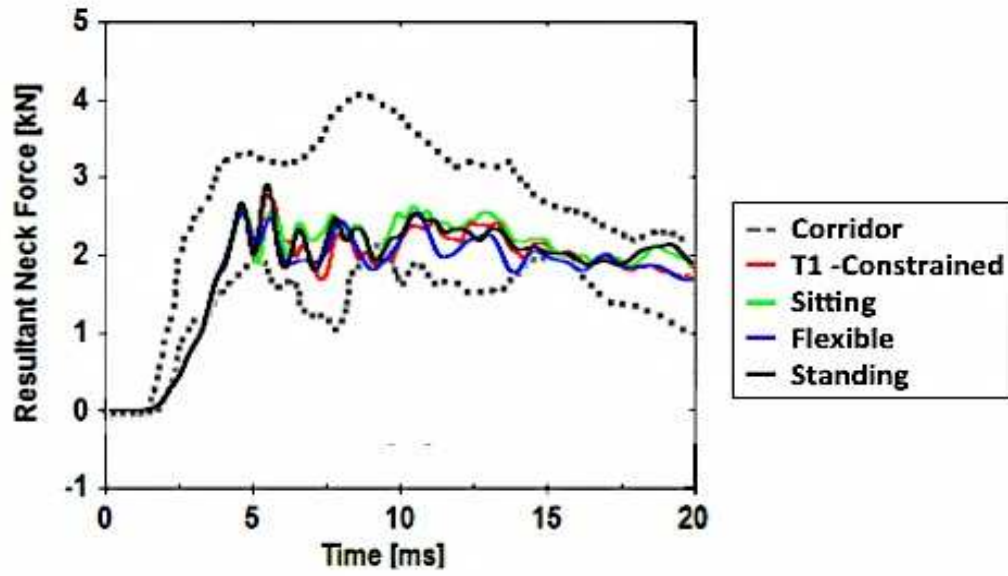


Figure D.2 Comparison of neck load curves for different drop configurations shown in Figure D.1.

Appendix E

Effect of Muscle Activation in Compressive Impacts

The knowledge related to the dynamics and the injury mechanisms of the neck or cervical spine is very limited in spite of the availability of a number of research outcomes. The main obstacle for the advancement of this knowledge is the absence of active muscles and in vivo cervical tissues in different studies. This appendix aimed to investigate the biological response of humanlike neck on inverted drop tests (as shown in Figure E.1) including the muscle activation, so that it can contribute to the proper test conditions and definition of a neck injury criterion.

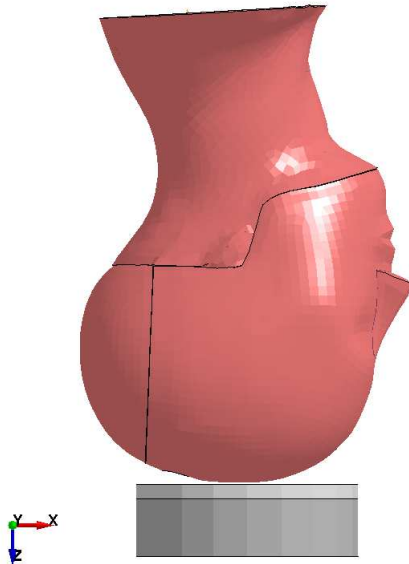


Figure E.1 Inverted drop test with the full neck model including the muscles and skin

In this analysis, three different curves (Figure E.2) were used to define the active muscle properties in order to represent the active state dynamics during an impact.

From Figure E.3, the peak neck resultant force was increased by $(5.4 \pm 3.2) \%$ due to the presence of muscles. The muscle activation of the neck affects the loading curves assuming that the activation state has influence on the resultant force.

Figure E.4 shows that the upper neck forces followed a different path when the muscles were included in the simulations.

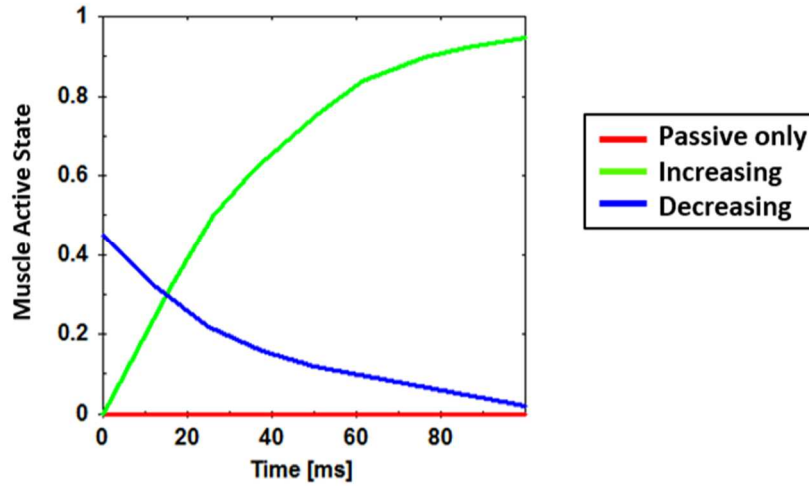


Figure E.2 The active state dynamics curves used in the simulation

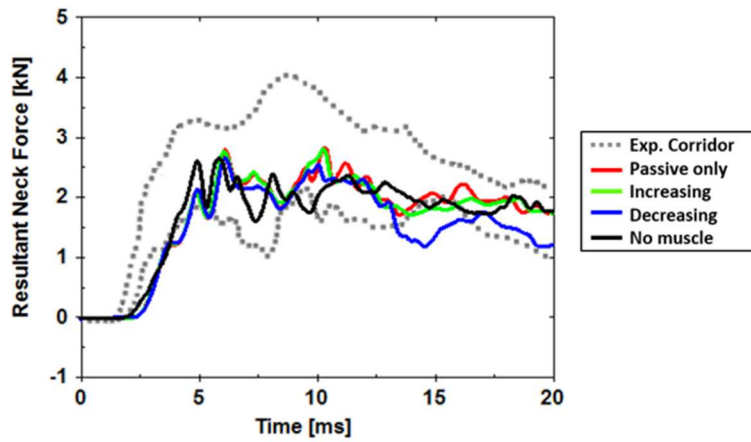


Figure E.3 The comparison of resultant neck force with experimental corridor

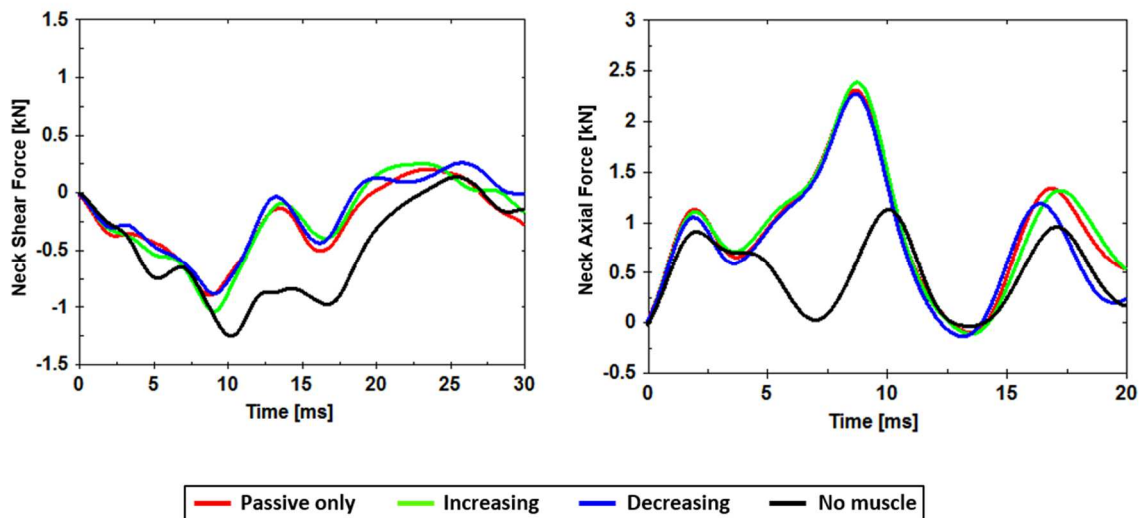


Figure E.4 The upper neck shear and axial forces due to muscle activation

Based on the above discussion and figures, it is assumed that the presence of the muscles on the inverted drop tests can be neglected for determining the peak neck resultant force, because the peak force appeared within 7 ms of the impact and less significant differences among the peak values were observed. However, the muscles effect should be taken into account for defining a neck injury criterion considering the flexion-extension movement.

The Author

Mohammed Nasim was born on 27th July, 1987 in Dhaka, Bangladesh. He completed his secondary school in 2003 from St. Gregory's High School, and higher secondary school from Notre Dame College in 2005. In the same year, he started his bachelors in Mechanical Engineering at Islamic University of Technology. His bachelors' thesis was titled as "Improvement of Hybrid Photovoltaic Thermal/Solar energy systems using three kind of RIBs". After the completion of his bachelors in 2009, he was employed by Aristopharma Ltd., a leading pharmaceuticals company of Bangladesh, as Engineering Officer, in 2010. After the first work experience, he was recruited by United Airways (BD) Ltd. (Bangladesh) as Trainee Engineer (Aerospace) in the same year. In 2011, he received Erasmus Mundus Scholarship in European Masters in Engineering Rheology (EURHEO). During this program, he went to Univerza v Ljubljana (Slovenia) to complete his first year courses; after that he finished fully integrated courses from Universidade do Minho (Portugal) in 2012. He completed his master thesis, at Université catholique de Louvain (Belgium) in 2013, on "Viscoelastic properties of PTHF based Thermoplastic elastomer (TPEs)", under the supervision of Prof. Evelyne Van Ruymbeke. The thesis was in cooperation with DSM (The Netherlands) and it aimed to study the viscoelastic properties of well-defined PTHF-T Φ T segmented block copolymers, which is a new class of thermoplastic elastomers (TPEs). After completing the course, he went back to Bangladesh and joined American International University – Bangladesh as a Lecturer in the Department of Electrical and Electronics Engineering in 2014. He was the course teacher of basic mechanical engineering and renewable energy technology courses. Moreover, he was the instructor in the lab of computer-aided design for electrical drafting. In 2015, he was granted the prestigious Marie-Sklodowska Curie Action fellowship and employed by Dainese S.p.A. for the project MOTORIST. His main objectives were to develop new PPE and standards. Considering the fact that there were no certified neck protectors, he started to work on neck protection development and its associated standards. Later in the same year, he was enrolled at University of Padova as a Ph.D. student. He continued on the same research project for his Ph.D. thesis under the supervision of Prof. Ugo Galvanetto, which was titled as "Neck Protection Development and a Proposal of the Associated Standard for the Motorcyclists".